Advances in Experimental Medicine and Biology 1115

Avia Rosenhouse-Dantsker
Anna N. Bukiya *Editors*

Cholesterol Modulation of Protein Function

Sterol Specificity and Indirect Mechanisms

Springer

Advances in Experimental Medicine and Biology

Volume 1115

More information about this series at http://www.springer.com/series/5584

Avia Rosenhouse-Dantsker • Anna N. Bukiya
Editors

Cholesterol Modulation of Protein Function

Sterol Specificity and Indirect Mechanisms

Springer

Editors
Avia Rosenhouse-Dantsker
Department of Chemistry
University of Illinois
Chicago, IL, USA

Anna N. Bukiya
The University of Tennessee Health
Science Center
Memphis, TN, USA

ISSN 0065-2598 ISSN 2214-8019 (electronic)
Advances in Experimental Medicine and Biology
ISBN 978-3-030-04277-6 ISBN 978-3-030-04278-3 (eBook)
https://doi.org/10.1007/978-3-030-04278-3

Library of Congress Control Number: 2018966812

This Springer imprint is published by the registered company Springer Nature Switzerland AG
The registered company address is: Gewerbestrasse 11, 6330 Cham, Switzerland

Preface

Cholesterol is one of the most talked-about molecules of modern times. This sterol was first obtained from gallstones in the mid-eighteenth century by French chemist François Poulletier de la Salle. His work was not published, but was referred to by his colleagues and collaborators. Another French chemist, Michel Eugène Chevreul, named the compound "cholesterine" in 1815, and this recognition opened an era of studies on cholesterol biosynthesis and physiological function that has persisted into the twenty-first century.

Cholesterol is a vital component of all animal cells. Cholesterol insertion into biological membranes conditions their physical properties by maintaining a proper rigidity, adjusting membrane thickness and curvature. In addition, cholesterol serves as a precursor for steroid hormones and as an essential component of lipoproteins. The human body produces around 1 g of cholesterol each day, resulting in total cholesterol levels in the body exceeding 30 g. Twenty-five percent of this amount is located in the brain, highlighting the vital role of cholesterol in maintaining neuronal cell excitability and homeostasis.

Despite over 200 years of scientific search into cholesterol properties, the role of cholesterol in physiology and pathology still remains a subject of investigation. On the one hand, excessive cholesterol consumption with Western diets and excessive production of cholesterol in the human body constitute a major risk factor for common pathological conditions, cardiovascular disease in particular. At the other extreme, very low cholesterol levels serve as indicators of a poor prognosis in critical illness. Our understanding of the multiple health consequences of cholesterol levels that depart from a normal "middle ground" is often hampered by the difficulty in interpreting the molecular mechanisms that underlie the cellular effects of cholesterol and, most importantly, the modulation of the effector molecular targets of cholesterol, cell proteins. This volume is the first of two volumes that captures the current state of our understanding of the molecular mechanisms that underlie cholesterol modulation of protein function.

Consistent with the two major physiological roles of cholesterol as a structural and signaling molecule, the general view of the molecular mechanisms that govern cholesterol modulation of protein function is conceptualized in two modes of

action: (a) indirect effects via cholesterol modulation of membrane physical properties and (b) protein targeting via direct interaction of the cholesterol molecule with sterol-sensing protein sites. This first volume focuses on sterol specificity as a means to distinguish between direct and indirect effects of cholesterol and on indirect mechanisms, whereas the second volume covers direct cholesterol-protein interactions.

Experimental discrimination between indirect and direct mechanisms of cholesterol effects on protein function is not straightforward. Cholesterol stereoisomers and cholesterol derivatives that exert differential effects on the physical properties of cell membranes are often used as tools to help distinguish between the potential mechanisms that underlie cholesterol-protein interactions. Thus, the first part of this volume introduces the reader to cholesterol chemistry and the use of both naturally occurring and synthetic derivatives that help to distinguish between indirect and direct modulations of protein function by cholesterol. Examples in this part include the well-studied G-protein-coupled receptors and two classes of potassium channels.

The second part of this volume focuses on studies that successfully use modern technologies to elucidate the effects of cholesterol on the physical properties of membranes and highlight these major driving forces behind this sterol's effect on proteins. These include the following studies on the various aspects of cholesterol's effects: modulation of the physical properties of membranes by means of nuclear magnetic resonance, modifications of dipole potential of lipid membranes, and mapping using mass spectrometry imaging. The volume concludes with a chapter on the cholesterol-dependent gating of a voltage-gated potassium channel demonstrating the lipid property-driven effect of cholesterol on protein function.

As the reader will discover, the depiction of cholesterol effects on protein function as either indirect or direct is somewhat oversimplified. In nature, these mechanisms are not mutually exclusive and likely coexist in the finely tuned cellular environment. Moreover, our knowledge of cholesterol modulation of protein function is far from being complete. There is little doubt that the field of cholesterol-protein interactions will remain an active and intriguing area of research for years to come.

The editors are deeply thankful to all the authors who contributed to this project aimed at portraying the complexity of the biomechanisms involving this lipid discovered 200 years ago. The editors are also grateful to senior mentors, collaborators, and emerging junior colleagues for the inspiration, for the fruitful exchange of ideas, and for providing a nurturing environment for the completion of this collection of important contributions to the field.

Chicago, IL, USA Avia Rosenhouse-Dantsker
Memphis, TN, USA Anna N. Bukiya

Contents

Contributors

G. Aditya Kumar CSIR-Centre for Cellular and Molecular Biology, Hyderabad, India

Nicolas Barbera Division of Pulmonary and Critical Care, Department of Medicine, University of Illinois at Chicago, Chicago, IL, USA

Jitendra D. Belani Thomas Jefferson University, College of Pharmacy, Philadelphia, PA, USA

Michael F. Brown Department of Chemistry and Biochemistry, University of Arizona, Tucson, AZ, USA

Department of Physics, University of Arizona, Tucson, AZ, USA

Anna N. Bukiya The University of Tennessee Health Science Center, Memphis, TN, USA

Amitabha Chattopadhyay CSIR-Centre for Cellular and Molecular Biology, Hyderabad, India

Academy of Scientific and Innovative Research, Ghaziabad, India

Ronald J. Clarke University of Sydney, School of Chemistry, Sydney, NSW, Australia

Stephanie M. Cologna Department of Chemistry and Laboratory of Integrated Neuroscience, University of Illinois at Chicago, Chicago, IL, USA

Alex M. Dopico The University of Tennessee Health Science Center, Memphis, TN, USA

Md. Jafurulla CSIR-Centre for Cellular and Molecular Biology, Hyderabad, India

Qiu-Xing Jiang Department of Microbiology and Cell Science, IFAS, University of Florida, Gainesville, FL, USA

Irena Levitan Division of Pulmonary and Critical Care, Department of Medicine, University of Illinois at Chicago, Chicago, IL, USA

Trivikram R. Molugu Department of Chemistry and Biochemistry, University of Arizona, Tucson, AZ, USA

Bhagyashree D. Rao CSIR-Indian Institute of Chemical Technology, Hyderabad, India

Academy of Scientific and Innovative Research, Ghaziabad, India

Part I
Sterol Specificity in Modulating Protein Function

Chirality Effect on Cholesterol Modulation of Protein Function

Jitendra D. Belani

Abstract Cholesterol is a key steroidal, lipid biomolecule found abundantly in plasma membranes of eukaryotic cells. It is an important structural component of cellular membranes and regulates membrane fluidity and permeability. Cholesterol is also essential for normal functioning of key proteins including ion-channels, G protein-coupled receptors (GPCRs), membrane bound steroid receptors, and receptor kinases. It is thought that cholesterol exerts its actions via specific binding to chiral proteins and lipids as well as through non-specific physiochemical interactions. Distinguishing between the specific and the non-specific interactions can be difficult. Although much remains unclear, progress has been made in recent years by utilizing *ent*-cholesterol, the enantiomer of natural cholesterol (*nat*-cholesterol) as a probe. *Ent*-Cholesterol is the non-superimposable mirror image of *nat*-cholesterol and exhibits identical physiochemical properties as *nat*-cholesterol. Hence, if the biological effects of cholesterol result solely due to membrane effects, it is expected that there will be no difference between *ent*-cholesterol and *nat*-cholesterol. However, when direct binding with chiral proteins and lipids is involved, the enantiomer is expected to potentially elicit significantly different, measurable effects due to formation of diastereomeric complexes. In this chapter, we have reviewed the literature related to *ent*-cholesterol and its use as a probe for various biophysical and biological interactions of cholesterol.

Keywords Cholesterol · Enantiomer · *ent*-Cholesterol · Synthesis · Stereospecificity · Sterol–membrane interactions

J. D. Belani (✉)
Thomas Jefferson University, College of Pharmacy, Philadelphia, PA, USA
e-mail: Jitendra.belani@jefferson.edu

A. Rosenhouse-Dantsker, A. N. Bukiya (eds.), *Cholesterol Modulation of Protein Function*, Advances in Experimental Medicine and Biology 1115,
https://doi.org/10.1007/978-3-030-04278-3_1

1 Introduction

A chiral racemic compound consists of an equimolar mixture of two enantiomeric forms. In the last few decades, scientists have tried to understand biogenesis and role of naturally occurring enantiomerically pure compounds. Chiral triterpenes found in nature undergo stereospecific cyclizations to produce enantiomerically pure steroids. Cholesterol and other steroids are thus produced in optically pure form as one enantiomer. Many of these steroidal biomolecules play a vital role in cellular functions. Molecular mechanisms underlying these cellular functions are still largely unclear. The unnatural enantiomers of these steroids can serve as valuable probes as their chemical composition, bonding pattern, and relative configuration are the same as the naturally occurring steroids. Since these unnatural enantiomers are not found in nature, these must be chemically synthesized in the laboratory. The non-superimposable mirror image of naturally occurring cholesterol is referred to as *ent*-cholesterol. A diastereomer of cholesterol with the configuration different only at C3 with α-OH group is referred to as 3-epicholesterol. The structures of cholesterol, 3-epicholesterol, and *ent*-cholesterol are given in Fig. 1. Both *ent*-cholesterol and 3-epicholesterol have been extensively used to elucidate cholesterol mechanisms and when compared to *nat*-cholesterol, these stereoisomers are expected to elicit different specific and non-specific interactions with lipids and proteins present in the membranes.

2 Chemical Structure and Synthesis

Chemical structure of natural cholesterol contains four rings (labeled A, B, C, and D) and a "side-chain" attached at the C17 of ring D. The structure contains eight stereocenters (C3, C8, C9, C10, C13, C14, C17, C20), seven of which are contiguous. In addition, there is an isolated double bond between C5 and C6 that contributes significantly to the three-dimensional shape of the steroid. Cellular biosynthesis of cholesterol is a tightly regulated process and involves enantioselective epoxidation of squalene followed by polyene cyclization to provide lanosterol in a concerted fashion. Lanosterol is further converted into cholesterol in a multistep process by the removal of three methyl groups, the reduction of one double bond by NADPH, and the migration of the other double bond [1]. Racemic syntheses of cholesterol in the laboratory by Woodward in 1952 [2] and by Johnson in 1964 [3, 4] are considered as scientific milestones. These two early and unique syntheses paved the way for synthesis of the enantiomer of this complex biomolecule.

Enantiomer of cholesterol, *ent*-cholesterol is a non-superimposable mirror image of the natural cholesterol. To prepare the enantiomer, the stereochemistry at all eight chiral carbons in cholesterol must be inverted. There is no simple way to achieve this and the enantiomer of cholesterol remains inaccessible without enormous synthetic effect [5]. Steroid nuclei with "near symmetry" such as in *ent*-19-

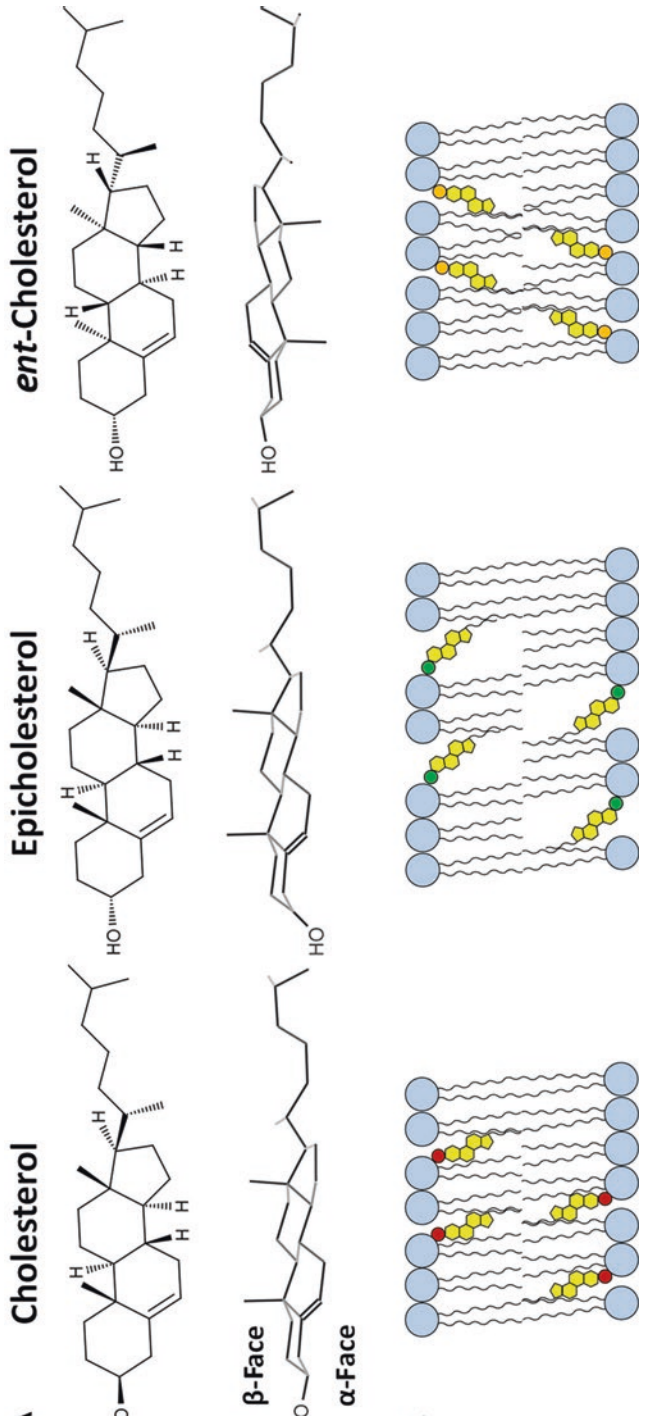

Fig. 1 (**a**) Chemical structures of cholesterol, *ent*-cholesterol, and epicholesterol; (**b**) Three-dimensional representation of the three steroids; (**c**) Schematic of the localization of the three cholesterol isomers within phospholipid bilayers and their effects on membrane packing (Adapted from Barbera et al. Current Topics in Membranes, 80, 2017, 25–50)

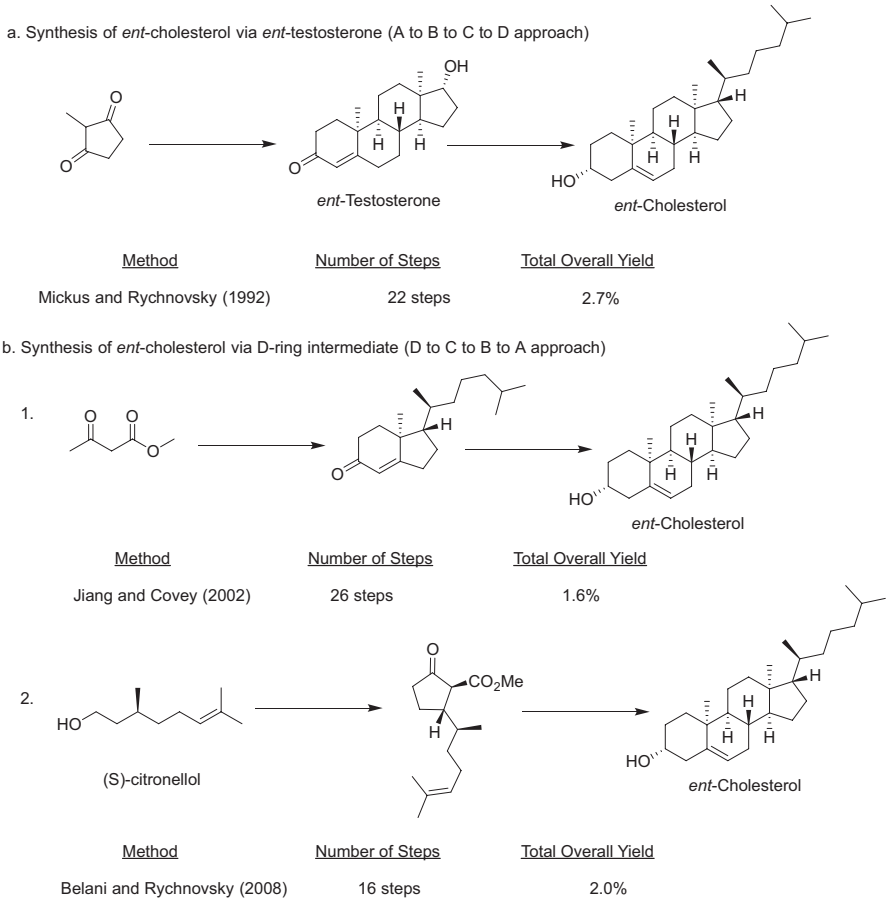

Fig. 2 The Two Different Synthetic approaches to *ent*-Cholesterol

nortestosterone have been synthesized from naturally occurring 19-nortestosterone. However, installation of the side-chain present in cholesterol poses significant additional challenges and the "inversion approach" for cholesterol offers no advantages over traditional total synthesis. Hence, the enantiomer of cholesterol must be prepared via total synthesis. There are essentially two different approaches to enantioselective synthesis of *ent*-cholesterol reported in the literature. The first involves synthesis of ABCD rings followed by installation of side chain on ring D. The other more efficient way is to first prepare a D-ring synthon with an intact side-chain and subsequent elaboration of CBA rings. The first stereoselective total synthesis was reported by Rychnovsky and Mickus in 1992 [6] and involved synthesis of the tetracyclic core of *ent*-testosterone using a modified Hoffman La Roche synthesis of 19-nor steroids [7]. Subsequently, the side chain on steroidal C17 was installed by a multistep protocol. Approximately 18 mg of *ent*-cholesterol was thus synthesized in 22 linear steps from commercially available starting materials in 2.7% overall yield (Fig. 2a). Jiang and Covey subsequently reported the first synthesis of *ent*-cholesterol

from a precursor containing the D-ring and the entire side of the steroid [8]. In this synthesis, approximately 80 mg of the enantiomer was synthesized in 26 linear steps and 1.6% overall yield from commercially available methylacetoacetate (Fig. 2b1). The third synthesis was reported in 2008 by Rychnovsky and Belani and was based on a ring D to C to B to A approach [9]. The synthesis provided approximately 120 mg of *ent*-cholesterol in 16 steps from commercially available (*S*)-citronellol with an overall yield of 2% (Fig. 2b2). Although all the syntheses described above are long and have some low yielding and limiting steps, they make *ent*-cholesterol more readily available to be used as a probe of function and metabolism of cholesterol. The last two routes also allow incorporation of ^{13}C-or^{2}H-labels toward the end of the syntheses by using CD_3I or $^{13}CH_3I$ for the installation of the axial C-18 methyl group in the A-ring of the steroid. These isotope labels allow for easy analysis of the steroid and its metabolites using various spectral techniques. Two other methods for standalone installation of the isooctyl side-chain on the steroid nucleus have been reported with good yield but preparation of steroid core is still tedious and low yielding [10, 11]. There is still an urgent need for more efficient routes with less number of steps that can allow gram scale preparation of *ent*-cholesterol. A convergent synthesis that can provide about 10% overall yield would certainly be a game-changer for this field.

3 Differential Effects of Cholesterol and Its Stereoisomers

It is now well understood that the biological interactions and functions of the molecule are related to its chirality [12]. Classical examples include (*S*)-thalidomide that is selectively teratogenic; ibuprofen, an anti-inflammatory drug which is sold as a racemate but only the (*S*)-enantiomer is active; and carvone, a monoterpene that interacts differently with olfactory receptors and smells like spearmint in the *R* form and caraway in the *S* form. For steroids, it was first shown that even simple diastereomers that are easily accessible have distinct interactions with lipids [13, 14]. It is anticipated that *ent*-steroids may also have biophysical and biological interactions that are different than those of the natural steroids [15]. In the last two decades, scientists have tried to study to understand these differences; however, many fascinating puzzles and anomalies still remain.

3.1 Effects on Membrane Proteins

Cholesterol plays a very important role in cellular function. It is vital for proper membrane protein function and plays a critical role in signal transduction and overall human health. For cholesterol, the first total synthesis of its enantiomer in >97% ee permitted investigation of the role of sterols in ion-channel formation [16]. Amphotericin B formed different channels in the presence of cholesterol and

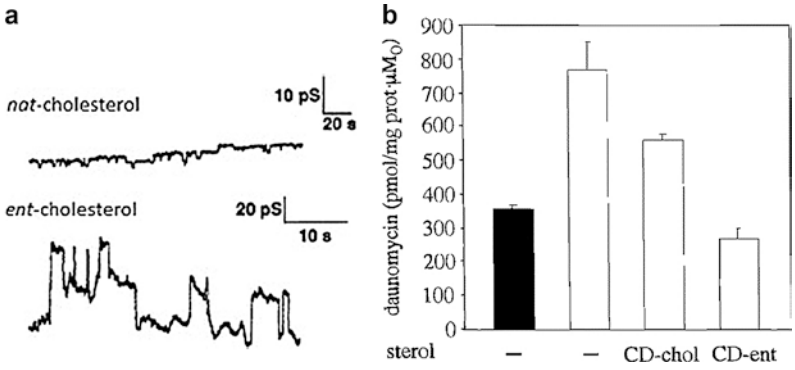

Fig. 3 (**a**) Amphotericin B ion channels in racemic glycerol monooleate (a) with cholesterol and (b) with *ent*-cholesterol with 2×10^{-8} M amphotericin B, (Adapted from [16]); (**b**) Accumulation of [^{3}H]-daunomycin in CHO cells in response to cholesterol depletion and repletion (Adapted from [18])

ent-cholesterol. Unlike natural cholesterol, membranes containing *ent*-cholesterol did not support any ion channels at amphotericin B concentrations of 2×10^{-8}, but ion channels were observed at a tenfold higher amphotericin B concentration (Fig. 3a). This constituted the first direct proof that amphotericin B binds to cholesterol in the ion channel structure. Further, to confirm if the antifungal activity of amphotericin B solely depends on changes in the physical properties of the phospholipid membrane and if they are stereospecific, Rychnovsky and coworkers used *ent*-cholesterol to probe the extent of suppression of antifungal activity of amphotericin B when compared with exogenous *nat*-cholesterol and ergosterol. It is known that when an exogenous sterol is added to fungal cell cultures, it results in suppression of the antifungal activity of amphotericin B. Ergosterol, the major phytosterol found in fungal cell membrane, was the most effective (62%) in suppressing the antifungal activity of amphotericin B. The antibiotic retained only 73% of its activity at 60 ppm of *nat*-cholesterol and 87% of activity at 30 ppm of *ent*-cholesterol. The results provide strong evidence in favor of enantiospecific interactions between amphotericin B and sterol being responsible for the activity of the antifungal agent [17].

Absolute configuration of cholesterol was however found to have minimal effects on localization of multidrug resistant P-glycoprotein (Pgp) in whole cell systems. These proteins generally localize in low density cholesterol enriched membranes. The structure of low density membrane domains of HepG2 cells was first disrupted by removing cholesterol using cyclodextrin (CD) and then repleted by with cholesterol or *ent*-cholesterol. Repletion with either sterol was equally effective in restoring total cellular content of cholesterol to baseline levels. In a separate experiment, effect of cholesterol on Pgp transport of daunomycin was studied using CHO cells in presence or absence of specific class I Pgp inhibitors. It was observed that daunomycin concentrations in CHO cells were increased three to four folds after cholesterol depletion by CD and treatment with Pgp inhibitors. Restoring the sterol

concentration with *nat*-cholesterol partially reversed the effect of CD on accumulation of daunomycin. However, treatment with the enantiomer of cholesterol before incubation with daunomycin led to significantly less accumulation of daunomycin (Fig. 3b) This observation predicted a specific interaction between cholesterol and the binding site of daunomycin on Pgp [18].

Cholesterol is required for activity and specificity of bacterial pore-forming toxins [19]. Palmer and coworkers studied sterol requirements of two different cholesterol-binding cytolysins—streptolysin O (SLO) and *Vibrio cholerae* cytolysin (VCC). Both SLO and VCC were able to permeabilize liposomal membranes containing *nat*-cholesterol and were inactive with vesicles lacking cholesterol. When cholesterol was replaced by *ent*-cholesterol, VCC had very low activity. However, SLO was only slightly less active with *ent*-cholesterol. The study suggested that although the cholesterol interaction with VCC is stereospecific, it is not with SLO [20]. Covey and coworkers also investigated the role of elevated levels of cholesterol in advanced atherosclerosis. Macrophages normally have cholesterol poor endoplasmic reticulum (ER) membrane. However, in advanced atherosclerotic lesions, free cholesterol accumulates in these ER membranes which subsequently inhibits ER calcium ATPase-2b pump (SERCA2b). To investigate the mechanism of cholesterol-induced SERCA2b inhibition, the authors incubated SERCA2b containing ER membranes with methyl-β-cyclodextrin-complexes with either *nat*-cholesterol or *ent*-cholesterol. It was observed that similar amounts of *nat*-cholesterol and *ent*-cholesterol were incorporated into the membranes and SERCA2b was inhibited to similar extent. This observation confirmed that the interaction between cholesterol and SERCA2b is not stereospecific and the excess free cholesterol simply reduces the conformational freedom of SERCA2b and depletion of ER calcium stores occurs [21].

Antibodies are proteins that are extremely specific and have been used to distinguish and separate enantiomers [22, 23]. Addadi and coworkers investigated interactions between a monoclonal antibody 36A1 and monolayers of sterols: *nat*-cholesterol, *ent*-cholesterol, and *epi*-cholesterol. The hydroxyl group at C3 was in α-position resulting in a diastereomer. When compared, layers of *nat*-cholesterol and *ent*-cholesterol interacted with the antibody to the same extent. The packing of the epimer in monolayer was distinct as the configuration at C3 position imposed a more acute angle between the hydroxyl group and the rigid steroid backbone. Hence the interaction of the antibody was not observed with the epimer. It was proposed that the interaction was dependent on the structure even more than on the chemical composition of the molecules comprising the monolayer. The antibody was able to overcome minor topographical differences between hydrophobic enantiomeric surfaces and bind equally well to the two cholesterol enantiomers. The study highlighted the fact that antibody recognition depends both on molecular structure and on the molecular packing [24, 25].

Structural features of sterols required for binding to and activating ACAT (acyl-CoA:Cholesterol acyltransferase), a membrane bound ER enzyme, were investigated by Covey and coworkers. The ACAT enzyme converts cholesterol and other sterols to long chain fatty acid acyl-CoA esters and consists of two isoforms ACAT1

and ACAT2. The enzymes contain a substrate binding site and an allosteric activator site. It is known that binding of cholesterol on the activator site makes the ACAT enzyme less discriminatory toward esterification and various modifications on sterol structure are tolerated [26]. Activation by cholesterol with equatorial 3β-OH group was compared with *ent*-cholesterol (equatorial, 3α-OH) and epicholesterol (axial, 3α-OH). Not surprisingly, epicholesterol was found to be a poor substrate for ACAT1 indicating axial orientation of the hydroxyl group at C3 is detrimental to the binding of the steroid. What was even more remarkable was the finding that *ent*-cholesterol, with equatorial C3–OH group and physical properties that were identical to *nat*-cholesterol, was also not a strong substrate for ACAT1. Rogers et al. separately studied esterification of pregnenolone, a poor ACAT substrate without the isooctyl side chain, and its activation by cholesterol and its enantiomer. Cholesterol was found to increase the V_{max} for pregnenolone esterification by 100 folds but *ent*-cholesterol only slightly activated the ACAT enzyme. *Ent*-Cholesterol is thus not only a poor substrate but also a poor activator. It has been proposed that the substrate binding site on ACAT enzyme prefers to bind with cholesterol and the interaction is stereospecific. It does not allow *ent*-cholesterol to bind. *Ent*-Cholesterol however does bind to the allosteric activating site albeit poorly [27]. These studies together clearly suggest that the overall shape of the molecule is very critical for ACAT1 substrate binding and allosteric activating site and not just the orientation of the C3-hydroxyl group [28, 29].

Bukiya et al. studied the effect of sterol structure on the activity of large-conductance voltage/Ca^{2+}-gated K^+ (BK) channels. Cholesterol is known to inhibit BK channels and this may affect regulation of neurotransmitter release and neuronal excitability. Although small changes in the steroid ring system or the side-chain had differential efficacy on reducing the activity of the BK channels, some more than the others, the enantiomer repeatedly failed to reduce the BK channel activity. This result again signifies the presence of enantiospecific spatial recognition site on the protein, in this case the BK α subunit [30]. Similar results were observed for bacterial and eukaryotic inward rectifier K^+ (Kir) channels. Cholesterol was found to inhibit purified prokaryotic and eukaryotic Kir channel as confirmed by $^{86}Rb^+$ uptake studies. *Ent*-Cholesterol did not inhibit the $^{86}Rb^+$ uptake even though it is expected to have the same effects on membrane properties as cholesterol. The study confirmed that cholesterol-Kir channel interactions are likely enantiospecific and occur at an evolutionary conserved site [31]. In a separate study conducted to understand mechanisms underlying cholesterol protection against alcohol-induced BK channel inhibition and resulting vasoconstriction, Bisen et al. showed that both cholesterol and *ent*-cholesterol reduced BK channel inhibition by alcohol in inside-out patches excised from freshly isolated cerebral artery myocytes. This observation that the two enantiomers have similar effects on the pharmacological properties of the channel suggests that either a protein site is not involved or that the protein site involved has very lax requirements for sterol recognition. It is more likely that this effect is mediated by non-specific lipid bilayer-mediated mechanism that both the enantiomers have the ability to affect equally [32].

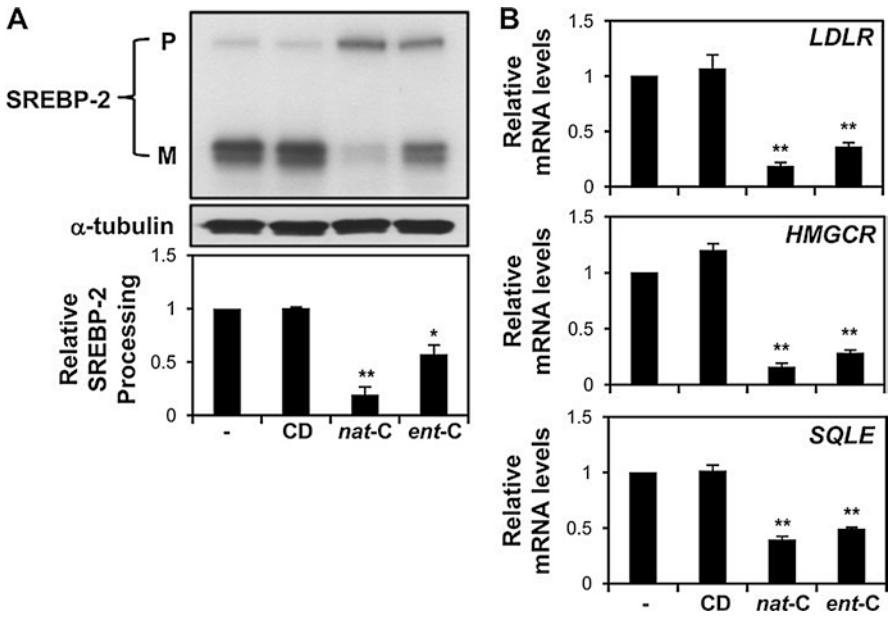

Fig. 4 (**a**, **b**) *Ent*-cholesterol suppresses activation of the SREBP-2 pathway (Adapted from [33])

To understand how cholesterol maintains its homeostasis, Kristiana et al. used the enantiomer to dissect the direct binding ability and its ability to alter the membrane properties [33]. It is known that low cellular cholesterol levels cause activation of sterol regulatory elem*ent*-binding protein-2 (SREBP) transcription factors. Alternatively at high concentrations, cholesterol binds to SREBP cleavage activating protein (Scap), causes a conformational change and eventually traps SREBP-2 in the ER and reduces the cholesterol concentration. In addition, at high concentration, cholesterol accelerates proteolytic cleavage of squalene monooxygenase (SM), a key enzyme required for biosynthesis of cholesterol. Understanding how these feedback mechanisms change when cholesterol is replaced by *ent*-cholesterol will allow elucidation of the role of non-specific membrane effects on regulation of cholesterol homeostasis. In-vitro assays with CHO-7 cells showed that *ent*-cholesterol not only suppressed SREBP-2 processing but also reduced the expression of three SREBP-2 target genes-LDLR, HMGCR, and SQLE (Fig. 4a, b). *ent*-Cholesterol was also equally able to induce a conformational change in Scap as determined by a trypsin-cleavage assay. And finally, *ent*-cholesterol also accelerated degradation of endogenous squalene monooxygenase in SRD-1 cells that lack sterol regulation as well as in CHO-7 cells that overexpress SM. All these findings suggest that the sterol-protein interactions involved in regulating cholesterol levels are not enantiospecific and that *ent*-cholesterol can also elicit these membrane effects that contribute significantly to cholesterol homeostasis [33].

3.2 *Effects on Lipid-Modified Proteins*

Both lipids and proteins affect formation of cholesterol-rich domains or rafts in membranes [34]. Since both proteins and most lipids are chiral, their interactions with cholesterol could require chiral recognition and affect formation of these rafts. Covey and coworkers compared capacity of the enantiomers to condense sphingomyelins in a monolayer system. Lipid-raft-forming capabilities of the enantiomers were compared by obtaining the surface pressure-average molecular area isotherms for mixtures of 70 mol% egg sphingomyelin and 30 mol% *nat*- or *ent*-cholesterol. These isotherms were identical for the two enantiomers indicating that the absolute configuration of the sterol does not affect its interaction with lipids such as sphingomyelin or phosphatidylcholine. In addition, both the enantiomers reversed to the same extent the enhanced phosphorylation of the EGF receptor that occurred following depletion of cholesterol with methyl-β-cyclodextrin [35]. This was direct evidence that the effects of cholesterol on EGF receptor function are most likely not enantioselective. Separately, Epand et al. studied how the enantiomers of cholesterol modulate lipid organization by small peptides. Interactions of two proteins, a 19-amino-acid, *N*-terminally myristoylated fragment (myristoyl-GGKLSKKKKGYNVNDEKAK-amide) of the protein NAP-22 [neuronal axonal membrane protein], and the segment LWYIK (Leu-Trp-Tyr-Ile-Lys) from the gp41 protein of HIV, were studied with *nat*-cholesterol and *ent*-cholesterol using differential scanning calorimetry (DSC) and nuclear Overhauser enhancement spectroscopy (NOESY-MAS-NMR). Phase transition properties of two lipid mixtures containing the lipid SOPC (1-stearoyl-2-oleoylphosphatidylcholine) and the phospholipid PtdIns(4,5)*P*2] were measured using DSC in presence of either cholesterol or *ent*-cholesterol. No significant difference was observed when *ent*-cholesterol replaced cholesterol. However, when 10 mol% myristoylated fragment of NAP-22 was added, a large increase in enthalpy of the chain melting transition was observed. The lipid mixture containing cholesterol underwent separation into cholesterol-rich and cholesterol-depleted domains. When *ent*-cholesterol was used instead of cholesterol, the chain melting transition had completely disappeared indicating stereospecific requirement for peptide-induced formation of cholesterol domains. Additionally, *N*-acetyl-LWYIK-amide increased the transition enthalpy of the phospholipid-sterol mixture containing cholesterol indicating separation of a cholesterol-depleted domain of SOPC. The effect on chain melting transition with *ent*-cholesterol was much less pronounced. Very similar effects were observed with the all D-isomer of N-acetyl-LWYIK providing evidence that peptide chirality is not essential for interaction with cholesterol containing membranes [36].

3.3 *Effects on Sterol-Lipid Interactions*

Covey and coworkers subsequently studied enantiospecific interactions between cholesterol and egg yolk sphingomyelin (SPM) measured as a difference in the plots of surface pressure (P) *vs.* mean molecular area (mmA) during the compression of

mixed monolayers containing the same mol% of either cholesterol enantiomer cospread on the surface with SPM. It was observed that enantioselectivity increased as the mol% of sterol is increased to 30%. *ent*-Cholesterol had a greater condensing effect on SPM than *nat*-cholesterol. It was thus proposed that the D-erythro-sphingosine base of SPM with its two chiral centers undergoes intermolecular hydrogen bonding with another molecule of SPM. Cholesterol alters these intermolecular SPM-SPM hydrogen bonds enantiospecifically [37]. In addition, Brewster angle microscopy showed that an additional phase was formed during compression of *ent*-cholesterol/egg yolk SPM monolayer that was not observed with *nat*-cholesterol/egg yolk SPM monolayer [38]. These experiments indicated that enantioselective interactions between cholesterol and cell membrane lipids can affect the physical properties of membranes.

To understand if enantiospecific effects that result from interactions of cholesterol and proteins occur via direct binding of the steroid to proteins or by modulation of the physical properties of the lipids bilayers, Alakoskela et al. studied the interaction of the two enantiomers with chiral phospholipid monolayers of 1,2-dipa lmitoylglycero-*sn*-3-phosphocholine (L-DPPC) and 2,3-dipalmitoylglycero-*sn*-1-phosphocholine (D-DPPC) using fluorescence imaging. These two chiral phospholipids form spiral-shaped solid domains with opposite senses in presence of low concentrations of cholesterol [39]. When comparing the two enantiomers, the authors did not observe any difference in domain shapes when cholesterol was replaced with *ent*-cholesterol. However, with racemic DPPC mixtures, the residual chirality with *ent*-cholesterol was found to be in the direction opposite that for cholesterol. This modest effect was attributed to cholesterol–cholesterol stacking at the solid–liquid interface leading to slightly different line tensions. The observation clearly indicated that cholesterol chirality requires solid like domains and is not likely to play a major role in biological membranes [40].

Cholesterol chirality and structure also affects membrane dipole potential. Electric dipoles of lipid and water molecules orient themselves in non-random fashion at the membrane interface to generate membrane dipole potential. Bandari et al. measured the membrane dipole potential using dual wavelength voltage sensitive fluorescence spectroscopy using POPC (1-palmitoyl-2-oleoyl-*sn*-glycero-3-phosphocholine) membranes. The membrane dipole potential increased with increasing concentration of cholesterol. Since generation of dipole potential arises due to membrane effects, *ent*-cholesterol that shares identical physicochemical properties with cholesterol showed comparable increase in the dipole potential. Epicholesterol however showed a modest decrease in dipole potential, indicating again that the C3 (α-OH) group significantly alters the physiochemical properties of the molecule. These effects of steroid structure on membrane dipole potential were correlated with a serotonin$_{1A}$ receptor functional assay. Comparable specific bindings of the agonist [^{3}H]8-OH-DPAT to the serotonin$_{1A}$ receptor were observed for solubilized hippocampal membranes that were enriched with cholesterol or *ent*-cholesterol. However, when epicholesterol was used, the percentage specific binding of the agonist dropped significantly suggesting that these interactions are diastereospecific and not enantiospecific [41]. To further confirm that these stereoisomers do not restore the specific binding to the serotonin$_{1A}$ receptor simply by

changing the membrane order, the fluorescence anisotropy measurements with the membrane probe DPH were conducted. All three stereoisomers including epi-cholesterol were found to increase fluorescence anisotropy similarly indicating no change in membrane order when compared to the native membrane [42]. In a separate study, Oakes and Domene performed extensive molecular dynamics to establish an atomic-level description of cholesterol-lipid leading to increase in membrane dipole potential by cholesterol and *ent*-cholesterol [43]. The authors performed molecular dynamic simulations using membranes containing 1-palmitoyl-2-oleoyl-sn-glycero-3-phosphocholine (POPC) molecules and *nat*-cholesterol, *ent*-cholesterol or *epi*-cholesterol. *Nat*-Cholesterol and *ent*-cholesterol exhibited greatest and almost identical effect on the biophysical properties of the membrane. *Epi*-Cholesterol exhibited weaker lipid-tail organization with increased mean tilt angles and lower calculated carbon-deuterium order parameter (S_{CD}) values. Both *nat*-cholesterol and *ent*-cholesterol augmented the membrane dipole potential and *epi*-cholesterol was found to decrease the membrane potential when compared to cholesterol-free membranes. Effectively, the authors showed that inclusion of small molecules with slight structural differences can modulate the dipole potential of the membranes, an important property that regulates transport processes [43].

3.4 Effects In Vivo

Importance of absolute configuration of cholesterol was established by studying effect of *ent*-cholesterol on growth, viability, and behavior of *Caenorhabditis elegans*. *C. elegans* is unable to synthesize its own cholesterol [44]. Substituting *nat*-cholesterol with *ent*-cholesterol did not significantly affect the first generation animals (Fig. 5a); however, all the second generation animals died or were arrested as embryos or larvae (Fig. 5b). The animals that did hatch were severely paralyzed (Fig. 5c). In contrast, *nat*-cholesterol animals continued to grow and behave normally (Fig. 5d). Late stage second-generation animals that survived in presence of only *ent*-cholesterol developed severe cuticle defects before dying (Fig. 5e). To confirm that effects were attributed to *ent*-cholesterol incorporation into the animals, the authors extracted and measured cholesterol content of first generation adult animals. It was confirmed that *ent*-deuterocholesterol replaced majority of the *nat*-cholesterol in the first generation animals. Separately, when animals were treated with a mixture of *ent*-cholesterol and *nat*-cholesterol, specifically in the ratio of 9:1 and 9.9:0.1, *ent*-cholesterol enhanced deleterious effects of *nat*-cholesterol reduction on the growth, movement and viability of the animals. This indicated for the first time that *ent*-cholesterol in fact antagonized essential functions of *nat*-cholesterol in vivo [45]. Covey and colleagues also compared direct ability of the enantiomers to interact with a protein. *Nat*-cholesterol was oxidized rapidly by cholesterol oxidase unlike *ent*-cholesterol, which was oxidized much more slowly under the same conditions. This clearly indicated distinct behavior of the enantiomers with a protein that has a specific sterol binding site [35].

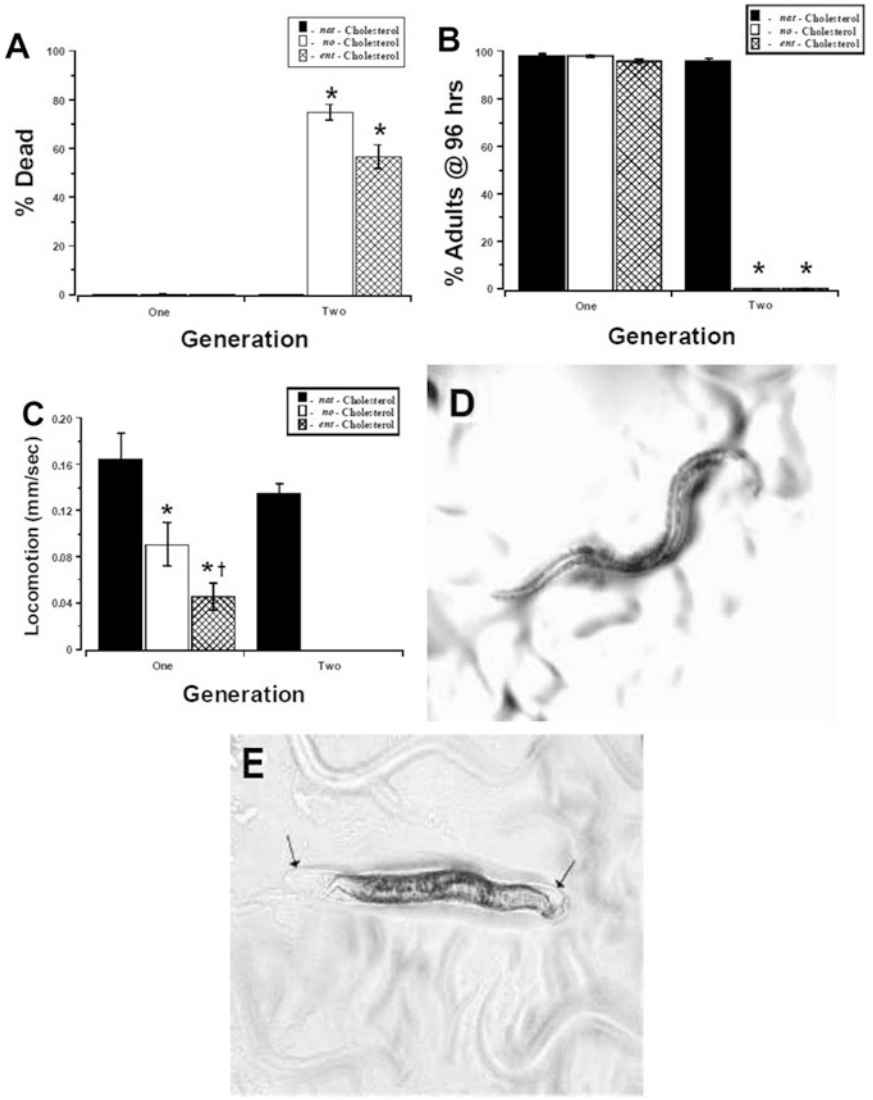

Fig. 5 Lethal, developmental, and behavioral effects of the enantiomer of cholesterol (Adapted from [45])

Xu et al. studied the sterol requirement to support mammalian cell growth using mutant CHO cells that have limited ability to synthesize cholesterol. These auxotrophic mutant cells must be provided with sterols exogenously for normal growth. Numerous sterols with slight modification of the side chain supported robust growth of these cells and these sterols comprised up to 96% of total cellular sterols after 10 days. These sterols were thus not converted to cholesterol. In addition, it was

confirmed that residual cholesterol synthesis (about 3%) was critical for cell growth. Blocking the residual endogenous cholesterol synthesis by treating the cells with NB-598, a squalene epoxide inhibitor, adversely affected the cell growth. These cholesterol requirements were surprisingly not enantiospecific confirming that the essential functions of cholesterol do not depend on its absolute configuration. *Ent*-Cholesterol supported the growth of these auxotrophic cells in presence or absence of NB-598 (Fig. 6). The results indicate that *ent*-cholesterol not only met the bulk requirement of the sterol but also satisfied the requirement of small amount of cholesterol itself [46].

Cholesterol absorption and metabolism is a complex process and better understanding pathways can provide new therapeutic regimens. Deuterium labeled *ent*-cholesterol (d_2) and *nat*-cholesterol (d_7) were used to elucidate pathways and specificity of absorption, secretion, and elimination of cholesterol in hamsters. Deuterium incorporation allowed easy measurement of the enriched cholesterol via mass spectrometry. Animals were administered deuterated enantiomers by oral gavage or via intracardiac injection. Substantial differences in absorption and excretion patterns were observed. *Ent*-Cholesterol was much more rapidly absorbed across mucosal membrane and the intestinal concentration peaked at ~1 h. Subsequently *ent*-cholesterol was as quickly secreted into the bile indicating possible enterohepatic recirculation. Finally, the enantiomer was quantitatively excreted in the stools over 3 days. The intracardiac injection revealed quick and preferential accumulation of *ent*-cholesterol in liver and bile. Unlike the enantiomer, orally administered *nat*-Cholesterol accumulated in mucosa mostly in the unesterified form and was absorbed very slowly. It took several days for serum concentration of *nat*-cholesterol to peak. The intracardiac administration of *nat*-cholesterol confirmed relatively slower elimination of the *nat*-cholesterol. This drastic difference in the rate of absorption and elimination of two enantiomers with identical physical properties indicates relevance of enantiospecific interactions and differential spatial recognition of the steroid with chiral proteins and lipids [47].

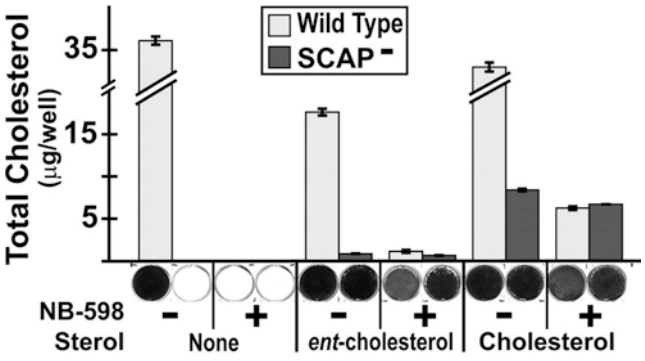

Fig. 6 Requirement for cholesterol in mammalian cells is not enantiospecific. *Ent*-cholesterol supports growth of auxotrophic CHO cells in presence or absence of NB-598 (Adapted from [46], Copyright (2005) National Academy of Sciences, U.S.A.)

4 Summary and Future Considerations

Much progress has been made to understand differential effects of cholesterol and its stereoisomers on membrane proteins, lipid-modified proteins, and membrane lipids. Utilization of *ent*-cholesterol, 3-epicholesterol, and their deuterium labeled forms has undoubtedly allowed us to understand the complex mechanisms of cholesterol and distinguish between specific and non-specific interactions of the steroid. Numerous direct effects of cholesterol with specific proteins have been established. Many of the effects have been confirmed to simply be due to membrane effects. The above studies clearly suggest that *ent*-cholesterol interacts differently with proteins and lipids. However, there are a number of studies that revealed lack of chiral discrimination between the enantiomers. In such cases, findings need to be further investigated. *Ent*-Cholesterol will continue to be utilized as a valuable probe and it is expected that advances in synthetic chemistry will allow gram scale synthesis and easier access to the enantiomer.

References

1. Yoder RA, Johnston JN. A case study in biomimetic total synthesis: polyolefin carbocyclizations to terpenes and steroids. Chem Rev. 2005;105(12):4730–56. https://doi.org/10.1021/cr0406231.
2. Woodward RB, Sondheimer F, Taub D, et al. The total synthesis of steroids. J Am Chem Soc. 1952;74(17):4223–51. https://doi.org/10.1021/ja01137a001.
3. Johnson WS, Marshall JA, Keana JFW, et al. Steroid total synthesis—hydrochrysene approach—XVI: racemic conessine, progesterone, cholesterol, and some related natural products. Tetrahedron. 1966;22:541–601.
4. Keana JFW, Johnson WS. Racemic cholesterol. Steroids. 1964;4(3):457–62.
5. Arnett EM, Gold JM. Chiral aggregation phenomena. 4. A search for stereospecific interactions between highly purified enantiomeric and racemic dipalmitoyl phosphatidylcholines and other chiral surfactants in monolayers, vesicles, and gels. J Am Chem Soc. 1982;104(2):636–9. https://doi.org/10.1021/ja00366a054.
6. Rychnovsky SD, Mickus DE. Synthesis of ent-cholesterol, the unnatural enantiomer. J Org Chem. 1992;57(9):2732–6. https://doi.org/10.1021/jo00035a036.
7. Micheli RA, Hojos ZG, Cohen N, et al. Total syntheses of optically active 19-nor steroids. (+)-Estr-4-ene-3,17-dione and (+)-13.beta.-ethylgon-4-ene-3,17-dione. J Org Chem. 1975;40(6):675–81. https://doi.org/10.1021/jo00894a003.
8. Jiang X, Covey DF. Total synthesis of ent-cholesterol via a steroid C,D-ring side-chain synthon. J Org Chem. 2002;67(14):4893–900.
9. Belani JD, Rychnovsky SD. A concise synthesis of ent-Cholesterol. J Org Chem. 2008;73(7):2768–73. https://doi.org/10.1021/jo702694g.
10. Kumar AS, Covey DF. A new method for the preparation of ent-cholesterol from ent-testosterone. Tetrahedron Lett. 1999;40(5):823–6.
11. Westover EJ, Covey DF. First synthesis of ent-desmosterol and its conversion to ent-deuterocholesterol. Steroids. 2003;68(2):159–66.
12. McConathy J, Owens MJ. Stereochemistry in drug action. Prim Care Companion J Clin Psychiatry. 2003;5(2):70–3.
13. Demel RA, Bruckdorfer KR, Van Deenen LLM. The effect of sterol structure on the permeability of lipomes to glucose, glycerol and Rb+. Biochim Biophys Acta Biomembr. 1972;255(1):321–30.

14. Demel RA, Bruckdorfer KR, van Deenen LLM. Structural requirements of sterols for the interaction with lecithin at the air-water interface. Biochim Biophys Acta Biomembr. 1972;255(1):311–20.
15. Biellmann JF. Enantiomeric steroids: synthesis, physical, and biological properties. Chem Rev. 2003;103(5):2019–33. https://doi.org/10.1021/cr020071b.
16. Mickus DE, Levitt DG, Rychnovsky SD. Enantiomeric cholesterol as a probe of ion-channel structure. J Am Chem Soc. 1992;114(1):359–60. https://doi.org/10.1021/ja00027a055.
17. Richter RK, Mickus DE, Rychnovsky SD, et al. Differential modulation of the antifungal activity of amphotericin B by natural and ent-cholesterol. Bioorg Med Chem Lett. 2004;14(1):115–8.
18. Luker GD, Pica CM, Kumar AS, et al. Effects of cholesterol and enantiomeric cholesterol on P-glycoprotein localization and function in low-density membrane domains. Biochemistry. 2000;39(29):8692.
19. Palmer M. The family of thiol-activated, cholesterol-binding cytolysins. Toxicon. 2001;39(11):1681–9.
20. Zitzer A, Westover EJ, Covey DF, et al. Differential interaction of the two cholesterol-dependent, membrane-damaging toxins, streptolysin O and Vibrio cholerae cytolysin, with enantiomeric cholesterol. FEBS Lett. 2003;553(3):229–31.
21. Li Y, Ge M, Ciani L, et al. Enrichment of endoplasmic reticulum with cholesterol inhibits sarcoplasmic-endoplasmic reticulum calcium ATPase-2b activity in parallel with increased order of membrane lipids: implications for depletion of endoplasmic reticulum calcium stores and apoptosis in cholesterol-loaded macrophages. J Biol Chem. 2004;279(35):37030–9. https://doi.org/10.1074/jbc.M405195200.
22. Got PA, Scherrmann JM. Stereoselectivity of antibodies for the bioanalysis of chiral drugs. Pharm Res. 1997;14(11):1516–23.
23. Knox JP, Galfre G. Use of monoclonal antibodies to separate the enantiomers of abscisic acid. Anal Biochem. 1986;155(1):92–4.
24. Merav G, David I, Mickus DE, et al. Stereoselective recognition of monolayers of cholesterol, ent-cholesterol, and epicholesterol by an antibody. Chembiochem. 2001;2(4):265–71. https://doi.org/10.1002/1439-7633(20010401)2:4<265::AID-CBIC265>3.0.CO;2-V.
25. Geva M, Addadi L. Stereospecific and structure specific recognition of two- and three-dimensionally organized surfaces by biological macromolecules. Mol Cryst Liq Cryst. 2003;390(1):57–66. https://doi.org/10.1080/15421400390193413.
26. Zhang Y, Yu C, Liu J, et al. Cholesterol is superior to 7-ketocholesterol or 7 alpha-hydroxycholesterol as an allosteric activator for acyl-coenzyme A:cholesterol acyltransferase 1. J Biol Chem. 2003;278(13):11642–7. https://doi.org/10.1074/jbc.M211559200.
27. Rogers MA, Liu J, Song BL, et al. Acyl-CoA:cholesterol acyltransferases (ACATs/SOATs): enzymes with multiple sterols as substrates and as activators. J Steroid Biochem Mol Biol. 2015;151:102–7. https://doi.org/10.1016/j.jsbmb.2014.09.008.
28. Liu J, Chang CC, Westover EJ, et al. Investigating the allosterism of acyl-CoA:cholesterol acyltransferase (ACAT) by using various sterols: in vitro and intact cell studies. Biochem J. 2005;391(Pt 2):389–97. https://doi.org/10.1042/BJ20050428.
29. Rogers MA, Liu J, Kushnir MM, et al. Cellular pregnenolone esterification by acyl-CoA:cholesterol acyltransferase. J Biol Chem. 2012;287(21):17483–92. https://doi.org/10.1074/jbc.M111.331306.
30. Bukiya AN, Belani JD, Rychnovsky S, et al. Specificity of cholesterol and analogs to modulate BK channels points to direct sterol-channel protein interactions. J Gen Physiol. 2011;137(1):93–110. https://doi.org/10.1085/jgp.201010519.
31. D'Avanzo N, Hyrc K, Enkvetchakul D, et al. Enantioselective protein-sterol interactions mediate regulation of both prokaryotic and eukaryotic inward rectifier K+ channels by cholesterol. PLoS One. 2011;6(4):e19393. https://doi.org/10.1371/journal.pone.0019393.
32. Bisen S, Seleverstov O, Belani J, et al. Distinct mechanisms underlying cholesterol protection against alcohol-induced BK channel inhibition and resulting vasoconstriction. Biochim Biophys Acta. 2016;1861(11):1756–66.

33. Kristiana I, Luu W, Stevenson J, et al. Cholesterol through the looking glass: ability of its enantiomer also to elicit homeostatic responses. J Biol Chem. 2012;287(40):33897–904. https://doi.org/10.1074/jbc.M112.360537.
34. Epand RM. Do proteins facilitate the formation of cholesterol-rich domains? Biochim Biophys Acta Biomembr. 2004;1666(1):227–38.
35. Westover EJ, Covey DF, Brockman HL, et al. Cholesterol depletion results in site-specific increases in epidermal growth factor receptor phosphorylation due to membrane level effects. Studies with cholesterol enantiomers. J Biol Chem. 2003;278(51):51125–33. https://doi.org/10.1074/jbc.M304332200.
36. Epand RM, Rychnovsky SD, Belani JD, et al. Role of chirality in peptide-induced formation of cholesterol-rich domains. Biochem J. 2005;390(Pt 2):541–8. https://doi.org/10.1042/BJ20050649.
37. Lalitha S, Kumar AS, Stine KJ, et al. Enantiospecificity of sterol-lipid interactions: first evidence that the absolute configuration of cholesterol affects the physical properties of cholesterol-sphingomyelin membranes. Chem Commun. 2001;(13):1192–3. https://doi.org/10.1039/B104081M.
38. Lalitha S, Sampath Kumar A, Stine KJ, et al. Chirality in membranes: first evidence that enantioselective interactions between cholesterol and cell membrane lipids can be a determinant of membrane physical properties. J Supramol Chem. 2001;1(2):53–61.
39. Weis RM, McConnell HM. Cholesterol stabilizes the crystal-liquid interface in phospholipid monolayers. J Phys Chem. 1985;89(21):4453–9. https://doi.org/10.1021/j100267a011.
40. Alakoskela JM, Sabatini K, Jiang X, et al. Enantiospecific interactions between cholesterol and phospholipids. Langmuir. 2008;24(3):830–6. https://doi.org/10.1021/la702909q.
41. Bandari S, Chakraborty H, Covey DF, et al. Membrane dipole potential is sensitive to cholesterol stereospecificity: implications for receptor function. Chem Phys Lipids. 2014;184:25–9. https://doi.org/10.1016/j.chemphyslip.2014.09.001.
42. Jafurulla M, Rao BD, Sreedevi S, et al. Stereospecific requirement of cholesterol in the function of the serotonin1A receptor. Biochim Biophys Acta. 2014;1838(1 Pt B):158–63. https://doi.org/10.1016/j.bbamem.2013.08.015.
43. Oakes V, Domene C. Stereospecific interactions of cholesterol in a model cell membrane: implications for the membrane dipole potential. J Membr Biol. 2018;251(3):507–19. https://doi.org/10.1007/s00232-018-0016-0.
44. Vinci G, Xia X, Veitia RA. Preservation of genes involved in sterol metabolism in cholesterol auxotrophs: facts and hypotheses. PLoS One. 2008;3(8):e2883. https://doi.org/10.1371/journal.pone.0002883.
45. Crowder CM, Westover EJ, Kumar AS, et al. Enantiospecificity of cholesterol function in vivo. J Biol Chem. 2001;276(48):44369–72. https://doi.org/10.1074/jbc.C100535200.
46. Xu F, Rychnovsky SD, Belani JD, et al. Dual roles for cholesterol in mammalian cells. Proc Natl Acad Sci U S A. 2005;102(41):14551–6. https://doi.org/10.1073/pnas.0503590102.
47. Westover EJ, Lin X, Riehl TE, et al. Rapid transient absorption and biliary secretion of enantiomeric cholesterol in hamsters. J Lipid Res. 2006;47(11):2374–81. https://doi.org/10.1194/jlr.M600165-JLR200.

A Critical Analysis of Molecular Mechanisms Underlying Membrane Cholesterol Sensitivity of GPCRs

Md. Jafurulla, G. Aditya Kumar, Bhagyashree D. Rao, and Amitabha Chattopadhyay

Abstract G protein-coupled receptors (GPCRs) are the largest and a diverse family of proteins involved in signal transduction across biological membranes. GPCRs mediate a wide range of physiological processes and have emerged as major targets for the development of novel drug candidates in all clinical areas. Since GPCRs are integral membrane proteins, regulation of their organization, dynamics, and function by membrane lipids, in particular membrane cholesterol, has emerged as an exciting area of research. Cholesterol sensitivity of GPCRs could be due to direct interaction of cholesterol with the receptor (specific effect). Alternately, GPCR function could be influenced by the effect of cholesterol on membrane physical properties (general effect). In this review, we critically analyze the specific and general mechanisms of the modulation of GPCR function by membrane cholesterol, taking examples from representative GPCRs. While evidence for both the proposed mechanisms exists, there appears to be no clear-cut distinction between these two mechanisms, and a combination of these mechanisms cannot be ruled out in many cases. We conclude that classifying the mechanism underlying cholesterol sensitivity of GPCR function merely into these two mutually exclusive classes could be somewhat arbitrary. A more holistic approach could be suitable for analyzing GPCR–cholesterol interaction.

Md. Jafurulla · G. Aditya Kumar
CSIR-Centre for Cellular and Molecular Biology, Hyderabad, India
e-mail: jafri@ccmb.res.in; adityakumar@ccmb.res.in

B. D. Rao
CSIR-Indian Institute of Chemical Technology, Hyderabad, India

Academy of Scientific and Innovative Research, Ghaziabad, India
e-mail: bhagyashree@ccmb.res.in

A. Chattopadhyay (✉)
CSIR-Centre for Cellular and Molecular Biology, Hyderabad, India

Academy of Scientific and Innovative Research, Ghaziabad, India
e-mail: amit@ccmb.res.in

A. Rosenhouse-Dantsker, A. N. Bukiya (eds.), *Cholesterol Modulation of Protein Function*, Advances in Experimental Medicine and Biology 1115,
https://doi.org/10.1007/978-3-030-04278-3_2

Keywords GPCR–cholesterol interaction · Specific effect · General effect · Cholesterol binding motifs

Abbreviations

7-DHC	7-Dehydrocholesterol
7-DHCR	3β-Hydroxy-steroid-Δ^7-reductase
24-DHCR	3β-Hydroxy-steroid-Δ^{24}-reductase
AY 9944	*trans*-1,4-*bis*(2-chlorobenzylaminoethyl)cyclohexane dihydrochloride
CB	Cannabinoid receptor
CCK	Cholecystokinin receptor
CCM	Cholesterol consensus motif
CCR5	CC chemokine receptor 5
CRAC	Cholesterol recognition/interaction amino acid consensus
CXCR4	CXC chemokine receptor 4
GalR2	Galanin receptor 2
GPCR	G protein-coupled receptor
MβCD	Methyl-β-cyclodextrin
MI	Metarhodopsin I
MII	Metarhodopsin II
mGluR	Metabotropic glutamate receptor
SLOS	Smith–Lemli–Opitz syndrome
Smo	Smoothened
T2R4	Bitter taste receptor 4

1 G Protein-Coupled Receptors as Signaling Hubs and Drug Targets

The G protein-coupled receptor (GPCR) superfamily is the largest and an extremely diverse family of proteins implicated in information transfer across biological membranes [1–3]. They are characterized by seven transmembrane domain topology and include >800 members which are encoded by ∼5% of genes in humans [4]. Signaling by GPCRs involves their activation by a wide variety of extracellular ligands that trigger the transduction of signals into the cellular interior through concerted structural rearrangements in their transmembrane and extramembranous domains [5, 6].

GPCRs are involved in the modulation of cellular responses to stimuli that encompass a variety of endogenous and exogenous ligands which even include photons. As a result, GPCRs mediate several essential physiological processes such as

neurotransmission, cellular metabolism, secretion, cellular differentiation, growth, and inflammatory/immune responses. GPCRs have therefore emerged as popular targets for the development of novel drug candidates in all clinical areas ranging from disorders of the central nervous system to cancer [7–11]. Importantly, ~50% of clinically prescribed drugs and 25 of the 100 top selling drugs target GPCRs [12–14]. However, only a small number of GPCRs are currently targeted by drugs [15, 16]. This presents the exciting possibility that the receptors which are not identified yet could be potential drug targets for diseases that pose a challenge to the available repertoire of drugs.

The role of membrane lipids in GPCR organization, dynamics, structure, and function has emerged as an exciting area in GPCR biology. GPCRs are integral membrane proteins with their transmembrane helices traversing the membrane seven times and as a consequence a major part of these receptors is surrounded by membrane lipids. For example, in case of rhodopsin, molecular dynamics simulations show that the lipid–protein interface corresponds to ~38% of the total surface area of the receptor [17]. In such a scenario, it is only realistic that the membrane lipid environment would modulate GPCR structure and function. Cellular membranes comprise of a wide variety of lipids, each of which uniquely modulates the physicochemical properties of the bilayer [18, 19]. Phospholipids, sphingolipids, and cholesterol constitute major lipid components of cell membranes, among which cholesterol has been extensively studied in the context of the organization, dynamics, structure, and function of GPCRs.

2 Membrane Cholesterol in GPCR Function

Cholesterol is a crucial and representative lipid in higher eukaryotic cell membranes and plays a key role in membrane organization, dynamics, function, and sorting. The unique molecular structure of cholesterol has been intricately fine-tuned over a very long timescale of natural evolution [20, 21]. The chemical structure of cholesterol comprises of the 3β-hydroxyl group, the rigid tetracyclic fused ring, and the flexible isooctyl side chain (Fig. 1a). The 3β-hydroxyl group (sole polar group) helps cholesterol anchor at the membrane interface and is believed to form hydrogen bonds with polar residues of membrane proteins. The tetracyclic fused ring and the isooctyl side chain constitute the apolar component of cholesterol. An inherent asymmetry about the plane of the sterol ring is generated by methyl substitutions on one of its faces (Fig. 1b). The protruding methyl groups (constituting the rough β face) are believed to participate in van der Waals interactions with the side chains of branched amino acids such as valine, leucine, and isoleucine. The other side of the sterol ring (constituting the smooth α face) exhibits favorable van der Waals interaction with the saturated fatty acyl chains of phospholipids (Fig. 1c; [22–24]). Cholesterol is nonrandomly distributed in specific domains (or pools) in biological and model membranes [22, 25–28]. Membrane cholesterol is essential for a range

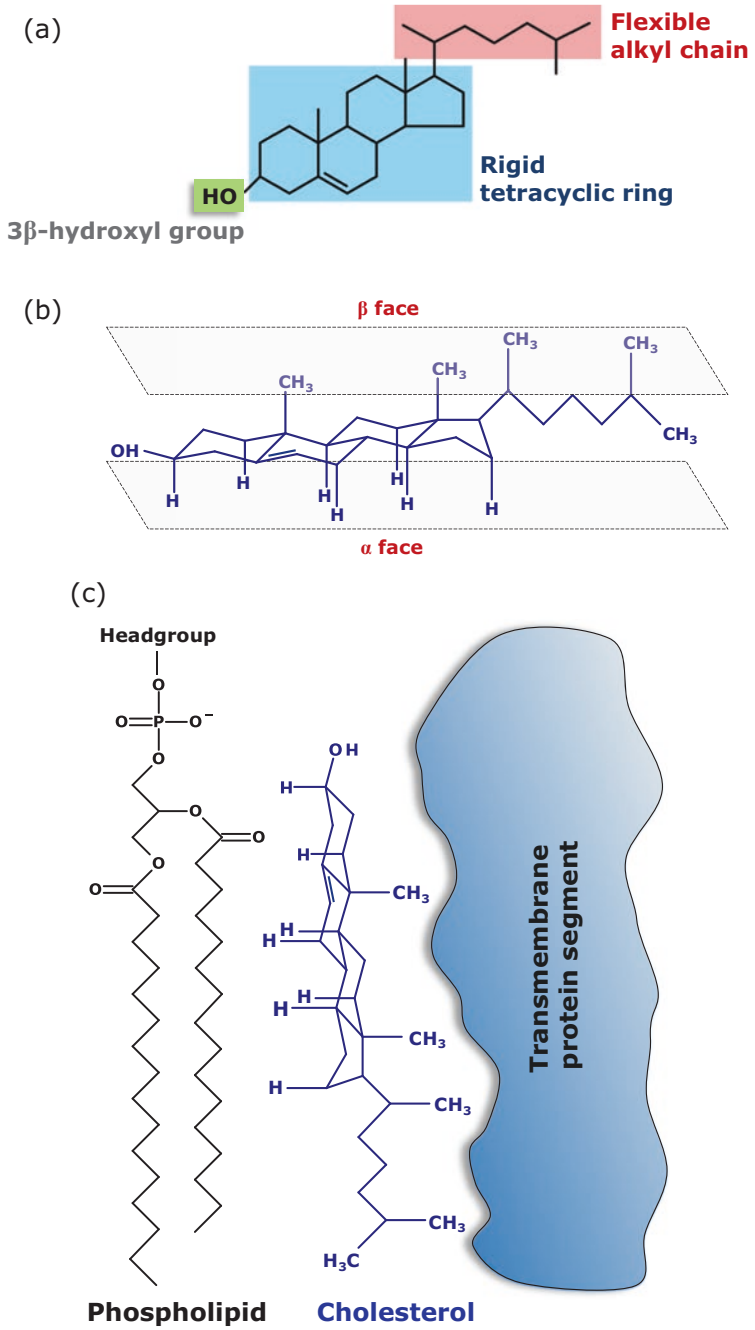

Fig. 1 Structural features of cholesterol and its orientation with respect to membrane components: (**a**) Chemical structure of cholesterol with its three structurally distinct regions (shown as shaded boxes): the 3β-hydroxyl group, the rigid tetracyclic fused ring, and the flexible isooctyl side chain.

of cellular processes such as membrane sorting and trafficking [29], signal transduction [30], and the entry of pathogens [31–35].

Membrane cholesterol has been shown to modulate the organization, dynamics, and function of several GPCRs (reviewed in [3, 36–42]). Understanding such dependence of the function of GPCRs on membrane cholesterol assumes significance since the function of GPCRs has been found to be compromised in pathological conditions with misregulated cholesterol metabolism [43]. In addition, cholesterol exhibits an inherent diversity in terms of its distribution across cell, tissue, and organ types. For example, although the central nervous system constitutes ~2% of the body mass, it accounts for ~25% of the cholesterol content in the body [44, 45]. Moreover, cellular cholesterol content is age-dependent [46] and developmentally regulated [47].

In spite of several studies showing the importance of cholesterol in GPCR function, the exact molecular mechanism underlying this remains elusive [48, 49]. The cholesterol dependence of the function of GPCRs could be attributed to either specific (direct) interaction or general (indirect) effect of membrane cholesterol on physical properties of the membrane in which the receptor is embedded. A combination of specific and general effects is yet another possibility. In this review, we discuss the cholesterol sensitivity of GPCRs with examples highlighting specific and general effects of membrane cholesterol on GPCR function, along with experimental strategies to explore such interactions.

3 Strategies to Explore Cholesterol Sensitivity of GPCRs

The mechanism of action of cholesterol on GPCRs has been explored using a battery of experimental strategies, each of which provides a unique perspective to address the molecular basis of these interactions. The strategies commonly used to study such interactions rely on the modulation of cholesterol content or its availability in membranes in order to probe its role in supporting the function and organization of GPCRs. These techniques, when used judiciously, could be helpful in delineating the specific and general effects of cholesterol on GPCR function. We discuss below a few important strategies that are used to explore the nature of the interaction of membrane cholesterol with GPCRs.

Fig. 1 (continued) (**b**) Two faces of cholesterol: asymmetry is due to the methyl groups on one plane of the sterol ring of cholesterol resulting in a rough (β) face, leaving the other plane with axial hydrogen atoms (smooth (α) face). (**c**) A schematic showing the possible orientation of cholesterol with respect to membrane components (phospholipid and transmembrane protein segment). The smooth α face of cholesterol contributes to favorable van der Waals interaction with the saturated fatty acyl chains of phospholipids and the rough β face interacts with uneven transmembrane domains of integral membrane proteins. Adapted and modified from [22]. See text for more details

3.1 Solubilization and Reconstitution

Solubilization is an important method used to understand the structural and functional aspects of GPCRs. Solubilization involves the isolation of the receptor from its native membrane environment and dispersing it in a relatively purified state using suitable amphiphilic detergents. The process of solubilization leads to dissociation of proteins and lipids which are held together in the native membrane, ultimately resulting in the formation of small clusters of protein, lipid, and detergent in an aqueous solution [50–54]. Solubilization has been utilized as an effective strategy to study GPCR–lipid interactions and probe lipid specificity by reconstitution of the receptor with specific lipids [54, 55]. The process of reconstitution involves removal of detergent, followed by incorporation of the receptor into membrane-mimics such as micelles, bicelles, liposomes, nanodiscs, and planar lipid bilayers [55, 56]. This strategy has been earlier utilized to explore the role of cholesterol in the function of the serotonin$_{1A}$ receptor [54]. Using this strategy, we further explored the structural stringency of cholesterol in the function of the serotonin$_{1A}$ receptor by reconstituting the solubilized receptor with close structural analogs (biosynthetic precursors and stereoisomers) of cholesterol [57–60].

3.2 Inhibition of Cholesterol Biosynthesis

Biosynthesis of cholesterol is carried out in a stringently regulated multi-step enzymatic pathway [61]. A physiologically relevant approach to study the role of cholesterol in GPCR function is metabolic (chronic) depletion by inhibiting specific enzymes in its biosynthetic pathway. A common strategy that has been used to chronically deplete cellular cholesterol is the use of statins [62, 63]. Statins are competitive inhibitors of HMG-CoA reductase, the enzyme that catalyzes the rate-limiting step in the cholesterol biosynthetic pathway (Fig. 2a; [64]). In addition, distal inhibitors such as AY 9944 (*trans*-1,4-*bis*(2-chlorobenzylaminoethyl)cyclohexane dihydrochloride) that inhibits 3β-hydroxy-steroid-Δ^7-reductase (7-DHCR), and triparanol which inhibits 3β-hydroxy-steroid-Δ^{24}-reductase (24-DHCR) have been extensively utilized [65, 66]. Inhibition of 7-DHCR and 24-DHCR that catalyze final steps in the Kandutsch-Russell pathway [67] and Bloch pathway [68] results in the accumulation of 7-dehydrocholesterol (7-DHC) and desmosterol, respectively (Fig. 2a). Importantly, malfunctioning of 7-DHCR and 24-DHCR has been identified as major factors for lethal neuropsychiatric disorders such as Smith–Lemli–Opitz syndrome (SLOS) and desmosterolosis [69, 70]. Therefore, inhibitors of 7-DHCR and 24-DHCR have been successfully utilized to generate cellular and animal model systems to study these disease conditions [65, 66, 71, 72]. We previously utilized this strategy to generate a cellular model for SLOS using AY 9944, and explored the function of the serotonin$_{1A}$ receptor (an important neurotransmitter receptor) in this neuropsychiatric disease condition [43].

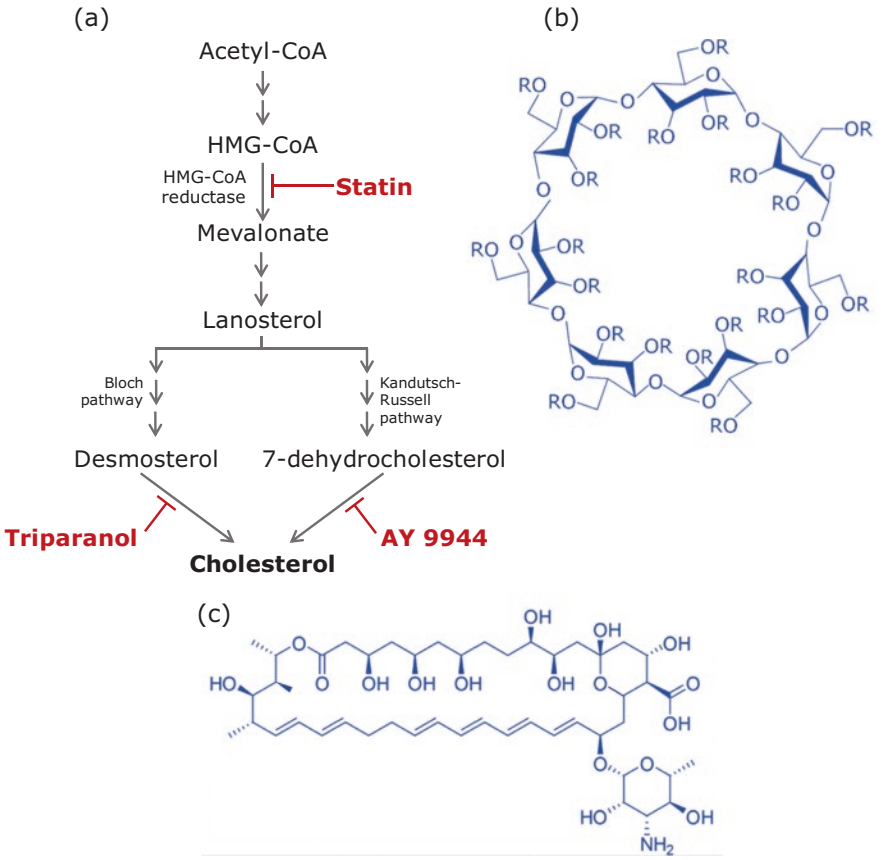

Fig. 2 Strategies to explore cholesterol-dependence of GPCR function. (**a**) A schematic representation of biosynthetic inhibitors of cholesterol. The role of cholesterol in GPCR function can be analyzed utilizing inhibitors of cholesterol biosynthesis that allow chronic depletion of cholesterol in a physiologically relevant manner. Statins inhibit the first rate-limiting step that involves the conversion of HMG-CoA to mevalonate at an early step in the cholesterol biosynthetic pathway. Inhibitors of the final steps in the Kandutsch-Russel and Bloch pathways of cholesterol biosynthesis include AY 9944 and triparanol that inhibit the synthesis of cholesterol from their immediate precursors, 7-dehydrocholesterol and desmosterol, respectively. (**b**) The chemical structure of methyl-β-cyclodextrin (MβCD), a specific carrier of cholesterol that selectively depletes membrane cholesterol. R denotes a methyl group. (**c**) Chemical structure of nystatin, a representative complexing agent

3.3 Specific Carriers

A commonly utilized strategy for acute and specific modulation of membrane cholesterol content is by using specific carriers. Methyl-β-cyclodextrin (MβCD), a member of the cyclodextrin family, is an oligomer of seven methylated-glucose residues that exhibits specificity for cholesterol over other membrane lipids

(see Fig. 2b; [34, 73, 74]). MβCD has been utilized as the carrier of choice to study the effect of cholesterol on GPCR function, organization, and dynamics in a large number of studies [36, 37]. The relatively small size and polar nature of MβCD allows its close interaction with membranes, thereby enabling efficient and selective modulation of cholesterol content. This strategy has been utilized to explore the cholesterol-dependent function of several GPCRs such as rhodopsin [75], oxytocin [76], galanin [77], serotonin$_{1A}$ [78, 79], cannabinoid [80–82], and bitter taste T2R4 receptors [83]. We have successfully utilized MβCD for controlled modulation of membrane cholesterol to study its role in the function of the serotonin$_{1A}$ receptor [78, 79, 84]. We further utilized MβCD to replace cholesterol with its various close structural analogs in order to explore the structural stringency of cholesterol for supporting receptor function [54]. Interestingly, we have recently shown that although both inhibition of cholesterol biosynthesis and specific carriers modulate cholesterol levels in cell membranes, the actual effect could differ a lot (even at same cholesterol concentrations), since the membrane dipolar environment in these cases turn out to be very different [85].

3.4 Enzymatic Oxidation

Specific modulation of membrane cholesterol could also be achieved by its oxidation using the enzyme cholesterol oxidase. Cholesterol oxidase catalyzes the oxidation of cholesterol to 4-cholestenone at the membrane interface [86], thereby modifying the chemical nature of cholesterol without physical depletion from membranes. Oxidation of cholesterol exhibits mild effect on global membrane properties relative to its physical depletion, and minimizes nonspecific effects of cholesterol modulation. This strategy has been earlier utilized to explore the structural specificity of cholesterol (the hydroxyl group in particular) in the function of several GPCRs such as the serotonin$_{1A}$ receptor [87, 88], oxytocin and cholecystokinin (CCK) receptors [76], galanin-GalR2 receptors [77], rhodopsin [89], and chemokine receptors CXCR4 and CCR5 [90].

3.5 Complexing Agents

Modulating availability of cholesterol in the membrane, rather than physical depletion, is yet another method to explore the cholesterol sensitivity of GPCR function. Cholesterol-complexing agents such as digitonin, filipin, nystatin, amphotericin B, and perfringolysin O [91–95] at appropriate concentrations partition into membranes and sequester cholesterol, thereby making it unavailable for interaction with GPCRs. These agents could be used to address the interaction of cholesterol with GPCRs by restricting cholesterol availability. Figure 2c shows the chemical

structure of nystatin, a representative complexing agent. This strategy has been earlier utilized to probe the requirement of membrane cholesterol for the function of the serotonin$_{1A}$ [96, 97], oxytocin [76], and galanin [77] receptors.

4 Mechanisms of Cholesterol Sensitivity of GPCRs

Cholesterol sensitivity of GPCRs is well documented. However, the underlying molecular mechanism remains elusive. The ongoing efforts to understand the structural and functional correlates underlying cholesterol sensitivity of GPCR function have provided evidence in favor of both specific interaction and general (membrane) effects. We discuss below representative studies on cholesterol sensitivity of GPCRs.

4.1 Specific Requirement of Membrane Cholesterol for GPCRs

4.1.1 Serotonin$_{1A}$ Receptor

The serotonin$_{1A}$ receptor is a key neurotransmitter GPCR that is implicated in the generation and modulation of various cognitive, behavioral, and developmental functions [98–102]. The serotonin$_{1A}$ receptor is the most well-studied GPCR in terms of specificity of cholesterol in the organization, dynamics, and function of the receptor. Earlier work from our laboratory has comprehensively demonstrated the specific requirement of membrane cholesterol for the function of the serotonin$_{1A}$ receptor utilizing an array of experimental approaches. By modulating the availability of membrane cholesterol by employing (1) MβCD [57, 78], (2) biosynthetic inhibitors such as statin [63] and AY 9944 [43], and (3) complexing agents such as nystatin [96] and digitonin [97], we have shown the requirement of cholesterol in receptor function. We generated a cellular model for SLOS (a fatal neuropsychiatric disorder) using AY 9944 and showed that the function of the serotonin$_{1A}$ receptor is compromised under this disease-like condition [43]. We have recently generated a rat model of SLOS by oral feeding of AY 9944 to dams for brain metabolic NMR studies. Importantly, enzymatic oxidation of cholesterol [87, 88] led to a change in receptor function, without any appreciable effect on membrane order (as reported by fluorescence anisotropy measurements), *thereby suggesting specific requirement of cholesterol for receptor function*. We further demonstrated the structural stringency of cholesterol in supporting the function of the serotonin$_{1A}$ receptor by replacing cholesterol with its immediate biosynthetic precursors (7-DHC and desmosterol) [58, 59, 103] and stereoisomers of cholesterol ([60]; reviewed in [54]). In addition, we showed that the stability of the serotonin$_{1A}$ receptor is enhanced in the presence of cholesterol using biochemical approaches [104], molecular modeling [105], and all atom molecular dynamics simulations [106]. Taken together, these studies bring out the cholesterol sensitivity of the serotonin$_{1A}$ receptor function, which in some cases (such as treatment with cholesterol oxidase) could have a specific mechanism.

4.1.2 Oxytocin Receptor

The oxytocin receptor plays an important role in several neuronal functions and in reproductive biology [107]. Cholesterol dependence of oxytocin receptor function was explored using multiple approaches [76, 108]. Modulation of membrane cholesterol content using MβCD resulted in a change in the affinity state of the receptor for oxytocin, with the receptor in a high affinity state in the presence of cholesterol [108]. In addition, utilizing cholesterol-complexing agent filipin, mere complexation of cholesterol was shown to be sufficient to modulate receptor function [76]. Importantly, treatment with cholesterol oxidase modulated the function of the receptor without a significant change in membrane order. The structural stringency of cholesterol for the function of the oxytocin receptor was demonstrated by replacing cholesterol with an array of its structural analogs [76]. Further, the oxytocin receptor was shown to be more stable in the presence of cholesterol [109]. These results point out the role of specific mechanism in the cholesterol-dependent function of the oxytocin receptor.

4.1.3 Galanin Receptor

Galanin receptors upon binding to the neuropeptide galanin mediate diverse physiological functions in the peripheral and central nervous systems. The requirement of cholesterol for galanin receptor (GalR2) function was shown by modulating cholesterol content in cellular membranes using MβCD or by culturing cells in lipoprotein-deficient serum [77]. Depletion of membrane cholesterol led to decrease in affinity of ligand binding to the receptor. In addition, complexation of cholesterol with filipin and enzymatic oxidation of cholesterol led to significant reduction in ligand binding activity of the receptor. The mechanistic basis of cholesterol sensitivity was evident from experiments in which cholesterol was replaced with its structural analogs, thereby implying a possible specific mechanism responsible for cholesterol sensitivity of GalR2 [77].

4.1.4 Chemokine Receptors

Chemokine receptors are important GPCRs implicated in immunity and infection. A wide range of chemokines bind to these receptors and mediate specific immune responses. Membrane cholesterol has been shown to be essential for stabilizing the functional conformation and signaling of CCR5 and CXCR4 receptors, members of the chemokine receptor family [90, 110, 111]. The cholesterol sensitivity of the function of CCR5 was shown using conformation-specific antibodies, whose binding to the receptor exhibited cholesterol dependence [110]. Treatment with cholesterol oxidase [90] resulted in reduction in binding of epitope-specific antibodies to CCR5 along with loss in receptor function. In addition, replacement of cholesterol with 4-cholesten-3-one showed reduction in specific ligand binding to the receptor [110]. Similar results were observed for CXCR4 where depletion or oxidation of membrane cholesterol resulted in reduction in binding of conformation-specific

antibodies and signaling of the receptor [90, 111]. These effects were reversed upon replenishment with membrane cholesterol.

4.1.5 Bitter Taste Receptors

The human bitter taste receptors (T2Rs) are chemosensory receptors with significant therapeutic potential [112]. Earlier work from our laboratory has shown that the T2R4 receptor, a representative member of the bitter taste receptor family, exhibits cholesterol sensitivity in its signaling [83]. The molecular basis of such cholesterol dependence of receptor function could be attributed to the putative cholesterol recognition/interaction amino acid consensus (CRAC) motif (see below), since mutation of a lysine residue in the CRAC sequence led to loss of cholesterol sensitivity of the receptor [83].

4.1.6 Cannabinoid and Cholecystokinin Receptors

Cannabinoid receptors are activated by endocannabinoids which mediate a variety of physiological and neuroinflammatory processes, and are implicated in several neurodegenerative and neuroinflammatory disorders. The cholesterol sensitivity of type-1 cannabinoid (CB1) receptors was shown from dependence of specific ligand binding and signaling of the receptor on membrane cholesterol [80, 81, 113]. Importantly, such a sensitivity of CB1 receptor function to membrane cholesterol is lost upon mutation of a lysine residue in the putative CRAC sequence. Interestingly, the type-2 cannabinoid (CB2) receptor has glycine instead of lysine (as in CB1 receptor) in the CRAC sequence [113] and does not show cholesterol dependence for its function [82, 113]. These studies point toward the possible involvement of the CRAC motif in cholesterol sensitivity of CB1 receptors.

Similar observations were reported for subtypes of cholecystokinin CCK1 and CCK2 receptors [114, 115]. CCK1 receptors were shown to be sensitive to membrane cholesterol by analyzing active conformation of the receptor, probed using fluorescence of a specific fluorescent ligand and intracellular calcium response [114]. Interestingly, a closely related subtype CCK2 receptor has been shown to be insensitive to membrane cholesterol [115]. Importantly, mutation in CRAC motif region in CCK1 receptor resulted in the loss of its cholesterol sensitivity.

4.2 Structural Evidence in Support of GPCR–Cholesterol Interaction

The specificity of cholesterol for the function of GPCRs has gained support from recently reported high-resolution crystal structures of GPCRs with bound cholesterol molecules. Crystal structures of several GPCRs have been resolved with bound cholesterol molecules over the last decade (see Table 1). Cholesterol was found to

Table 1 GPCR structures with bound cholesterol[a]

Receptor	PDB ID	# Chol[b]	Reference
β_2-adrenergic receptor	2RH1	3	[116]
	3D4S	2	[117]
	3NYA, 3NY8, 3NY9	2	[118]
	3PDS	1	[119]
	5JQH	1	[120]
	5D5A, 5D5B	3	[121]
	5X7D	2	[122]
	5D6L	3	[123]
Adenosine A_{2A} receptor	4EIY 5K2A, 5K2B, 5K2C, 5K2D	3 3	[124] [125]
	5IU4, 5IU7, 5IU8, 5IUA 5IUB	4 3	[126] [126]
	5UVI	3	[127]
	5NLX, 5NM2, 5NM4	3	[128]
	5MZJ, 5N2R 5MZP	3 4	[129] [129]
	5JTB	3	[130]
	5VRA	3	[131]
	6AQF	3	[132]
	5OLH, 5OLO 5OM4, 5OLV, 5OM1, 5OLG, 5OLZ	3 4	[133] [133]
κ-opioid receptor	6B73	1	[134]
μ-opioid receptor	4DKL	1	[135]
	5C1M	1	[136]
Metabotropic glutamate receptor 1	4OR2	6 (per dimer)	[137]
Smoothened	5L7D	1 (per dimer)	[138]
	6D35	1	[139]
Serotonin$_{2B}$ receptor	4IB4	1	[140]
	4NC3	1	[141]
	5TVN	1	[142]
Cannabinoid receptor 1	5XR8, 5XRA	1	[143]
CC chemokine receptor type 9	5LWE	1 (per dimer)	[144]
Endothelin receptor type-B	5X93	1	[145]
US28 in complex with the chemokine domain of human CX3CL1	4XT1 5WB2	2 2	[146]
$P2Y_1$ receptor	4XNV	1	[147]
$P2Y_{12}$ receptor	4PXZ 4NTJ	1 2	[148] [149]

[a]The list was generated by searching the PDB database for GPCR structures with cholesterol as a small molecule ligand

[b]Number of cholesterol molecules bound per GPCR monomer

be bound between transmembrane helices (interhelical) within the receptor or between monomers of a receptor dimer. Interestingly, cholesterol sensitivity has been demonstrated in few of these GPCRs. We discuss below examples of GPCRs (see Fig. 3) which display cholesterol sensitivity in their function.

4.2.1 β_2-Adrenergic Receptor

One of the first high-resolution crystal structures of a GPCR with bound cholesterol molecules was for the β_2-adrenergic receptor, in which three cholesterol molecules were found per receptor monomer (Fig. 3a; [116]). In addition, in a subsequent structure, two cholesterol molecules were identified in a shallow cleft formed by transmembrane helices I–IV of the receptor (Fig. 3b; [117]). Importantly, this structure was instrumental in defining one of the putative cholesterol interaction sites in GPCRs, the cholesterol consensus motif (CCM) (see below). The cholesterol dependence of the stability and function of the β_2-adrenergic receptor has been previously reported [150–153].

4.2.2 Adenosine A_{2A} Receptor

The high-resolution crystal structure of the adenosine A_{2A} receptor showed three bound molecules of cholesterol, all of them located at the extracellular half of the transmembrane helices of the receptor (Fig. 3c; [124]). The three cholesterol molecules were found between transmembrane helices II/III, V/VI, and VI/VII. Interestingly, transmembrane helix VI which is implicated in ligand binding appears to be stabilized by cholesterol [124], and could provide structural basis for the reported cholesterol sensitivity of adenosine A_{2A} receptor function [154].

4.2.3 Opioid Receptors

In case of κ-, μ-, and δ-opioid receptors, cholesterol has been shown to modulate the affinity of ligand binding and signaling [62, 155, 156]. Recent crystal structures of the κ-opioid receptor ([134]; Fig. 3d) and μ-opioid receptor [135, 136]; Fig. 3e) showed cholesterol bound to transmembrane helices of the receptors. Cholesterol was found to interact with the transmembrane helices VI and VII of the μ-opioid receptor.

4.2.4 Metabotropic Glutamate Receptor

Unlike class A GPCRs discussed above in which transmembrane domains constitute predominant sites for ligand binding, the metabotropic glutamate receptor mGluR belongs to class C and has large extracellular domain(s) responsible for

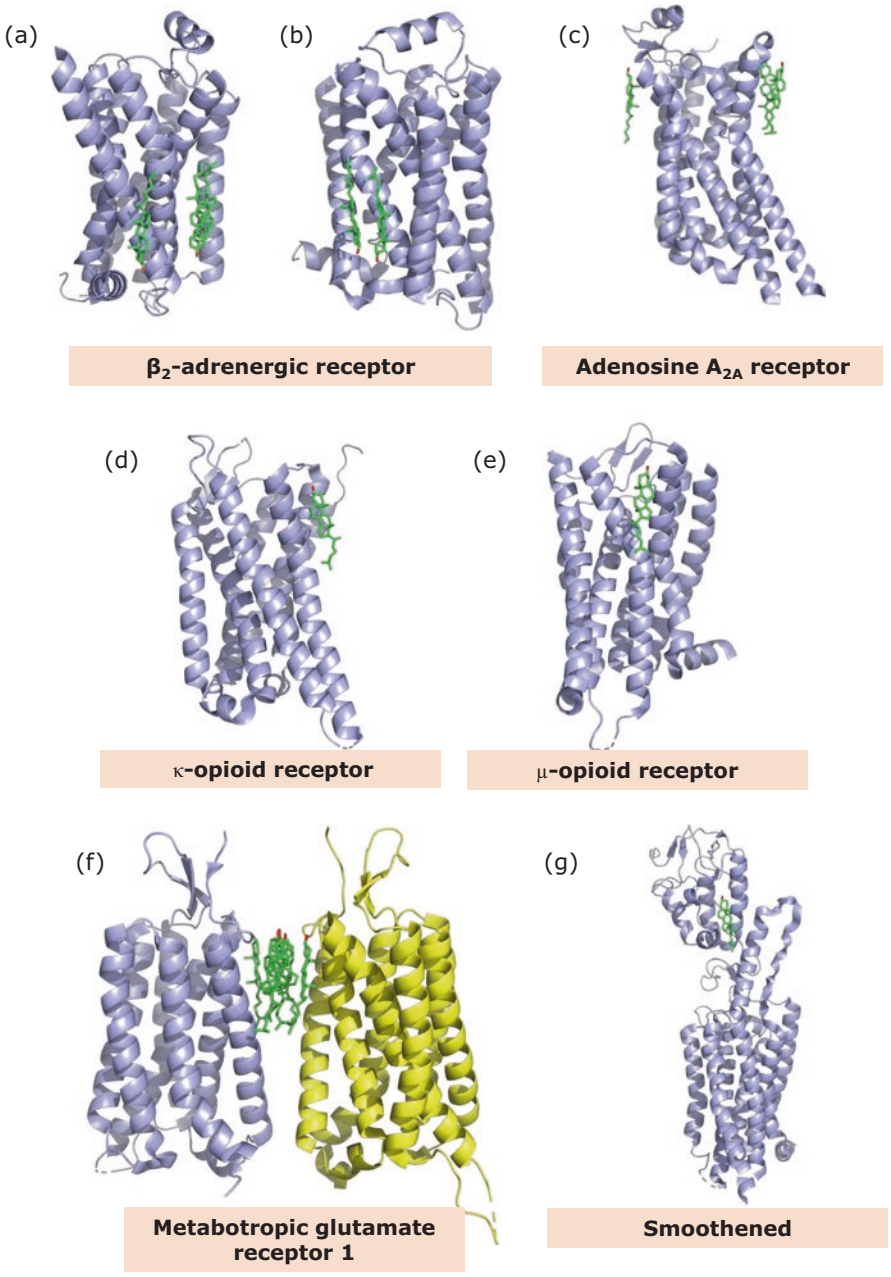

Fig. 3 Crystal structures of representative GPCRs with bound cholesterol molecules. Bound cholesterol molecules have been identified in crystal structures of several GPCRs (the corresponding PDB IDs are indicated in parentheses): (**a**, **b**) β_2-adrenergic receptor (2RH1, 3D4S), (**c**) adenosine A_{2A} receptor (4EIY), (**d**) κ-opioid receptor (6B73), (**e**) μ-opioid receptor (4DKL), (**f**) metabotropic glutamate receptor 1 (4OR2), and (**g**) smoothened (5L7D). Snapshots of cholesterol-bound

ligand binding. It has been earlier shown that membrane cholesterol modulates the ligand binding affinity and signaling of the mGluR [157, 158]. However, it was not clear how membrane cholesterol could modulate ligand binding at the extracellular domain of the receptor. The structural basis of such modulation of receptor function by membrane cholesterol was recently shown in a cholesterol-bound crystal structure of the mGluR [137]. In the receptor structure, six cholesterol molecules were bound symmetrically in the extracellular side of transmembrane helices I and II at the dimer interface (Fig. 3f). These structural evidences could form the basis of the observed role of cholesterol in mGluR function.

4.2.5 Smoothened Receptor

One of the most compelling functional correlates of cholesterol interaction with GPCRs was shown in the recently reported structure of the sterol binding frizzled (class F) GPCR, smoothened (Smo) [138, 139, 159]. Smo is a component of the hedgehog signaling pathway involved in embryonic development and programmed cell death, and the role of cholesterol in this pathway is well documented [160]. Cholesterol acts as the endogenous activator of Smo by inducing conformational changes in the receptor that stimulates the hedgehog pathway. The structure of Smo showed a cholesterol molecule bound to the extracellular cysteine-rich domain of the receptor which is crucial for transduction of hedgehog signals (Fig. 3g). Importantly, the structure helped to predict key residues for this interaction, mutating which impaired hedgehog signaling [159].

We would like to end this section with a cautionary note. Although crystallography is an excellent technique to resolve detailed high-resolution structures of GPCRs, it suffers from some inherent limitations. Despite the fact that the extramembranous regions of GPCRs play crucial roles in receptor function and signaling [161–163], the flexible loops corresponding to these regions are generally stabilized using a monoclonal antibody or replaced with lysozyme [116, 164, 165], since the inherent conformational flexibility of the loops poses a problem for crystallography. In addition, crystallography is often carried out in detergent dispersions or lipidic cubic phases using a heavily engineered (mutated) and antibody-bound receptor. In spite of the popularity of lipidic cubic phase membranes for GPCR crystallization [166], the physiological significance of bound cholesterol molecules in GPCR crystal structures in lipidic cubic phases is not clear [167]. It is possible that the bound cholesterol molecules and the CCM site could be specific to membrane lipid environment (which is different in lipidic cubic phase relative to the lamellar phase). It would therefore be prudent to be careful in extrapolating bound cholesterol in crystal structures of GPCRs to their cholesterol-sensitive function.

Fig. 3 (continued) (cholesterol shown in green with its hydroxyl group in red) structures of GPCRs were generated from their respective PDB structures using PyMOL Molecular Graphics System (version 2.0.6 Schrödinger, LLC). Function of these GPCRs has been shown to be sensitive to membrane cholesterol. See text and Table 1 for more details

4.3 Cholesterol Interaction Motifs

The specific association of cholesterol with GPCRs that could possibly mediate cholesterol-dependent function is proposed to be manifested through conserved sequence motifs on these receptors. We discuss here few putative cholesterol interaction motifs that have been identified in GPCRs.

4.3.1 Cholesterol Recognition/Interaction Amino Acid Consensus (CRAC) Motif

CRAC motif is one of the most well-studied sequence motifs proposed to be implicated in the interaction of proteins with cholesterol. The CRAC motif is characterized by the sequence -L/V-$(X)_{1-5}$-Y-$(X)_{1-5}$-R/K- (from N-terminus to C-terminus of the protein), where $(X)_{1-5}$ represents between one and five residues of any amino acid [24, 168]. Subsequent to the first report on the presence of CRAC motif in the peripheral-type benzodiazepine receptor [169], the motif has been identified in several membrane proteins such as HIV transmembrane protein gp41 [170], caveolin-1 [171], and receptors implicated in pathogen entry [35]. We reported, for the first time, the presence of CRAC motifs in representative GPCRs such as rhodopsin, β_2-adrenergic receptor, and the serotonin$_{1A}$ receptor [172].

We have previously shown that the serotonin$_{1A}$ receptor consists of three CRAC motifs in transmembrane helices II, V, and VII ([172]; see Fig. 4a). Interestingly, coarse-grain molecular dynamics simulations identified high cholesterol occupancy at the CRAC motif in transmembrane helix V of the serotonin$_{1A}$ receptor ([173]; see Fig. 4b). A characteristic feature of these sites is the inherent dynamics exhibited by cholesterol, ranging from ns to μs timescale. The corresponding energy landscape of cholesterol association with GPCRs can be described as a series of shallow minima, interconnected by low energy barriers (see Fig. 4c; [40]). Ongoing work in our laboratory aims to elucidate the role of CRAC motifs in the function of the serotonin$_{1A}$ receptor. In addition, CRAC motifs have been identified and correlated to cholesterol-dependent function of GPCRs such as CB1 [113], CCK1 [115], and bitter taste T2R4 receptors [83]. Importantly, as described earlier (see Sect. 4.1), mutation of key residues in the respective CRAC motifs in these GPCRs led to the modulation of cholesterol sensitivity of their function.

4.3.2 CARC: An Inverted CRAC Motif

The search for cholesterol interaction sites led to the recent identification of CARC, a motif which is similar to CRAC sequence, but with opposite orientation along the polypeptide chain, i.e., -(K/R)-X_{1-5}-(Y/F)-X_{1-5}-(L/V)- [24, 174]. The CARC motif was first identified in the nicotinic acetylcholine receptor and was found to be

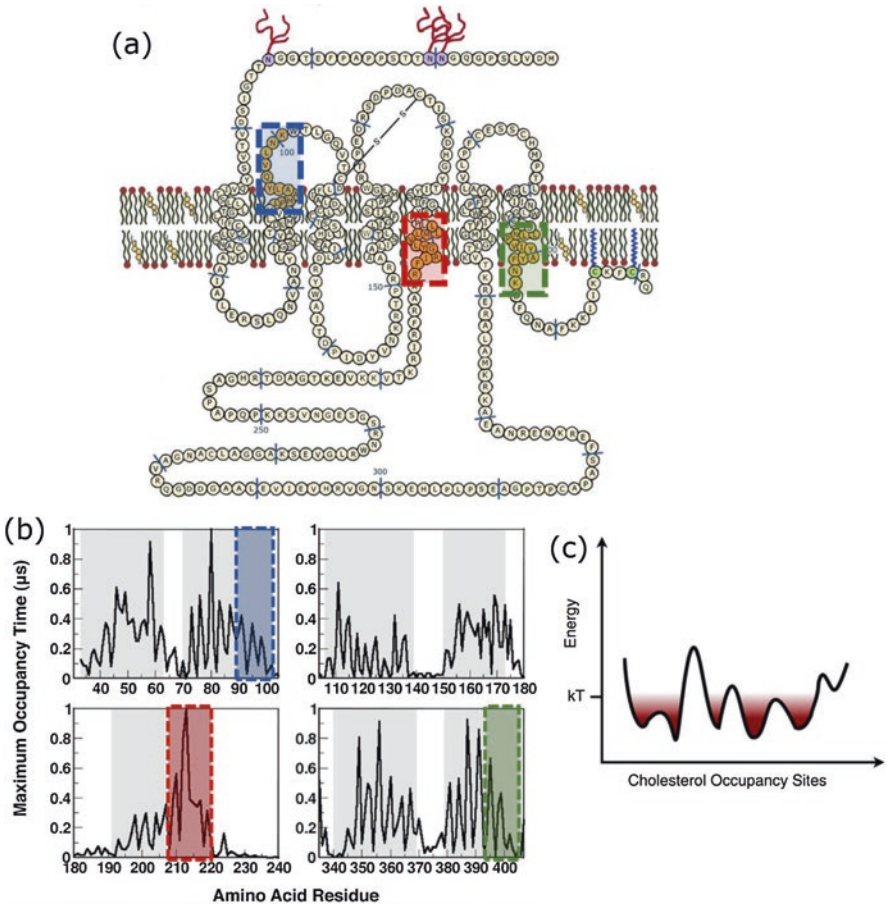

Fig. 4 (**a**) A schematic representation depicting the topological features and amino acid sequence of the human serotonin$_{1A}$ receptor embedded in a membrane bilayer consisting of phospholipids and cholesterol. The serotonin$_{1A}$ receptor consists of three CRAC motifs in transmembrane helices II (boxed in blue), V (boxed in red), and VII (boxed in green). Adapted and modified from [172]. (**b**) Residue-wise maximum occupancy of cholesterol at the serotonin$_{1A}$ receptor, obtained by coarse-grain molecular dynamics simulations. Maximum occupancy time (defined as the longest time a given cholesterol molecule is bound at a particular residue) of cholesterol at each amino acid of the serotonin$_{1A}$ receptor was averaged over simulations carried out at varying concentrations of cholesterol. Transmembrane helices are represented as gray bands, and CRAC motifs are highlighted as in (**a**). The high cholesterol occupancy observed at the CRAC motif on transmembrane helix V is noteworthy. Adapted and modified with permission from [173] (copyright 2018 American Chemical Society). (**c**) Energy landscape corresponding to cholesterol interaction sites in GPCRs. The interaction of cholesterol with GPCRs is weak, yet dynamic with varying occupancy times ranging from ns to μs timescale. This feature of the interaction of cholesterol with GPCRs is reflected in the energy landscape of cholesterol interaction which shows a series of shallow minima interconnected by low energy barriers. Adapted from [40]

conserved over natural evolution among members of this family of receptors [174]. Interestingly, the CARC motif was found in several GPCRs such as rhodopsin, β_2-adrenergic receptor, δ-opioid receptor, galanin receptor type 1, metabotropic glutamate receptor, and chemokine receptor CXCR4 [174]. Some of these receptors display cholesterol sensitivity in their function. The simultaneous presence of the CARC and CRAC motifs in two leaflets of the membrane bilayer in membrane proteins has been proposed as a potential "mirror code" [175].

4.3.3 Cholesterol Consensus Motif (CCM)

CCM was one of the first putative cholesterol interaction sites identified in GPCRs from the crystal structure of the β_2-adrenergic receptor [117]. On the basis of homology, the CCM site has been defined as [4.39-4.43(R,K)]-[4.50(W,Y)]-[4.46(I,V,L)]-[2.41(F,Y)] (according to the Ballesteros–Weinstein nomenclature [176]). We have previously shown high cholesterol occupancy at the CCM site located at the groove of transmembrane helices II and IV of the β_2-adrenergic receptor using coarse-grain molecular dynamics simulations [177]. We have earlier identified a characteristic CCM in the serotonin$_{1A}$ receptor which was found to be evolutionarily conserved [49].

However, it should be noted that mere presence of cholesterol interaction motif(s) does not necessarily translate to cholesterol-dependence of receptor function. For example, the neurotensin receptor 1 does not exhibit cholesterol sensitivity for its function, although the receptor has CCM in its sequence [178].

4.3.4 The Accessibility Issue: Nonannular Binding Sites

In the context of cholesterol binding sites in GPCRs, we previously proposed that these sites could represent "nonannular" binding sites whose possible locations could be inter or intramolecular (interhelical) protein interfaces [49]. Transmembrane proteins are surrounded by a shell (or annulus) of lipid molecules, termed as "annular" lipids [179]. The rate of exchange of lipids between the annular lipid shell and the bulk lipid phase was shown to be approximately an order of magnitude slower than the rate of exchange of bulk lipids [37, 179]. In addition, it was previously proposed that cholesterol binding sites could be "nonannular" in nature [180, 181]. Nonannular sites are characterized by relative lack of accessibility (due to their location in deep clefts or cavities on the protein surface) to the annular lipids [182], and therefore it is proposed that lipids in these sites are difficult to be replaced by competition with annular lipids [181]. Binding to the nonannular sites is considered to be more specific compared to annular sites. Interestingly, a recent study, employing experimental and simulation approaches, has proposed that membrane cholesterol could enter the deep orthosteric ligand binding pocket in the adenosine A_{2A} receptor [183].

5 General Effects of Membrane Cholesterol on GPCRs

The influence of cholesterol on bulk (global) membrane properties has been extensively studied. Cholesterol has been shown to modulate membrane physical properties such as fluidity, curvature, phase, elasticity, dipole potential, and thickness [184–193]. Such effects of cholesterol on general membrane properties have been shown to modulate the organization and function of GPCRs (see Fig. 5; [75, 76, 194–196]).

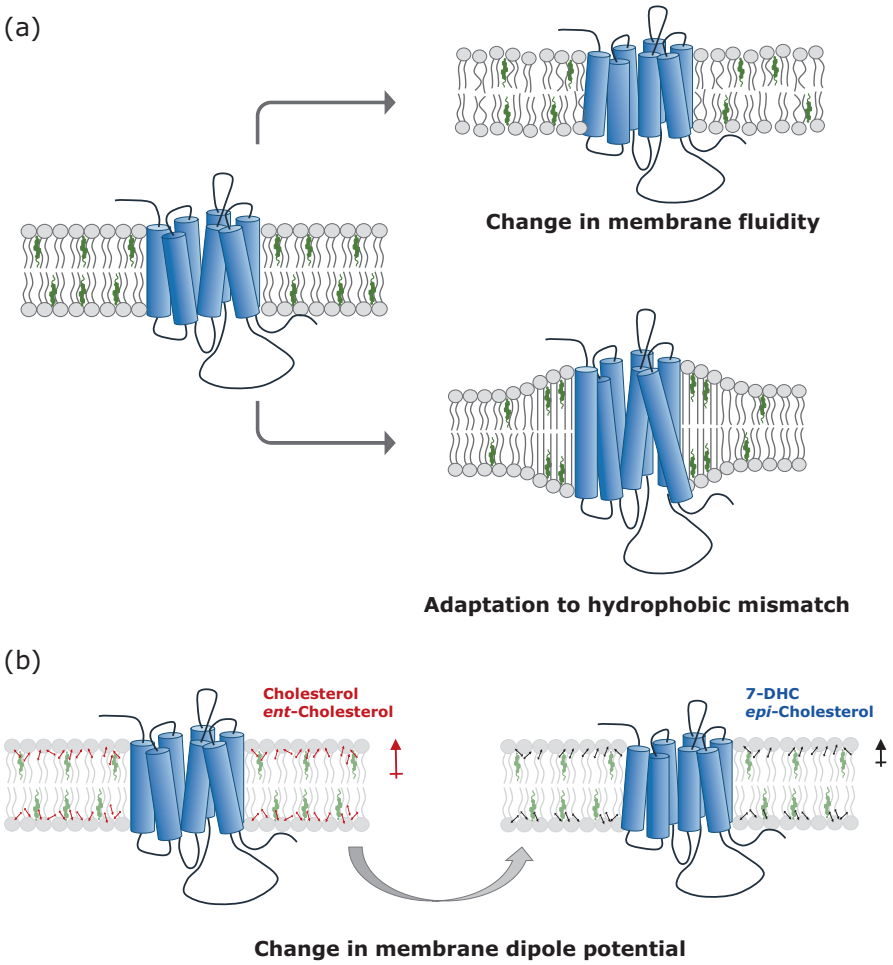

Fig. 5 A schematic representation depicting general effects of cholesterol on membrane physical properties. (**a**) Changes in membrane fluidity and adaptation to hydrophobic mismatch could modulate GPCR function. (**b**) Dipole potential of membranes containing cholesterol and its close structural analogs. Membranes containing cholesterol and *ent*-cholesterol exhibit higher dipole potential (shown as arrows, the length of which represents the magnitude of dipole potential) relative to 7-dehydrocholesterol (7-DHC) and *epi*-cholesterol. Such changes in membrane dipole potential have implications in GPCR function. See text for more details

As discussed above, the specific requirement of cholesterol has been implicated in the function of several GPCRs. The other mechanism by which membrane cholesterol could modulate GPCR function is by affecting general (bulk) membrane properties. What follows below is a brief overview of some of the studies on representative GPCRs where cholesterol-induced modulation of general membrane properties has been implicated in receptor function.

5.1 Rhodopsin

Rhodopsin is a photoreceptor of retinal rod cells and upon exposure to light, undergoes a series of conformational changes. Light-activated rhodopsin exists in equilibrium with a number of intermediates, collectively termed metarhodopsins. Cholesterol is known to regulate the activation of rhodopsin by influencing the equilibrium between the inactive metarhodopsin I (MI) and active metarhodopsin II (MII) states of the receptor [197, 198]. Membrane cholesterol has been shown to stabilize the inactive MI state of the receptor by inducing ordering of membrane lipids, thereby reducing the equilibrium MII (active state) concentration [199]. By increasing the lipid acyl chain ordering, cholesterol reduces the free volume in membrane bilayers [75, 200]. This change in free volume by cholesterol is implied in the observed shift in equilibrium of MI and MII states of rhodopsin [75]. Interestingly, the extent of MII formation displayed a positive correlation with free volume in membranes over a range of cholesterol concentration.

In addition, a variety of mechanisms such as adaptation of rhodopsin to bilayer thickness (in case of hydrophobic mismatch) and membrane curvature have been proposed to regulate MI-MII equilibrium [195]. Interestingly, cholesterol is known to modulate membrane thickness [186] and induce membrane curvature [188]. It is therefore possible that the observed effects of cholesterol on rhodopsin function (MI-MII equilibrium) could be partly due to its effect on membrane thickness (hydrophobic mismatch) and curvature.

5.2 Serotonin$_{1A}$ Receptor

The role of cholesterol in the function of the serotonin$_{1A}$ receptor has been well worked out by our laboratory [3, 37, 40, 42, 201]. Utilizing multiple approaches, we showed that serotonin$_{1A}$ receptors exhibit stringent requirement for cholesterol to support their function, with evidence pointing toward a specific mechanism in many cases (see Sect. 4.1). However, the role of bulk membrane effects of cholesterol on the receptor function cannot be ruled out. With an overall objective of addressing the role of membrane physical properties in receptor function, we monitored the microviscosity of membranes of varying cholesterol content using a fluorescent molecular rotor which allows measurement of membrane viscosity through its

characteristic viscosity-sensitive fluorescence depolarization [196]. A noteworthy feature of our results was that specific agonist binding by the serotonin$_{1A}$ receptor exhibited close correlation with membrane viscosity. This prompted us to speculate that global membrane properties modulated by cholesterol are important in the function of the serotonin$_{1A}$ receptor.

Along similar lines, we measured membrane dipole potential of membranes of varying cholesterol content using an electrochromic fluorescent probe [202]. This provides a convenient method to measure dipole potential, utilizing the probe fluorescence, which is sensitive to the electric field in which the probe is localized [192]. Membrane dipole potential is the potential difference within the membrane bilayer, generated due to the nonrandom arrangement (orientation) of amphiphile dipoles in the membrane interfacial region [203]. Importantly, membrane dipole potential has been shown to play a role in the function of membrane proteins and peptides [204, 205]. In this case too, we noted a correlation between membrane dipole potential and receptor activity [202], reinforcing the above conclusion that global membrane properties could be crucial for the function of the serotonin$_{1A}$ receptor, even if that may not be the whole story.

5.3 Cholecystokinin Receptor

The function of cholecystokinin receptors has been shown to be sensitive to membrane cholesterol content [76]. Interestingly, replacement of membrane cholesterol with sterol analogs that restored membrane fluidity (to levels comparable to membrane fluidity when cholesterol was used) supported the function of the receptor. The specific ligand binding to the receptor exhibited a positive correlation with membrane fluidity, thereby implying the general effect of cholesterol on receptor function.

6 Conclusions

While examples of membrane cholesterol sensitivity of GPCR function have increased over the years, the mechanism underlying such phenomena remains elusive. The notion that cholesterol sensitivity of GPCR function has two underlying mutually exclusive mechanisms appears somewhat arbitrary (although may have provided some early insights). A major reason for this is the fact that it is not always possible to dissect out specific and general effects in a cooperative molecular assembly such as membranes. We would like to illustrate this with recent work done by us [60, 206] and others [207]. In our ongoing work on the role of membrane cholesterol on the function of the serotonin$_{1A}$ receptor, we utilized two stereoisomers of cholesterol, *ent*-cholesterol and *epi*-cholesterol [60]. These are enantiomer and diastereomer of cholesterol, respectively. While *ent*-cholesterol is the non-superimposable

mirror image of natural cholesterol, only the orientation of the hydroxyl group at carbon-3 is inverted relative to natural cholesterol in *epi*-cholesterol. Interestingly, *ent*-cholesterol is often used to distinguish specific interaction of cholesterol from nonspecific effects [208–211]. Typically, enantiomers are characterized by identical physicochemical properties (except for the direction of rotation of plane-polarized light).

We showed that *ent*-cholesterol, but not *epi*-cholesterol, could replace cholesterol in supporting the function of the serotonin$_{1A}$ receptor [60]. In other words, our results demonstrated that the requirement of membrane cholesterol for the serotonin$_{1A}$ receptor function is diastereospecific, but not enantiospecific. A direct implication of these results is that a key structural feature of natural cholesterol in terms of its ability to support the function of the serotonin$_{1A}$ receptor is the *equatorial* configuration of the 3-hydroxyl group. We attributed these results to the fact that *epi*-cholesterol, differing with cholesterol only in the *axial* orientation of the 3-hydroxyl group, was unable to support receptor function. We therefore concluded that the interaction of membrane cholesterol with the serotonin$_{1A}$ receptor is specific in nature [60]. A recent paper reported the detailed physical properties of membranes containing *epi*-cholesterol determined by atomistic molecular dynamics simulations [207]. A closer examination of this paper reveals that physical properties of membranes such as lipid headgroup area, tilt angle, order parameter, and extent of interdigitation are different for membranes containing cholesterol and *epi*-cholesterol. Similar observations were also reported earlier [212]. In addition, we earlier reported that dipole potential of membranes containing cholesterol and *epi*-cholesterol is very different ([206]; see Fig. 5b). Keeping in mind all of the above, whether the difference in receptor function reported by us [60] could be due to these differences in membrane physical properties, or difference in specific interaction due to the orientation of the 3-hydroxyl group, remains a moot question. At this point in time, it is not easy to dissect out a precise answer to this question with available approaches. In addition, specific and general effects of cholesterol may not be mutually exclusive and the observed effect could be a combination of both. Clearly, a judicious combination of experimental and computational approaches would provide more holistic insight into the mechanism of cholesterol sensitivity of GPCR function.

Acknowledgments A.C. gratefully acknowledges support from SERB Distinguished Fellowship (Department of Science and Technology, Govt. of India). G.A.K. and B.D.R. thank the Council of Scientific and Industrial Research and University Grants Commission for the award of Senior Research Fellowships, respectively. A.C. is a Distinguished Visiting Professor at Indian Institute of Technology, Bombay (Mumbai), and Adjunct Professor at Tata Institute of Fundamental Research (Mumbai), RMIT University (Melbourne, Australia), and Indian Institute of Science Education and Research (Kolkata). Some of the work described in this article was carried out by former members of A.C.'s research group whose contributions are gratefully acknowledged. We thank members of the Chattopadhyay laboratory, particularly Parijat Sarkar, for comments and discussions.

References

1. Pierce KL, Premont RT, Lefkowitz RJ. Seven-transmembrane receptors. Nat Rev Mol Cell Biol. 2002;3:639–50.
2. Rosenbaum DM, Rasmussen SGF, Kobilka BK. The structure and function of G-protein-coupled receptors. Nature. 2009;459:356–63.
3. Chattopadhyay A. GPCRs: lipid-dependent membrane receptors that act as drug targets. Adv Biol. 2014;2014:143023.
4. Zhang Y, DeVries ME, Skolnick J. Structure modeling of all identified G protein-coupled receptors in the human genome. PLoS Comput Biol. 2006;2:e13.
5. Gether U. Uncovering molecular mechanisms involved in activation of G protein-coupled receptors. Endocr Rev. 2000;21:90–113.
6. Weis WI, Kobilka BK. The molecular basis of G protein-coupled receptor activation. Annu Rev Biochem. 2018;87:897–919.
7. Heilker R, Wolff M, Tautermann CS, Bieler M. G-protein-coupled receptor-focused drug discovery using a target class platform approach. Drug Discov Today. 2009;14:231–40.
8. Cooke RM, Brown AJH, Marshall FH, Mason JS. Structures of G protein-coupled receptors reveal new opportunities for drug discovery. Drug Discov Today. 2015;20:1355–64.
9. Jacobson KA. New paradigms in GPCR drug discovery. Biochem Pharmacol. 2015;98:541–55.
10. Kumari P, Ghosh E, Shukla AK. Emerging approaches to GPCR ligand screening for drug discovery. Trends Mol Med. 2015;21:687–701.
11. Gutierrez AN, McDonald PH. GPCRs: emerging anti-cancer drug targets. Cell Signal. 2018;41:65–74.
12. Thomsen W, Frazer J, Unett D. Functional assays for screening GPCR targets. Curr Opin Biotechnol. 2005;16:655–65.
13. Schlyer S, Horuk R. I want a new drug: G-protein-coupled receptors in drug development. Drug Discov Today. 2006;11:481–93.
14. Hauser AS, Attwood MM, Rask-Andersen M, Schiöth HB, Gloriam DE. Trends in GPCR drug discovery: new agents, targets and indications. Nat Rev Drug Discov. 2017;16:829–42.
15. Lin SHS, Civelli O. Orphan G protein-coupled receptors: targets for new therapeutic interventions. Ann Med. 2004;36:204–14.
16. Stockert JA, Devi LA. Advancements in therapeutically targeting orphan GPCRs. Front Pharmacol. 2015;6:100.
17. Huber T, Botelho AV, Beyer K, Brown MF. Membrane model for the G-protein-coupled receptor rhodopsin: hydrophobic interface and dynamical structure. Biophys J. 2004;86:2078–100.
18. van Meer G, Voelker DR, Feigenson GW. Membrane lipids: where they are and how they behave. Nat Rev Mol Cell Biol. 2008;9:112–24.
19. van Meer G, de Kroon AIPM. Lipid map of the mammalian cell. J Cell Sci. 2011;124:5–8.
20. Brown AJ, Galea AM. Cholesterol as an evolutionary response to living with oxygen. Evolution. 2010;64:2179–83.
21. Kumar GA, Chattopadhyay A. Cholesterol: an evergreen molecule in biology. Biomed Spectrosc Imaging. 2016;5:S55–66.
22. Chaudhuri A, Chattopadhyay A. Transbilayer organization of membrane cholesterol at low concentrations: implications in health and disease. Biochim Biophys Acta. 2011;1808:19–25.
23. Fantini J, Barrantes FJ. Sphingolipid/cholesterol regulation of neurotransmitter receptor conformation and function. Biochim Biophys Acta. 2009;1788:2345–61.
24. Fantini J, Barrantes FJ. How cholesterol interacts with membrane proteins: an exploration of cholesterol-binding sites including CRAC, CARC, and tilted domains. Front Physiol. 2013;4:31.
25. Simons K, Ikonen E. How cells handle cholesterol. Science. 2000;290:1721–6.
26. Xu X, London E. The effect of sterol structure on membrane lipid domains reveals how cholesterol can induce lipid domain formation. Biochemistry. 2000;39:843–9.

27. Mukherjee S, Maxfield FR. Membrane domains. Annu Rev Cell Dev Biol. 2004;20:839–66.
28. Lingwood D, Simons K. Lipid rafts as a membrane organizing principle. Science. 2010;327:46–50.
29. Simons K, van Meer G. Lipid sorting in epithelial cells. Biochemistry. 1988;27:6197–202.
30. Simons K, Toomre D. Lipid rafts and signal transduction. Nat Rev Mol Cell Biol. 2000;1:31–9.
31. van der Goot FG, Harder T. Raft membrane domains: from a liquid-ordered membrane phase to a site of pathogen attack. Semin Immunol. 2001;13:89–97.
32. Pucadyil TJ, Chattopadhyay A. Cholesterol: a potential therapeutic target in *Leishmania* infection? Trends Parasitol. 2007;23:49–53.
33. Vieira FS, Corrêa G, Einicker-Lamas M, Coutinho-Silva R. Host-cell lipid rafts: a safe door for micro-organisms? Biol Cell. 2010;102:391–407.
34. Chattopadhyay A, Jafurulla M. Role of membrane cholesterol in leishmanial infection. Adv Exp Med Biol. 2012;749:201–13.
35. Kumar GA, Jafurulla M, Chattopadhyay A. The membrane as the gatekeeper of infection: cholesterol in host-pathogen interaction. Chem Phys Lipids. 2016;199:179–85.
36. Pucadyil TJ, Chattopadhyay A. Role of cholesterol in the function and organization of G-protein coupled receptors. Prog Lipid Res. 2006;45:295–333.
37. Paila YD, Chattopadhyay A. Membrane cholesterol in the function and organization of G-protein coupled receptors. Subcell Biochem. 2010;51:439–66.
38. Oates J, Watts A. Uncovering the intimate relationship between lipids, cholesterol and GPCR activation. Curr Opin Struct Biol. 2011;21:802–7.
39. Jafurulla M, Chattopadhyay A. Membrane lipids in the function of serotonin and adrenergic receptors. Curr Med Chem. 2013;20:47–55.
40. Sengupta D, Chattopadhyay A. Molecular dynamics simulations of GPCR-cholesterol interaction: an emerging paradigm. Biochim Biophys Acta. 2015;1848:1775–82.
41. Gimpl G. Interaction of G protein coupled receptors and cholesterol. Chem Phys Lipids. 2016;199:61–73.
42. Sengupta D, Prasanna X, Mohole M, Chattopadhyay A. Exploring GPCR-lipid interactions by molecular dynamics simulations: excitements, challenges and the way forward. J Phys Chem B. 2018;122:5727–37.
43. Paila YD, Murty MRVS, Vairamani M, Chattopadhyay A. Signaling by the human serotonin$_{1A}$ receptor is impaired in cellular model of Smith–Lemli–Opitz syndrome. Biochim Biophys Acta. 2008;1778:1508–16.
44. Dietschy JM, Turley SD. Cholesterol metabolism in the brain. Curr Opin Lipidol. 2001;12:105–12.
45. Chattopadhyay A, Paila YD. Lipid-protein interactions, regulation and dysfunction of brain cholesterol. Biochem Biophys Res Commun. 2007;354:627–33.
46. Martin M, Dotti CG, Ledesma MD. Brain cholesterol in normal and pathological aging. Biochim Biophys Acta. 2010;1801:934–44.
47. Karnell FG, Brezski RJ, King LG, Silverman MA, Monroe JG. Membrane cholesterol content accounts for developmental differences in surface B cell receptor compartmentalization and signaling. J Biol Chem. 2005;280:25621–8.
48. Paila YD, Chattopadhyay A. The function of G-protein coupled receptors and membrane cholesterol: specific or general interaction? Glycoconj J. 2009;26:711–20.
49. Paila YD, Tiwari S, Chattopadhyay A. Are specific nonannular cholesterol binding sites present in G-protein coupled receptors? Biochim Biophys Acta. 2009;1788:295–302.
50. Seddon AM, Curnow P, Booth PJ. Membrane proteins, lipids and detergents: not just a soap opera. Biochim Biophys Acta. 2004;1666:105–17.
51. Kalipatnapu S, Chattopadhyay A. Membrane protein solubilization: recent advances and challenges in solubilization of serotonin$_{1A}$ receptors. IUBMB Life. 2005;57:505–12.
52. Privé GG. Detergents for the stabilization and crystallization of membrane proteins. Methods. 2007;41:388–97.
53. Duquesne K, Sturgis JN. Membrane protein solubilization. Methods Mol Biol. 2010;601:205–17.

54. Chattopadhyay A, Rao BD, Jafurulla M. Solubilization of G protein-coupled receptors: a convenient strategy to explore lipid-receptor interaction. Methods Enzymol. 2015;557:117–34.
55. Goddard AD, Dijkman PM, Adamson RJ, dos Reis RI, Watts A. Reconstitution of membrane proteins: a GPCR as an example. Methods Enzymol. 2015;556:405–24.
56. Serebryany E, Zhu GA, Yan ECY. Artificial membrane-like environments for *in vitro* studies of purified G-protein coupled receptors. Biochim Biophys Acta. 2012;1818:225–33.
57. Chattopadhyay A, Jafurulla M, Kalipatnapu S, Pucadyil TJ, Harikumar KG. Role of cholesterol in ligand binding and G-protein coupling of serotonin$_{1A}$ receptors solubilized from bovine hippocampus. Biochem Biophys Res Commun. 2005;327:1036–41.
58. Chattopadhyay A, Paila YD, Jafurulla M, Chaudhuri A, Singh P, Murty MRVS, et al. Differential effects of cholesterol and 7-dehydrocholesterol on ligand binding of solubilized hippocampal serotonin$_{1A}$ receptors: implications in SLOS. Biochem Biophys Res Commun. 2007;363:800–5.
59. Singh P, Jafurulla M, Paila YD, Chattopadhyay A. Desmosterol replaces cholesterol for ligand binding function of the serotonin$_{1A}$ receptor in solubilized hippocampal membranes: support for nonannular binding sites for cholesterol? Biochim Biophys Acta. 2011;1808:2428–34.
60. Jafurulla M, Rao BD, Sreedevi S, Ruysschaert J-M, Covey DF, Chattopadhyay A. Stereospecific requirement of cholesterol in the function of the serotonin$_{1A}$ receptor. Biochim Biophys Acta. 2014;1838:158–63.
61. Nes WD. Biosynthesis of cholesterol and other sterols. Chem Rev. 2011;111:6423–51.
62. Levitt ES, Clark MJ, Jenkins PM, Martens JR, Traynor JR. Differential effect of membrane cholesterol removal on μ- and δ-opioid receptors: a parallel comparison of acute and chronic signaling to adenylyl cyclase. J Biol Chem. 2009;284:22108–22.
63. Shrivastava S, Pucadyil TJ, Paila YD, Ganguly S, Chattopadhyay A. Chronic cholesterol depletion using statin impairs the function and dynamics of human serotonin$_{1A}$ receptors. Biochemistry. 2010;49:5426–35.
64. Istvan ES, Deisenhofer J. Structural mechanism for statin inhibition of HMG-CoA reductase. Science. 2001;292:1160–4.
65. Mizuno GR, Chapman CJ, Chipault JR, Pfeiffer DR. Lipid composition and (Na^++K^+)-ATPase activity in rat lens during triparanol-induced cataract formation. Biochim Biophys Acta. 1981;644:1–12.
66. Kolf-Clauw M, Chevy F, Wolf C, Siliart B, Citadelle D, Roux C. Inhibition of 7-dehydrocholesterol reductase by the teratogen AY9944: a rat model for Smith-Lemli-Opitz syndrome. Teratology. 1996;54:115–25.
67. Kandutsch AA, Russell AE. Preputial gland tumor sterols. A metabolic pathway from lanosterol to cholesterol. J Biol Chem. 1960;235:2256–61.
68. Bloch KE. Sterol structure and membrane function. CRC Crit Rev Biochem. 1983;14:47–92.
69. Porter FD, Herman GE. Malformation syndromes caused by disorders of cholesterol synthesis. J Lipid Res. 2011;52:6–34.
70. Kanungo S, Soares N, He M, Steiner RD. Sterol metabolism disorders and neurodevelopment-an update. Dev Disabil Res Rev. 2013;17:197–210.
71. Gaoua W, Wolf C, Chevy F, Ilien F, Roux C. Cholesterol deficit but not accumulation of aberrant sterols is the major cause of the teratogenic activity in the Smith-Lemli-Opitz syndrome animal model. J Lipid Res. 2000;41:637–46.
72. Chevy F, Illien F, Wolf C, Roux C. Limb malformations of rat fetuses exposed to a distal inhibitor of cholesterol biosynthesis. J Lipid Res. 2002;43:1192–200.
73. Zidovetzki R, Levitan I. Use of cyclodextrins to manipulate plasma membrane cholesterol content: evidence, misconceptions and control strategies. Biochim Biophys Acta. 2007;1768:1311–24.
74. López CA, de Vries AH, Marrink SJ. Computational microscopy of cyclodextrin mediated cholesterol extraction from lipid model membranes. Sci Rep. 2013;3:2071.
75. Niu S-L, Mitchell DC, Litman BJ. Manipulation of cholesterol levels in rod disk membranes by methyl-β-cyclodextrin: effects on receptor activation. J Biol Chem. 2002;277:20139–45.

76. Gimpl G, Burger K, Fahrenholz F. Cholesterol as modulator of receptor function. Biochemistry. 1997;36:10959–74.
77. Pang L, Graziano M, Wang S. Membrane cholesterol modulates galanin-GalR2 interaction. Biochemistry. 1999;38:12003–11.
78. Pucadyil TJ, Chattopadhyay A. Cholesterol modulates ligand binding and G-protein coupling to serotonin$_{1A}$ receptors from bovine hippocampus. Biochim Biophys Acta. 2004;1663:188–200.
79. Pucadyil TJ, Chattopadhyay A. Cholesterol depletion induces dynamic confinement of the G-protein coupled serotonin$_{1A}$ receptor in the plasma membrane of living cells. Biochim Biophys Acta. 2007;1768:655–68.
80. Bari M, Battista N, Fezza F, Finazzi-Agrò A, Maccarrone M. Lipid rafts control signaling of type-1 cannabinoid receptors in neuronal cells. Implications for anandamide-induced apoptosis. J Biol Chem. 2005;280:12212–20.
81. Bari M, Paradisi A, Pasquariello N, Maccarrone M. Cholesterol-dependent modulation of type 1 cannabinoid receptors in nerve cells. J Neurosci Res. 2005;81:275–83.
82. Bari M, Spagnuolo P, Fezza F, Oddi S, Pasquariello N, Finazzi-Agrò A, et al. Effect of lipid rafts on Cb2 receptor signaling and 2-arachidonoyl-glycerol metabolism in human immune cells. J Immunol. 2006;177:4971–80.
83. Pydi SP, Jafurulla M, Wai L, Bhullar RP, Chelikani P, Chattopadhyay A. Cholesterol modulates bitter taste receptor function. Biochim Biophys Acta. 2016;1858:2081–7.
84. Chattopadhyay A, Jafurulla M, Pucadyil TJ. Ligand binding and G-protein coupling of the serotonin$_{1A}$ receptor in cholesterol-enriched hippocampal membranes. Biosci Rep. 2006;26:79–87.
85. Sarkar P, Chakraborty H, Chattopadhyay A. Differential membrane dipolar orientation induced by acute and chronic cholesterol depletion. Sci Rep. 2017;7:4484.
86. Sampson NS, Vrielink A. Cholesterol oxidases: a study of nature's approach to protein design. Acc Chem Res. 2003;36:713–22.
87. Pucadyil TJ, Shrivastava S, Chattopadhyay A. Membrane cholesterol oxidation inhibits ligand binding function of hippocampal serotonin$_{1A}$ receptors. Biochem Biophys Res Commun. 2005;331:422–7.
88. Jafurulla M, Nalli A, Chattopadhyay A. Membrane cholesterol oxidation in live cells enhances the function of serotonin$_{1A}$ receptors. Chem Phys Lipids. 2017;203:71–7.
89. Boesze-Battaglia K, Albert AD. Cholesterol modulation of photoreceptor function in bovine retinal rod outer segments. J Biol Chem. 1990;265:20727–30.
90. Nguyen DH, Taub D. Inhibition of chemokine receptor function by membrane cholesterol oxidation. Exp Cell Res. 2003;291:36–45.
91. Holz RW. The effects of the polyene antibiotics nystatin and amphotericin B on thin lipid membranes. Ann N Y Acad Sci. 1974;235:469–79.
92. Nishikawa M, Nojima S, Akiyama T, Sankawa U, Inoue K. Interaction of digitonin and its analogs with membrane cholesterol. J Biochem. 1984;96:1231–9.
93. Bolard J. How do the polyene macrolide antibiotics affect the cellular membrane properties? Biochim Biophys Acta. 1986;864:257–304.
94. Coutinho A, Prieto M. Cooperative partition model of nystatin interaction with phospholipid vesicles. Biophys J. 2003;84:3061–78.
95. Savinov SN, Heuck AP. Interaction of cholesterol with perfringolysin O: what have we learned from functional analysis? Toxins. 2017;9:381.
96. Pucadyil TJ, Shrivastava S, Chattopadhyay A. The sterol-binding antibiotic nystatin differentially modulates ligand binding of the bovine hippocampal serotonin$_{1A}$ receptor. Biochem Biophys Res Commun. 2004;320:557–62.
97. Paila YD, Pucadyil TJ, Chattopadhyay A. The cholesterol-complexing agent digitonin modulates ligand binding of the bovine hippocampal serotonin$_{1A}$ receptor. Mol Membr Biol. 2005;22:241–9.
98. Pucadyil TJ, Kalipatnapu S, Chattopadhyay A. The serotonin$_{1A}$ receptor: a representative member of the serotonin receptor family. Cell Mol Neurobiol. 2005;25:553–80.

99. Kalipatnapu S, Chattopadhyay A. Membrane organization and function of the serotonin$_{1A}$ receptor. Cell Mol Neurobiol. 2007;27:1097–116.
100. Müller CP, Carey RJ, Huston JP, De Souza Silva MA. Serotonin and psychostimulant addiction: focus on 5-HT$_{1A}$-receptors. Prog Neurobiol. 2007;81:133–78.
101. Lacivita E, Leopoldo M, Berardi F, Perrone R. 5-HT$_{1A}$ receptor, an old target for new therapeutic agents. Curr Top Med Chem. 2008;8:1024–34.
102. Fiorino F, Severino B, Magli E, Ciano A, Caliendo G, Santagada V, et al. 5-HT$_{1A}$ receptor: an old target as a new attractive tool in drug discovery from central nervous system to cancer. J Med Chem. 2014;57:4407–26.
103. Singh P, Paila YD, Chattopadhyay A. Differential effects of cholesterol and 7-dehydrocholesterol on the ligand binding activity of the hippocampal serotonin$_{1A}$ receptor: implications in SLOS. Biochem Biophys Res Commun. 2007;358:495–9.
104. Saxena R, Chattopadhyay A. Membrane cholesterol stabilizes the human serotonin$_{1A}$ receptor. Biochim Biophys Acta. 2012;1818:2936–42.
105. Paila YD, Tiwari S, Sengupta D, Chattopadhyay A. Molecular modeling of the human serotonin$_{1A}$ receptor: role of membrane cholesterol in ligand binding of the receptor. Mol BioSyst. 2011;7:224–34.
106. Patra SM, Chakraborty S, Shahane G, Prasanna X, Sengupta D, Maiti PK, et al. Differential dynamics of the serotonin$_{1A}$ receptor in membrane bilayers of varying cholesterol content revealed by all atom molecular dynamics simulation. Mol Membr Biol. 2015;32:127–37.
107. Burger K, Gimpl G, Fahrenholz F. Regulation of receptor function by cholesterol. Cell Mol Life Sci. 2000;57:1577–92.
108. Klein U, Gimpl G, Fahrenholz F. Alteration of the myometrial plasma membrane cholesterol content with β-cyclodextrin modulates the binding affinity of the oxytocin receptor. Biochemistry. 1995;34:13784–93.
109. Gimpl G, Fahrenholz F. Cholesterol as stabilizer of the oxytocin receptor. Biochim Biophys Acta. 2002;1564:384–92.
110. Nguyen DH, Taub D. Cholesterol is essential for macrophage inflammatory protein 1 beta binding and conformational integrity of CC chemokine receptor 5. Blood. 2002;99:4298–306.
111. Nguyen DH, Taub D. CXCR4 function requires membrane cholesterol: implications for HIV infection. J Immunol. 2002;168:4121–6.
112. Behrens M, Meyerhof W. Bitter taste receptors and human bitter taste perception. Cell Mol Life Sci. 2006;63:1501–9.
113. Oddi S, Dainese E, Fezza F, Lanuti M, Barcaroli D, De Laurenzi V, et al. Functional characterization of putative cholesterol binding sequence (CRAC) in human type-1 cannabinoid receptor. J Neurochem. 2011;116:858–65.
114. Harikumar KG, Puri V, Singh RD, Hanada K, Pagano RE, Miller LJ. Differential effects of modification of membrane cholesterol and sphingolipids on the conformation, function, and trafficking of the G protein-coupled cholecystokinin receptor. J Biol Chem. 2005;280:2176–85.
115. Potter RM, Harikumar KG, Wu SV, Miller LJ. Differential sensitivity of types 1 and 2 cholecystokinin receptors to membrane cholesterol. J Lipid Res. 2012;53:137–48.
116. Cherezov V, Rosenbaum DM, Hanson MA, Rasmussen SGF, Thian FS, Kobilka TS, et al. High-resolution crystal structure of an engineered human β_2-adrenergic G protein-coupled receptor. Science. 2007;318:1258–65.
117. Hanson MA, Cherezov V, Griffith MT, Roth CB, Jaakola V-P, Chein YET, et al. A specific cholesterol binding site is established by the 2.8 Å structure of the human β_2-adrenergic receptor. Structure. 2008;16:897–905.
118. Wacker D, Fenalti G, Brown MA, Katritch V, Abagyan R, Cherezov V, et al. Conserved binding mode of human β_2 adrenergic receptor inverse agonists and antagonist revealed by X-ray crystallography. J Am Chem Soc. 2010;132:11443–5.
119. Rosenbaum DM, Zhang C, Lyons JA, Holl R, Aragao D, Arlow DH, et al. Structure and function of an irreversible agonist-β_2 adrenoceptor complex. Nature. 2011;469:236–40.

120. Staus DP, Strachan RT, Manglik A, Pani B, Kahsai AW, Kim TH, et al. Allosteric nanobodies reveal the dynamic range and diverse mechanisms of G-protein-coupled receptor activation. Nature. 2016;535:448–52.
121. Huang C-Y, Olieric V, Ma P, Howe N, Vogeley L, Liu X, et al. *In meso in situ* serial X-ray crystallography of soluble and membrane proteins at cryogenic temperatures. Acta Crystallogr D Struct Biol. 2016;72:93–112.
122. Liu X, Ahn S, Kahsai AW, Meng K-C, Latorraca NR, Pani B, et al. Mechanism of intracellular allosteric β_2AR antagonist revealed by X-ray crystal structure. Nature. 2017;548:480–4.
123. Ma P, Weichert D, Aleksandrov LA, Jensen TJ, Riordan JR, Liu X, et al. The cubicon method for concentrating membrane proteins in the cubic mesophase. Nat Protoc. 2017;12:1745–62.
124. Liu W, Chun E, Thompson AA, Chubukov P, Xu F, Katritch V, et al. Structural basis for allosteric regulation of GPCRs by sodium ions. Science. 2012;337:232–6.
125. Batyuk A, Galli L, Ishchenko A, Han GW, Gati C, Popov PA, et al. Native phasing of x-ray free-electron laser data for a G protein-coupled receptor. Sci Adv. 2016;2:e1600292.
126. Segala E, Guo D, Cheng RKY, Bortolato A, Deflorian F, Doré AS, et al. Controlling the dissociation of ligands from the adenosine A_{2A} receptor through modulation of salt bridge strength. J Med Chem. 2016;59:6470–9.
127. Martin-Garcia JM, Conrad CE, Nelson G, Stander N, Zatsepin NA, Zook J, et al. Serial millisecond crystallography of membrane and soluble protein microcrystals using synchrotron radiation. IUCrJ. 2017;4:439–54.
128. Weinert T, Olieric N, Cheng R, Brünle S, James D, Ozerov D, et al. Serial millisecond crystallography for routine room-temperature structure determination at synchrotrons. Nat Commun. 2017;8:542.
129. Cheng RKY, Segala E, Robertson N, Deflorian F, Doré AS, Errey JC, et al. Structures of human A_1 and A_{2A} adenosine receptors with xanthines reveal determinants of selectivity. Structure. 2017;25:1275–85.
130. Melnikov I, Polovinkin V, Kovalev K, Gushchin I, Shevtsov M, Shevchenko V, et al. Fast iodide-SAD phasing for high-throughput membrane protein structure determination. Sci Adv. 2017;3:e1602952.
131. Broecker J, Morizumi T, Ou W-L, Klingel V, Kuo A, Kissick DJ, et al. High-throughput *in situ* X-ray screening of and data collection from protein crystals at room temperature and under cryogenic conditions. Nat Protoc. 2018;13:260–92.
132. Eddy MT, Lee M-Y, Gao Z-G, White KL, Didenko T, Horst R, et al. Allosteric coupling of drug binding and intracellular signaling in the A_{2A} adenosine receptor. Cell. 2018;172:68–80.
133. Rucktooa P, Cheng RKY, Segala E, Geng T, Errey JC, Brown GA, et al. Towards high throughput GPCR crystallography: *in meso* soaking of adenosine A_{2A} receptor crystals. Sci Rep. 2018;8:41.
134. Che T, Majumdar S, Zaidi SA, Ondachi P, McCorvy JD, Wang S, et al. Structure of the nanobody-stabilized active state of the kappa opioid receptor. Cell. 2018;172:55–67.
135. Manglik A, Kruse AC, Kobilka TS, Thian FS, Mathiesen JM, Sunahara RK, et al. Crystal structure of the μ-opioid receptor bound to a morphinan antagonist. Nature. 2012;485:321–6.
136. Huang W, Manglik A, Venkatakrishnan AJ, Laeremans T, Feinberg EN, Sanborn AL, et al. Structural insights into μ-opioid receptor activation. Nature. 2015;524:315–21.
137. Wu H, Wang C, Gregory KJ, Han GW, Cho HP, Xia Y, et al. Structure of a class C GPCR metabotropic glutamate receptor 1 bound to an allosteric modulator. Science. 2014;344:58–64.
138. Byrne EFX, Sircar R, Miller PS, Hedger G, Luchetti G, Nachtergaele S, et al. Structural basis of smoothened regulation by its extracellular domains. Nature. 2016;535:517–22.
139. Huang P, Zheng S, Wierbowski BM, Kim Y, Nedelcu D, Aravena L, et al. Structural basis of smoothened activation in hedgehog signaling. Cell. 2018;174:1–13.
140. Wacker D, Wang C, Katritch V, Han GW, Huang X-P, Vardy E, et al. Structural features for functional selectivity at serotonin receptors. Science. 2013;340:615–9.
141. Liu W, Wacker D, Gati C, Han GW, James D, Wang D, et al. Serial femtosecond crystallography of G protein-coupled receptors. Science. 2013;342:1521–4.

142. Wacker D, Wang S, McCorvy JD, Betz RM, Venkatakrishnan AJ, Levit A, et al. Crystal structure of an LSD-bound human serotonin receptor. Cell. 2017;168:377–89.
143. Hua T, Vemuri K, Nikas SP, Laprairie RB, Wu Y, Qu L, et al. Crystal structures of agonist-bound human cannabinoid receptor CB_1. Nature. 2017;547:468–71.
144. Oswald C, Rappas M, Kean J, Doré AS, Errey JC, Bennett K, et al. Intracellular allosteric antagonism of the CCR9 receptor. Nature. 2016;540:462–5.
145. Shihoya W, Nishizawa T, Yamashita K, Inoue A, Hirata K, Kadji FMN, et al. X-ray structures of endothelin ET_B receptor bound to clinical antagonist bosentan and its analog. Nat Struct Mol Biol. 2017;24:758–64.
146. Burg JS, Ingram JR, Venkatakrishnan AJ, Jude KM, Dukkipati A, Feinberg EN, et al. Structural basis for chemokine recognition and activation of a viral G protein-coupled receptor. Science. 2015;347:1113–7.
147. Zhang D, Gao Z-G, Zhang K, Kiselev E, Crane S, Wang J, et al. Two disparate ligand-binding sites in the human $P2Y_1$ receptor. Nature. 2015;520:317–21.
148. Zhang J, Zhang K, Gao Z-G, Paoletta S, Zhang D, Han GW, et al. Agonist-bound structure of the human $P2Y_{12}$ receptor. Nature. 2014;509:119–22.
149. Zhang K, Zhang J, Gao Z-G, Zhang D, Zhu L, Han GW, et al. Structure of the human $P2Y_{12}$ receptor in complex with an antithrombotic drug. Nature. 2014;509:115–8.
150. Yao Z, Kobilka B. Using synthetic lipids to stabilize purified *β*2 adrenoceptor in detergent micelles. Anal Biochem. 2005;343:344–6.
151. Pontier SM, Percherancier Y, Galandrin S, Breit A, Galés C, Bouvier M. Cholesterol-dependent separation of the β2-adrenergic receptor from its partners determines signaling efficacy: insight into nanoscale organization of signal transduction. J Biol Chem. 2008;283:24659–72.
152. Paila YD, Jindal E, Goswami SK, Chattopadhyay A. Cholesterol depletion enhances adrenergic signaling in cardiac myocytes. Biochim Biophys Acta. 2011;1808:461–5.
153. Zocher M, Zhang C, Rasmussen SGF, Kobilka BK, Müller DJ. Cholesterol increases kinetic, energetic, and mechanical stability of the human β2-adrenergic receptor. Proc Natl Acad Sci U S A. 2012;109:E3463–72.
154. Lam RS, Nahirney D, Duszyk M. Cholesterol-dependent regulation of adenosine A_{2A} receptor-mediated anion secretion in colon epithelial cells. Exp Cell Res. 2009;315:3028–35.
155. Xu W, Yoon S-I, Huang P, Wang Y, Chen C, Chong PL-G, et al. Localization of the κ opioid receptor in lipid rafts. J Pharmacol Exp Ther. 2006;317:1295–306.
156. Huang P, Xu W, Yoon S-I, Chen C, Chong PL-G, Liu-Chen LY. Cholesterol reduction by methyl-β-cyclodextrin attenuates the delta opioid receptor-mediated signaling in neuronal cells but enhances it in non-neuronal cells. Biochem Pharmacol. 2007;73:534–49.
157. Eroglu C, Brügger B, Wieland F, Sinning I. Glutamate-binding affinity of *Drosophila* metabotropic glutamate receptor is modulated by association with lipid rafts. Proc Natl Acad Sci U S A. 2003;100:10219–24.
158. Kumari R, Castillo C, Francesconi A. Agonist-dependent signaling by group I metabotropic glutamate receptors is regulated by association with lipid domains. J Biol Chem. 2013;288:32004–19.
159. Huang P, Nedelcu D, Watanabe M, Jao C, Kim Y, Liu J, et al. Cellular cholesterol directly activates smoothened in hedgehog signaling. Cell. 2016;166:1176–87.
160. Porter JA, Young KE, Beachy PA. Cholesterol modification of hedgehog signaling proteins in animal development. Science. 1996;274:255–9.
161. Turner JH, Gelasco AK, Raymond JR. Calmodulin interacts with the third intracellular loop of the serotonin 5-hydroxytryptamine$_{1A}$ receptor at two distinct sites. Putative role in receptor phosphorylation by protein kinase C. J Biol Chem. 2004;279:17027–37.
162. Wheatley M, Wootten D, Conner MT, Simms J, Kendrick R, Logan RT, et al. Lifting the lid on GPCRs: the role of extracellular loops. Br J Pharmacol. 2012;165:1688–703.
163. Pal S, Aute R, Sarkar P, Bose S, Deshmukh MV, Chattopadhyay A. Constrained dynamics of the sole tryptophan in the third intracellular loop of the serotonin$_{1A}$ receptor. Biophys Chem. 2018;240:34–41.

164. Day PW, Rasmussen SGF, Parnot C, Fung JJ, Masood A, Kobilka TS, et al. A monoclonal antibody for G protein-coupled receptor crystallography. Nat Methods. 2007;4:927–9.
165. Rosenbaum DM, Cherezov V, Hanson MA, Rasmussen SGF, Thian FS, Kobilka TS, et al. GPCR engineering yields high-resolution structural insights into β_2-adrenergic receptor function. Science. 2007;318:1266–73.
166. Caffrey M. A comprehensive review of the lipid cubic phase or *in meso* method for crystallizing membrane and soluble proteins and complexes. Acta Crystallogr F Struct Biol Commun. 2015;71:3–18.
167. Khelashvili G, Albornoz PBC, Johner N, Mondal S, Caffrey M, Weinstein H. Why GPCRs behave differently in cubic and lamellar lipidic mesophases. J Am Chem Soc. 2012;134:15858–68.
168. Epand RM. Cholesterol and the interaction of proteins with membrane domains. Prog Lipid Res. 2006;45:279–94.
169. Li H, Papadopoulos V. Peripheral-type benzodiazepine receptor function in cholesterol transport. Identification of a putative cholesterol recognition/interaction amino acid sequence and consensus pattern. Endocrinology. 1998;139:4991–7.
170. Vincent N, Genin C, Malvoisin E. Identification of a conserved domain of the HIV-1 transmembrane protein gp41 which interacts with cholesteryl groups. Biochim Biophys Acta. 2002;1567:157–64.
171. Epand RM, Sayer BG, Epand RF. Caveolin scaffolding region and cholesterol-rich domains in membranes. J Mol Biol. 2005;345:339–50.
172. Jafurulla M, Tiwari S, Chattopadhyay A. Identification of cholesterol recognition amino acid consensus (CRAC) motif in G-protein coupled receptors. Biochem Biophys Res Commun. 2011;404:569–73.
173. Sengupta D, Chattopadhyay A. Identification of cholesterol binding sites in the serotonin$_{1A}$ receptor. J Phys Chem B. 2012;116:12991–6.
174. Baier CJ, Fantini J, Barrantes FJ. Disclosure of cholesterol recognition motifs in transmembrane domains of the human nicotinic acetylcholine receptor. Sci Rep. 2011;1:69.
175. Fantini J, Di Scala C, Evans LS, Williamson PTF, Barrantes FJ. A mirror code for protein-cholesterol interactions in the two leaflets of biological membranes. Sci Rep. 2016;6:21907.
176. Ballesteros JA, Weinstein H. Integrated methods for the construction of three-dimensional models and computational probing of structure-function relations in G protein-coupled receptors. Methods Neurosci. 1995;25:366–428.
177. Prasanna X, Chattopadhyay A, Sengupta D. Cholesterol modulates the dimer interface of the β_2-adrenergic receptor via cholesterol occupancy sites. Biophys J. 2014;106:1290–300.
178. Oates J, Faust B, Attrill H, Harding P, Orwick M, Watts A. The role of cholesterol on the activity and stability of neurotensin receptor 1. Biochim Biophys Acta. 2012;1818:2228–33.
179. Lee AG. Lipid-protein interactions in biological membranes: a structural perspective. Biochim Biophys Acta. 2003;1612:1–40.
180. Simmonds AC, East JM, Jones OT, Rooney EK, McWhirter J, Lee AG. Annular and nonannular binding sites on the ($Ca^{2+} + Mg^{2+}$)-ATPase. Biochim Biophys Acta. 1982;693:398–406.
181. Jones OT, McNamee MG. Annular and nonannular binding sites for cholesterol associated with the nicotinic acetylcholine receptor. Biochemistry. 1988;27:2364–74.
182. Marius P, Zagnoni M, Sandison ME, East JM, Morgan H, Lee AG. Binding of anionic lipids to at least three nonannular sites on the potassium channel KcsA is required for channel opening. Biophys J. 2008;94:1689–98.
183. Guixà-González R, Albasanz JL, Rodriguez-Espigares I, Pastor M, Sanz F, Martí-Solano M, et al. Membrane cholesterol access into a G-protein-coupled receptor. Nat Commun. 2017;8:14505.
184. McIntosh TJ. The effect of cholesterol on the structure of phosphatidylcholine bilayers. Biochim Biophys Acta. 1978;513:43–58.
185. Simon SA, McIntosh TJ, Latorre R. Influence of cholesterol on water penetration into bilayers. Science. 1982;216:65–7.

186. Nezil FA, Bloom M. Combined influence of cholesterol and synthetic amphiphilic peptides upon bilayer thickness in model membranes. Biophys J. 1992;61:1176–83.
187. McMullen TPW, Lewis RNAH, McElhaney RN. Differential scanning calorimetric study of the effect of cholesterol on the thermotropic phase behavior of a homologous series of linear saturated phosphatidylcholines. Biochemistry. 1993;32:516–22.
188. Chen Z, Rand RP. The influence of cholesterol on phospholipid membrane curvature and bending elasticity. Biophys J. 1997;73:267–76.
189. Arora A, Raghuraman H, Chattopadhyay A. Influence of cholesterol and ergosterol on membrane dynamics: a fluorescence approach. Biochem Biophys Res Commun. 2004;318:920–6.
190. Bacia K, Schwille P, Kurzchalia T. Sterol structure determines the separation of phases and the curvature of the liquid-ordered phase in model membranes. Proc Natl Acad Sci U S A. 2005;102:3272–7.
191. Starke-Peterkovic T, Turner N, Vitha MF, Waller MP, Hibbs DE, Clarke RJ. Cholesterol effect on the dipole potential of lipid membranes. Biophys J. 2006;90:4060–70.
192. Haldar S, Kanaparthi RK, Samanta A, Chattopadhyay A. Differential effect of cholesterol and its biosynthetic precursors on membrane dipole potential. Biophys J. 2012;102:1561–9.
193. Yeagle P. The membranes of cells. 3rd ed. Orlando, FL: Academic Press; 2016. p. 200–7.
194. Brejchová J, Sýkora J, Dlouhá K, Roubalová L, Ostašov P, Vošahlíková M, et al. Fluorescence spectroscopy studies of HEK293 cells expressing DOR-$G_i1\alpha$ fusion protein; the effect of cholesterol depletion. Biochim Biophys Acta. 2011;1808:2819–29.
195. Soubias O, Gawrisch K. The role of the lipid matrix for structure and function of the GPCR rhodopsin. Biochim Biophys Acta. 2012;1818:234–40.
196. Pal S, Chakraborty H, Bandari S, Yahioglu G, Suhling K, Chattopadhyay A. Molecular rheology of neuronal membranes explored using a molecular rotor: implications for receptor function. Chem Phys Lipids. 2016;196:69–75.
197. Brown MF. Modulation of rhodopsin function by properties of the membrane bilayer. Chem Phys Lipids. 1994;73:159–80.
198. Brown MF. Soft matter in lipid-protein interactions. Annu Rev Biophys. 2017;46:379–410.
199. Mitchell DC, Straume M, Miller JL, Litman BJ. Modulation of metarhodopsin formation by cholesterol-induced ordering of bilayer lipids. Biochemistry. 1990;29:9143–9.
200. Falck E, Patra M, Karttunen M, Hyvönen MT, Vattulainen I. Impact of cholesterol on voids in phospholipid membranes. J Chem Phys. 2004;121:12676–89.
201. Jafurulla M, Chattopadhyay A. Structural stringency of cholesterol for membrane protein function utilizing stereoisomers as novel tools: a review. Methods Mol Biol. 2017;1583:21–39.
202. Singh P, Haldar S, Chattopadhyay A. Differential effect of sterols on dipole potential in hippocampal membranes: implications for receptor function. Biochim Biophys Acta. 2013;1828:917–23.
203. Clarke RJ. The dipole potential of phospholipid membranes and methods for its detection. Adv Colloid Interface Sci. 2001;89-90:263–81.
204. Duffin RL, Garrett MP, Busath DD. Modulation of lipid bilayer interfacial dipole potential by phloretin, RH421, and 6-ketocholestanol as probed by gramicidin channel conductance. Langmuir. 2003;19:1439–42.
205. Starke-Peterkovic T, Turner N, Else PL, Clarke RJ. Electric field strength of membrane lipids from vertebrate species: membrane lipid composition and Na^+-K^+-ATPase molecular activity. Am J Physiol Regul Integr Comp Physiol. 2005;288:R663–70.
206. Bandari S, Chakraborty H, Covey DF, Chattopadhyay A. Membrane dipole potential is sensitive to cholesterol stereospecificity: implications for receptor function. Chem Phys Lipids. 2014;184:25–9.
207. Oakes V, Domene C. Stereospecific interactions of cholesterol in a model cell membrane: implications for the membrane dipole potential. J Membr Biol. 2018;251:507–19.
208. Mickus DE, Levitt DG, Rychnovsky SD. Enantiomeric cholesterol as a probe of ion-channel structure. J Am Chem Soc. 1992;114:359–60.

209. Covey DF. *ent*-Steroids: novel tools for studies of signaling pathways. Steroids. 2009; 74:577–85.
210. D'Avanzo N, Hyrc K, Enkvetchakul D, Covey DF, Nichols CG. Enantioselective protein-sterol interactions mediate regulation of both prokaryotic and eukaryotic inward rectifier K^+ channels by cholesterol. PLoS One. 2011;6:e19393.
211. Kristiana I, Luu W, Stevenson J, Cartland S, Jessup W, Belani JD, et al. Cholesterol through the looking glass: ability of its enantiomer also to elicit homeostatic responses. J Biol Chem. 2012;287:33897–904.
212. Westover EJ, Covey DF. The enantiomer of cholesterol. J Membr Biol. 2004;202:61–72.

Regulation of BK Channel Activity by Cholesterol and Its Derivatives

Anna N. Bukiya and Alex M. Dopico

Abstract Cholesterol (CLR) is an essential structural lipid in the plasma membrane of animal cells. In addition, CLR has been widely recognized as a critical modulator of protein function, including ion channels. Voltage- and Ca^{2+}-gated K^+ (BK) channels control a wide variety of physiological processes, including cell excitability, smooth muscle contractility, sensory perception, neurotransmitter release, and hormone secretion. Thus, disruption of BK currents has been implicated in the pathophysiology of prevalent human diseases. The current chapter reviews the literature documenting CLR modulation of BK channel function at a variety of levels ranging from organ systems to artificial lipid bilayers. We discuss the use of CLR isomers and structural analogs as a tool to help in discerning the mechanisms underlying CLR-driven modification of BK current. The chapter is finalized with an overview of the phenomenology and potential mechanisms that govern CLR control over the alcohol (ethyl alcohol, ethanol) sensitivity of BK channels. Studies on CLR regulation of BK currents may ultimately pave the way for novel therapeutic approaches to combat prevalent pathophysiological and morbid conditions.

Keywords MaxiK channel · Alcohol · Cerebral artery · High cholesterol diet · Hypercholesterolemia

Abbreviations

BK	Voltage- and Ca^{2+}-gated K^+ (channels)
CLR	Cholesterol
CTD	Cytosolic tail domain
LDL	Low-density lipoprotein
LRRC	Leucine-rich repeat-containing (protein)

A. N. Bukiya (✉) · A. M. Dopico
The University of Tennessee Health Science Center, Memphis, TN, USA
e-mail: abukiya@uthsc.edu; adopico@uthsc.edu

A. Rosenhouse-Dantsker, A. N. Bukiya (eds.), *Cholesterol Modulation of Protein Function*, Advances in Experimental Medicine and Biology 1115,
https://doi.org/10.1007/978-3-030-04278-3_3

MβCD	Methyl-β-cyclodextrin
PGD	Pore-gate domain
RCK	Regulator of conductance of potassium (domain)
SPM	Sphingomyelin
TM	Transmembrane
VSD	Voltage-sensing domain

1 Introduction

Cholesterol (CLR) is an essential structural lipid in the plasma membrane of animal cells. In addition, CLR has been widely recognized as a critical modulator of protein function, including ion channels. Voltage- and Ca^{2+}-gated K^+ (BK) channels control a plethora of tissue functions, including cell excitability, smooth muscle contractility, sensory perception, neurotransmitter release, and hormone secretion. Thus, disruption of BK currents has been implicated in the pathophysiology of prevalent human diseases. The current chapter reviews the literature documenting CLR modulation of BK channel function at the organ level, on individual cells, in isolated membrane patches, and in artificial lipid bilayers. First, we will introduce the reader to BK channel basic structure, subunit composition, and physiological roles. Second, we will review the phenomenology of BK channel regulation by CLR. This section contains two sub-sections, in which we describe CLR modulation of BK current following manipulation of CLR levels in vivo and in vitro. The section on phenomenology is followed by an overview of the diverse mechanisms that govern CLR modulation of BK channel function. These include cellular mechanisms, lipid membrane microdomain mechanisms, protein–protein interactions, and the contribution of differential subunits to the BK channel sensitivity to CLR. We will emphasize the use of CLR isomers and other structural analogs to discern between membrane- and protein-mediated effects of CLR on BK channel function. Finally, we will review the literature that describes the CLR control of alcohol (ethyl alcohol, ethanol) effect on BK currents in cell-free systems: artificial lipid bilayers and excised membrane patches. While the mechanisms of CLR control over alcohol effect on BK channels remain a topic of investigation, we will highlight the use of the enantiomer of CLR to elucidate the driving forces behind CLR–alcohol interactions that modify BK currents.

2 BK Channels: Protein Structure, Macromolecular Subunit Composition, and Physiological Role

Functional BK channels are formed by a tetramer of channel-forming proteins usually termed slo (invertebrates), slo1 (vertebrates), or alpha subunits. This protein is the product of the *KCNMA1* gene in mammals [1]. Slo1 channels belong to the

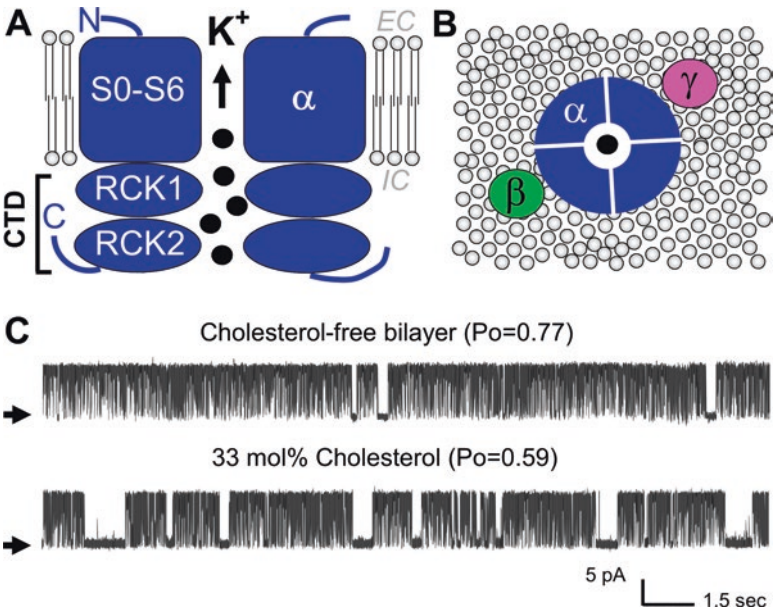

Fig. 1 Schematic structure of BK channel. (**a**) Side view of two alpha subunits. *CTD* cytosolic tail domain, *EC* extracellular, *IC* intracellular, *RCK* regulator of conductance of potassium (domain). (**b**) Top view of the mammalian BK channel complex. Functional BK channels are formed by alpha subunit tetramers. In most mammalian tissue types, alpha tetramers are accompanied by accessory subunits of beta and/or gamma type. Stoichiometry of alpha, beta, and gamma assembly remains a topic of investigation [112]. (**c**) Representative single-channel recordings obtained after incorporation of BK channel-forming alpha subunit protein cloned from rat cerebral artery myocytes (cbv1) into control, CLR-free (top recordings), or CLR-containing (bottom recording) POPE/POPS (3:1 wt/wt) bilayers. Channel openings are shown as upward deflections; arrows point at the baseline level (channel closed). The membrane potential was set to 0 mV (asymmetric K^+) and free calcium bathing BK CTD was set at ≈10 μM. *Po* open probability

superfamily of six transmembrane domain (TM6) voltage-gated ion channels [1]. Following the design that is common for these superfamily members, BK alpha subunits include an S1–S6 "core" that is highly conserved with that of purely voltage-gated potassium channels (Fig. 1). The core contains a voltage-sensing domain (VSD) formed by segments S1–S4, and a pore-gate domain (PGD) formed by S5–S6 [2]. In addition, BK alpha subunits also possess two unique features that set BK aside from other voltage-gated potassium channels. First, the BK alpha subunit includes an S0 segment added to the S1–S6 core, which places the BK alpha N-terminus outside the cell [1–3]. The S0 segment contributes to voltage-gating [4], and has also been implicated in BK alpha subunit interactions with accessory proteins (see below) [5]. Second, the BK alpha protein includes a large (>800 amino acids) C-terminal, referred to as the cytosolic tail domain (CTD) [2]. The CTD hosts two regulator of conductance of potassium domains, RCK1 and RCK2 [2] that contain high-affinity sites for calcium recognition [6]. In addition to calcium- and

voltage-sensing, the alpha subunit activity is governed by magnesium interaction with a low-affinity, divalent site, often referred to as a magnesium-binding site [7–9], which has been mapped to the RCK1 region [2].

A variety of BK alpha protein isoforms results from pre-mRNA processing by alternative splicing, editing, and regulation by miRNA, followed by an array of post-translational modifications such as phosphorylation and glycosylation, among others [10–12]. The functional diversity of BK channels, however, is further enhanced by accessory proteins globally known as BK regulatory subunits. Thus, in most mammalian tissues, slo1 channels are tightly associated with proteins that constitute the family of BK beta subunits (Fig. 1) [13]. These accessory proteins contain around 200 amino acids, and are composed of short N- and C-termini, and two TM domains connected by a loop. Four beta subunit types have been identified, each encoded by a different gene (*KCNMB1-4*) [14–16]. It is noteworthy that BK beta subunit expression is highly tissue-specific. While BK beta1 is almost uniquely expressed in smooth muscle [13, 15, 16], the beta2 subunit is present in adrenal chromaffin cells and, to a lesser extent, in central neurons [13, 15]. In turn, the beta3 subunit (several isoforms exist) accompanies slo1 channels in skeletal muscle, while beta4 is highly prevalent in central neurons throughout the brain [14, 15, 17].

Notably, BK beta subunits cannot form functional channels themselves, rather they substantially modify the slo1 current phenotype, including its pharmacological properties. Furthermore, beta1 subunit co-expression with slo1 slows down the macroscopic current activation and deactivation kinetics, and increases the apparent calcium sensitivity of the channel [15, 18]. The BK beta1 subunit confers sensitivity of the BK channel complex to the activating properties of lithocholic acid, leukotriene B4, and the synthetic non-steroidal compound HENA [19–22]. These activators are presumed to form a hydrogen bond with Thr169 of beta1, which is not present in any other type of beta subunits [20–23].

BK beta2 subunit co-expression with slo1 results in fast inactivation of BK current, while partial inactivation is observed in the presence of the beta3, 3b-V4 subunit variant [13, 15, 24]. The latter also right-shifts the voltage dependence of ionic current activation [24]. In contrast, the beta4 subunit decreases BK channel activity at low intracellular calcium concentrations (1 μM) but increases channel activity at high (50 μM) concentrations [15]. The beta4 subunit also confers unique resistance of the BK channel complex to the peptide blockers, iberiotoxin and charybdotoxin [25].

In addition to beta subunits, the leucine-rich repeat-containing (LRRC) protein family has been identified as BK channel accessory proteins and termed BK gamma subunits [26]. Like beta subunits, LRRC26 and its paralogous proteins, LRRC52, LRRC55, and LRRC38, have a differential tissue expression profile. However, unlike beta subunits, BK gamma subunits contain a single membrane-spanning domain with N- and C-termini protruding from the membrane [26]. Gamma subunit association with the BK channel pore-forming alpha subunit leads to an increase in the apparent Ca^{2+}-sensitivity of the channel [26]. Moreover, LRRC26 assembly with the BK channel allows channel opening at physiologically relevant voltages in the absence of intracellular calcium [26].

BK channels critically control a wide array of cellular processes. These include the circadian clock, tumor progression, neuronal firing, neurotransmitter and hormone release, sensory function, smooth muscle contractility, and arterial tone [27–32]. Moreover, BK channel and its coding genes are critical targets for alcohol, one of the most widely abused drugs worldwide [33]. In addition to the plasma membrane, BK channels of intracellular location have been found in the mitochondria, nuclear envelope, endoplasmic reticulum, and the Golgi apparatus [34]. Studies on the physiological role of these intracellular channels are only emerging [34–38].

Considering the critical contribution of BK channels to the most fundamental physiological processes, pharmacological targeting of BK channels has been considered for the treatment of prevalent health disorders such as asthma, stroke, cancer, and hypertension, among others [28, 39–41]. In this regard, studies with a focus on BK channel modulation by endogenous compounds gain additional significance, as they may improve our understanding of BK function in physiology and pathology, and the influence of endogenous mediators on modification of BK channel function by exogenous compounds.

3 Phenomenology of BK Channel Regulation by CLR

3.1 BK Channel Function Modification by Manipulations of CLR Levels In Vivo

The current interest in BK channel modulation by cholesterol stems not only from the key roles that BK channels play in physiology and pathology (see previous section), and the increasing recognition of cholesterol as a lipid that modulates protein function, but also from the high prevalence of elevated blood cholesterol levels and their influence on human health. It is estimated that 1 out of 3 US adults may require treatment with cholesterol-lowering medications (https://www.cdc.gov/cholesterol/facts.htm, retrieved June 6, 2018). Clinically defined hypercholesterolemia is reached when blood CLR level exceeds 240 mg/dL in blood serum. Hypercholesterolemia represents a risk factor for a variety of health disorders, including hypertension, stroke, atherosclerosis, and cognitive deficits [42–45]. Noteworthy, not only increased (hypercholesterolemia), but also decreased blood CLR levels (hypocholesterolemia) pose an enhanced risk for disease and death [46]. Indeed, hypocholesterolemia accompanies major trauma, infectious conditions, and poor evolution from surgery, and serves as a negative prognostic factor in critically ill patients [47–50]. Understanding the fundamentals of blood cholesterol influence on physiology and pathology, as well as the development of effective therapeutic interventions, requires addressing molecular mechanisms that underlie the effects of CLR on its molecular targets. The latter include BK channels [51, 52].

Several reports, including work from our lab, underscore the sensitivity of plasmalemmal BK channels to modifications in blood cholesterol. Considering the

well-established link between fluctuations in blood CLR and cardiovascular health, the majority of studies focus on cholesterol modulation of BK channel function in the cardiovascular system. For instance, an increase in the open probability of BK channels was observed in *cell-attached* patch recordings from human vascular myocytes in areas of atherosclerotic plaque in coronary arteries compared to recordings on myocytes from extra-plaque regions [53]. However, this difference disappeared when the comparison of BK channel activity was made using excised (i.e., "cell-free"), membrane patches [53]. It was thus proposed that an unidentified cytosolic signal(s) may play a role in the link between blood cholesterol and BK channels [53].

Animal models of hypercholesterolemia provided further insights into the influence of blood CLR influence over BK channel activity and, ultimately, organ function [54]. Hypercholesterolemia can be achieved by subjecting laboratory animals to a high-CLR diet as reviewed elsewhere [55, 56]. In this regard, rabbits are one of the most sensitive animal models to manipulation of blood CLR levels by dietary CLR [56]. An in vivo study on rabbits that were subjected to a high-CLR diet versus normal chaw showed a similar degree of vasodilation in response to aortic injection of sodium nitroprusside [57]. However, vasodilation by aortic injection of acetylcholine or bradykinin was significantly smaller in high-CLR diet-fed animals when compared to the control group [57]. This difference persisted in the presence of the nitric oxide synthase antagonist *N*-nitro-L-arginine methyl ester (L-NAME). In addition, the tetraethylammonium-sensitive component of vasodilation elicited by acetylcholine was reduced in CLR-fed rabbits as compared to the control group [57]. These observations led to the conclusion that a high-CLR diet and the resulting hypercholesterolemia modify the contribution of potassium currents to organ function.

Similar to the above hindlimb findings in vivo, a study on endothelium-dependent and independent in vitro relaxations of carotid artery rings from hypercholesterolemic rabbits failed to detect differences between control and high-CLR diet-fed rabbits in their vasodilation to sodium nitroprusside [58]. Relaxation by nitric oxide and 8-bromoguanosine 3′,5′-cyclic monophosphate was also similar in the two groups [58]. However, nitric oxide-driven relaxation of artery rings from hypercholesterolemic animals was more sensitive to the BK channel blocker charybdotoxin. This suggested that hypercholesterolemia increased the contribution of BK channels to nitric oxide relaxation or, alternatively, up-regulated BK channel activity.

Our group studied BK channel contribution to the regulation of cerebral artery diameter in a rat model of high-CLR diet. The latter resulted in a significant increase in both total CLR in blood serum and CLR content within de-endothelialized cerebral artery [59]. Paxilline-induced constriction of in vitro pressurized arteries from rats on high-CLR diet was diminished when compared to that from control rat donors [59]. Yet, arteries from both groups showed similar sensitivity to depolarization-induced vasoconstriction evoked by 60 mM KCl [59]. These results were in agreement with findings obtained using the rabbit model. In these studies it was shown that, while basic responses of arteries to vasomodulator stimuli remained unmodified, BK channel contribution to the regulation of artery diameter was reduced by the high-CLR diet [57]. The reduction in paxilline-induced cerebral artery constriction

by high-CLR diet and the resulting hypercholesterolemia may stem from several mechanisms that may not be mutually exclusive. These may include a decrease in the number of functional BK channels in arterial smooth muscle, modification of the channel's affinity to the blocker, or reduction in the channel's basal activity, and thereby the ability to regulate vascular smooth muscle contractility.

Interestingly, we detected up-regulation of the BK beta1 subunit-associated fluorescence signal following immunofluorescence staining and confocal microscope imaging of myocytes that were isolated from cerebral arteries of rats on high-CLR diet compared to their controls [59]. Consistently, daily administration of the antihyperlipidemic drug atorvastatin to rats on high-CLR diet decreased the amount of BK beta1 subunit-associated fluorescence signal [60]. In contrast to our findings, immunohistochemical staining and Western blots suggested downregulation of BK beta1 protein level in the Oddi sphincter circular smooth muscle strips from rabbits on high-CLR diet [61]. Thus, there may be tissue and/or species differences in the effect of high-CLR diet with resulting hypercholesterolemia on the amount of BK protein subunit levels.

In summary, several studies demonstrate that in vivo manipulations of CLR levels affect the influence of the BK channel activity on organ function. In particular, BK channel complex protein amounts in smooth muscle are sensitive to CLR levels in the blood.

3.2 BK Channel Function Modification by Manipulations of CLR Levels In Vitro

The most straightforward way of manipulating the CLR amount in the membrane is to create artificial phospholipid membranes with a known amount of CLR in the lipid mixture. Multiple studies of native brain or recombinant BK channels incorporated into artificial lipid bilayers consistently correlated a decrease in the channel's open probability with an increase in the molar fraction of CLR in the bilayer lipid mixture up to 50 mol% (Fig. 1c) [62–65].

Manipulation of CLR levels in cellular membranes is usually achieved using chemical carriers for steroids. In particular, CLR depletion is achieved by exposing cells to methyl-β-cyclodextrin (MβCD). The opposite effect is accomplished by incubating cells in MβCD complexed with CLR [66]. In addition, in some tissue types, a mild increase in CLR level can be obtained by incubation in low-density lipoprotein (LDL) media [67].

BK current sensitivity to the modulation of membrane CLR levels has been reported in a wide range of cell types including human and rabbit aorta cultured myocytes [51, 68], human myometrial cultured myocytes [69], melanoma IGR39 and glioma cell lines [70, 71], bovine aortic endothelial cells [72], rat uterine [73], ureteric [74], cardiac myocytes [75], pituitary tumor GH3 cells [76], mouse colonic epithelial cells [77], and chicken hair cells [78]. Most studies concur that CLR

depletion in vitro enhances BK currents while CLR enrichment depresses the currents. However, these findings are not universal and, when considered at the cellular level, the CLR effect on BK current varies as a result of a variety of mechanisms (see below) [52].

4 Mechanisms and Sites of CLR Action on the BK Channel

4.1 Cellular Mechanisms

Unexpectedly, CLR depletion from mouse portal vein myocytes did not facilitate BK currents but inhibited them [79]. A similar phenomenon was observed in glioma cells [71]. CLR depletion-driven reduction of BK current was not attributed to internalization or a change in calcium sensitivity of glioma cell BK channels. Rather, CLR depletion disrupted BK channel activation by calcium release from inositol 1,4,5-trisphosphate (IP_3) receptors [71]. Another study documenting an unexpected decrease in BK currents upon CLR depletion used rat uterine myocytes to demonstrate that such a decrease could be driven by channel internalization from the plasmalemma [73]. Thus, at the cellular level, the final effect of manipulating CLR levels is determined by several factors, which include the amount of channel-forming protein within the plasma membrane and/or modulation of BK channel activity by physiological stimuli that, in turn, could be modified by CLR.

4.2 Microdomain Mechanisms and Protein–Protein Interactions

Several reports have linked CLR-driven modification in BK currents in native cells to a preferential location of BK channels in membrane rafts. Indeed, studies in IGR39 human melanoma cells, rat ureter myocytes, mouse colonic epithelial cells, and Madin-Darby canine kidney cells demonstrated that the BK alpha subunit protein was preferentially located in the membrane fraction representing detergent-resistant “raft-like” domains [70, 74, 77, 80]. Moreover, BK channels have been found to reside in caveolae of human myometrium [69] and rat ureter [74] myocytes. Indeed, BK channels physically associate with caveolin-1 via a binding motif located in the CTD of the BK channel alpha subunit [72, 81]. Such association has been proposed to tether the CTD of slo1 to the membrane [81]. CLR depletion results in a decrease of caveolin-1 in the caveolae fraction [81] and drives the BK channel into the detergent-soluble membrane areas [77].

Raft disruption by CLR depletion is generally reported to increase BK currents. This has been shown in IGR39 human melanoma cells [70], mouse colonic epithelium [77], and GH3 pituitary tumor cells [76].

4.3 Contribution of Different Subunits to BK Channel Sensitivity to CLR

In mammalian tissue, the BK channel-forming tetramer of alpha subunits is usually accompanied by accessory proteins (see above). A nearly universal finding of BK currents modulation by CLR favors the idea that CLR action does not require a specific BK subunit combination. Indeed, BK current sensitivity to CLR has been documented in Madin-Darby canine and human embryonic kidney cells following transfection with pore-forming alpha subunit cloned from human brain (hslo1) [80, 82]. Thus, BK accessory subunits are not necessary for CLR modulation of BK currents. This conclusion is further supported by reports on artificial lipid membranes showing CLR-induced BK currents' inhibition upon incorporation of alpha subunit protein into the bilayer [63–65].

Whether accessory subunits are able to modify the effect of CLR on the BK alpha protein remains largely unknown. A study in planar lipid bilayers demonstrated that co-incorporation of the BK alpha subunit with the beta1 protein into an artificial lipid membrane did not alter the CLR-induced inhibition of BK currents [64]. However, the study was performed at a single CLR molar fraction (33 mol%) and at a fixed concentration of calcium (≈10 μM) bathing the CTD of the BK alpha protein. The presence of functional beta1 subunits within the BK complex was confirmed by an increase in the BK channel apparent calcium sensitivity: the open probability-voltage curve of the beta1-containing BK complex displayed a leftward shift compared to the curve of the homomeric channel. It remains to be determined, however, whether the beta1 protein can modify the sensitivity of the BK channel to CLR over a wide range of CLR molar fractions in the membrane-forming lipid mixture, and over a wide range of calcium levels being sensed by the CTD of the BK alpha protein. Moreover, detailed analysis of CLR-driven modifications in BK channel gating in the absence versus presence of the beta1 subunit is currently being performed in our lab. This analysis will determine whether the accessory beta1 subunit contributes to the effect of CLR on BK channel function.

The role of the BK beta2 and beta4 subunits in CLR sensitivity of BK channels has been studied using hslo1 channels transfected into HEK293 cells [83]. In this study, 10 μM CLR did not evoke modifications in the amplitude of macroscopic currents resulting from either beta2- or beta4-containing BK channels. The concentration of CLR used in this work was rather small. Thus, it is possible that CLR levels in the membrane did not reach the critical value required for modification of BK current amplitude. An alternative explanation is that beta2 and beta4 are involved in a negative feedback mechanism that controls the sensitivity of the BK channel-forming alpha subunit on CLR, or even confer CLR resistance to the channel protein. Detailed analysis of beta2 and beta4-driven modifications in BK channel CLR sensitivity is yet to be performed. A possible role of beta3 and gamma subunits in the CLR sensitivity of BK complex also remains to be explored.

In summary, regardless of the complexity of the mechanisms that may contribute to the final effect of CLR on BK current, a simple model of CLR modulation of BK channel function only requires including the BK channel-forming alpha subunit and its immediate lipid environment.

4.4 Cell-Free Mechanisms: Use of CLR Derivatives

CLR is able to modulate BK channel activity in cell-free environments such as the one obtained following BK protein reconstitution into 1–3 lipid species bilayers. Whether using native BK [62] or recombinant slo1 proteins [63–65, 82], all of the studies performed using a lipid bilayer came to similar conclusions. Specifically, elevation of CLR level in the bilayer-forming lipid mixture significantly decreased the open probability of BK channels in a concentration-dependent manner. The EC_{50} for reducing channel activity by CLR was approximately 15–20 mol% [63, 64]. This CLR level was at the lower end of the physiologically relevant CLR levels commonly found in native cellular membranes [84, 85]. The reduction in the open probability of BK channels resulted from both a decrease in mean open and an increase in mean closed times [62, 63, 65]. One study reported that in addition to a reduction in the open probability of BK channels, an increase in cholesterol levels also led to a minor (≈7%) decrease in the unitary conductance of the channel [62].

CLR modulation of the open probability of BK channels may arise from two mechanisms that may not be mutually exclusive. First, CLR insertion into membranes is known to alter the bulk physical properties of the lipid bilayer. Indeed, a CLR-driven increase in lateral elastic stress, modifications in phospholipid fatty acid tails order parameter, and membrane "fluidity," membrane curvature, thickness, and membrane dipole have all been reported [86–90]. Second, CLR may directly interact with a sensing region on the BK alpha subunit. In an attempt to distinguish between these two possible mechanisms, our group incorporated the BK alpha subunit into planar POPE:POPS (3:1 w/w) bilayers that contained the enantiomeric CLR isomer, ent-CLR [91]. Ent-CLR constitutes a "mirror" image of the CLR molecule, in which the stereochemistry at all chiral centers is opposite to the stereochemistry in natural CLR (Fig. 2a, b). As optical isomers, CLR and ent-CLR share the same relative configuration and conformations of all four rings, and do not extensively differ in their modification of membrane physical properties [82, 92]. As such, the specificity of the protein response to a particular enantiomer of the two optical CLR isomers is considered to reflect the involvement of a CLR-recognizing protein site [93–95]. Studies of homotetramers of the BK alpha subunit reconstituted in lipid bilayers demonstrated that ent-CLR failed to decrease the open probability of the channel (Fig. 2c) [91]. This suggests that the changes in BK currents observed following alterations in CLR levels require recognition via a CLR-sensing protein site. This conclusion was further bolstered by data demonstrating that cholestanol and coprostanol were both effective in reducing the open probability of the BK channel (Fig. 2c) despite the striking differences in the abilities of

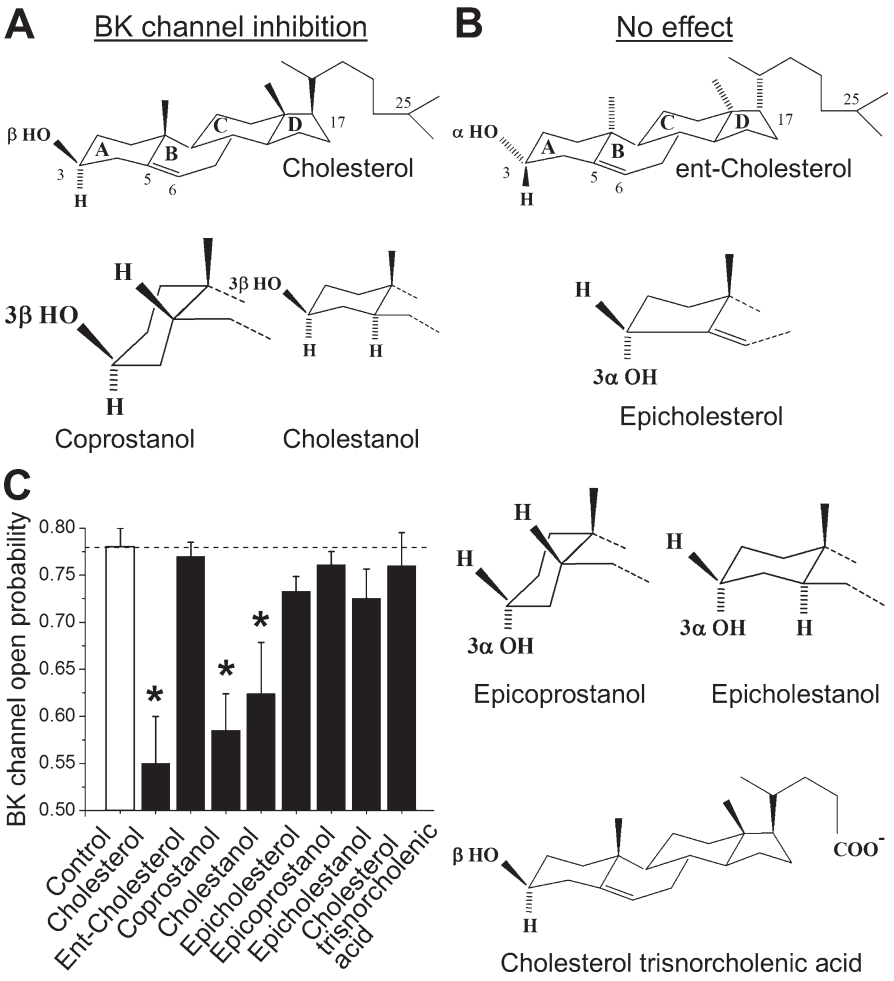

Fig. 2 Structural requirements for CLR and analogs to inhibit homomeric BK channel following reconstitution of BK pore-forming α subunit protein (cbv1) into planar lipid bilayers. (**a**) Chemical structure of BK channel-inhibiting CLR and its derivatives. (**b**) Molecular structures of CLR analogs that failed to inhibit BK channel activity efficiently. (**c**) Average open probability (Po) values show that CLR, coprostanol, and cholestenol, but not their epi-isomers, ent-CLR, or CLR trisnorcholenic acid significantly reduced BK channel activity when compared to steroid-free bilayers (control). *Significantly different from control ($p < 0.05$). Control refers to steroid-free POPE/POPS (3:1 wt/wt) bilayer

coprostanol, cholestanol, and CLR to modify several major bilayer physical properties such as lipid condensing [96, 97].

In contrast, none of the steroid epimers at carbon atom 3 (C3) studied (epiCLR, epicoprostanol, and epicholestanol) were able to reduce BK current [91]. Indeed, steroid inhibition of BK channel activity required the β configuration of the hydroxyl

group at C3 (Fig. 2). Moreover, we established that BK channel inhibition was favored by the hydrophobic nature of the alkyl side chain at C17, as CLR trisnorcholenic acid failed to decrease the open probability of the BK channel (Fig. 2b, c). Together, these findings support a protein-mediated mechanism of the CLR effect on the BK channel alpha subunit. The CLR-sensing site, however, has lax structural selectivity toward the steroid nucleus, while having strict specificity toward the orientation of the steroid single hydroxyl group and the hydrophobicity of the steroid's alkyl side chain.

4.5 CLR-Sensing Sites in the BK Alpha Subunit Protein

CLR recognition amino acid consensus (CRAC) motifs have been widely accepted as plausible CLR-sensing regions [98, 99]. The BK alpha subunit protein sequence contains ten CRAC motifs: three in the S0–S6 transmembrane core and seven in the CTD (Fig. 3a). To pinpoint the slo1 subunit CLR-sensing region(s) we probed CLR on an engineered slo1 protein that resulted from truncating the BK alpha subunit cloned from rat cerebral artery myocytes (cbv1) immediately after S6, between Ile322 and Ile323. Single channel protein function was evaluated under identical recording conditions after channel reconstitution into CLR-free or CLR-containing (25 mol%) POPE:POPS (3:1 w/w) bilayers. The truncated cbv1 (trcbv1S6) channels retained the basic characteristics of the BK currents, but were insensitive to CLR [100]. This result indicated that the CTD was necessary for CLR inhibition of BK channel activity [100]. Whether the CTD actually provided CLR-recognition sites or rather a distant control over CLR-sensing via the transmembrane core remains unknown.

Further work, however, helped to elucidate the contribution of the CTD CRAC regions to the CLR-sensitivity of BK currents. Cbv1 CTD contains 7 CRAC motifs that are scattered over the CTD sequence (Fig. 3a). Computational protein homology modeling based on the crystal structure of the hslo1 CTD (Protein Data Bank ID 3MT5, [101]) allowed mapping of the CRAC motifs on the folded intracellular part of the protein. Such mapping shows scattered distribution of CRAC motifs over the CTD globular structure in the aqueous media (Fig. 3b). The role of individual CRAC motifs within the CTD in CLR-sensing is currently under investigation. However, CRAC4 seemed to play a critical role in CLR modification of BK currents: tyrosine 450 substitution to phenylalanine (Y450F) within CRAC4 resulted in a decrease in CLR-induced BK channel inhibition (Fig. 3c) whereas a similar

Fig. 3 (continued) computational homology modeling (Molecular Operating Environment software; Chemical Computing Group) based on a template of hslo1 CTD crystal structure [Protein Data Bank (PDB) ID 3MT5; 101]. The CRAC motifs are color-coded, the numbers reflect the sequential numbering of the CTD CRAC motifs from 4 through 10. (**c**) Averaged inhibition of wild-type cbv1 versus cbv1Y450F channel activity by CLR. *Significantly different from CLR-induced inhibition of unmutated cbv1 ($p < 0.05$). With modifications from [100]

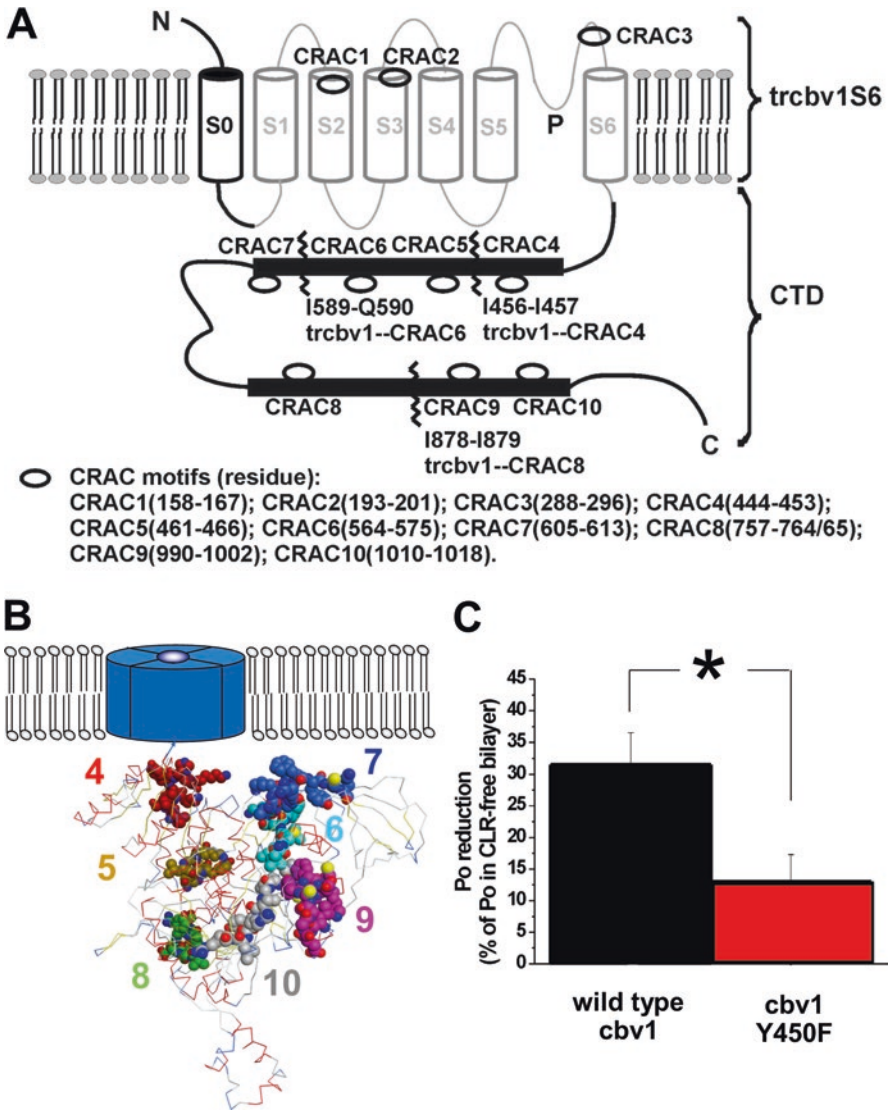

Fig. 3 The cholesterol recognition amino acid consensus motif 4 (CRAC4) within the BK channel α subunit protein CTD region is necessary for CLR-induced reduction in open probability of the homomeric BK channel. (**a**) Schematic structure of CRAC motifs identified within the BK channel sequence (cloned from rat cerebral artery myocytes, cbv1). CRAC motifs are consequently numbered from 1 to 10. Three CRAC motifs are identified within transmembrane core of the protein, while the remaining seven reside within CTD. Scheme was originally published in the Journal of Biological Chemistry, Singh AK, McMillan J, Bukiya AN, Burton B, Parrill AL, Dopico AM. Multiple cholesterol recognition/interaction amino acid consensus (CRAC) motifs in cytosolic C tail of Slo1 subunit determine cholesterol sensitivity of Ca^{2+}- and voltage-gated K^+ (BK) channels. J. Biol. Chem. 2012; 287: 20509–20521. © the American Society for Biochemistry and Molecular Biology. (**b**) Location of CRAC motifs on the CTD structure that was built using the

substitution (Y429F) located upstream of CRAC4 did not affect CLR modification of the open probability of the BK channel. Remarkably, sequential substitution of central tyrosine residues into phenylalanine in CRACs4-10 gradually ablated the sensitivity of the BK channel to CLR. However, when the cbv1 channel was truncated after CRAC4 (i.e., rendering a CRAC5-10-lacking sequence), the Y450F substitution within CRAC4 totally ablated CLR-induced BK channel inhibition. This outcome suggested that CTD CRAC motifs might interact among themselves for CLR-sensing. Future work will shed light on the mechanisms that underlie this phenomenon.

5 CLR Modulation of BK Channel Responses to Alcohol

Alcohol (ethyl alcohol, ethanol) is one of the most widely used drugs worldwide. Indeed, a recent National Survey on Drug Use and Health revealed that around 86% of people 18 years and older consumed alcohol at some time point in life while 56% of people reported consumption within the past month (https://www.samhsa.gov/data/sites/default/files/NSDUH-DetTabs-2015/NSDUH-DetTabs-2015/NSDUH-DetTabs-2015.htm#tab2-41b, retrieved June 9, 2018). In excessive amounts, alcohol poses substantial health risks: approximately 88,000 people are estimated to die from alcohol-related causes each year. This statistic places alcohol misuse at third place in the list of leading preventable causes of death in the USA (https://www.niaaa.nih.gov/alcohol-health/overview-alcohol-consumption/alcohol-facts-and-statistics, retrieved June 9, 2018). Remarkably, the BK channel constitutes one of the molecular targets of ethanol [102, 103].

Ethanol effect on BK channels is tuned by several factors, including subunit composition, post-translational modification of the slo1 subunit, the lipid microenvironment, the duration and pattern of ethanol exposure, and the level of free calcium at the intracellular part of the protein [17, 33]. When calcium levels were below 10 μM, ethanol concentrations reached in the blood during intoxication (15–75 mM) led to an increase in BK currents [104–106]. At higher levels of calcium, on the other hand, ethanol-induced inhibition of homomeric BK channels was observed [105, 106]. These effects of ethanol on the BK alpha subunit homotetramers were due to modification in the open probability of the BK channel along with only a slight, if any, effect on the unitary current amplitude of the channel [104]. Moreover, ethanol-induced increase in the open probability of the BK channel could be observed in cell-free systems such as two-lipid species (POPE:POPS 3:1 w/w) artificial bilayers [63, 65]. The effect of ethanol on the open probability of the BK channel was facilitated by a decrease in the average duration of BK channel long closures, and by a shift of channel closures from long to rather brief events. The channel open times did not undergo such apparent changes. The ethanol-driven increase in the open probability of the BK channel homotetramer was opposite to the effect of CLR, and CLR antagonism of ethanol-induced activation of the BK channel was observed in cell-free lipid bilayers [63]. It was observed that CLR

prevented ethanol from modifying channel dwell times, namely that CLR prevented ethanol effect on long closure events [63]. Thus, it has been proposed that CLR and ethanol may share common pathway(s) in regulating BK channel activity, with these pathways not requiring the presence of complex cytoarchitecture or proteolipid domain organization.

Modifications in the membrane lipid profile qualitatively changed the pattern of CLR control over the effect of ethanol on the BK channel. In particular, hslo1 protein incorporation into a DOPE:sphingomyelin (SPM) (3:2 molar ratio) bilayer rendered an ethanol-induced increase in the channel's open probability in the presence of <20 mol% CLR. Higher CLR levels, on the other hand, resulted in ethanol-induced BK channel inhibition. Such a complex profile of ethanol effect on BK currents in a bilayer-forming lipid mixture as a function of the concentration of CLR has been linked to a modification in the bilayer thickness [82]. SPM-containing bilayers are of particular interest, as CLR and SPM form lipid microdomains that model lipid raft behavior of native membranes [107–110]. Ent-CLR at either low (20 mol%) or high (40 mol%) concentrations in the lipid mixture failed to modulate the effect of ethanol on the BK channel when compared to natural CLR [82]. In summary, data from artificial lipid bilayers led to the conclusion that although the CLR modification of the effect of ethanol on the BK channel is tuned by the surrounding lipids, there is very likely a protein site that could sense CLR but not ent-CLR in controlling the channel's ethanol sensitivity.

An additional layer of complexity is introduced by the BK channel accessory beta1 subunit. In beta1 subunit-containing BK channels, ethanol-induced activation was only seen at low micromolar calcium levels, while ethanol-driven inhibition could be observed when calcium exceeded 2 μM [106]. Indeed, application of 50 mM ethanol to rat or mouse cerebral artery myocyte BK channels for 3–10 min resulted in a significant decrease in the open probability of the channel [65, 111]. Moreover, ethanol-induced inhibition of the beta1-containing BK channel could not be observed in CLR-free bilayers or upon CLR depletion by MβCD from membrane patches excised from freshly isolated cerebral artery myocytes [65]. Such depletion decreased CLR level by 50% [65].

Surprisingly, rat or mouse cerebral artery myocyte enrichment with CLR using different carriers (either MβCD or LDL-CLR) also blunted ethanol-induced BK channel inhibition (Fig. 4a, b) [67]. In this case, the CLR-enriching treatment increased the CLR levels up to 1.5 times on an average compared to control [59, 65, 67]. Thus, CLR represents a critical component in ethanol sensitivity of the beta1 subunit-containing BK channel: there is an optimal level of CLR that supports ethanol effect on BK current. While ent-CLR in lipid bilayers largely failed to modulate open probability [91] and ethanol sensitivity [82] of homotetrameric BK channels, enrichment of rat cerebral artery myocytes with ent-CLR resulted in blunting of the ethanol effect on BK currents (Fig. 4c). This effect was similar to the action of natural CLR (Fig. 4b, c) [67].

The difference between ent-CLR action on BK ethanol sensitivity in bilayers versus native membranes may be due to several key differences between these experimental settings. First, the differences observed in ent-CLR action on ethanol

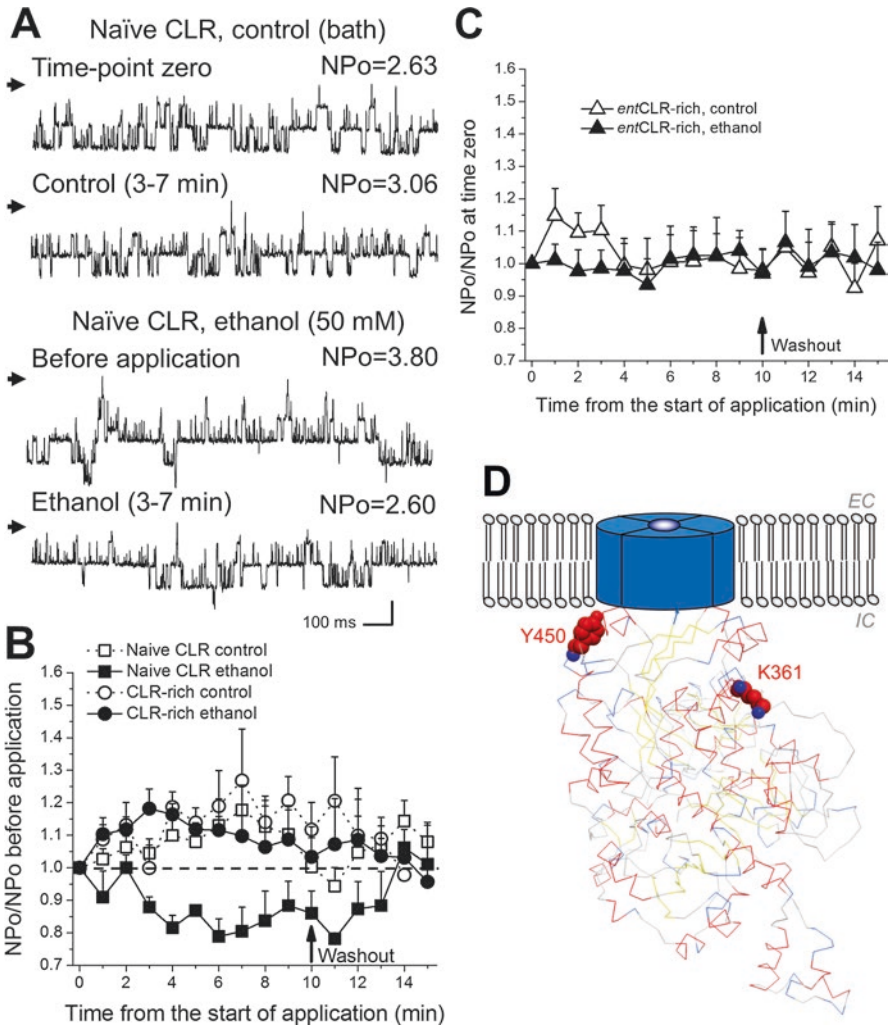

Fig. 4 CLR and ent-CLR similarly protect against ethanol-induced BK channel inhibition in membrane patches from rat cerebral artery myocytes. (**a**) Original records demonstrating ethanol-induced inhibition of BK currents in membrane patches excised from cerebral artery myocytes of rat. Arrows point at baseline (all channels are closed). Recordings were performed with 30 μM calcium bathing the intracellular membrane leaflet; the transmembrane voltage was set at −40 mV. (**b**) Averaged changes in BK channel open probability (NPo) over time in myocyte membrane excised patches from middle cerebral artery myocytes of rat suggesting CLR protection against ethanol-induced BK channel inhibition. Here and in (**c**), "Control" refers to application of patch-clamp recording bath solution; "Ethanol" refers to application of 50 mM ethanol in the bath solution. Washout was performed with a patch-clamp recording bath solution. (**c**) Averaged changes in the BK channel open probability (NPo) over time in myocyte membrane excised patches from ent-CLR-enriched middle cerebral arteries of rat. Panels (**a**–**c**) were originally published in [67]. (**d**) Relative location of individual amino acids lysine 361 and tyrosine 450 on BK channel alpha subunit protein CTD that have been implicated in ethanol and CLR sensitivity, respectively [100, 113]

sensitivity of BK currents may arise from differences in amino acid sequence between the rat cerebral artery myocyte BK alpha subunit protein (cbv1) and the hslo1 cloned from human brain used in the studies with the DOPE:SPM (3:2 molar ratio) lipid bilayers. This scenario is unlikely as cbv1 and hslo1 share >99% identity in their CTD amino acid sequences. It is noteworthy that ent-CLR failed to modulate BK current generated by cbv1 [91] and hslo1 [82]. Thus, the differential effect of CLR and ent-CLR on ethanol sensitivity is dissociated from the ent-CLR effect on the channel's basal function. Of note, alcohol- and CLR-sensing sites in slo1 proteins appear to be spatially separated in the folded alpha subunit CTD (Fig. 4d). If such separation indeed exists, it would favor the idea that CLR (and ent-CLR) modulation of BK ethanol sensitivity involves third-party mechanisms and/or additional channel regions that link steroid and alcohol sensing.

These mechanisms may involve modulation by membrane lipid composition including the presence of BK channel modulatory proteins. BK channels in patches excised from cerebral artery myocytes contain functional beta1 subunits [16, 106]. Thus, the presence of this subunit could constitute a critical factor contributing to the differential profile of the sensitivities of BK currents to CLR versus ent-CLR and to ethanol-induced modulation of BK channels in artificial bilayers versus native membranes. Notably, the BK beta1 subunit contains two CRAC domains in its sequence. The role of these domains in CLR control over ethanol sensitivity of the beta1 subunit-containing BK channel is currently under study in our group.

Using a rat model of high-CLR diet, our group has established that high-CLR dietary intake significantly increased CLR levels within the cerebral artery, and thus protected against ethanol-induced constriction of cerebral vessels in vitro and in vivo [59]. Conceivably, widely prescribed CLR-lowering atorvastatin removed excessive CLR from cerebral arteries and restored arterial sensitivity to the constrictive effect of ethanol [60]. The consequences of CLR modulation of BK channel's alcohol sensitivity in organs other than cerebral vessels remain unknown.

6 Conclusions

An overview of the current literature shows that despite several decades of studies into the modulation of BK channel function by CLR, our knowledge about both the phenomenology and the underlying mechanisms of such modulation is far from complete. First, in an overly simplified system that includes the BK alpha subunit protein incorporated into two species-phospholipid bilayer, there is a multitude of possible CLR-recognition sites presented by CRAC motifs and perhaps others yet to be determined. The individual contribution of each motif to the overall effect of CLR on BK currents remains to be established. Second, the phenomenology of CLR effect on BK current is diverse, with both current activation and inhibition by CLR being reported. Thus, systematic studies are needed to further elucidate the causes of this diversity. Third, the recent discovery of an accessory gamma subunit in the BK complex raises the question of a possible contribution of this subunit to CLR

effect on BK currents. Last but not least, the ability of a high-CLR diet and statin therapy to modulate the effect of a widely used drug such as alcohol via modulation of CLR content in target organs (i.e., the cerebral artery) sets a precedent for further investigation of the ability of CLR level manipulation to modulate BK channel-dependent physiological processes.

The use of CLR isomers and structural analogs will help to shed light on the variegated roles played by CLR in tuning the functional and pharmacological profile of the BK channel complex. Further studies are necessary to unveil mechanisms and structural requirements for CLR modulation of BK currents at all levels of resolution spanning from atomistic to organismal.

Acknowledgements This work was supported by National Institute of Alcohol Abuse and Alcoholism and National Heart and Lung Institute grants R37 AA11560 (AMD), R01 HL104631 (AMD), and R01 AA023764 (ANB).

References

1. Salkoff L, Butler A, Ferreira G, Santi C, Wei A. High-conductance potassium channels of the SLO family. Nat Rev Neurosci. 2006;7(12):921–31.
2. Lee US, Cui J. BK channel activation: structural and functional insights. Trends Neurosci. 2010;33(9):415–23.
3. Meera P, Wallner M, Song M, Toro L. Large conductance voltage- and calcium-dependent K^+ channel, a distinct member of voltage-dependent ion channels with seven N-terminal transmembrane segments (S0-S6), an extracellular N terminus, and an intracellular (S9-S10) C terminus. Proc Natl Acad Sci U S A. 1997;94(25):14066–71.
4. Koval OM, Fan Y, Rothberg BS. A role for the S0 transmembrane segment in voltage-dependent gating of BK channels. J Gen Physiol. 2007;129(3):209–20.
5. Liu G, Zakharov SI, Yao Y, Marx SO, Karlin A. Positions of the cytoplasmic end of BK α S0 helix relative to S1-S6 and of β1 TM1 and TM2 relative to S0-S6. J Gen Physiol. 2015;145(3):185–99.
6. Hite RK, Tao X, Mac Kinnon R. Structural basis for gating the high-conductance Ca^{2+}-activated K^+ channel. Nature. 2017;541(7635):52–7.
7. Yang H, Hu L, Shi J, Cui J. Tuning magnesium sensitivity of BK channels by mutations. Biophys J. 2006;91(8):2892–900.
8. Chen RS, Geng Y, Magleby KL. $Mg^{(2+)}$ binding to open and closed states can activate BK channels provided that the voltage sensors are elevated. J Gen Physiol. 2011;138(6):593–607.
9. Miranda P, Giraldez T, Holmgren M. Interactions of divalent cations with calcium binding sites of BK channels reveal independent motions within the gating ring. Proc Natl Acad Sci U S A. 2016;113(49):14055–60.
10. Meredith A. Genetic methods for studying ion channel function in physiology and disease. In: Zheng J, Trudeau MC, editors. Handbook of ion channels. Boca Raton: CRC Press; 2015. p. 165–86.
11. Shipston MJ, Tian L. Posttranscriptional and posttranslational regulation of BK channels. Int Rev Neurobiol. 2016;128:91–126.
12. Latorre R, Castillo K, Carrasquel-Ursulaez W, Sepulveda RV, Gonzalez-Nilo F, Gonzalez C, et al. Molecular determinants of BK channel functional diversity and functioning. Physiol Rev. 2017;97(1):39–87.
13. Orio P, Rojas P, Ferreira G, Latorre R. New disguises for an old channel: MaxiK channel beta-subunits. News Physiol Sci. 2002;17:156–61.

14. Behrens R, Nolting A, Reimann F, Schwarz M, Waldschütz R, Pongs O. hKCNMB3 and hKCNMB4, cloning and characterization of two members of the large-conductance calcium-activated potassium channel beta subunit family. FEBS Lett. 2000;474(1):99–106.
15. Brenner R, Jegla TJ, Wickenden A, Liu Y, Aldrich RW. Cloning and functional characterization of novel large conductance calcium-activated potassium channel beta subunits, hKCNMB3 and hKCNMB4. J Biol Chem. 2000;275(9):6453–61.
16. Brenner R, Peréz GJ, Bonev AD, Eckman DM, Kosek JC, Wiler SW, et al. Vasoregulation by the beta1 subunit of the calcium-activated potassium channel. Nature. 2000;407(6806):870–6.
17. Contet C, Goulding SP, Kuljis DA, Barth AL. BK channels in the central nervous system. Int Rev Neurobiol. 2016;128:281–342.
18. Li Q, Yan J. Modulation of BK channel function by auxiliary beta and gamma subunits. Int Rev Neurobiol. 2016;128:51–90.
19. Bukiya AN, Liu J, Toro L, Dopico AM. Beta1 (KCNMB1) subunits mediate lithocholate activation of large-conductance Ca^{2+}-activated K^+ channels and dilation in small, resistance-size arteries. Mol Pharmacol. 2007;72(2):359–69.
20. Bukiya AN, McMillan J, Liu J, Shivakumar B, Parrill AL, Dopico AM. Activation of calcium- and voltage-gated potassium channels of large conductance by leukotriene B4. J Biol Chem. 2014;289(51):35314–25.
21. Bukiya AN, McMillan JE, Fedinec AL, Patil SA, Miller DD, Leffler CW, et al. Cerebrovascular dilation via selective targeting of the cholane steroid-recognition site in the BK channel β1-subunit by a novel nonsteroidal agent. Mol Pharmacol. 2013;83(5):1030–44.
22. Bukiya AN, Singh AK, Parrill AL, Dopico AM. The steroid interaction site in transmembrane domain 2 of the large conductance, voltage- and calcium-gated potassium (BK) channel accessory β1 subunit. Proc Natl Acad Sci U S A. 2011;108(50):20207–12.
23. Bukiya AN, Vaithianathan T, Toro L, Dopico AM. Channel beta2-4 subunits fail to substitute for beta1 in sensitizing BK channels to lithocholate. Biochem Biophys Res Commun. 2009;390(3):995–1000.
24. Hu S, Labuda MZ, Pandolfo M, Goss GG, McDermid HE, Ali DW. Variants of the KCNMB3 regulatory subunit of maxi BK channels affect channel inactivation. Physiol Genomics. 2003;15(3):191–8.
25. Wang B, Jaffe DB, Brenner R. Current understanding of iberiotoxin-resistant BK channels in the nervous system. Front Physiol. 2014;5:382.
26. Yan J, Aldrich RW. BK potassium channel modulation by leucine-rich repeat-containing proteins. Proc Natl Acad Sci U S A. 2012;109(20):7917–22.
27. Vandael DH, Marcantoni A, Mahapatra S, Caro A, Ruth P, Zuccotti A, et al. Ca(v)1.3 and BK channels for timing and regulating cell firing. Mol Neurobiol. 2010;42(3):185–98.
28. Ge L, Hoa NT, Wilson Z, Arismendi-Morillo G, Kong XT, Tajhya RB, et al. Potassium (BK) ion channels in biology, disease and possible targets for cancer immunotherapy. Int Immunopharmacol. 2014;22(2):427–43.
29. Duncan PJ, Shipston MJ. BK channels and the control of the pituitary. Int Rev Neurobiol. 2016;128:343–68.
30. Pyott SJ, Duncan RK. BK channels in the vertebrate inner ear. Int Rev Neurobiol. 2016;128:369–99.
31. Whitt JP, Montgomery JR, Meredith AL. BK channel inactivation gates daytime excitability in the circadian clock. Nat Commun. 2016;7:10837.
32. Dopico AM, Bukiya AN, Jaggar JH. Calcium- and voltage-gated BK channels in vascular smooth muscle. Pflugers Arch. 2018;470(9):1271–89.
33. Dopico A.M., Bukiya A.N., Bettinger J.C. (2017) Voltage-Sensitive Potassium Channels of the BK Type and Their Coding Genes Are Alcohol Targets in Neurons. In: Handbook of Experimental Pharmacology. Springer, Berlin, Heidelberg.
34. Li B, Gao TM. Functional role of mitochondrial and nuclear BK channels. Int Rev Neurobiol. 2016;128:163–91.

35. Singh H, Stefani E, Toro L. Intracellular $BK_{(Ca)}$ ($iBK_{(Ca)}$) channels. J Physiol. 2012;590(23):5937–47.
36. Gu XQ, Pamenter ME, Siemen D, Sun X, Haddad GG. Mitochondrial but not plasmalemmal BK channels are hypoxia-sensitive in human glioma. Glia. 2014;62(4):504–13.
37. Leanza L, Venturini E, Kadow S, Carpinteiro A, Gulbins E, Becker KA. Targeting a mitochondrial potassium channel to fight cancer. Cell Calcium. 2015;58(1):131–8.
38. Balderas E, Zhang J, Stefani E, Toro L. Mitochondrial BK_{Ca} channel. Front Physiol. 2015;6:104.
39. Goldklang MP, Perez-Zoghbi JF, Trischler J, Nkyimbeng T, Zakharov SI, Shiomi T, et al. Treatment of experimental asthma using a single small molecule with anti-inflammatory and BK channel-activating properties. FASEB J. 2013;27(12):4975–86.
40. Joseph BK, Thakali KM, Moore CL, Rhee SW. Ion channel remodeling in vascular smooth muscle during hypertension: implications for novel therapeutic approaches. Pharmacol Res. 2013;70(1):126–38.
41. Bentzen BH, Olesen SP, Rønn LC, Grunnet M. BK channel activators and their therapeutic perspectives. Front Physiol. 2014;5:389.
42. Hu G, Antikainen R, Jousilahti P, Kivipelto M, Tuomilehto J. Total cholesterol and the risk of Parkinson disease. Neurology. 2008;70:1972–9.
43. Bui QT, Prempeh M, Wilensky RL. Atherosclerotic plaque development. Int J Biochem Cell Biol. 2009;41:2109–13.
44. Granger DN, Rodrigues SF, Yildirim A, Senchenkova EY. Microvascular responses to cardiovascular risk factors. Microcirculation. 2010;17:192–205.
45. Miller AA, Budzyn K, Sobey CG. Vascular dysfunction in cerebrovascular disease: mechanisms and therapeutic intervention. Clin Sci (Lond). 2010;119:1–17.
46. Jacobs D. Report of the conference on low blood cholesterol: mortality associations. Circulation. 1992;86:1046–60.
47. Stachon A, Böning A, Weisser H, Laczkovics A, Skipka G, Krieg M. Prognostic significance of low serum cholesterol after cardiothoracic surgery. Clin Chem. 2000;46:1114–20.
48. Dunham CM, Fealk MH, Sever WE III. Following severe injury, hypocholesterolemia improves with convalescence but persists with organ failure or onset of infection. Crit Care. 2003;7:R145–53.
49. Guimarães SM, Lima EQ, Cipullo JP, Lobo SM, Burdmann EA. Low insulin-like growth factor-1 and hypocholesterolemia as mortality predictors in acute kidney injury in the intensive care unit. Crit Care Med. 2008;36:3165–70.
50. Vyroubal P, Chiarla C, Giovannini I, Hyspler R, Ticha A, Hrnciarikova D, et al. Hypocholesterolemia in clinically serious conditions–review. Biomed Pap Med Fac Univ Palacky Olomouc Czech Repub. 2008;152:181–9.
51. Bolotina V, Omelyanenko V, Heyes B, Ryan U, Bregestovski P. Variations of membrane cholesterol alter the kinetics of Ca^{2+}-dependent K^+ channels and membrane fluidity in vascular smooth muscle cells. Pflugers Arch. 1989;415:262–8.
52. Dopico AM, Bukiya AN, Singh AK. Large conductance, calcium- and voltage-gated potassium (BK) channels: regulation by cholesterol. Pharmacol Ther. 2012;135(2):133–50.
53. Wiecha J, Schläger B, Voisard R, Hannekum A, Mattfeldt T, Hombach V. Ca^{2+}-activated K^+ channels in human smooth muscle cells of coronary atherosclerotic plaques and coronary media segments. Basic Res Cardiol. 1997;92:233–9.
54. Sobey CG. Potassium channel function in vascular disease. Arterioscler Thromb Vasc Biol. 2001;21:28–38.
55. Chan J, Karere G, Cox L, VandeBerg J. Animal models of diet-induced hypercholesterolemia. In: Kumar SA, editor. Hypercholesterolemia. Den Haag: INTECH; 2015. p. 3–31.
56. Bukiya A, Rosenhouse-Dantsker A. Hypercholesterolemia effect on potassium channels. In: Kumar SA, editor. Hypercholesterolemia. Den Haag: INTECH; 2015. p. 95–119.
57. Jeremy RW, McCarron H. Effect of hypercholesterolemia on Ca^{2+}-dependent K^+ channel-mediated vasodilatation in vivo. Am J Physiol Heart Circ Physiol. 2000;279:H1600–8.

58. Najibi S, Cohen RA. Enhanced role of K^+ channels in relaxations of hypercholesterolemic rabbit carotid artery to NO. Am J Phys. 1995;269(3 Pt 2):H805–11.
59. Bukiya A, Dopico AM, Leffler CW, Fedinec A. Dietary cholesterol protects against alcohol-induced cerebral artery constriction. Alcohol Clin Exp Res. 2014;38(5):1216–26.
60. Simakova MN, Bisen S, Dopico AM, Bukiya AN. Statin therapy exacerbates alcohol-induced constriction of cerebral arteries via modulation of ethanol-induced BK channel inhibition in vascular smooth muscle. Biochem Pharmacol. 2017;145:81–93.
61. Du P, Cui GB, Wang YR, Zhang XY, Ma KJ, Wei JG. Down regulated expression of the beta1 subunit of the big-conductance Ca^{2+} sensitive K^+ channel in sphincter of Oddi cells from rabbits fed with a high cholesterol diet. Acta Biochim Biophys Sin Shanghai. 2006;38(12):893–9.
62. Chang HM, Reitstetter R, Mason RP, Gruener R. Attenuation of channel kinetics and conductance by cholesterol: an interpretation using structural stress as a unifying concept. J Membr Biol. 1995;143:51–63.
63. Crowley JJ, Treistman SN, Dopico AM. Cholesterol antagonizes ethanol potentiation of human brain BK_{Ca} channels reconstituted into phospholipid bilayers. Mol Pharmacol. 2003;64(2):365–72.
64. Bukiya AN, Vaithianathan T, Toro L, Dopico AM. The second transmembrane domain of the large conductance, voltage- and calcium-gated potassium channel beta(1) subunit is a lithocholate sensor. FEBS Lett. 2008;582(5):673–8.
65. Bukiya AN, Vaithianathan T, Kuntamallappanavar G, Asuncion-Chin M, Dopico AM. Smooth muscle cholesterol enables BK β1 subunit-mediated channel inhibition and subsequent vasoconstriction evoked by alcohol. Arterioscler Thromb Vasc Biol. 2011;31:2410–23.
66. Zidovetzki R, Levitan I. Use of cyclodextrins to manipulate plasma membrane cholesterol content: evidence, misconceptions and control strategies. Biochim Biophys Acta. 2007;1768(6):1311–24.
67. Bisen S, Seleverstov O, Belani J, Rychnovsky S, Dopico AM, Bukiya AN. Distinct mechanisms underlying cholesterol protection against alcohol-induced BK channel inhibition and resulting vasoconstriction. Biochim Biophys Acta. 2016;1861(11):1756–66.
68. Bregestovski PD, Bolotina VN. Membrane fluidity and kinetics of Ca^{2+}-dependent potassium channels. Biomed Biochim Acta. 1989;48:S382–7.
69. Brainard AM, Miller AJ, Martens JR, England SK. Maxi-K channels localize to caveolae in human myometrium: a role for an actin-channel-caveolin complex in the regulation of myometrial smooth muscle K+ current. Am J Physiol Cell Physiol. 2005;289:C49–57.
70. Tajima N, Itokazu Y, Korpi ER, Somerharju P, Käkelä R. Activity of $BK_{(Ca)}$ channel is modulated by membrane cholesterol content and association with Na^+/K^+-ATPase in human melanoma IGR39 cells. J Biol Chem. 2011;286:5624–38.
71. Weaver AK, Olsen ML, McFerrin MB, Sontheimer H. BK channels are linked to inositol 1,4,5-triphosphate receptors via lipid rafts: a novel mechanism for coupling $[Ca^{2+}]_i$ to ion channel activation. J Biol Chem. 2007;282:31558–68.
72. Wang XL, Ye D, Peterson TE, Cao S, Shah VH, Katusic ZS, et al. Caveolae targeting and regulation of large conductance Ca^{2+}-activated K^+ channels in vascular endothelial cells. J Biol Chem. 2005;280:11656–64.
73. Shmygol A, Noble K, Wray S. Depletion of membrane cholesterol eliminates the Ca^{2+}-activated component of outward potassium current and decreases membrane capacitance in rat uterine myocytes. J Physiol. 2007;581(Pt 2):445–56.
74. Babiychuk EB, Smith RD, Burdyga T, Babiychuk VS, Wray S, Draeger A. Membrane cholesterol regulates smooth muscle phasic contraction. J Membr Biol. 2004;198:95–101.
75. Prendergast C, Quayle J, Burdyga T, Wray S. Cholesterol depletion alters coronary artery myocyte Ca^{2+} signalling in a stimulus-specific manner. Cell Calcium. 2010;47:84–91.
76. Lin MW, Wu AZ, Ting WH, Li CL, Cheng KS, Wu SN. Changes in membrane cholesterol of pituitary tumor (GH3) cells regulate the activity of large-conductance Ca^{2+}-activated K^+ channels. Chin J Physiol. 2006;49:1–13.
77. Lam RS, Shaw AR, Duszyk M. Membrane cholesterol content modulates activation of BK channels in colonic epithelia. Biochim Biophys Acta. 2004;1667:241–8.

78. Purcell EK, Liu L, Thomas PV, Duncan RK. Cholesterol influences voltage-gated calcium channels and BK-type potassium channels in auditory hair cells. PLoS One. 2011;6:e26289.
79. Sones WR, Davis AJ, Leblanc N, Greenwood IA. Cholesterol depletion alters amplitude and pharmacology of vascular calcium-activated chloride channels. Cardiovasc Res. 2010;87:476–84.
80. Bravo-Zehnder M, Orio P, Norambuena A, Wallner M, Meera P, Toro L, et al. Apical sorting of a voltage- and Ca^{2+}-activated K^+ channel alpha -subunit in Madin-Darby canine kidney cells is independent of N-glycosylation. Proc Natl Acad Sci U S A. 2000;97:13114–9.
81. Alioua A, Lu R, Kumar Y, Eghbali M, Kundu P, Toro L, et al. Slo1 caveolin-binding motif, a mechanism of caveolin-1-Slo1 interaction regulating Slo1 surface expression. J Biol Chem. 2008;283(8):4808–17.
82. Yuan C, Chen M, Covey DF, Johnston LJ, Treistman SN. Cholesterol tuning of BK ethanol response is enantioselective, and is a function of accompanying lipids. PLoS One. 2011;6:e27572.
83. King JT, Lovell PV, Rishniw M, Kotlikoff MI, Zeeman ML, McCobb DP. Beta2 and beta4 subunits of BK channels confer differential sensitivity to acute modulation by steroid hormones. J Neurophysiol. 2006;95:2878–88.
84. Gennis RB. Biomembranes: molecular structure and function. New York: Springer; 1989.
85. Sackmann E. Biological membranes architecture and function. In: Lypowsky R, Sackmann E, editors. Structure and dynamics of membranes. Amsterdam: Elsevier; 1995. p. 1–63.
86. Lis LJ, McAlister M, Fuller N, Rand RP, Parsegian VA. Measurement of the lateral compressibility of several phospholipid bilayers. Biophys J. 1982;37(3):667–72.
87. Starke-Peterkovic T, Turner N, Vitha MF, Waller MP, Hibbs DE, Clarke RJ. Cholesterol effect on the dipole potential of lipid membranes. Biophys J. 2006;90(11):4060–70.
88. Heiner AL, Gibbons E, Fairbourn JL, Gonzalez LJ, McLemore CO, Brueseke TJ, et al. Effects of cholesterol on physical properties of human erythrocyte membranes: impact on susceptibility to hydrolysis by secretory phospholipase A2. Biophys J. 2008;94:3084–93.
89. Molugu TR, Brown MF. Cholesterol-induced suppression of membrane elastic fluctuations at the atomistic level. Chem Phys Lipids. 2016;199:39–51.
90. Alobeedallah H, Cornell B, Coster H. The effect of cholesterol on the dielectric structure of lipid bilayers. J Membr Biol. 2018;251(1):153–61.
91. Bukiya AN, Belani JD, Rychnovsky S, Dopico AM. Specificity of cholesterol and analogs to modulate BK channels points to direct sterol-channel protein interactions. J Gen Physiol. 2011;137(1):93–110.
92. Alakoskela J, Sabatini K, Jiang X, Laitala V, Covey DF, Kinnunen PK. Enantiospecific interactions between cholesterol and phospholipids. Langmuir. 2008;24(3):830–6.
93. Crowder CM, Westover EJ, Kumar AS, Ostlund RE Jr, Covey DF. Enantiospecificity of cholesterol function in vivo. J Biol Chem. 2001;276:44369–72.
94. Romanenko VG, Rothblat GH, Levitan I. Modulation of endothelial inward-rectifier K^+ current by optical isomers of cholesterol. Biophys J. 2002;83:3211–22.
95. Westover EJ, Covey DF. The enantiomer of cholesterol. J Membr Biol. 2004;202:61–72.
96. Xu X, London E. The effect of sterol structure on membrane lipid domains reveals how cholesterol can induce lipid domain formation. Biochemistry. 2000;39:843–9.
97. Le Goff G, Vitha MF, Clarke RJ. Orientational polarisability of lipid membrane surfaces. Biochim Biophys Acta. 2007;1768:562–70.
98. Epand RM. Cholesterol and the interaction of proteins with membrane domains. Prog Lipid Res. 2006;45(4):279–94.
99. Fantini J, Di Scala C, Baier CJ, Barrantes FJ. Molecular mechanisms of protein-cholesterol interactions in plasma membranes: functional distinction between topological (tilted) and consensus (CARC/CRAC) domains. Chem Phys Lipids. 2016;199:52–60.
100. Singh AK, McMillan J, Bukiya AN, Burton B, Parrill AL, Dopico AM. Multiple cholesterol recognition/interaction amino acid consensus (CRAC) motifs in cytosolic C tail of Slo1 subunit determine cholesterol sensitivity of Ca^{2+}- and voltage-gated K^+ (BK) channels. J Biol Chem. 2012;287(24):20509–21.

101. Yuan P, Leonetti MD, Pico AR, Hsiung Y, MacKinnon R. Structure of the human BK channel Ca^{2+}-activation apparatus at 3.0 Å resolution. Science. 2010;329(5988):182–6.
102. Chu B, Dopico AM, Lemos JR, Treistman SN. Ethanol potentiation of calcium-activated potassium channels reconstituted into planar lipid bilayers. Mol Pharmacol. 1998;54(2):397–406.
103. Dopico AM, Lemos JR, Treistman SN. Ethanol increases the activity of large conductance, $Ca^{(2+)}$-activated K^+ channels in isolated neurohypophysial terminals. Mol Pharmacol. 1996;49(1):40–8.
104. Dopico AM, Anantharam V, Treistman SN. Ethanol increases the activity of $Ca^{(++)}$-dependent K^+ (mslo) channels: functional interaction with cytosolic Ca^{++}. J Pharmacol Exp Ther. 1998;284(1):258–68.
105. Liu J, Vaithianathan T, Manivannan K, Parrill A, Dopico AM. Ethanol modulates BK_{Ca} channels by acting as an adjuvant of calcium. Mol Pharmacol. 2008;74(3):628–40.
106. Bukiya AN, Liu J, Dopico AM. The BK channel accessory beta1 subunit determines alcohol-induced cerebrovascular constriction. FEBS Lett. 2009;583(17):2779–84.
107. London E. Insights into lipid raft structure and formation from experiments in model membranes. Curr Opin Struct Biol. 2002;12:480–6.
108. London E. How principles of domain formation in model membranes may explain ambiguities concerning lipid raft formation in cells. Biochim Biophys Acta. 2005;1746:203–20.
109. Yuan C, Furlong J, Burgos P, Johnston LJ. The size of lipid rafts: an atomic force microscopy study of ganglioside GM1 domains in sphingomyelin/DOPC/cholesterol membranes. Biophys J. 2002;82:2526–35.
110. Johnston LJ. Nanoscale imaging of domains in supported lipid membranes. Langmuir. 2007;23:5886–95.
111. Liu P, Xi Q, Ahmed A, Jaggar JH, Dopico AM. Essential role for smooth muscle BK channels in alcohol-induced cerebrovascular constriction. Proc Natl Acad Sci U S A. 2004;101(52):18217–22.
112. Gonzalez-Perez V, Xia XM, Lingle CJ. Two classes of regulatory subunits coassemble in the same BK channel and independently regulate gating. Nat Commun. 2015;6:8341.
113. Bukiya AN, Kuntamallappanavar G, Edwards J, Singh AK, Shivakumar B, Dopico AM. An alcohol-sensing site in the calcium- and voltage-gated, large conductance potassium (BK) channel. Proc Natl Acad Sci U S A. 2014;111(25):9313–8.

Chiral Specificity of Cholesterol Orientation Within Cholesterol Binding Sites in Inwardly Rectifying K^+ Channels

Nicolas Barbera and Irena Levitan

Abstract Cholesterol is an integral component of cellular membranes and has been shown to be an important functional regulator for many different ion channels, including inwardly rectifying potassium (Kir) channels. Consequently, understanding the molecular mechanisms underlying this regulation represents a critical field of study. Broadly speaking, cholesterol can mediate ion channel function either directly by binding to specific sites or indirectly by altering surrounding membrane properties. Owing to the similar effects of cholesterol and its chiral isomers (epicholesterol and ent-cholesterol) on membrane properties, comparative analysis of these sterols can be an effective tool for discriminating between these direct and indirect effects. Indeed, this strategy was used to demonstrate the direct effect of cholesterol on Kir channel function. However, while this approach can discriminate between direct and indirect effects, it does not account for the promiscuity of cholesterol binding sites, which can potentially accommodate cholesterol *or* its chiral isomers. In this chapter, we use docking analyses to explore the idea that the specificity of cholesterol's effect on Kir channels is dependent on the specific orientation of cholesterol within its putative binding pocket which its chiral isomers cannot replicate, even when bound themselves.

Keywords Kir channels · Cholesterol binding · Cholesterol stereoisomers

1 Introduction

A crucial feature of many organic molecules is the specific geometric arrangement of their constituent atoms with respect to molecular symmetry. This feature arises from the tendency of carbon atoms to form bonds arranged tetrahedrally and means that, depending on the different moieties bond to a given carbon atom, even very

N. Barbera · I. Levitan (✉)
Division of Pulmonary and Critical Care, Department of Medicine,
University of Illinois at Chicago, Chicago, IL, USA
e-mail: levitan@uic.edu

A. Rosenhouse-Dantsker, A. N. Bukiya (eds.), *Cholesterol Modulation of Protein Function*, Advances in Experimental Medicine and Biology 1115,
https://doi.org/10.1007/978-3-030-04278-3_4

simple molecules with identical chemical formulas can adopt structurally distinct geometries, called stereoisomers. The importance of these different arrangements is that stereoisomers cannot be superimposed on one another and represent unique, separate molecules in their own right with distinct chemical and physical properties. In biological systems, specific ligand–protein interactions are typically stereo-specific, meaning that the functional interaction occurs only with a specific isomer but not with its chiral analogue. In contrast, non-specific interactions are typically not stereo-sensitive. Multiple studies, therefore, use comparative analysis of stereo-isomers to determine the specificity of the particular interaction between proteins and different ligands.

In the last two decades, several groups including ours pioneered this approach to discriminate between two general mechanisms of cholesterol regulation of ion channels: specific sterol–protein interactions and regulation of channel function by changes in the physical properties of the lipid bilayer [1–5]. The rationale of this approach is that cholesterol stereoisomers have similar effects on the physical properties of the membrane bilayer but are expected to be strongly distinct in their ability to interact with the proteins via specific sterol–protein interactions. It is important to note, however, that as discussed below, these assumptions are not always correct. First, it must be acknowledged that while stereoisomers are identical in an achiral environment, cholesterol interactions with phospholipids have a degree of stereo-specificity, which may affect their impact on the physical properties of the lipid bilayer [6, 7]. Extensive studies, however, documented how cholesterol stereoisomers affect the properties of the lipid bilayer and found that the differences are rather minor [8, 9]. It also became clear that a specific interaction of cholesterol with a channel protein is not always stereo-specific, as some channels have "lax" cholesterol binding sites that can accommodate not only cholesterol but also its chiral isomers, as was shown for nicotinic acetylcholine receptor (nAChR) [2]. Thus, while the stereo-specificity of cholesterol's effect on a channel provides strong evidence for a specific sterol–protein interaction, a lack of stereo-specificity does not exclude this possibility. Furthermore, *our studies provide an increasing amount of evidence for a new possibility: a cholesterol binding site that has lax binding requirements, accommodating both cholesterol and its isomers, but a stereo-specific orientation of the isomers within the binding site which leads to a stereo-specific functional effect*.

Our studies focus on elucidating the mechanism of cholesterol regulation of inwardly rectifying K^+ channels. Inwardly rectifying K^+ channels (Kir) form a major class of K^+ channels responsible for the maintenance of membrane potential and K^+ homeostasis in multiple cell types [10–12]. Most of our studies focused on Kir2 channels, a major sub-family of Kir, that are ubiquitously expressed in a variety of cell types, including neurons, cardiomyocytes, smooth muscle cells, endothelial cells, and macrophages [13]. Kir2 channels are known to be critically involved in regulating membrane excitability in cardiac and smooth muscle cells [14–16] and neurovascular coupling [17]. Early studies from the Davies group also showed that Kir channels expressed in vascular endothelial cells are sensitive to a mechanical force generated by fluid shear stress [18] leading to the hypothesis that endothelial

Kir channels may be one of the putative shear stress sensors [19]. As expected from their biophysical profiles, endothelial Kir channels were later identified as Kir2.1 and Kir2.2 [20, 21] and our recent studies demonstrated that Kir2.1 channels play a major role in endothelial control of vascular tone via activation of endothelial nitric oxide synthase (eNOS) regulation of NO release [21]. Furthermore, most recently, we established that cholesterol-induced suppression of endothelial Kir2.1 channels has a major impact on vascular function in dyslipidemia: it is responsible for the impairment of flow-induced vasodilation and augments the development of atherosclerosis [22]. It is clearly critical, therefore, to elucidate the molecular basis of cholesterol regulation of these channels.

2 Stereo-Specific Cholesterol Regulation of Kir2 Channels

Structurally, cholesterol (3β-hydroxy-5-cholestene) has a distinct shape composed of an asymmetric tetracyclic ring system with a smooth α-face and a methylated "rough" β-face with a single hydroxyl group oriented toward the β-face. Cholesterol has eight distinct stereocenters, which all inform the chirality of the cholesterol analogue in question. These are located at C3, C8, C9, C10, C13, C14, C17, and C20. The two commonly used chiral isomers of cholesterol are the synthetic analogues epicholesterol (3α-hydroxy-5-cholestene) and ent-cholesterol (enantiomeric cholesterol). Epicholesterol has an almost identical structure to cholesterol, with the sole difference being the placement of its hydroxyl group at the 3α position rather than the 3β position of C3. In contrast, ent-cholesterol is the mirror image of cholesterol with an opposite arrangement at each of the eight stereocenters of cholesterol (Fig. 1). Both analogues constitute powerful tools to elucidate the nature of the molecular interactions between sterols and the channels. It is important to keep in mind, however, that as described in our recent review [23], the difference between the orientation of the stereocenters of epi-cholesterol and ent-cholesterol yields major differences in the 3-dimensional structures of these analogues and their position within the bilayer, a distinction that will become important in our analysis of the interactions of these sterols with the cholesterol binding site in Kir2.2 channels.

Differential effects of cholesterol stereoisomers on ion channels were first discovered for $GABA_A$ receptors [24], a pentameric ligand-gated chloride channel, belonging to the Cys loop ligand-gated ion channel superfamily, which also includes nicotinic acetylcholine receptors and glycine receptors [25]. Similarly to nAChR, depletion of membrane cholesterol resulted in a loss of agonist-dependent opening of $GABA_A$ and in the case of $GABA_A$ this effect was stereo-specific, as repleting cells with epicholesterol failed to support channel function [24]. At the same time, enriching cells with cholesterol also had a detrimental effect on $GABA_A$ function and this effect could be supported by the addition of epicholesterol [24]. The authors concluded that "normal" cholesterol level in the membrane is required to maintain the functionality of $GABA_A$ but that the excess of cholesterol should regulate the

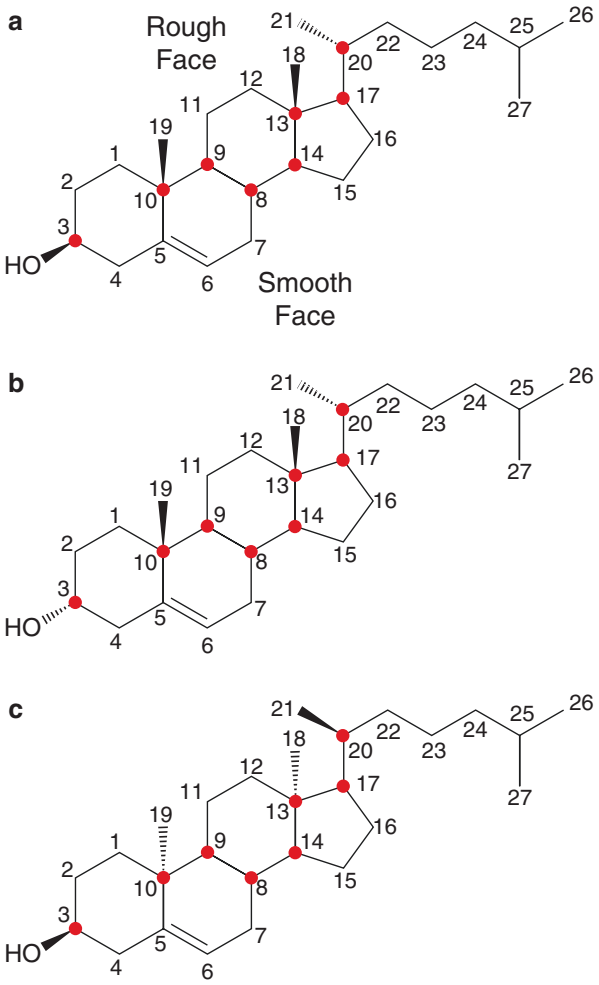

Fig. 1 Cholesterol Chirality. The chemical structures of (**a**) cholesterol, (**b**) epicholesterol, and (**c**) ent-cholesterol are shown with the 27 constituent carbon atoms labeled by number. The *solid wedges* indicate bonds pointing above the plane of the page and *dashed wedges* indicate bonds pointing below the plane of the page. The chiral centers are identified with red dots in each

channels in a non-specific way via changes in membrane fluidity [24]. This conclusion, however, should be challenged in light of later studies of nAChR, another pentameric Cys loop ligand-gated ion channel, where it was shown that cholesterol and epicholesterol can both bind to the channel protein [2]. Thus, while it is clear that cholesterol has a complex effect on $GABA_A$, the contributions of the specific and non-specific effects remained unclear. One of the difficulties in interpreting these observations is the uncertainty about the levels of cholesterol/epicholesterol substitutions in these experiments.

In applying this approach to elucidate the mechanism of cholesterol regulation of Kir2 channels, our first goal was to develop a system to quantitatively substitute native membrane cholesterol with epicholesterol in a mammalian cell. Similarly to previous studies, cells were exposed either to methyl-β-cyclodextrin (MβCD) alone (empty MβCD), MβCD saturated with cholesterol (MβCD-cholesterol) or MβCD saturated with epicholesterol (MβCD-epicholesterol) [1]. The levels of the sterols were quantified using gas-liquid chromatography (GLC). As expected, exposing endothelial cells to empty MβCD resulted in cholesterol depletion and exposing the cells to MβCD-cholesterol resulted in cholesterol enrichment. The degree of cholesterol depletion is highly dependent on MβCD concentration and the duration of the exposure, and could be as high as a 90% decrease (tenfold decrease in free membrane cholesterol). At this level of cholesterol depletion, however, cell viability is jeopardized and in most of our experiments, we maintained the level of cholesterol depletion at 50%. The dynamic range of cholesterol enrichment is significantly smaller than that of cholesterol depletion: exposing cells to MβCD-cholesterol consistently increased the level of cellular cholesterol up to twofold. Prolonging the exposure from 1–2 h, which is a standard protocol, to 24–48 h did not enhance the level of the incorporation suggesting that the system become equilibrated between the membrane and the MβCD-cholesterol shuttle. Also, this range is not unique for endothelial cells, as the same twofold increase was consistently found in cells exposed to MβCD-cholesterol for several other cell types [26–28]. It is important to note that a twofold increase range is specific for the "free cholesterol" or cholesterol that is found in cellular membranes and not applicable for cholesterol-ester, a modification of free cholesterol that can be accumulated in much higher amount inside the cells. Notably, a twofold increase in cellular cholesterol is found not only in cells exposed to MβCD-cholesterol in vitro but also in cells isolated from hypercholesterolemic animals [29].

In terms of cholesterol/epicholesterol substitution, we determined using GLC that while, as expected, cholesterol and epicholesterol peaks overlap, they are distinct enough to discriminate between the two stereoisomers and determine their levels in the cellular lipid extracts (Fig. 2a), [1]. This allowed us not only to verify that epicholesterol is indeed incorporated into the cells but also analyze the relative amounts of epicholesterol and native cholesterol in the same cells. The incorporation of epicholesterol can be detected as a shoulder of the cholesterol peak at low incorporation levels and as a clear second peak when the levels of cholesterol and epicholesterol in the cells are comparable (Fig. 2b). We found that exposing the cells to MβCD-epicholesterol results in an efficient incorporation of epicholesterol and that this incorporation is not in addition to the normal levels of cholesterol but rather there is an exchange of native cholesterol by epicholesterol. The latter finding was not really surprising because as MβCD is a high affinity sterol shuttle [30], it is expected that when MβCD-epicholesterol releases its epicholesterol into the cellular membrane, it can bind to the available cholesterol removing it from the membrane. As a result, we could optimize the conditions of the exposure in such a way that about 50% of native cholesterol was substituted with a similar amount of epicholesterol resulting in the total sterol amount being unchanged.

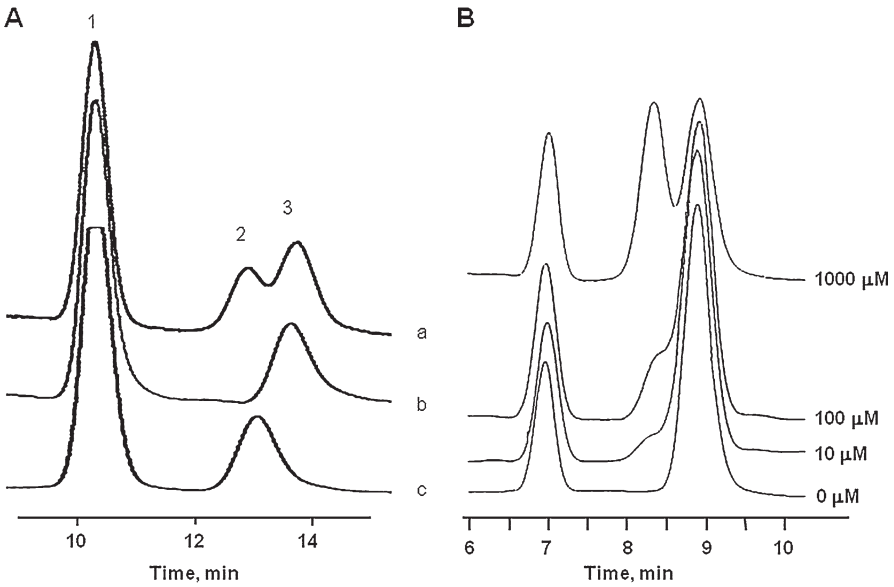

Fig. 2 Chromatographic profiles of cholesterol and epicholesterol in lipid extracts of endothelial cells exposed to MβCD-epicholesterol. Cholesterol and epicholesterol separated and quantified using GLC: peak 1—CME (internal standard), peak 2—epicholesterol, peak 3—cholesterol. (**a**) The chromatographic profiles of: a—lipid extracts of the cells treated with 5 mM MβCD-epicholesterol for 60 min, b—mixture of CME and cholesterol, c—mixture of CME and epicholesterol [1]. (**b**) The chromatographic profiles of lipid extracts of the cells treated with 10, 100 or 1000 μM MβCD-epicholesterol for 60 min

Using this system, we showed that while an increase in membrane cholesterol resulted in a strong suppression of Kir current in these cells, partial substitution of cholesterol by epicholesterol led to an opposite effect and resulted in a strong augmentation of the current [1]. This was surprising first of all because at that time, the prevailing belief was that ion channels should be regulated by cholesterol via non-specific changes in the physical properties of the lipid bilayer, in which case removal of cellular cholesterol and substituting it with a similar amount of epicholesterol should have little or no effect on the currents. The opposite effects of cholesterol and epicholesterol on Kir currents could not be explained by subtle differences in their effects on the physical properties of the bilayer because while not fully identical, the effects of the two sterols on the physical properties of the bilayer are similar and definitely not opposite [8, 9, 23]. We interpreted these findings, therefore, as evidence that cholesterol regulates Kir channels by specific sterol–protein interaction. It is important to note, however, that this observation alone cannot be interpreted as evidence that cholesterol binds directly to the channel, as sometimes is done mistakenly. The specificity of cholesterol regulation of an ion channel or any other protein in the complex milieu of the plasma membrane may also indicate a specific interaction between cholesterol and a regulatory protein, which in turn may affect channel

function. This possibility can be directly addressed only by using purified systems, as was done in our further studies described below. Furthermore, the fact that enriching cells with epicholesterol resulted in an increase in Kir current density, suggested to us that epicholesterol actually competes with cholesterol for a binding site either on the channel itself or on an intermediate regulator. This was one of the first indications that cholesterol regulates ion channels by specific sterol–protein interactions.

Our further studies identified Kir2.1 and Kir2.2 channels as the major components of endothelial Kir current [31] and reconfirmed that both Kir2.1 and Kir2.2 are strongly suppressed by the elevation of membrane cholesterol, whereas two other members of Kir2 family, Kir2.3 and Kir2.4 are less cholesterol sensitive [26]. Overall, cholesterol sensitivity was observed in all Kir families with the predominant effect being suppression of the channel function [32]. Interestingly, however, some of the Kir channels, specifically belonging to the Kir3 family (G-protein coupled Kir channels, GIRK) were found to be enhanced by cholesterol enrichment [32–34] but the stereo-specificity of this effect has not been established yet. The stereo-specificity of cholesterol-induced suppression of Kir2.1 channels and the opposite effects of cholesterol and epicholesterol on Kir2.1 function were also reconfirmed in a heterologous expression system when the channels were overexpressed in a null cell line, in this case CHO cells [35].

To address the question of whether the stereo-specificity of cholesterol-induced suppression of Kir can be a result of its binding to a regulatory intermediate, we turned to purified channels incorporated into liposomes, a system that lacks any regulatory intermediates. Using this approach with a bacterial homologue of Kir channels, KirBac1.1, we demonstrated that the channels are still sensitive to cholesterol and confirmed the stereo-specific effect [36]. The same approach was used to reconfirm the stereo-specificity of Kir2 channels in a purified system [37].

Differential effects of cholesterol and epicholesterol on ion channel function are definitely not unique to Kir channels and growing number of studies demonstrate that stereo-specificity is a prevailing feature of cholesterol effects on different types of ion channels (Fig. 3). Specifically, consistent with our studies of Kir channels described above, but in contrast to previous belief that cholesterol regulates Large-conductance Ca^{2+}-sensitive K+ channels (BK) by altering lateral stress in the lipid bilayer [38, 39], Bukiya et al. [4] demonstrated strong differences between cholesterol and two of its chiral analogues, epicholesterol and ent-cholesterol in regulation of BK. Furthermore, comparative analysis of an array of steroids known to have different impact on the physical properties of the lipid bilayer strengthen their conclusion that cholesterol regulates BK channels via specific sterol–protein interactions, which was further tested and confirmed in their subsequent studies, as described in detail in their recent review [40]. The stereo-specificity of cholesterol effects was also demonstrated for TRPV1 channels, a major member of the family of transient receptor potential channels, which were shown to be inhibited by cholesterol but not by epicholesterol [5]. Notably, cholesterol has multiple diverse effects on different members of the TRP family, including both inhibitory and facilitatory effects, as well as direct effects on channel function and effects on channel trafficking [41].With the exception of cholesterol-induced suppression of TRPV1

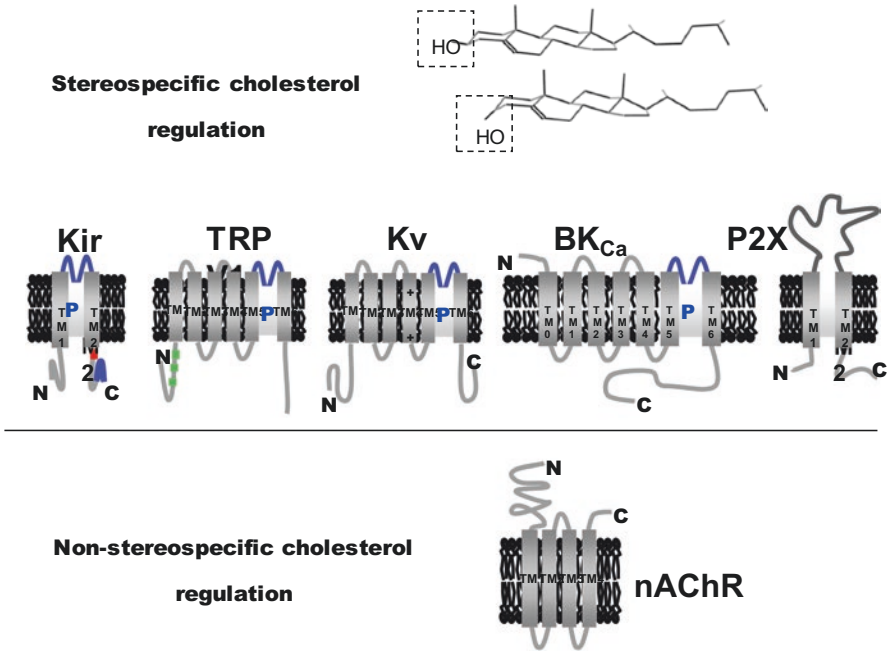

Fig. 3 Ion channels known to be regulated by cholesterol in a stereo-specific and non-stereo-specific way. Chemical structures of cholesterol and epi-cholesterol are shown, highlighting the difference in hydroxyl groups as well as schematic representations of Kir, TRPV1, Kv, BK_{Ca}, P2X, and nAChR, sorted according to their regulation. Channels shown to be regulated by cholesterol stereo-specifically are grouped on top. The channel nAChR, which was regulated by cholesterol in a non-stereo-specific manner, is shown below

channels, the stereo-specificity of these effects is not known and it would be very interesting to establish whether cholesterol may regulate different types of TRP channels by both direct and indirect mechanisms. Interestingly and surprisingly, a recent study by Minke et al. demonstrated that cholesterol can also regulate invertebrate TRP channels (TRPL), even though these channels are not exposed to cholesterol in their native environment [42]. This leads us to the question of possible promiscuity of cholesterol binding sites.

A striking example of a cholesterol binding site that can accommodate different sterols including epicholesterol is nicotinic acetylcholine receptor (nAChR). Cholesterol regulation of nAChR has been extensively studied, as discussed in several excellent reviews [43, 44]. Briefly, in terms of cholesterol stereo-specificity and binding, it was shown that while the effect of cholesterol on these channels is not stereo-specific [2], it binds directly to the channels, as evidenced using photo-activatable cholesterol analogues that cross-linked with the nAChR [45, 46]. A lack of stereo-specificity was also found for cholesterol-induced suppression of volume-regulated anion channels (VRAC) [3] but since at that time, the molecular identity of the channels was unknown, it was impossible to probe further whether the effect

could be non-stereo-specific by direct. Recent identification of I_{swell} as a protein underlying VRAC current [47] opens the possibility to explore this possibility in the future.

Taken together, these experiments lead to several key points and conclusions. One, the stereo-specificity of cholesterol effect on a specific ion channel provides strong evidence for specific sterol–protein interaction: if the effect of cholesterol cannot be substituted by its analogues or even more so, if chiral analogues of cholesterol yield opposite effects on the channel function, it is possible to claim with confidence that specific sterol–protein interactions play a key role in this effect. The opposite, however, is not true and as is clearly seen in case of nAChR, a lack of stereo-specificity does not exclude specific direct binding.

This led us to the next question—what is the mechanistic basis of the stereo-specificity of cholesterol effects on ion channels. Traditionally, it is believed that "stereo-specific" indicates a lack of binding of an isomer to the binding site. This is definitely true for numerous ligands and proteins. However, the lax nature of cholesterol binding sites in nAChR, as well as expected predominance of hydrophobic interactions within the binding site, led us to question this assumption. Instead, we hypothesize that even when the effect of cholesterol is stereo-specific, it is possible that stereoisomers can still bind to the same binding site. If this is the case, it will indicate that the stereo-specificity of the regulatory effect does not come from the lack of binding but from the specific configuration of the sterol within the binding site. This idea is explored computationally in the next part of the chapter.

3 Stereo-Specific Interaction of Cholesterol with the Kir2.2 Cholesterol Binding Site

As described above, we discovered that a partial substitution of membrane cholesterol with epicholesterol not only abrogates the inhibitory effect, but also increases the channel activity. This led us to hypothesize that epicholesterol acts as a competitive inhibitor of cholesterol, occupying cholesterol binding sites without affecting channel function. If this is indeed the case, then the key factor determining cholesterol's functional effect is its specific conformation and orientation within the channel binding site as compared to epicholesterol. Thus, after our initial studies established the stereo-specific effect of cholesterol on the regulation of Kir channels, the next step was to uncover the specific sites within these channels where cholesterol is directly interacting and mediating channel function.

3.1 Identification of Kir2 Cholesterol Binding Sites

Earlier studies identified two types of cholesterol binding motifs in ion channels and membrane receptors: (1) the Cholesterol Recognition Amino Acid Consensus (CRAC) motif ((L/V)-$X_{1–5}$-(Y)-$X_{1–5}$-(K/R)) and the reverse CARC motif

((K/R)-X_{1-5}-(Y/F)-X_{1-5}-(L/V)) found in multiple ion channels including nAChR, TRPV1, BK channels, KV channels, and GPCRs, and (2) the Cholesterol Consensus Motif (CCM) first identified in human β2-andrenergic receptors [43, 48, 49]. Interestingly, these cholesterol binding motifs were found in both the transmembrane and cytosolic domains of different channels. Specifically, in the nicotinic acetylcholine receptor (nAChR) and in transient receptor potential vanilloid 1 (TRPV1) channels, the CRAC/CARC motifs are found in the transmembrane domains [41, 43]. This is to be expected, as cholesterol is an integral membrane lipid and should interact with the transmembrane domains of the channels. There are also several examples when CRAC/CARC motifs are found in the cytosolic domains of the channels, as was shown for BK [40, 50], KV [51] and P2X [52]. Specifically, with respect to BK channels, ten CRAC motifs were identified, seven of which were located in the cytosolic domain. Since the authors showed that removal of cytosolic part of the protein totally blunted cholesterol sensitivity, they focused on the cytosolic CRAC motifs. However, while mutations in the cytosolic CRAC motifs were shown to blunt the sensitivity of the channels to cholesterol, it is still not clear how membrane cholesterol can interact with these cytosolic motifs, and whether such cytosolic motifs directly bind cholesterol or act to translate cholesterol binding at membrane sites into channel activity.

Our search for the known cholesterol binding motifs in Kir2 channels yielded mixed results [53]. Only one partial CRAC domain and two CARC domains were identified in Kir2.1, and of these three, two are located at the interface of the slide helix and the transmembrane domain. No CRAC/CARC domains were identified in the transmembrane region of the channel. Consequently, we decided to apply a different strategy, which was not limited to previously known cholesterol binding motifs. Our approach followed a three-step process: (1) molecular docking (2) molecular dynamics simulations, and (3) mutagenesis and electrophysiology experiments [53]. A docking analysis was used to predict which locations within the transmembrane region of the protein could contain favorable cholesterol–channel interactions. The advantage of this approach is that it is data agnostic, and in absence of any information provides a useful starting point for identifying interaction sites. With respect to Kir2, since the crystal structures of none of the Kir2 channels were known at the time, we used a homology model of Kir2.1 constructed based on the structure of the TM domain of a bacterial analogue of Kir, KirBac1.3, and the cytosolic domain of Kir3.1 [54]. Docking analysis of cholesterol on the entire transmembrane region of the Kir2.1 homology model was performed, and yielded five different predicted clusters for possible cholesterol interaction sites. Each of the predicted conformations was then verified with molecular dynamics simulations to measure their stability and it was found that the five predicted docking sites converged into two "cholesterol recognition regions." Within these two cholesterol recognition regions, several residues were identified as interacting with cholesterol during the simulations and confirmed by site-directed mutagenesis and electrophysiological studies. These residues formed the basis of the prediction for the binding sites.

More recently, after the crystal structure of Kir2.2 channel was published, Fürst et al. [55] undertook a similar study to identify a putative cholesterol binding site in

Kir2.2. In their approach, docking analyses of both cholesterol and ent-cholesterol were performed. Predicted cholesterol poses were considered only when the hydroxyl group was oriented towards the intra- or extracellular leaflet, and the sterol moiety was found entirely in one half of the membrane or the other. Only these poses were considered because of the orientation of cholesterol in a native membrane environment: it was assumed that when cholesterol diffuses to a binding pocket, it does so in a similar orientation to its native membrane orientation. Putative binding clusters were then identified by comparing high frequency cholesterol poses to ent-cholesterol poses. It was assumed that due to the lack of effect of ent-cholesterol on Kir, the most physiologically relevant poses would be those that exist for cholesterol but not ent-cholesterol. Consequently, those poses with minimal cholesterol/ent-cholesterol overlap or large predicted energy differences were further tested through MD simulations. Two of the predicted residues were verified with electrophysiological experiments. Significantly, the putative binding site identified in this study is similar to one of the cholesterol recognition regions identified in our previous work. Furthermore, as in our studies, cholesterol binding CRAC and CARC domains were not identified in Kir2.2, suggesting a CRAC-independent interaction mechanism for cholesterol with Kir channels. This idea is further substantiated by the recent work of Rosenhouse-Dantsker, who showed that CRAC, CARC, and CCM form only a subset of the existing cholesterol binding sites in crystallized protein structures [56].

The identification of cholesterol binding sites on Kir2 channels provided the basis to elucidate the nature of the stereo-specific effect of cholesterol on the channel's function. This was done through a comparative docking analysis of the interactions of cholesterol, epicholesterol, and ent-cholesterol with a recently identified crystal structure of Kir2.2. Our expectation was that if the stereoisomers of cholesterol also directly interact with the channel (that is to say, direct binding itself is not stereo-specific), then docking analyses would predict similar binding pockets and similar binding energies for the three sterols. Indeed, our analysis showed that this is in fact the case. As discussed in detail below, we found that all three stereoisomers of cholesterol directly interact with the channel with similar binding energies but different orientations within the binding sites.

3.2 Differential Docking of Cholesterol Isomers to Kir2.2 Binding Site

In molecular docking, the general goal is to simulate the interactions between a target receptor and ligand in order to find the optimal conformation of the ligand with minimized energy (i.e., in the most favorable position) [57, 58]. This technique is used extensively in the drug pipeline, and is as an effective method for screening potential drug candidates and estimating their binding affinity [59, 60]. Molecular docking can be divided into two parts: the *search algorithm* and the *scoring function*. The search algorithm simulates an ensemble of configurations for the

ligand on the surface of the receptor. Typical molecular docking programs consider four types of molecular interactions between ligands and receptors: electrostatic forces (dipoles/charges), electrodynamics forces (van der Waals), steric forces (entropy), and solvent-related forces (hydrogen bonds and hydrophobic interactions), with these interactions usually estimated through a force field. The resulting poses are then clustered together according to their similarity, and scored according to a scoring function. With respect to our docking analyses, this scoring function is based on the predicted binding energy of the cluster, with clusters ranked in order of highest predicted binding affinity. As described above, in the case of cholesterol and Kir2 channels, molecular docking allowed for an unbiased scanning of the channel for potential binding sites independent of the previously identified motifs leading to the identification of novel cholesterol binding regions [56] (Fig. 4).

In our more recent study, we used a similar approach to compare the putative binding sites and the binding affinity of cholesterol and its stereoisomers [23]. In this study, comparative molecular docking of cholesterol, epicholesterol, and ent-cholesterol was done using AutoDock 4 [61]. The general methodology of the AutoDock program is as follows: a search space is defined on the target receptor, and this search space is discretized into a grid. After a search space is defined, the ligand is randomly placed into the grid for a configuration search. For our studies, we used a grid with 0.375 Å spacing (the default for AutoDock) centered on Val^{168}, right above the glycine hinge, similar to the center of the search space we defined in our previous study. The grid size was 90 × 78 × 126 grid points, or 33.75 × 29.95 × 48 Å. These dimensions were chosen because they covered the entire transmembrane region of the protein across two subunits. By doing so, we could search for potential sites on a

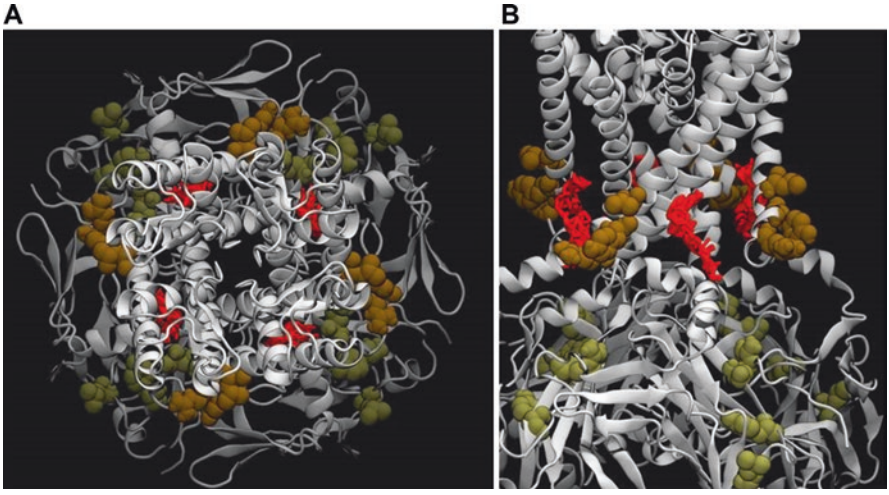

Fig. 4 Kir-cholesterol binding site shows no overlap with known cholesterol binding motifs. The putative binding site of cholesterol in Kir2.2 is visualized as a "cloud" of cholesterol poses, as predicted by docking analysis. The two CARC motifs present in Kir2.2 are rendered in brown and green, respectively. (**a**) A top-down view of the channel. (**b**) A side view of the channel, showing the predicted location of cholesterol binding relative to the two CARC motifs

single subunit and between two subunits. Moreover, due to the "random seeding" process inherent in AutoDock's algorithm, we performed three separate docking analyses for each of the three sterol isomers. The results of the separate docking analyses for each sterol were compared with one another to identify the most reproducible sites. The results of each docking analysis were clustered according to their configurational similarity and their location in the search space by calculating pairwise root-mean-square deviation (RMSD) values and grouping together those in the population with RMSDs that are less than 2 Å (Fig. 5). These clusters were

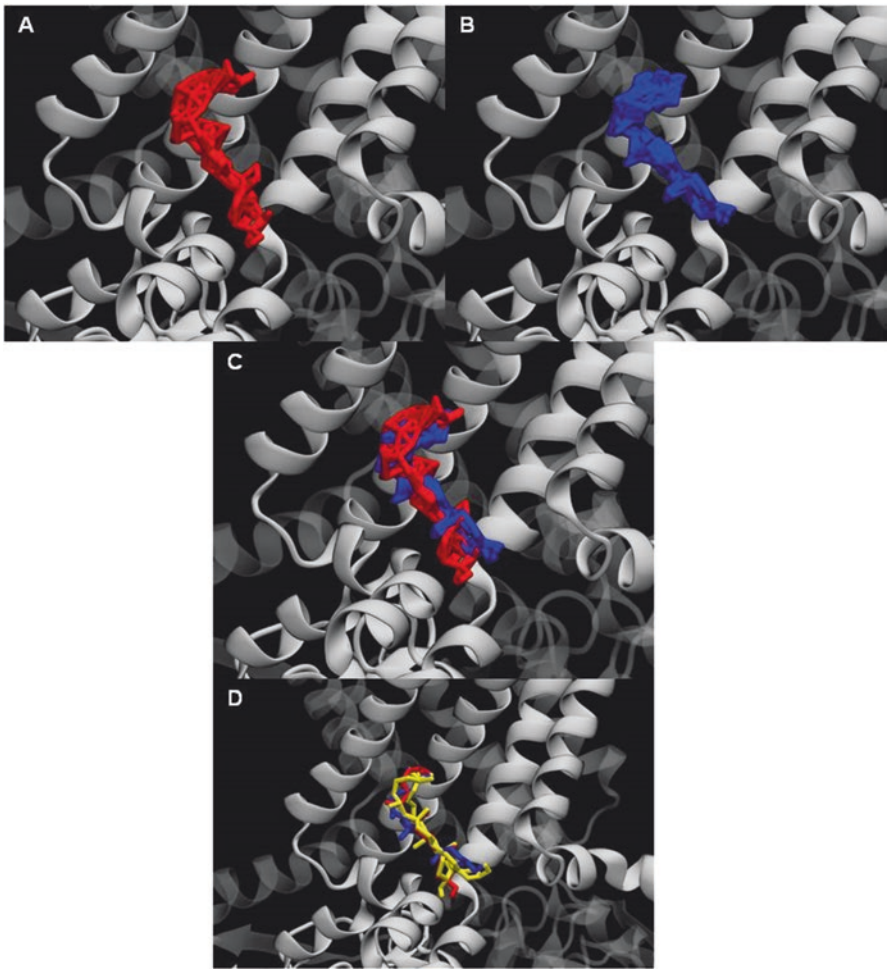

Fig. 5 Overlap of predicted sterol binding sites. Docking analyses predicted a similar binding site for cholesterol, epi-cholesterol, and ent-cholesterol. (**a**) The predicted binding site for cholesterol, represented as a "cloud" of representative poses from the docking analysis. (**b**) the predicted binding site for ent-cholesterol, also represented as a "cloud". (**c**) Overlay of the cholesterol and ent-cholesterol clouds. (**d**) A single representation of the most energetically favorable poses for cholesterol (red), ent-cholesterol (blue), and epicholesterol (yellow). Modified from Barbera et al. [23]

ranked according to their predicting binding affinity. Typically, each cluster represents a putative binding site. However, it is important to note that within each cluster there is a "cloud" of configurationally similar predicted poses, and that the predicted binding energy for the cluster corresponds to the binding energy of the most favorable pose within the cluster. In comparing the results of the separate sterols, our initial observation was that the predicted binding conformations for cholesterol, epicholesterol, and ent-cholesterol show considerable overlap in predicted conformation, binding location, and energetic favorability.

For cholesterol, we found that while nine total clusters were generated, 70% of all predicted poses were grouped together into one large cluster. Furthermore, this cluster represented the most energetically favorable cluster, with a predicted binding energy of −9.75 kcal/mol, and showed good agreement with a similarly predicted binding configuration in Fürst et al.: the orientation of cholesterol is such that the methyl groups of the "rough" face of cholesterol (carbon atoms C18 and C19 in Fig. 1a) are oriented towards away from the slide helix and towards the center of the protein, with the hydroxyl group oriented towards the cytoplasmic region. Similarly, for ent-cholesterol, we also found that 75% of the poses were grouped in one most energetically favorable cluster with practically identical predicted binding energy of −9.9 kcal/mol. The two clusters strongly overlap: both are in a non-annular region between the two alpha helices of the transmembrane region, just above the slide helix of the channel. Furthermore in comparing the arrangement of the poses, the sterol groups of cholesterol and ent-cholesterol almost perfectly overlap when overlaid on one another.

However, and most interestingly, while the clusters of cholesterol and ent-cholesterol poses strongly overlap in space, we also found a difference in their preferred orientations within the binding site. For cholesterol, the most favorable orientation is such that the methyl groups of the "rough" face of cholesterol are oriented away from the slide helix, towards the center of the channel, with the hydroxyl group oriented towards the cytoplasmic region. In contrast, for ent-cholesterol the most favorable predicted configuration was oriented in a mirror image to cholesterol, with the tetracyclic rings of cholesterol and ent-cholesterol overlapping and the methyl and hydroxyl groups facing opposite directions. While the bulk of the two sterols overlap in their predicted pose, this mirroring of orientation affects the residues predicted to interact with the sterols. Based on the docking analysis, both sterols are predicted to interact with ten residues, and of these, eight are identical between the two (Fig. 6). One of the differences is in the location of their hydrogen bonds: in the case of cholesterol, the hydroxyl group is oriented towards Lys^{189}, on the adjacent subunit. In contrast, ent-cholesterol is predicted to interact with Trp^{79} on the adjacent subunit. In both of these cases, the other sterol is not predicted to interact with the residue. Additionally, cholesterol is predicted to interact with Ala^{68}, while ent-cholesterol is predicted to interact with Cys^{74} through one of its methyl groups.

For epicholesterol, two configurations were predicted (56 and 40% of poses). Similar to ent-cholesterol, the location of the predicted poses overlapped with the

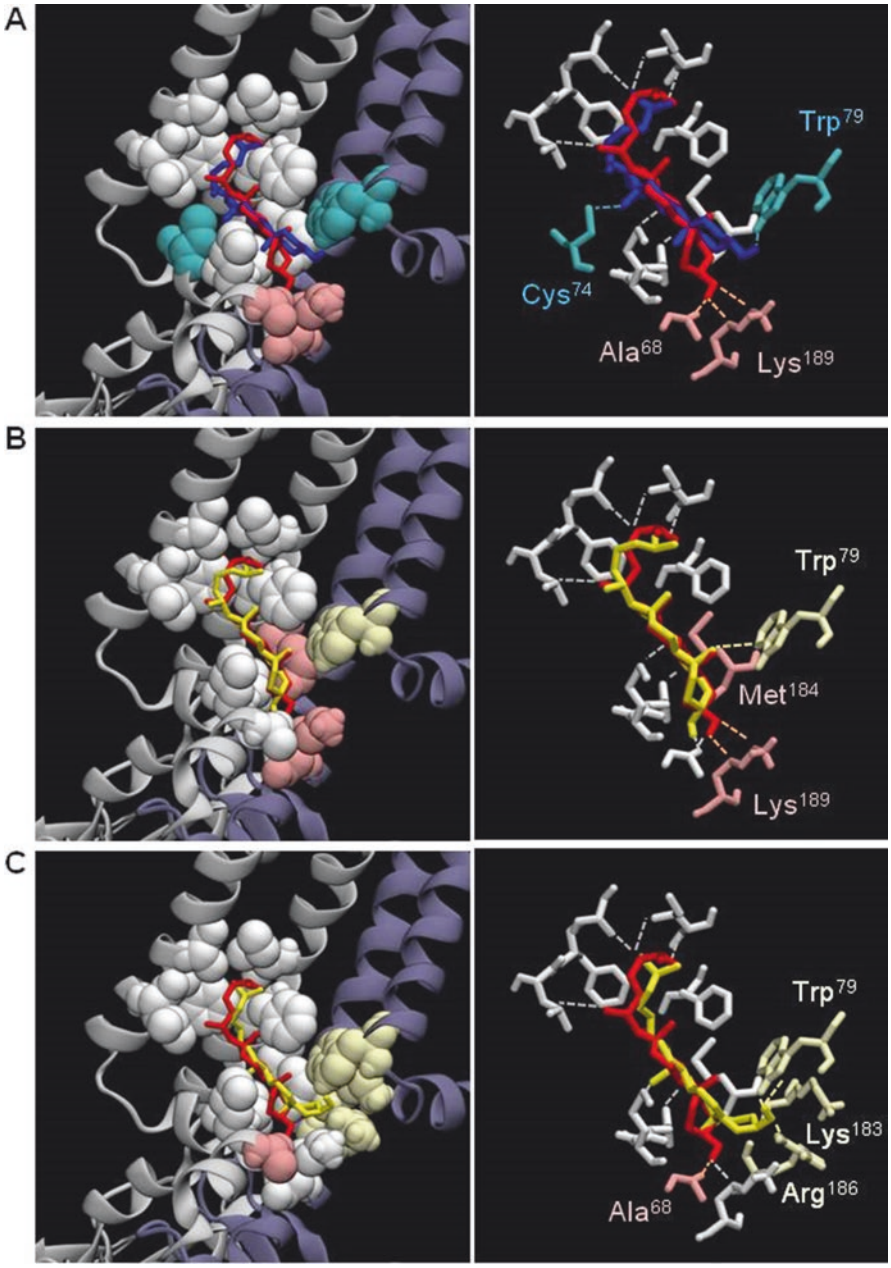

Fig. 6 Binding residues predicted by comparative docking analysis. Each docking analysis yielded a set of residues predicted to interact with the most energetically favorable pose of cholesterol (red), ent-cholesterol (blue), or epicholesterol (yellow). Shown here are pairwise comparisons between cholesterol and ent-cholesterol (**a**), as well as comparisons between cholesterol and the two most favorable poses of epicholesterol (**b**, **c**). Residues shown in white are predicted to interact with both cholesterol and the given sterol. Residues represented in pink are those predicted only to interact with cholesterol. Residues represented in cyan and light yellow are residues predicted only to interact with ent-cholesterol and epicholesterol

predicted pose of cholesterol, situated between the slide helix and the two alpha helices of the transmembrane region. Notably, only one of the two predicted conformations for epi-cholesterol also showed similar overlap with the tetracyclic rings of cholesterol as ent-cholesterol. In this orientation, the methyl groups are oriented similarly to cholesterol, but the hydroxyl group is oriented in the opposite direction to cholesterol, instead facing Ala^{68}, not Lys^{189}. Furthermore, the predicted binding energy is very similar to that of cholesterol, −9.8 kcal/mol. In the other configuration, the sterol rings are mirror and the methyl groups are aligned in the same direction as those of ent-cholesterol. In this configuration, the hydroxyl group is oriented towards Trp^{79} and Arg^{186}, as in ent-cholesterol. The predicted binding energy in this case was −10.4 kcal/mol.

Overall, these docking analyses suggest key differences in the specific residues interacting with cholesterol versus epi- or ent-cholesterol. In our analysis, both ent-cholesterol and epi-cholesterol were predicted to interact with a very similar set of residues as cholesterol. However, only in the case of cholesterol was the sterol predicted to interact with both Ala^{68} and Lys^{189}. While either epi-cholesterol or ent-cholesterol was predicted to interact with one of these, in none of the other cases was the sterol configured such that interaction with both of these residues occurs. We propose that the differences in the specific interactions of the cholesterol and its isomers with the channel residues within its binding site are responsible for their differential effects on the channel function.

4 Conclusions and Future Directions

Cholesterol regulation of ion channels was found to be stereo-specific in the majority of cases analyzed so far by different labs including ours. Our recent computational work with cholesterol stereoisomers and Kir2.2 channels suggests, however, that envisioning the different regulatory effects of these sterols from the perspective of "binding vs non-binding" provides an incomplete picture. As was shown in the case of nAChR, cholesterol binding sites on ion channels can indeed be promiscuous. Likewise, our docking analyses here imply that cholesterol, epi-cholesterol, and ent-cholesterol can interact in the same binding site with very similar binding configurations. If indeed this promiscuity is a consistent phenomenon in a range of ion channels, it requires then a much more detailed look at the binding process of cholesterol. It is not sufficient to ask whether cholesterol or a chiral isomer binds. Rather, it must also be asked: how is it oriented in its bound state, and what interactions are unique to cholesterol that are absent for epi-cholesterol and ent-cholesterol?

Acknowledgements We are very grateful to Ibra Fancher for the critical reading of the manuscript. We thank Manuela Ayee for critical discussions and Victor Romanenko for contributing GLC measurements shown in Fig. 2. We also thank Mr. Gregory Kowalsky for his help in designing Figs. 2 and 3. This work was supported by the National Institute of Health grants HL073965 and HL083298 (to I.L.).

References

1. Romanenko VG, Rothblat GH, Levitan I. Modulation of endothelial inward-rectifier K+ current by optical isomers of cholesterol. Biophys J. 2002;83(6):3211–22.
2. Addona GH, Sandermann H, Kloczewiak MA, Miller KW. Low chemical specificity of the nicotinic acetylcholine receptor sterol activation site. Biochim Biophys Acta Biomembr. 2003;1609(2):177–82.
3. Romanenko VG, Rothblat GH, Levitan I. Sensitivity of volume-regulated anion current to cholesterol structural analogues. J Gen Physiol. 2004;123(1):77–88.
4. Bukiya AN, Singh AK, Parrill AL, Dopico AM. The steroid interaction site in transmembrane domain 2 of the large conductance, voltage-and calcium-gated potassium (BK) channel accessory β1 subunit. Proc Natl Acad Sci. 2011;108(50):20207–12.
5. Picazo-Juarez G, Romero-Suarez S, Nieto-Posadas A, Llorente I, Jara-Oseguera A, Briggs M, et al. Identification of a binding motif in the S5 helix that confers cholesterol sensitivity to the TRPV1 ion channel. J Biol Chem. 2011;286(28):24966–76.
6. Demel RA, Bruckdorfer KR, van Deenen LLM. The effect of sterol structure on the permeability of liposomes to glucose, glycerol and Rb+. Biochim Biophys Acta. 1972;255:321–30.
7. Westover EJ, Covey DF. The enantiomer of cholesterol. J Membr Biol. 2004;202(2):61.
8. Gimpl G, Burger K, Fahrenholz F. Cholesterol as modulator of receptor function. Biochemistry. 1997;36:10959–74.
9. Xu X, London E. The effect of sterol structure on membrane lipid domains reveals how cholesterol can induce lipid domain formation. Biochemistry. 2000;39:843–9.
10. Kubo Y, Adelman JP, Clapham DE, Jan LY, Karschin A, Kurachi Y, et al. International Union of Pharmacology. LIV. Nomenclature and molecular relationships of inwardly rectifying potassium channels. Pharmacol Rev. 2005;57(4):509–26.
11. Hibino H, Inanobe A, Furutani K, Murakami S, Findlay I, Kurachi Y. Inwardly rectifying potassium channels: their structure, function, and physiological roles. Physiol Rev. 2010;90(1):291–366.
12. Levitan I, Ahn SJ, Fancher I, Rosenhouse-Dantsker A. Physiological roles and cholesterol sensitivity of endothelial inwardly-rectifying K+ channels: specific cholesterol-protein interactions through non annular binding sites. In: Levitan I, Dopico A, editors. Vascular ion channels in health and disease. Berlin: Springer; 2016.
13. Levitan I. Cholesterol and Kir channels. IUBMB Life. 2009;61:781–90.
14. Zaritsky JJ, Eckman DM, Wellman GC, Nelson MT, Schwarz TL. Targeted disruption of Kir2. 1 and Kir2. 2 genes reveals the essential role of the inwardly rectifying K+ current in K+-mediated vasodilation. Circ Res. 2000;87(2):160–6.
15. Miake J, Marban E, Nuss HB. Functional role of inward rectifier current in heart probed by Kir2.1 overexpression and dominant-negative suppression. J Clin Invest. 2003;111:1529–36.
16. Piao L, Li J, McLerie M, Lopatin A. Transgenic upregulation of IK1 in the mouse heart is proarrhythmic. Basic Res Cardiol. 2007;102(5):416–28.
17. Filosa JA, Bonev AD, Straub SV, Meredith AL, Wilkerson MK, Aldrich RW, et al. Local potassium signaling couples neuronal activity to vasodilation in the brain. Nat Neurosci. 2006;9(11):1397.
18. Olesen S-P, Clapham DE, Davies PF. Hemodynamic shear stress activates a K+ current in vascular endothelial cells. Nature. 1988;331(6152):168–70.
19. Davies PF. Flow-mediated endothelial mechanotransduction. Physiol Rev. 1995;75:519–60.
20. Fang Y, Schram G, Romanenko VG, Shi C, Conti L, Vandenberg CA, et al. Functional expression of Kir2.x in human aortic endothelial cells: the dominant role of Kir2.2. Am J Physiol Cell Physiol. 2005;289(5):C1134–44.
21. Ahn SJ, Fancher IS, Bian J-T, Zhang CX, Schwab S, Gaffin R, et al. Inwardly rectifying K+ channels are major contributors to flow-induced vasodilatation in resistance arteries. J Physiol. 2017;595(7):2339–64.

22. Fancher IS, Ahn SJ, Adamos C, Osborn C, Oh M-J, Fang Y, et al. Hypercholesterolemia-induced loss of flow-induced vasodilation and lesion formation in apolipoprotein E-deficient mice critically depend on inwardly rectifying K+ channels. J Am Heart Assoc. 2018;7(5):e007430.
23. Barbera N, Ayee MAA, Akpa BS, Levitan I. Differential effects of sterols on ion channels: stereospecific binding vs stereospecific response. Curr Top Membr. 2017;80:25–52.
24. Sooksawate T, Simmonds M. Effects of membrane cholesterol on the sensitivity of the GABAA receptor to GABA in acutely dissociated rat hippocampal neurones. Neuropharmacology. 2001;40(2):178–84.
25. Sigel E, Steinmann ME. Structure, function, and modulation of GABAA receptors. J Biol Chem. 2012;287(48):40224–31.
26. Romanenko VG, Fang Y, Byfield F, Travis AJ, Vandenberg CA, Rothblat GH, et al. Cholesterol sensitivity and lipid raft targeting of Kir2. 1 channels. Biophys J. 2004;87(6):3850–61.
27. Tikku S, Epshtein Y, Collins H, Travis AJ, Rothblat GH, Levitan I. Relationship between Kir2. 1/Kir2. 3 activity and their distributions between cholesterol-rich and cholesterol-poor membrane domains. Am J Phys Cell Phys. 2007;293(1):C440–C50.
28. Han H, Rosenhouse-Dantsker A, Gnanasambandam R, Epshtein Y, Chen Z, Sachs F, et al. Silencing of Kir2 channels by caveolin-1: cross-talk with cholesterol. J Physiol. 2014;592(18):4025–38.
29. Fang Y, Shaffer RG, Moore J, Mohler E, Levitan I. Hypercholesterolemia alters the functional properties of inwardly-rectifying K channels in side-population endothelial progenitor cells in a pig model. Vasc Pharmacol. 2006;45(3):e28–e9.
30. Zidovetzki R, Levitan I. Use of cyclodextrins to manipulate plasma membrane cholesterol content: evidence, misconceptions and control strategies. Biochim Biophys Acta Biomembr. 2007;1768(6):1311.
31. Fang Y, Schram G, Romanenko VG, Shi C, Conti L, Vandenberg CA, et al. Functional expression of Kir2.x in human aortic endothelial cells: the dominant role of Kir2.2. Am J Phys Cell Phys. 2005;289(5):C1134–C44.
32. Rosenhouse-Dantsker A, Leal-Pinto E, Logothetis DE, Levitan I. Comparative analysis of cholesterol sensitivity of Kir channels: role of the CD loop. Channels. 2010;4(1):63–6.
33. Deng W, Bukiya AN, Rodríguez-Menchaca AA, Zhang Z, Baumgarten CM, Logothetis DE, et al. Hypercholesterolemia induces up-regulation of KACh cardiac currents via a mechanism independent of phosphatidylinositol 4,5-bisphosphate and Gβγ. J Biol Chem. 2012;287(7):4925–35.
34. Bukiya AN, Durdagi S, Noskov S, Rosenhouse-Dantsker A. Cholesterol up-regulates neuronal G protein-gated inwardly rectifying potassium (GIRK) channel activity in the hippocampus. J Biol Chem. 2017;292(15):6135–47.
35. Epshtein Y, Chopra AP, Rosenhouse-Dantsker A, Kowalsky GB, Logothetis DE, Levitan I. Identification of a C-terminus domain critical for the sensitivity of Kir2. 1 to cholesterol. Proc Natl Acad Sci. 2009;106(19):8055–60.
36. Singh DK, Rosenhouse-Dantsker A, Nichols CG, Enkvetchakul D, Levitan I. Direct regulation of prokaryotic Kir channel by cholesterol. J Biol Chem. 2009;284(44):30727–36.
37. D'Avanzo N, Hyrc K, Enkvetchakul D, Covey DF, Nichols CG. Enantioselective protein-sterol interactions mediate regulation of both prokaryotic and eukaryotic inward rectifier K+ channels by cholesterol. PLoS One. 2011;6(4):e19393.
38. Chang H, Reitstetter R, Mason R, Gruener R. Attenuation of channel kinetics and conductance by cholesterol: an interpretation using structural stress as a unifying concept. J Membr Biol. 1995;143(1):51–63.
39. Bolotina V, Omelyanenko V, Heyes B, Ryan U, Bregestovski P. Variations of membrane cholesterol alter the kinetics of Ca2+-dependent K+ channels and membrane fluidity in vascular smooth muscle cells. Pflugers Arch. 1989;415(3):262–8.
40. Dopico AM, Bukiya AN. Regulation of Ca^{2+}-sensitive K^+ channels by cholesterol and bile acids via distinct channel subunits and sites. Curr Top Membr. 2017;80:53–94.
41. Morales-Lázaro SL, Rosenbaum T. Multiple mechanisms of regulation of transient receptor potential ion channels by cholesterol. Curr Top Membr. 2017;80:139–62.

42. Peters M, Katz B, Lev S, Zaguri R, Gutorov R, Minke B. Depletion of membrane cholesterol suppresses drosophila transient receptor potential-like (TRPL) channel activity. Curr Top Membr. 2017;80:233–54.
43. Di Scala C, Baier CJ, Evans LS, Williamson PTF, Fantini J, Barrantes FJ. Relevance of CARC and CRAC cholesterol-recognition motifs in the nicotinic acetylcholine receptor and other membrane-bound receptors. Curr Top Membr. 2017;80:3–24.
44. Baenziger JE, Domville JA, Therien JD. The role of cholesterol in the activation of nicotinic acetylcholine receptors. Curr Top Membr. 2017;80:95–137.
45. Corbin J, Wang HH, Blanton MP. Identifying the cholesterol binding domain in the nicotinic acetylcholine receptor with [125 I] azido-cholesterol. Biochim Biophys Acta Biomembr. 1998;1414(1):65–74.
46. Hamouda AK, Chiara DC, Sauls D, Cohen JB, Blanton MP. Cholesterol interacts with transmembrane α-helices M1, M3, and M4 of the Torpedo nicotinic acetylcholine receptor: photolabeling studies using [3H] azicholesterol. Biochemistry. 2006;45(3):976–86.
47. Syeda R, Qiu Z, Dubin AE, Murthy SE, Florendo MN, Mason DE, et al. LRRC8 proteins form volume-regulated anion channels that sense ionic strength. Cell. 2016;164(3):499–511.
48. Fantini J, Barrantes FJ. How cholesterol interacts with membrane proteins: an exploration of cholesterol-binding sites including CRAC, CARC, and tilted domains. Front Physiol. 2013;4:31.
49. Hanson MA, Cherezov V, Griffith MT, Roth CB, Jaakola V-P, Chien EY, et al. A specific cholesterol binding site is established by the 2.8 Å structure of the human β2-adrenergic receptor. Structure. 2008;16(6):897–905.
50. Singh AK, McMillan J, Bukiya AN, Burton B, Parrill AL, Dopico AM. Multiple cholesterol recognition/interaction amino acid consensus (CRAC) motifs in cytosolic C tail of Slo1 subunit determine cholesterol sensitivity of Ca2+-and voltage-gated K+ (BK) channels. J Biol Chem. 2012;287(24):20509–21.
51. Balajthy A, Hajdu P, Panyi G, Varga Z. Sterol regulation of voltage-gated K^+ channels. Curr Top Membr. 2017;80:255–91.
52. Murell-Lagnado RD. Regulation of P2X purinergic receptor signaling by cholesterol. Curr Top Membr. 2017;80:211–32.
53. Rosenhouse-Dantsker A, Noskov S, Durdagi S, Logothetis DE, Levitan I. Identification of novel cholesterol-binding regions in Kir2 channels. J Biol Chem. 2013;288(43):31154–64.
54. Nishida M, Cadene M, Chait BT, MacKinnon R. Crystal structure of a Kir3.1-prokaryotic Kir channel chimera. EMBO J. 2007;26(17):4005–15.
55. Fürst O, Nichols CG, Lamoureux G, D'Avanzo N. Identification of a cholesterol-binding pocket in inward rectifier K+(Kir) channels. Biophys J. 2014;107(12):2786–96.
56. Rosenhouse-Dantsker A. Insights into the molecular requirements for cholesterol binding to ion channels. Curr Top Membr. 2017;80:187–210.
57. Kitchen DB, Decornez H, Furr JR, Bajorath J. Docking and scoring in virtual screening for drug discovery: methods and applications. Nat Rev Drug Discov. 2004;3(11):935.
58. Huang S-Y, Zou X. Advances and challenges in protein-ligand docking. Int J Mol Sci. 2010;11(8):3016–34.
59. Chaudhary KK, Mishra N. A review on molecular docking: novel tool for drug discovery. Database. 2016;3:4.
60. de Ruyck J, Brysbaert G, Blossey R, Lensink MF. Molecular docking as a popular tool in drug design, an in silico travel. Adv Appl Bioinforma Chem. 2016;9:1.
61. Morris GM, Huey R, Lindstrom W, Sanner MF, Belew RK, Goodsell DS, et al. AutoDock4 and AutoDockTools4: automated docking with selective receptor flexibility. J Comput Chem. 2009;30(16):2785–91.

Part II
Indirect Modulation of Protein Function by Cholesterol

Cholesterol Effects on the Physical Properties of Lipid Membranes Viewed by Solid-state NMR Spectroscopy

Trivikram R. Molugu and Michael F. Brown

Abstract In this chapter, we review the physical properties of lipid/cholesterol mixtures involving studies of model membranes using solid-state NMR spectroscopy. The approach allows one to quantify the average membrane structure, fluctuations, and elastic deformation upon cholesterol interaction. Emphasis is placed on understanding the membrane structural deformation and emergent fluctuations at an atomistic level. Lineshape measurements using solid-state NMR spectroscopy give equilibrium structural properties, while relaxation time measurements study the molecular dynamics over a wide timescale range. The equilibrium properties of glycerophospholipids, sphingolipids, and their binary and tertiary mixtures with cholesterol are accessible. Nonideal mixing of cholesterol with other lipids explains the occurrence of liquid-ordered domains. The entropic loss upon addition of cholesterol to sphingolipids is less than for glycerophospholipids, and may drive formation of lipid rafts. The functional dependence of ^{2}H NMR spin–lattice relaxation (R_{1Z}) rates on segmental order parameters (S_{CD}) for lipid membranes is indicative of emergent viscoelastic properties. Addition of cholesterol shows stiffening of the bilayer relative to the pure lipids and this effect is diminished for lanosterol. Opposite influences of cholesterol and detergents on collective dynamics and elasticity at an atomistic scale can potentially affect lipid raft formation in cellular membranes.

Keywords Area per lipid · Cholesterol · Lanosterol · Lipid rafts · Membrane elasticity · Solid-state NMR

The original version of this chapter was revised. The correction to this chapter is available at https://doi.org/10.1007/978-3-030-04278-3_9

T. R. Molugu
Department of Chemistry and Biochemistry, University of Arizona, Tucson, AZ, USA

M. F. Brown (✉)
Department of Chemistry and Biochemistry, University of Arizona, Tucson, AZ, USA

Department of Physics, University of Arizona, Tucson, AZ, USA
e-mail: mfbrown@u.arizona.edu

A. Rosenhouse-Dantsker, A. N. Bukiya (eds.), *Cholesterol Modulation of Protein Function*, Advances in Experimental Medicine and Biology 1115,
https://doi.org/10.1007/978-3-030-04278-3_5

1 Introduction

Cholesterol is an essential component of mammalian cells constituting up to about 50 mol% of the total lipids in the plasma membrane [1, 2]. It plays key roles in maintaining the membrane integrity and regulating cell permeability [3]. Cellular functions are modulated by cholesterol in two different ways: either indirectly by affecting membrane properties due to lipid-cholesterol interactions [4–7] or directly by cholesterol-protein interactions [8–10]. As a steroid molecule, cholesterol has four fused rings and a hydrocarbon chain, which are hydrophobic, and a polar hydroxyl group making it overall amphiphilic as for other lipids (Fig. 1). Due to its

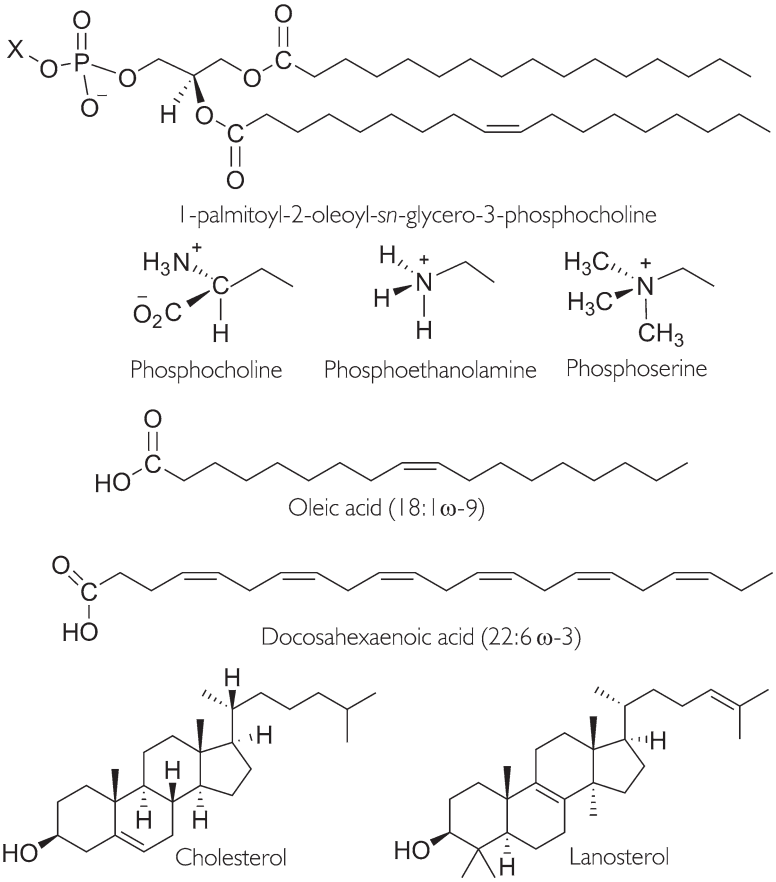

Fig. 1 Selected glycerophospholipid chemical structures, cholesterol, and lanosterol. The polar head groups vary in size, hydrogen bonding, and charge. Examples are shown for zwitterionic phosphocholine (PC) and phosphoethanolamine (PE) head groups, and for the anionic phosphoserine (PS) head group. Nonpolar acyl chains differ in length and degree of unsaturation, as illustrated by oleic acid (18:1ω-9) and docosahexaenoic acid (22:6ω-3). Cholesterol differs in the absence of methylation at the α-face relative to its biological precursor lanosterol. Figure adapted from [11]

chemical composition, most of the steroidal core structure fits into the lipid bilayer, with the fused rings in close proximity and interacting with the hydrocarbon chains of the lipids, while the polar hydroxyl group orients the molecule at the aqueous interface. When cholesterol is present in the liquid-ordered (l_o) phase, the lipid hydrocarbon chains become more ordered relative to the cholesterol-free (liquid-disordered, l_d) state. The lipid chain ordering induces alterations in the structural, dynamical [12], and physical properties of the lipid membrane, and thus can affect cellular signaling. The balance of attractive and repulsive forces for the membrane lipids is the consequence of both the polar headgroups and the nonpolar moieties, and yields a substantial polymorphism involving both lamellar and nonlamellar phases [13–20]. Notably, the structural and dynamical properties of biomembranes are mediated by the lipid composition and interactions with the proteins, water, cholesterol, and surfactants [7, 21–33]. Membrane remodeling requires mesoscopic elastic deformations of the lipids [30] that can play a central role in biological functioning with regard to lipid-protein interactions [6, 34, 35], domain formation, and various nano- and microstructures implicated in key cellular functions [34, 36–38]. Because the composition of lipids and cholesterol in cell membranes influences the lipid organization and membrane properties, it is not surprising that disorders in cellular cholesterol levels are implicated in various diseases [39, 40].

Many of the molecular species of lipids and proteins in membranes do not mix ideally [19, 20, 41–47]—cholesterol is one such component that is unequally distributed in cellular membranes, allowing for the presence of liquid-ordered raft-like domains [19, 20, 32, 42, 46–52]. Such raft-like domains have attracted considerable attention as platforms for signaling regulation in cellular biology and pharmacology [53–60]. The concept that biomembranes are homogeneous two-dimensional fluids with randomly distributed proteins (the fluid mosaic model) is challenged by the hypothesis that cellular membranes may contain such areas of lateral segregation [20, 55, 61–73]. By analysis of the liquid-ordered (l_o) phase [74, 75] and its possible connection with rafts in biological membranes [76, 77], the effect of cholesterol on domain formation in liquid-crystalline bilayers has been of great interest for membrane biophysicists [78]. For instance, raft-like domains are believed to occur in lipid systems with coexisting liquid-disordered (l_d) and liquid-ordered (l_o) phases. The l_d phase in these systems typically contains highly unsaturated lipids with a low phase-transition temperature, while the l_o phase predominantly consists of saturated glycerophospholipids or a sphingolipid component and cholesterol [2, 77]. Moreover, various proteins are endowed with the ability to interact with cholesterol via specific sensing mechanisms. The cholesterol recognition/interaction amino acid consensus (CRAC) sequence motif [79–82] is an example of such a recognition element. In some cases, they include cationic clusters that allow interactions with phosphatidylinositol 4,5-bisphosphate (PIP_2) in a cholesterol-dependent manner. Notably, such CRAC domains are found in the *Rhodopsin* (Family A) G-protein-coupled receptors (GPCRs) [83], and moreover posttranslational lipid modifications [84, 85] can promote sequestration into cholesterol-rich regions or microdomains.

Improving our understanding of complex lipid mixtures is an important aspect for current research in pharmacology, biophysics, and biochemistry as well as in

cellular biology. Various experimental methods have been used to study lipid–cholesterol interactions, including electron spin resonance (ESR) [86–94], Raman [95–97], Fourier transform infrared (FT-IR) [98, 99], and fluorescence spectroscopy [100–102]; atomic force microscopy (AFM) [103–105]; multidimensional nuclear magnetic resonance (NMR) spectroscopy [70, 73, 106, 107]; solid-state NMR spectroscopy [65, 101, 108–119]; and X-ray [72, 120, 121] and neutron diffraction methods [122–124]. Still, a thorough understanding of the physical basis for these observations in relation to the intricate lipid compositions of many biological membranes remains a conundrum [20, 51, 71, 125, 126]. This chapter covers recent developments in understanding lipid–cholesterol interactions in model membrane systems and implications for cellular function as seen by solid-state nuclear magnetic resonance (NMR) spectroscopy. First, we give a brief introduction to solid-state NMR methods for nonexperts to appreciate the results as applied to lipid-cholesterol systems. Next, we explain how solid-state NMR technology is applied for obtaining membrane structural and dynamical properties. We then discuss the sterol interactions with phospholipids in model membranes, including the role of configurational entropy in lipid raft formation. Emphasis is placed on how the average material properties emerge from the atomistic level interactions in lipid bilayers, as investigated by combining NMR spectroscopy with relaxation methods [11, 111, 112, 127].

2 Solid-State NMR Spectroscopy of Lipid Membranes

Solid-state NMR spectroscopy [29, 128–130] offers a versatile and noninvasive method for studying the molecular organization of lipids within membranes. In particular, isotopic substitution of ^{2}H for ^{1}H constitutes a minimal structural perturbation [131]. Interpretation of the ^{2}H NMR spectra is relatively straightforward, due to the intramolecular nature of the quadrupolar interaction that dominates the lineshape. There are a number of reviews that give a comprehensive treatment of ^{2}H NMR spectral analysis [30, 128, 129, 131–135]. An essential feature of ^{2}H NMR spectroscopy is that one introduces site-specific ^{2}H-labels, corresponding to the individual C–^{2}H bonds. In this way, we obtain atomistically resolved information for noncrystalline amorphous or liquid-crystalline systems. Because the coupling interactions in solid-state NMR are sensitive to orientation and/or distance, their values correspond to the average structure of the system of interest. On the other hand, molecular motions are manifested by the relaxation parameters that are also accessible in NMR spectroscopy. A unique feature is that in solid-state ^{2}H NMR of biomolecular systems, we acquire both lineshape data [118] and relaxation times [136] for investigating structural dynamics. Measurement of the ^{2}H NMR lineshapes yields knowledge of the average structure through the principal values of the coupling tensor as well as the principal axis system. Yet, if we only determine the coupling tensors, then the method mainly provides us with structural knowledge as in X-ray crystallography. An important feature of solid-state ^{2}H NMR spectroscopy

is that information is also obtained regarding the molecular motions, encompassing a range of different timescales. Through the combined measurement of residual quadrupolar couplings (RQCs) and relaxation rates, we thereby obtain knowledge of the geometry as well as investigate the multiscale molecular motions and their amplitudes in the membrane systems of interest. An analogous approach is introduced in the case of solid-state ^{13}C NMR spectroscopy of membrane lipids and biomembranes at natural isotopic abundance.

2.1 Deuterium Solid-State NMR Spectroscopy

Notably, ^{2}H NMR spectroscopy gives us a particularly simple illustration of the principles of magnetic resonance as applied to molecular solids, liquid crystals, and biomembranes. This is because the very large electric quadrupolar interaction dominates over the magnetic dipolar couplings of the ^{2}H and ^{1}H nuclei as well as the ^{2}H chemical shifts [134, 136]. The ^{2}H nucleus has a spin of $I = 1$, and hence there are three Zeeman energy levels due to projecting the nuclear spin angular momentum onto the magnetic field direction. The three eigenstates $|m\rangle = |0\rangle$ and $|\pm1\rangle$ are given by the Hamiltonian $\hat{H}_Z$ for interaction of the nuclear magnetic moment with the static magnetic field. We learn in quantum mechanics that the transitions between adjacent spin energy levels are allowed, which yields the two single-quantum nuclear spin transitions. Moreover, the degeneracy of the allowed transitions in ^{2}H NMR is removed by the quadrupolar coupling. Here, the perturbing Hamiltonian $\hat{H}_Q$ is due to interaction of the quadrupole moment of the ^{2}H nucleus with the electric field gradient (EFG) of the C–^{2}H bond. It follows that for each inequivalent site, two spectral branches are observed in the experimental spectrum.

In solid-state ^{2}H NMR spectroscopy, the experimentally observed quadrupolar coupling is given by the difference in the frequencies $\Delta\nu_Q^{\pm} \equiv \Delta\nu_Q^{+} - \Delta\nu_Q^{-}$ of the spectral lines due to the perturbing Hamiltonian. The result for the quadrupolar frequencies ($\nu_Q^{\pm}$) thus reads:

$$\nu_Q^{\pm} = \pm\frac{3}{4}\chi_Q\left\{D_{00}^{(2)}(\Omega_{PL}) - \frac{\eta_Q}{\sqrt{6}}\left[D_{-20}^{(2)}(\Omega_{PL}) + D_{20}^{(2)}(\Omega_{PL})\right]\right\}. \quad (1)$$

In the above formula, $\chi_Q \equiv e^2qQ/h$ is the *static* quadrupolar coupling constant, η_Q corresponds to the asymmetry parameter of the EFG tensor, $D_{00}^{(2)}(\Omega_{PL})$ is a Wigner rotation matrix element, and $\Omega_{PL} \equiv (\alpha_{PL}, \beta_{PL}, \gamma_{PN})$ are the Euler angles [137] relating the principal axis system (PAS) of the EFG tensor (P) to the laboratory frame (L) [29, 128, 136]. Furthermore, it turns out that the static EFG tensor of the C–^{2}H bond is nearly axially symmetric ($\eta_Q \approx 0$), which leads us to the simpler result:

$$\nu_Q^{\pm} = \pm\frac{3}{4}\chi_Q D_{00}^{(2)}(\Omega_{PL}). \quad (2)$$

The experimental quadrupolar splitting is thus given by:

$$\Delta\nu_{\mathrm{Q}} = \frac{3}{2}\chi_{\mathrm{Q}} D_{00}^{(2)}\left(\Omega_{\mathrm{PL}}\right). \tag{3}$$

Now in liquid-crystalline membranes, the motions of the constituent molecules are often cylindrically symmetric about the bilayer normal, an axis known as the director. The overall rotation of the principal axis system of the coupling tensor to the laboratory frame, described by the Ω_{PL} Euler angles, can thus be represented by the effect of two consecutive rotations. First, the Euler angles $\Omega_{\mathrm{PD}}(t)$ represent the (time-dependent) rotation from the principal axis frame to the director frame, and second the Euler angles Ω_{DL} represent the (static) rotation from the director frame to laboratory frame. Using the closure property of the rotation group [136], and considering the cylindrical symmetry about the director, we can then expand Eq. (3), which now reads

$$\Delta\nu_{\mathrm{Q}} = \frac{3}{2}\chi_{\mathrm{Q}}\left\langle D_{00}^{(2)}\left(\Omega_{\mathrm{PD}}\right)\right\rangle D_{00}^{(2)}\left(\Omega_{\mathrm{DL}}\right) \tag{4a}$$

$$= \frac{3}{2}\chi_{\mathrm{Q}}\frac{1}{2}\left\langle 3\cos^2\beta_{\mathrm{PD}} - 1\right\rangle \frac{1}{2}\left(3\cos^2\beta_{\mathrm{DL}} - 1\right). \tag{4b}$$

Here, $\beta_{\mathrm{DL}} \equiv \theta$ is the angle of the bilayer normal to the static external magnetic field. The segmental order parameter S_{CD} is given by:

$$S_{\mathrm{CD}} = \frac{1}{2}\left\langle 3\cos^2\beta_{\mathrm{PD}} - 1\right\rangle \tag{5}$$

where the angular brackets denote a time/ensemble average. It follows that

$$\Delta\nu_{\mathrm{Q}} = \frac{3}{2}\chi_{\mathrm{Q}} S_{\mathrm{CD}} P_2\left(\cos\beta_{\mathrm{DL}}\right) \tag{6}$$

where $P_2(\cos\beta_{\mathrm{DL}}) \equiv (3\cos^2\beta_{\mathrm{DL}} - 1)/2$ is the second-order Legendre polynomial. The above expression describes the dependence of the quadrupolar splitting on the (Euler) angles that rotate the coupling tensor from its principal axes system to the laboratory frame, as defined by the main magnetic field. Figure 2 illustrates the effect of cholesterol on the solid-state deuterium NMR lineshape for 1,2-diperdeuteriomyristoyl-*sn*-glycero-3-phosphocholine (DMPC-d_{54}) bilayers. A gradual increase in the quadrupolar splittings ($\Delta\nu_{\mathrm{Q}}$) for the acyl segments is observed as cholesterol concentration is increased, which reflects increased orientational order of the acyl chain segments with respect to the bilayer normal. This finding explains the well-known condensing effect of cholesterol at the molecular level, involving a reduction of the area per phospholipid molecule at the aqueous interface, accompanied by an increase in the bilayer hydrocarbon thickness.

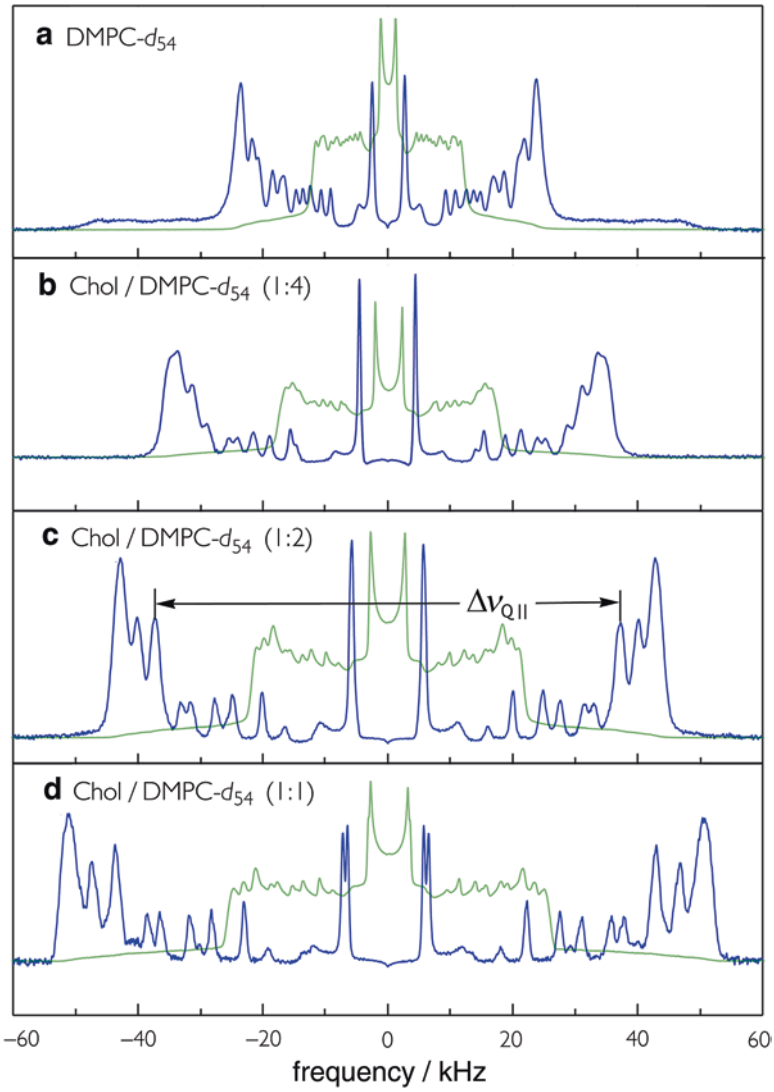

Fig. 2 Solid-state ^{2}H NMR spectra demonstrate the reduction in conformational degrees of freedom for the acyl chain orientation due to cholesterol: (**a**) DMPC-d_{54} in the liquid-disordered (l_d) phase, and (**b**–**d**) DMPC-d_{54} containing various mole fractions of cholesterol in the liquid-ordered (l_o) phase. Data were acquired at a magnetic field strength of 11.7 T (76.8 MHz) at $T = 44$ °C. Powder-type spectra (green) of randomly oriented multilamellar dispersions were numerically inverted (de-Paked) to yield sub-spectra corresponding to the $\theta = 0°$ orientation (blue). Note that a distribution of residual quadrupolar couplings (RQCs) corresponds to the various C^2H_2 and C^2H_3 groups with a progressive increase due to cholesterol. Data are taken from [112]

We can now introduce simplifying precepts from statistical mechanics to further explain the solid-state NMR lineshapes in terms of membrane structural dynamics. For detailed explanations and applications of the statistical mean-torque theory, the interested reader is referred to the literature [30, 65, 70, 73, 138]. The microscopic observables from ^{2}H NMR spectroscopy can then be related to the nano- or microstructure of the membrane lipid assembly. Structural quantities of interest for the lamellar state correspond to the mean interfacial area $\langle A \rangle$, together with the average thickness D_C of the bilayer hydrocarbon region, and the mean aqueous distance separating the lamellae [28, 128, 139–142]. Clearly, the area per lipid molecule plays an important role in molecular dynamics (MD) simulations of lipid membranes [71, 124, 142–148]. The various nanostructures are the result of a balance of forces acting at the level of the polar head groups and hydrocarbon chains [5, 13, 16, 138, 149, 150]. Notably, the deformation of a membrane film away from the equilibrium state is characterized by four material constants: (1) the surface tension γ (which is zero for a membrane bilayer at equilibrium), (2) the area expansion modulus K_A or alternatively the lateral compressibility $C_A \equiv 1/K_A$, (3) the bending rigidity K_C, and (4) the monolayer spontaneous H_0 curvature. The above structural quantities are fundamental to the forces governing the nano- and microstructures of assemblies of membrane lipids and amphiphiles. Representative applications of solid-state ^{2}H NMR spectroscopy to lipid membranes include studies of the influences of cholesterol [151–153] as well as acyl chain polyunsaturation [36, 67, 143, 150, 154–158].

2.2 *Temperature–Composition Phase Diagram of Lipid/Sterol Mixtures*

Lipid-lipid interactions have been investigated for a variety of systems and are important determinants of membrane organization. The lipid composition of the outer leaflet of a typical mammalian plasma membrane mainly comprises sphingomyelin (SM), cholesterol, and unsaturated phosphatidylcholine (PC) [59, 159]. Preferential association of SM and cholesterol has been observed in various membrane environments including enrichment in detergent-resistant membranes [53, 160]; formation of ordered phases in three-component giant unilamellar vesicles [64]; and the direct observation of small domains in the membranes of living cells [161]. Despite the research efforts by many groups into lipid-cholesterol interactions, however, important questions remain concerning the role of cholesterol and other sterols in forming the tightly packed liquid-ordered (l_o) phase. For instance, liquid-disordered (l_d) and (l_o)phases coexist in 1,2-dipalmitoyl-*sn*-glycero-3-phosphocholine (DPPC)/sterol model membranes [75, 162]. Still, the two phases remain submicroscopic in size. Because their small size makes these dynamic domains invisible by most imaging techniques, it has been postulated that l_d/l_o phase coexistence is absent in DPPC/cholesterol model membranes. An alternative explanation

for membrane heterogeneity invokes lipid compositional fluctuations due to proximity to a critical point [126, 163, 164]. Complicating matters further in biological membranes is the asymmetric distribution of lipid molecules between the inner and outer leaflets [165]. In this regard, theoretical descriptions of phospholipid/sterol interactions are extensive [74, 166–170]. The original PC/sterol condensed complex model [166] has been modified to predict phase coexistence in DPPC/cholesterol model membranes above the main transition temperature [171] as well as DPPC phase diagrams with ergosterol [172] and lanosterol [173]. Research in this area remains very active as molecular simulations improve, and experimental input parameters become more accurate [174].

Using solid-state ^{2}H NMR spectroscopy, influences of cholesterol on both the lipid head groups [151] and the acyl chains [152] have been extensively investigated. Cholesterol is located beneath the polar head groups, where it can interact strongly with the acyl chains and act as a spacer molecule, as first suggested [151] in terms of an umbrella-like model. Influences of the acyl chain ordering and dynamics are further discussed below. Previous NMR spectra of DPPC gave the first detailed phase diagram of this cholesterol/lipid mixture [74, 75] and entailed acquiring solid-state ^{2}H NMR spectra for temperatures from 25 to 70 °C and cholesterol concentrations from 0 to 30%. Recently, the binary cholesterol/DPPC phase diagram has been confirmed and extended with 1-palmitoyl-2-perdeuteriopalmitoyl-*sn*-glycero-3-phosphocholine (DPPC-d_{31})/cholesterol membranes [175]. Analogous experiments have been conducted for DPPC-d_{62} using ergosterol [162] and lanosterol [173] as well as N-perdeuteriopalmitoyl-D-erythro-sphingosylphosphorylcholine (PSM-d_{31}). These comparative studies allow insightful comparisons to be made for data obtained using palmitoyl chains with similar conformations. Partial phase diagrams for multilamellar dispersions of *sn*-2 palmitoyl chain-perdeuterated DPPC-d_{31}/cholesterol and for N-linked palmitoyl chain-perdeuterated PSM-d_{31}/cholesterol mixtures have been constructed solely from ^{2}H NMR measurements. Examples of the phase diagrams for the DPPC-d_{31}/cholesterol and PSM-d_{31}/cholesterol multilamellar dispersions obtained from the ^{2}H NMR spectral analysis for various temperatures and cholesterol compositions are shown in Fig. 3. The phase diagrams are very similar and exhibit solid-ordered (s_o) + (l_o) and l_d + l_o coexistence regions with a clear three-phase line separating them [75, 175]. Three regions of two-phase coexistence and a three-phase line are identified in DPPC-d_{31}/cholesterol multilamellar dispersions, as well as in the PSM-d_{31}/cholesterol multilamellar dispersions, thus confirming the basic features of the phase diagram [75]. Narrowing of the l_d + l_o coexistence region at high temperature implies a critical point that corresponds to a cholesterol concentration between ~25 and 30 mol%.

Notably, macroscopic (micron-sized) coexistence of l_d and l_o phases is not observed with solid-state ^{2}H NMR spectroscopy. Instead, spectral line broadening in the l_d + l_o coexistence region points to intermediate exchange of lipids between the two types of domains. The length scales associated with the domains are estimated to be 75–150 nm for DPPC-d_{31}/cholesterol and PSM-d_{31}/cholesterol model membrane mixtures [175]. Distances have been estimated between l_d/l_o domain interfaces in DPPC/cholesterol and PSM/cholesterol multilamellar dispersions to be

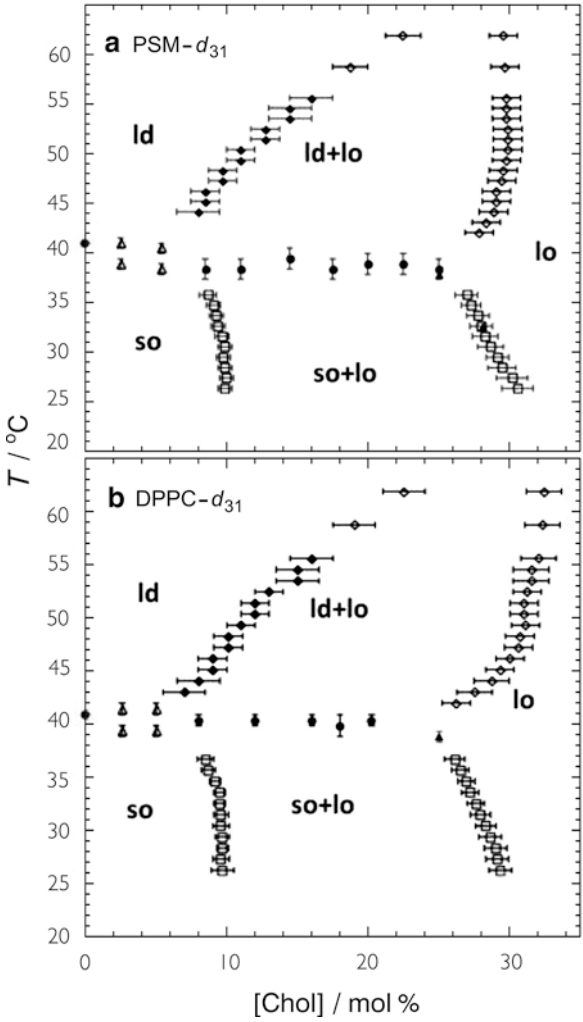

Fig. 3 Partial phase diagrams of: (**a**) PSM-d_{31}/cholesterol and (**b**) DPPC-d_{31}/cholesterol membranes obtained from solid-state ^{2}H NMR spectroscopy. Symbols denote (filled circles) the midpoint of the transition obtained from the de-Paked ^{2}H NMR spectra as a function of temperature; the onset or end of the transition as obtained (open triangles) by inspection of the temperature-dependent spectra, (open squares) from spectral subtractions, (open diamonds) from first-moment M_1 curves, or (filled diamonds) by inspection of the de-Paked spectra against cholesterol concentration; and lastly (filled triangles) the onset of the transition in the first-moment $M_1(T)$ curves. Data are for multilamellar dispersions having cholesterol concentrations of 25 or 28.1 mol% in (**a**) PSM-d_{31}/cholesterol bilayers and 25 mol% in (**b**) DPPC-d_{31}/cholesterol bilayers. Figure modified from [175]

~80 nm. The sizes are on the order of the dimensions of putative rafts in cellular membranes [165]. Hence, if rafts exist in cell membranes, they will be strongly governed by lipid/lipid interactions. The high cholesterol concentration found in many plasma membranes suggests that their preferred physical organization is most likely similar to the l_o phase. With the availability of a detailed picture of the DPPC/cholesterol and PSM/cholesterol binary systems in hand, future ^{2}H NMR studies of ternary raft-like systems [65, 113] can be then conducted to gain added insight into the behavior of lipid rafts in cellular plasma membranes.

2.3 *Separated Local-Field ^{13}C NMR Spectroscopy: ^{13}C–^{1}H Dipolar Couplings Allow Calculations of Lipid Bilayer Structure*

Lipid membrane systems clearly can benefit from precise structural characterization using solid-state NMR methods. As explained in the previous section, solid-state ^{2}H NMR spectroscopy is prominent among these methods. However, such applications are foreshadowed by the need for ^{2}H-isotope labeling involving synthetic organic chemistry [154, 176]. By the introduction of dipolar-recoupling methods, it is possible to extend the approaches originally developed with regard to solid-state ^{2}H NMR spectroscopy to other classes of biologically relevant lipids, as they occur in a membrane environment. In this regard, separated local-field (SLF) ^{13}C NMR spectroscopy [70, 73, 115, 177, 178] at natural abundance expands the range of applications of solid-state NMR spectroscopy in membrane biophysics. For example, sphingolipids and other natural lipids may be investigated, together with their interactions with cholesterol in raft-like lipid mixtures and with membrane proteins. Additional applications of natural abundance ^{13}C NMR methods to polyunsaturated lipid bilayers [178, 179] have been described. In these examples and others, we are interested in how the molecular properties of membrane lipids explain their biological functions within the broad context of structural biophysics [5, 6, 18, 180].

In what are called separated local-field (SLF) experiments, typically measurements of the direct ^{13}C–^{1}H dipolar couplings are carried out involving liquid-crystalline systems, such as lipid bilayers at natural isotopic abundance. Through-space direct ^{13}C–^{1}H dipolar interactions report on the orientations of the individual ^{13}C–^{1}H bonds with respect to the bilayer normal, and are mathematically isomorphous to the C–^{2}H bond order parameters, measured in solid-state ^{2}H NMR spectroscopy. Various SLF methods include for example dipolar-recoupling methods [70, 73, 106, 115, 177, 181], switched-angle spinning, and off-magic-angle spinning experiments [182]. Segmental order parameters can be unambiguously determined by SLF methods, and hence it is a useful technique for lipid structural studies. In lipid systems, correspondingly the segmental order parameters are defined as:

$$S_{CH} = \frac{1}{2}\left\langle 3\cos^2 \beta_{CH} - 1 \right\rangle \tag{7}$$

where β_{CH} is the instantaneous angle between the ^{13}C–^{1}H bond direction and the bilayer normal. Based on the geometrical considerations, the S_{CH} order parameters for a polymethylene chain are negative. Note that here we refer to the absolute order parameters $|S_{CH}|$, which are calculated from the relation:

$$\left|S_{CH}\right| = \frac{\left|\Delta\nu_D\right|}{\chi_D \chi_P}. \tag{8}$$

In the above formula, $\chi_D = \left(-\mu_0 \gamma_C \gamma_H / 4\pi^2\right)\left\langle r_{CH}^{-3} \right\rangle$ is the dipolar coupling constant (40.783 kHz corresponding to $b_{CH}/2\pi$ = 20.392 kHz for an aliphatic ^{13}C–^{1}H bond), χ_P = 0.393 is the pulse sequence scaling factor [73, 177], and $\Delta\nu_D$ is the measured residual dipolar coupling (RDC) evaluated at the $\theta = 90°$ orientation of the lineshape (Pake powder pattern). An illustration of the results obtained for mixtures of lipids and cholesterol using the dipolar recoupling with shape and scaling preservation (DROSS) experiment is shown in Fig. 4 [73]. The solid-state NMR spectra show well-resolved ^{13}C chemical shifts on the horizontal axis and the site-specific ^{1}H–^{13}C dipolar couplings on the vertical axis. A representative INEPT ^{13}C NMR spectrum showing highly resolved ^{13}C chemical shift resonances for POPC lipid and cholesterol is provided in Fig. 5 [73], which is indicative of the applicability of separated local-field NMR experiments for obtaining the site-specific information about lipid bilayers and lipid mixtures.

3 Molecular Distributions of Lipids are Obtained Using Solid-State ^{2}H NMR Spectral Lineshapes

The solid-state ^{2}H NMR spectrum for 1,2-diperdeuteriomyristoyl-*sn*-glycero-3-phosphocholine (DMPC-d_{54}) at 30 °C shown in Fig. 2a is illustrative of applications to phospholipids with perdeuterated chains in the physiologically relevant, liquid-crystalline state [111, 127]. Because the sample consists of bilayers randomly oriented in the aqueous medium relative to the direction of the magnetic field, the spectrum is a powder-type pattern that is a superposition of signals from the lamellae at all orientations. At each angle, the signal consists of doublets from the chain methyl and methylene positions along the perdeuterated chains [183]. The resulting spectrum has well-defined edges at ~±15 kHz due to a roughly constant order for the acyl methylene segments nearest to the head group of the lipid molecule. Individual peaks within the spectrum arise from less ordered methylene groups in the lower portion of the chains, and the highly disordered terminal methyl group produces the central pair of peaks [128]. From the distribution of the RQCs, structural quantities such as mean area per lipid $\langle A \rangle$ and volumetric bilayer thickness D_C

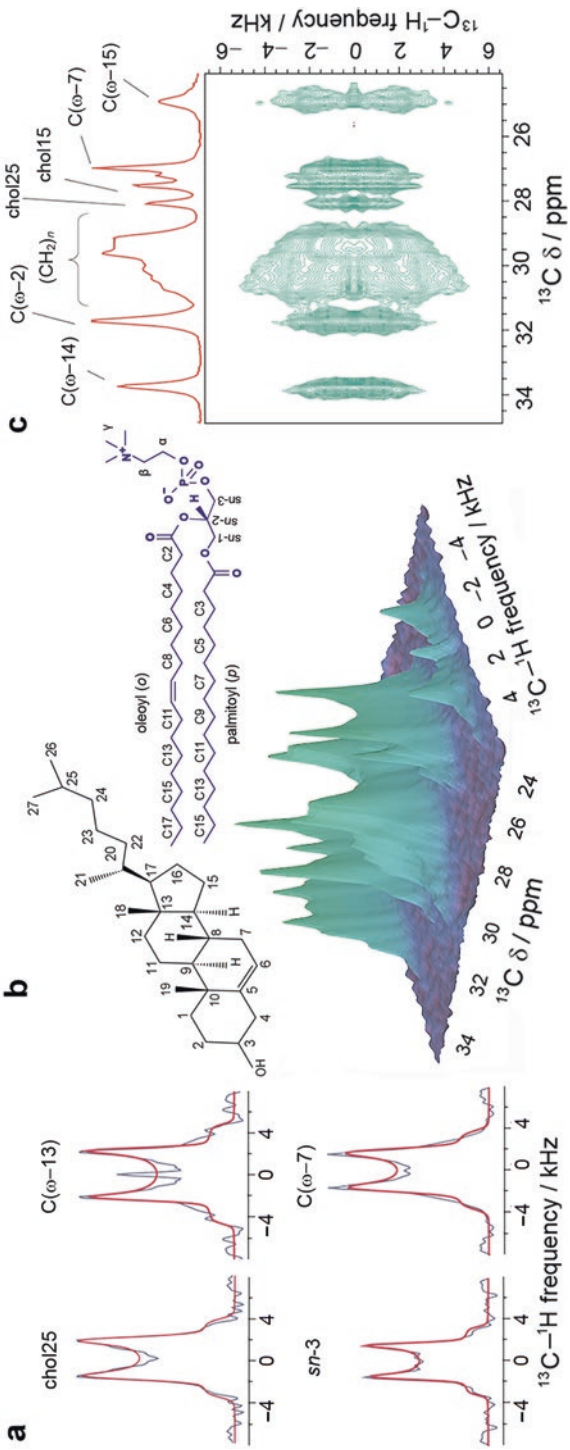

Fig. 4 Site-specific ^{13}C–^{1}H residual dipolar couplings (RDCs) are measured using two-dimensional separated local-field ^{13}C NMR (DROSS) spectrum for POPC/cholesterol (1:1) binary mixture at $T = 30$ °C. (**a**) Selected recoupled powder patterns, showing experimental (gray) and simulated (red) lineshapes. (**b**) Oblique view of aliphatic fingerprint region of the DROSS spectrum of binary system POPC/cholesterol. (**c**) The 2D plane of the spectrum shown in (**b**). The ^{13}C isotropic chemical shift (δ) spectrum is on the horizontal axis (red). The peak separation of the Pake doublet yields the site-specific ^{13}C–^{1}H dipolar couplings along the vertical axis. Figure modified from [73]

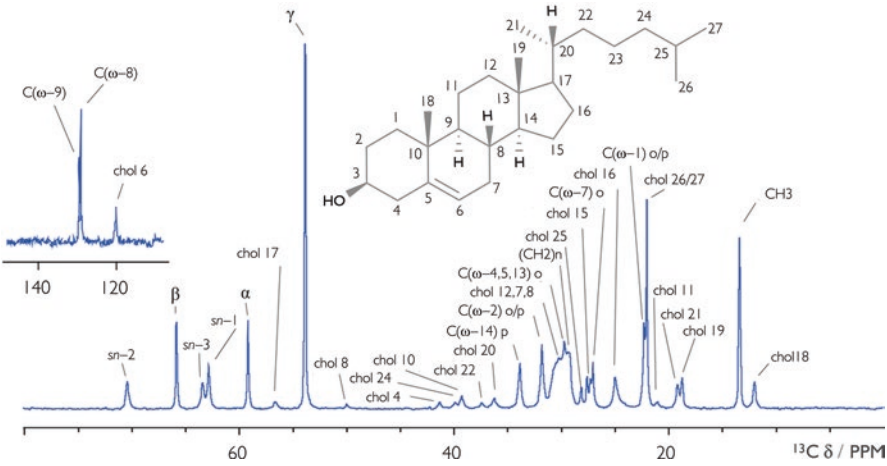

Fig. 5 Experimental INEPT ^{13}C NMR spectrum of the unsaturated lipid 1-palmitoyl-2-oleoyl-*sn*-glycero-3-phosphocholine (POPC) in the presence of 33% cholesterol (chol) at 30 °C. The INEPT experiment is used as part of the separated local-field experiment DROSS. Several highly resolved ^{13}C chemical shifts for POPC and cholesterol show the applicability of separated local-field NMR experiments for obtaining site-specific information on the lipid/cholesterol mixtures. Data obtained from [73]

are readily derived by a mean-torque (MT) model, and can be related to the corresponding material constants or elastic moduli [28, 30, 138]. The significant increase in the observed RQCs upon addition of cholesterol to DMPC bilayers is also shown in a series of spectra from Fig. 2b–d.

3.1 Bilayers Containing Cholesterol Enable Testing of Theories for Dynamical Structures of Membrane Assemblies

In general, lipid bilayers containing cholesterol allow an excellent model for testing theories for the configurational ordering and structural dynamics of liquid-crystalline membranes [30]. As we can see in Fig. 6, for the DMPC-d_{54} bilayer, both in the absence and presence of cholesterol, a well-defined profile of the segmental order parameters $S_{CD}^{(i)}$ versus the acyl segment position (i) is evident. An approximate order parameter plateau occurs over the middle part of the chains, followed by a progressive decrease, which manifests the end effects within the bilayer central hydrocarbon core (Fig. 6). In addition, due to the orientation of the glycerol backbone nearly perpendicular to the membrane surface, the *sn*-1 and *sn*-2 acyl chains are inequivalent [29, 129, 132]. The initial chain geometry leads to smaller order parameters for the beginning of the *sn*-2 chain [143, 184]. Beyond the first few segments, the order parameters of the *sn*-2 chain become larger than those of the *sn*-1

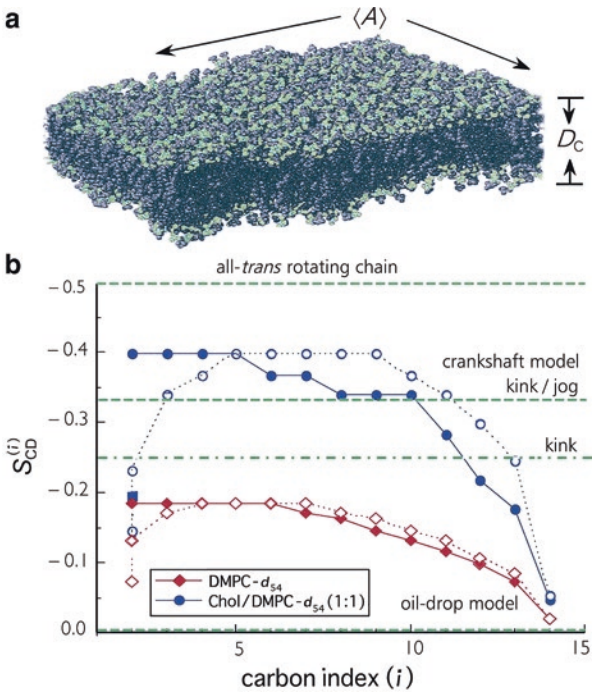

Fig. 6 Comparison of theoretical and solid-state ^{2}H NMR spectroscopy results for the configurational ordering and structural dynamics of liquid-crystalline membranes. The bilayer dimensions correspond to the interfacial membrane area per lipid $\langle A \rangle$ and volumetric thickness D_C. Structural parameters are calculated from the acyl chain volume V_C and moments $\langle \cos \beta \rangle$ and $\langle \cos^2 \beta \rangle$ obtained from the order parameter plateau, where β is the angle between the virtual bond connecting two neighboring carbons of the *i*th segment and bilayer normal [138]. Profiles of segmental order parameters $S_{CD}^{(i)}$ as a function of acyl chain position (i) for DMPC-d_{54} and DMPC-d_{54}/cholesterol (1:1) are shown at $T = 44$ °C [111]. Filled and open symbols refer to inequivalent *sn*-1 and *sn*-2 acyl chains, respectively. Reference order parameters are indicated for limiting cases of an oil-drop model with $S_{CD} = 0$, a crankshaft model having $S_{CD} = -1/3$, and an all-*trans* rotating chain with $S_{CD} = -1/2$. Data are taken from [153]

chain [154]. Smaller statistical fluctuations are associated with greater travel (flux) of the *sn*-2 chain to compensate for the initial position closer to the aqueous interface. The order profile clearly suggests that variations in the degree of acyl chain entanglement occur as a function of depth within the bilayer hydrocarbon region. As a result, it is unlikely that the phospholipids move individually within the bilayer, even in the presence of cholesterol [153, 185, 186].

The approach of using a model membrane, comprising a lipid that forms a fluid bilayer together with a lipid known to form a more ordered bilayer, as well as cholesterol in varying amounts, is probably most accessible as a mimic of biomembranes with a vast number of components [1, 15]. Interestingly, cholesterol has two different functions in model membrane systems: on the one hand, it increases the hydrophobic mismatch of the lipids at low concentrations and thereby enhances

phase separation. On the other hand, it functions as a mixing agent at high concentrations. Let us consider in greater detail the results in Fig. 6 for the DMPC-d_{54} bilayer, both in the absence and presence of cholesterol. To calibrate our intuition, at this point it might be helpful for readers to consider some simple motional models as heuristic guides or limiting cases. Referring again to Fig. 6, the first example is an all-*trans* rotating polymethylene chain, where Eq. (2) with $\beta_{PD} = 90^{o}$ then yields $S_{CD} = -1/2$ as a reference value. Next, we can consider a crankshaft model involving a polymethylene chain that is saturated with kink configurations *gauche*$^{\pm}$-*trans*-*gauche*$^{\mp}$, leading to $S_{CD} = -1/3$ for comparison. Last, the classical oil-drop model completely neglects tethering of the acyl chains to the aqueous interface, in which case the isotropic motion gives $S_{CD} = 0$ as a limit. One can then compare the experimental order profiles to the above limiting cases as benchmarks.

As we have already seen in Fig. 2, for the DMPC-d_{54}/cholesterol (1:1) binary mixture, in the liquid-ordered (l_o) phase there is a dramatic increase in the RQCs versus the liquid-disordered (l_d) phase of DMPC-d_{54} alone. This is due to a substantial reduction of the degrees of freedom of the flexible phospholipids, coming from the van der Waals interactions with the rigid sterol frame. The corresponding plateau in the order profile, cf. Fig. 6, can be understood in terms of a relatively constant probability of the acyl chain configurations, resulting from their tethering via the polar head groups to the aqueous interface, together with their travel (flux) toward the bilayer interior. For the top part of the acyl chains, the segmental order parameters approach the limiting value of $S_{CD} = -1/2$ when cholesterol is present, as expected for an all-*trans* rotating polymethylene chain [112]. However, there is still an approximate plateau indicating entanglement of the chain ends. Note that in the absence of cholesterol, the additional acyl disorder can arise from internal degrees of freedom of the phospholipids, e.g., due to segmental isomerizations, molecular motions, or collective thermal excitations of the bilayer. These additional degrees of freedom lead to smaller absolute S_{CD} values for the DMPC-d_{54} bilayer. Provided that the disorder of the DMPC-d_{54} bilayer is due mainly to rotational isomerism, then the acyl chains fall somewhere between the limiting crankshaft model with $S_{CD} = -1/3$, and the classical oil-drop model for which $S_{CD} = 0$. For the DMPC-d_{54} bilayer, both in the presence and absence of cholesterol, the acyl chains are more disordered within the hydrocarbon core to fill in the free volume that would otherwise be present due to chain terminations, approaching the classical "oil-drop" limit only in the center of the bilayer.

3.2 Order Parameter Profiles of Binary Mixtures of Cholesterol with Phospholipids and Sphingolipids: Implications for Rafts in Cellular Membranes

In addition to glycerophospholipids, most eukaryotic cells contain sphingolipids and sterols as additional classes of lipids (30–40 mol% cholesterol and 10–20 mol% sphingomyelin). Notably, plasma membranes of animal cells are enriched in cholesterol,

which is metabolically derived from lanosterol by removal of the methyl groups from the α-face of the molecule, raising the question of their evolution and function in the organization of the bilayer. Despite extensive research, whether the well-known ordering effect of cholesterol for sphingomyelin and other saturated glycerophospholipids leads to lateral phase segregation and microdomains remains under discussion, as the situation in vivo is far too complex to be exactly determined. However, the structural properties and phase-transition temperatures of sphingomyelins near body temperature (37 °C) suggest that they may play an important role in the formation of specialized domains in membranes, such as lipid rafts [47, 55, 69, 187].

Various studies have been reported on the comparison of order parameter profiles for sphingolipids and phospholipids, and their binary and tertiary mixtures with cholesterol [65, 73, 113, 152, 153]. Results have been obtained from solid-state ^{2}H NMR lineshapes of both POPC-d_{31} and PSM-d_{31} in a complementary way in the corresponding ternary systems. Addition of cholesterol at 20 mol% has been shown to have a major impact on the spectra of PSM-d_{31} in ternary mixtures with POPC (1:1). The range of phase coexistence is increased by the addition of POPC, thereby resisting the formation of the l_d phase from the l_o phase. By contrast, addition of PSM shows an increased ordering effect on the palmitoyl chain in POPC relative to the PSM-free POPC-d_{31}/cholesterol mixture. Analysis of solid-state ^{2}H NMR data using a first-order mean-torque model [65, 138] has uncovered interesting insights into the effect of cholesterol on the lateral organization of lipid-cholesterol mixtures. As described by Bartels et al. [65], the addition of cholesterol initially drives the phase separation (l_d–l_o) by inducing greater lateral order in sphingomyelin than in POPC lipids. However, at 20 mol% cholesterol, discrete components due to POPC-d_{31} and PSM-d_{31} phase separations are observed. At physiological temperature, the lipids in the ternary mixture (1:1 PSM/POPC with 20 mol% cholesterol) show distinct structural parameters (bilayer thickness and area per lipid). Structural parameters of POPC are highly temperature dependent, whereas sphingomyelin shows resistance to thermally driven structural deformation, and stronger affinity of cholesterol that can drive the formation of membrane domains. In mixtures with high amounts of cholesterol (33 mol%), saturation of the ordering effect for PSM seems to facilitate ideal mixing of the components, and hence similar results are observed. These observations naturally bring the intuition that the phase separation is driven by hydrophobic mismatch of the acyl chains of the various lipids, e.g., it is assumed the thickness difference is induced by unequal sterol partitioning into the two phases.

Another study using solid-state ^{13}C NMR spectroscopy [73] has shown that the cholesterol-mediated structural perturbations are less pronounced for egg-yolk sphingomyelin (EYSM) than for POPC. In Fig. 7, the order parameter profiles derived using separated local-field (SLF) ^{13}C NMR spectroscopy for EYSM and POPC bilayers are shown. The influence of cholesterol for the l_o phase of POPC and EYSM is clearly distinguishable. The higher-order parameter values for both the lipid bilayers at various carbon positions are an arresting indication of the l_o phase [6, 65, 92, 106, 111–113, 188–190], due to interaction with cholesterol [191–193]. In addition, the nonequivalence of the segments of the *sn*-1 and *sn*-2 chains [132] is

clearly reflected in the case of the POPC bilayers (Fig. 6a, b). Monounsaturation of the oleoyl chain at the C9 and C10 sites renders the two vinyl ^{13}C–^{1}H positions orientationally nonequivalent, both to each other and to the other saturated chain segments. The terminal methyl groups of the acyl chains exhibit very small residual dipolar couplings (RDC), because of the reorientation and three-fold symmetry of the methyl ^{13}C–^{1}H bonds. The largest couplings of these sites are observed at the C3 position, which may participate in interfacial exchange-type C3–OH hydrogen bonding, and/or C3–OH acceptor and NH donor hydrogen bonding. The large value is suggestive of a glycerol backbone conformation that is stabilized through lipid packing assisted by hydrogen bonding in the l_d phase.

Most striking, upon addition of 50 wt% cholesterol, the increment in segmental order parameters is $\Delta|S_{CH}| \approx 0.25$ for POPC and ≈ 0.12 for EYSM, as indicated in Fig. 7 (comparisons are for the maximum absolute $|S_{CH}|$ values due to the plateau region of the $|S_{CD}|$ profiles). Correspondingly, the increment in the hydrocarbon thickness and condensation of the area per lipid for EYSM is lower than for POPC. Such a remarkable difference indicates that EYSM is in a relatively ordered state in the single-component membrane. The higher acyl segmental order parame-

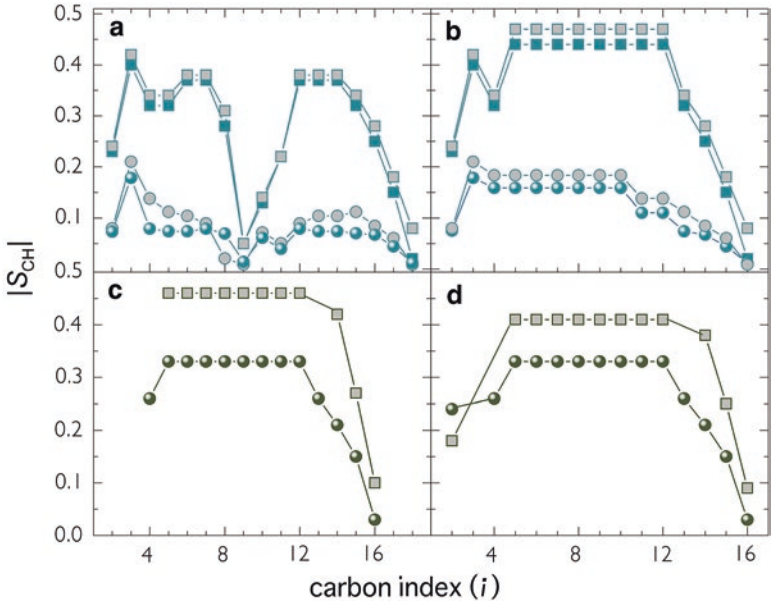

Fig. 7 Segmental order parameter S_{CH} profiles from solid-state ^{13}C NMR spectroscopy (separated local-field) indicate lipid-specific loss of conformational disorder due to cholesterol. Absolute order profiles are plotted for: (**a**) the *sn*-2 oleoyl chain of POPC, (**b**) the *sn*-1 palmitoyl chain of POPC, (**c**) the *sn*-2 sphingosine chain of EYSM, and (**d**) the *sn*-1 palmitoyl chain of EYSM. Circles represent pure lipids and squares represent lipid mixtures with cholesterol (1:1). For POPC, data are shown at two temperatures, $T = 28$ °C (gray-filled symbols) and $T = 48$ °C (solid symbols), and for EYSM at $T = 48$ °C. Note that upon adding cholesterol the absolute S_{CH} order parameters increase more for POPC than in EYSM. Figure adapted from [73]

ters in single-component bilayers at a given temperature, for EYSM relative to POPC, indicate the high propensity of self-association for the hydrophobic moieties of sphingomyelin lipids [55, 69]. Notably, these observations suggest that upon adding cholesterol, the entropic loss is less pronounced for EYSM than for POPC, as discussed in [29]. Mixing of cholesterol is more favorable for sphingolipids compared to phosphatidylcholines, potentially driving the formation of lipid rafts in multicomponent biomembranes [194, 195]. In other words, like dissolves like, as we learn in our introductory chemistry courses.

4 Nuclear Spin Relaxation Reveals Multiscale Dynamics of Membrane Lipids

An important further aspect is that analysis of the nuclear spin relaxation rates yields experimental information about the molecular dynamics that is unobtainable with other biophysical methods [128]. The possible types of motions that occur in lyotropic liquid crystals are: (1) segmental motions due to rotational isomerizations of the flexible surfactant or lipid molecules; (2) slower effective rotations of the entangled molecules; and (3) collective deformations of the bilayer which span a broad range, and can influence interactions involving the assembly [29, 111, 112, 129, 196]. At the high frequencies, bond stretching and bending vibrations are most likely too fast to influence significantly the nuclear spin relaxation, but rather lead to a pre-averaging of the coupling tensor [196, 197]. Identifying the predominant contributions within the various motional regimes, and characterizing their energetic parameters, would reveal the atomistic interactions that lead to bulk material properties based on the current NMR technology [29]. For liquid-crystalline membranes, elastic deformations (modeled as splay, twist, and bend) within the hydrocarbon core are interpreted as collective lipid dynamics on the order of membrane dimensions [127]. It follows that NMR relaxation studies of lipid membranes in the l_o and l_d phases can strongly benefit our understanding of the atomistic lipid–cholesterol interactions, leading to changes in bulk membrane physical properties, with striking biological consequences.

4.1 Fluctuating Molecular Interactions Due to Various Types of Lipid Motions Within the Bilayer Cause the Nuclear Spin Relaxation

The process of NMR relaxation is due to fluctuations of the coupling Hamiltonian, on account of the various possible motions of the lipid molecules within the bilayer. According to time-dependent perturbation theory, these fluctuations give rise to transitions between the various adjacent energy levels [136]. In ^{2}H NMR relaxometry of

liquid-crystalline membrane lipids, one is often interested in the spin–lattice (R_{1Z}) relaxation rates. Experimental R_{1Z} relaxation rate measurements involve perturbation of the magnetization away from the equilibrium value, and then following the attainment of equilibrium by observing the magnetization recovery as a function of time. The observable relaxation rates are related to the spectral densities of motion in the laboratory frame by:

$$R_{1Z} = \frac{3}{4}\pi^2 \chi_Q^2 \left[J_1(\omega_0) + 4J_2(2\omega_0) \right]. \tag{9}$$

In the above expression, R_{1Z} is the spin–lattice (longitudinal) relaxation rate, and $J_m(\omega_0)$ denotes the irreducible spectral densities of motion, where $m = 1$, 2, and ω_0 is the deuteron Larmor frequency. The spectral densities $J_m(\omega_0)$ describe the power spectrum of the motions as a function of frequency ω_0 in terms of fluctuations of the Wigner rotation matrix elements for transformation of the coupling (EFG) tensor from its principal axis system to the laboratory frame. They are the Fourier transform partners of the orientational correlation functions $G_m(t)$ which depend on time, and characterize the C–^{2}H bond fluctuations.

4.2 Generalized Model-Free Aspects of the Nuclear Spin Relaxation of Membrane Lipid Bilayers

Here, we give a brief introduction to the model-free interpretation of the relaxation rates for general readers, while dealing with actual lipid relaxation data. For a more complete description of generalized model-free (GMF) analysis, readers are referred to the review by Xu et al. [136]. Contributions to the nuclear spin relaxation from motions with different characteristic mean-squared amplitudes and timescales are possible in terms of a hierarchical energy landscape [185]. They include: (1) the static coupling tensor that is modulated by rapid local segmental motions, such as *trans-gauche* isomerizations of the hydrocarbon chains of the lipid or surfactant molecules; and (2) the residual coupling tensor (leftover from the fast motions) that is further modulated by slower motions. The slower motions in principle might include whole-molecule motions of the flexible phospholipids, or alternatively collective thermal excitations involving the various lipid molecules [146, 198]. Clearly, the segmental order parameters depend only on the amplitudes of the C–^{2}H bond fluctuations. On the other hand, the relaxation rates depend on both the orientational amplitudes and the rates of the C–^{2}H bond fluctuations. According to the GMF approach of relaxation rate analysis [136, 197, 199], a simple linear dependence of the R_{1Z} rates on the squared segmental order parameters (S_{CD}^2) (square-law) along the chain would result (Fig. 8). In the limit of short-wavelength excitations, on the order of the bilayer thickness and less, the spectral density reads [200]:

$$J_m(\omega) = \frac{5}{2} S_{CD}^2 D \omega^{-(2-d/2)} \left[\left| D_{-1m}^{(2)}(\beta_{DL}) \right|^2 + \left| D_{1m}^{(2)}(\beta_{DL}) \right|^2 \right]. \tag{10}$$

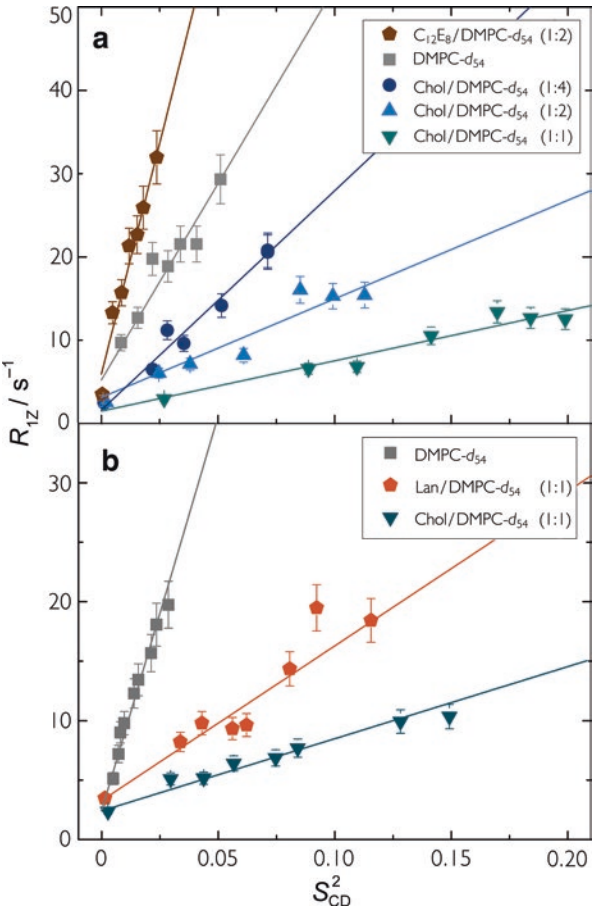

Fig. 8 Solid-state ^{2}H NMR relaxation at 76.8 MHz (11.8 T) shows emergence of membrane elastic fluctuations and their suppression by sterols. Striking differences are uncovered in membrane elastic fluctuations from cholesterol versus lanosterol at the atomistic level. (**a**) Dependence of spin–lattice relaxation rates $R_{1Z}^{(i)}$ on squared order parameters $S_{CD}^{(i)}$ for resolved ^{2}H NMR splittings of DMPC-d_{54} showing influences of cholesterol in the liquid-ordered (l_o) phase at T = 44 °C. The presence of cholesterol leads to a large decrease in the square-law slopes, corresponding to a progressive reduction in bilayer elasticity. An opposite increase is seen for bilayers containing $C_{12}E_8$ nonionic detergent at T = 42 °C. Data are taken from [129]. (**b**) Dependence of spin–lattice relaxation rates $R_{1Z}^{(i)}$ on squared order parameters $S_{CD}^{(i)}$ in liquid-ordered phase (l_o) for resolved ^{2}H NMR splittings of DMPC-d_{54} showing influences of lanosterol and cholesterol at T = 55 °C. Note that the decrease in the square-law slopes is consistent with a gradual reduction in bilayer elasticity on going from lanosterol to cholesterol. Data are taken from [112]

Here, ω is the angular frequency, D is the viscoelastic constant, d is the dimensionality, and $D^{(2)}$ indicates the second-rank Wigner rotation matrix [137]. The irreducible spectral densities $J_m(\omega)$ depend on the square of the observed S_{CD} order

parameters, and the slope of the square-law plot is inversely related to the softness of the membrane. For 3D quasielastic fluctuations, the viscoelastic constant is given by $D = 3k_{\mathrm{B}}T\sqrt{\eta}\,/\,5\pi\sqrt{2K^3}S_{\mathrm{s}}^2$, where a single elastic constant K is assumed, in which η is the corresponding viscosity coefficient, S_s is the order parameter for the relatively slow motions, and other symbols have their usual meanings. No distinction is made between splay, twist, and bend deformations. In addition to the bending modulus κ, the compression modulus K_B may come into play [141].

4.3 Nuclear Spin Relaxation of Lipid Membranes in the Liquid-Ordered Phases Reveals Atomistic Lipid–Cholesterol Interactions and Bulk Membrane Physical Properties

In the example presented here, a solid-state ^{2}H NMR relaxation study of effect of cholesterol on lipid bilayers shows that a square-law functional dependence of the R_{1Z} rates versus the order parameters S_{CD} is evident along the entire acyl chain for the multilamellar dispersions of DMPC-d_{54}/cholesterol bilayers (Fig. 8a) [111]. This dependence on the motional amplitudes signifies relatively slow bilayer motions that modulate the residual coupling tensors leftover from faster segmental motions (Fermi's golden rule). Given a simple composite membrane deformation model [196, 201], the R_{1Z} rates are due to a broad spectrum of 3D collective bilayer excitations, with effective rotations of the lipids. Transverse ^{2}H NMR spin relaxation studies also provide evidence for 2D collective motions of the membrane film, albeit at lower frequencies [202–205]. By contrast, local *trans-gauche* isomerizations along the chains modulate the same *static* NMR coupling tensor, and do not yield such a square-law. With regard to splay deformations, the so-called bending rigidity is $\kappa \approx Kt$, where $t = 2D_{\mathrm{C}}$ is the bilayer thickness, giving a $\kappa^{-3/2}$ dependence of the R_{1Z} rates [127]. Moreover, 3D director fluctuations ($d = 3$) yield a $\omega^{-1/2}$ frequency dispersion as a characteristic signature [185, 206]. In this case, the reduction in the square-law slope, cf. Fig. 8a, b, reflects an increase in κ and/or S_{s} due to short-range cholesterol–phospholipid interactions. One should also note that at the molecular level, a dynamical protrusion of cholesterol across the midplane, i.e., between the apposed monolayers, is suggested by quasielastic neutron scattering studies [27, 207]. Indeed, the square-law functional dependence as first discussed [185] is a model-free correlation among the experimental observables, and it does not rest on any specific molecular interpretation. For the longitudinal relaxation rates of liquid-crystalline lipid membranes, the above analysis is expected to be generally applicable.

4.4 The Progressive Increase in Bilayer Rigidity from Lanosterol to Cholesterol Parallels the Metabolic Pathway of Sterol Biogenesis

Influences of cholesterol on the physical properties of DMPC bilayers have also been compared to its metabolic precursor lanosterol in a related study [112] (Fig. 8b). Notably, cholesterol is a two-faced molecule—the α-face is smooth and the β-face is molecularly rough due to the methyl substituents. Even so, lanosterol is methylated on both the α-face and the β-face (Fig. 1), and it presents a more balanced countenance to the phospholipids [208]. In terms of biomolecular NMR spectroscopy, it has been observed that the slope of the square-law plot is greater for lanosterol than for cholesterol, consistent with the bilayer stiffness being less for lanosterol versus its metabolic product cholesterol [25, 112, 209]. Again, it is found that the site-specific analysis of the solid-state NMR results based on atomistic observables matches the results for the macroscopic bilayer elasticity [207, 210] (Fig. 9). The more molecularly smooth van der Waals surface of the α-face of cholesterol [92, 193, 211, 212] enables a large increase in bilayer rigidity and stabilizes the liquid-ordered phase to an even greater degree than lanosterol. Figure 9a illustrates the comparison of the bending rigidity (modulus) (κ) for the DMPC bilayers using deuterium NMR relaxometry and thermal shape fluctuation data. The progressive increase in the bilayer rigidity on going from lanosterol to cholesterol (Fig. 9b) parallels the metabolic pathway of sterol biogenesis [162, 173, 213–217], and may be related to the optimization or evolution of the biophysical properties of cholesterol. In a similar study, the effect of several sterols on the lipid order and bilayer rigidity has been investigated for macroscopically aligned bilayers of DMPC or DPPC using ^{2}H NMR spectra and spin–lattice relaxation rates [25]. The bending modulus of the bilayers was calculated from plots of the relaxation rates versus the square of the order parameter. Clear differences were obtained in the efficiency of the sterols to increase the stiffness of the bilayers. These differences are correlated to the ability of the sterols to induce the liquid-ordered phase in binary as well as in ternary systems.

5 Biophysical Conclusions and Outlook

Solid-state NMR methods offer excellent experimental techniques in medicine and biology. They uniquely probe the physical properties of lipid membranes and provide information complementary to other spectroscopic methods. Interestingly, owing to their physiological liquid-crystalline nature, membrane elastic deformations together with their multiscale molecular dynamics clearly fall in the solid-state ^{2}H NMR time- and length scales. The membrane stiffening effect upon addition of sterols has been investigated at an atomistically resolved level, showing a direct correspondence with bulk elasticity. Phase separation in bilayers of ternary lipid

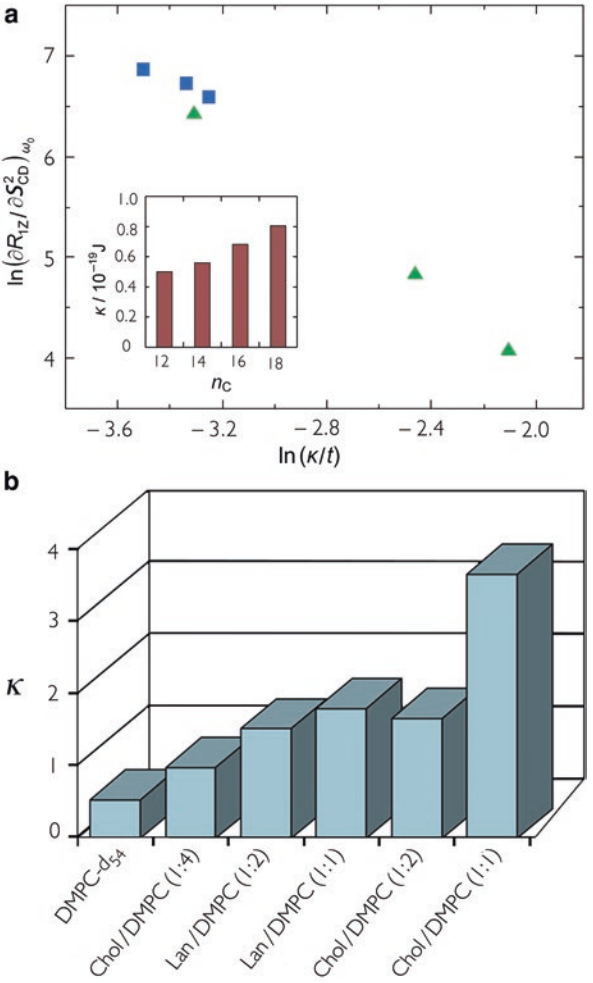

Fig. 9 Bending rigidity of lipid bilayers obtained from solid-state ^{2}H NMR relaxation analysis. (**a**) Comparison of solid-state ^{2}H NMR square-law slopes to bending rigidity κ obtained from thermal shape fluctuation data for lipid vesicles. Results for homologous series of PCs with acyl carbon lengths of n_C = 12, 14, and 16 in the liquid-disordered (l_d) phase at 55.4 MHz (squares); data at 76.8 MHz for DMPC/cholesterol mixtures with X_C = 0, 0.33, and 0.50 in the liquid-ordered (l_o) phase (triangles). The inset shows the values of κ estimated from the ^{2}H NMR model for the homologous series of PCs. Bending rigidity estimates from solid-state ^{2}H NMR are in good agreement with the values obtained from thermal shape fluctuation data. Figure adapted from [111]. (**b**) Comparison of bending rigidities of DMPC lipid bilayers obtained by solid-state ^{2}H NMR relaxation at various compositions of DMPC and cholesterol (Chol/DMPC), and DMPC and lanosterol (Lan/DMPC) mixtures. Significant difference is seen in the influence of cholesterol versus lanosterol on the elastic properties of DMPC membrane bilayers. Data taken from [112]

mixtures occurs mainly due to dissimilar affinities for different cholesterol concentrations. It is likely that configurational entropy plays a major role in the formation of the lipid domains called rafts [73]. It has also been shown in model membranes [20, 46, 47, 218] that formation of such domains entails Gibbs free energies that are lower than those for protein-lipid interactions, which therefore may indicate a role for proteins in domain formation. Further detailed information regarding protein–lipid interactions can contribute to understanding the lateral organization of cellular plasma membranes, and how lipid rafts may be implicated in their functional mechanisms. Moreover, nuclear spin–lattice relaxation studies of fluid lipid bilayers manifest their quasielastic deformation on short length and timescales, on the order of the membrane thickness and less. Interpretation of the atom-specific NMR relaxation data is in broad agreement with molecular dynamics (MD) simulations of flexible surfactant films and lipid membranes [51, 142, 146, 198, 219]. Molecular simulations [219] show that local *trans-gauche* isomerizations are accompanied by concerted isomerizations about multiple bonds in the assembly of lipid acyl chains. The continuum model for NMR relaxation approximates the collective excitations in mathematical closed form, wherein the influences of cholesterol and the membrane thickness correspond to the bilayer bending energy. A key remaining question is how the bilayer softness as studied with NMR relaxation may be significant to lipid–protein interactions in fluid membranes [6, 220–222], where elastic curvature deformation may play an important role.

Acknowledgments This research was supported by the US National Institutes of Health (R01EY012049 and R01EY026041) and the US National Science Foundation (MCB-1817862 and CHE-1904125).

References

1. van Meer G, Voelker DR, Feigenson GW. Membrane lipids: where they are and how they behave. Nat Rev Mol Cell Biol. 2008;9:112–24.
2. Krause MR, Regen SL. The structural role of cholesterol in cell membranes: from condensed bilayers to lipid rafts. Acc Chem Res. 2014;47:3512–21.
3. Maxfield FR, Tabas I. Role of cholesterol and lipid organization in disease. Nature. 2005; 438:612–21.
4. Yeagle PL. Modulation of membrane function by cholesterol. Biochimie. 1991;73:1303–10.
5. Brown MF. Modulation of rhodopsin function by properties of the membrane bilayer. Chem Phys Lipids. 1994;73:159–80.
6. Brown MF. Curvature forces in membrane lipid-protein interactions. Biochemistry. 2012;51: 9782–95.
7. Brown MF. Soft matter in lipid–protein interactions. Annu Rev Biophys. 2017;46:379–410.
8. Sheng R, Chen Y, Gee HY, Stec E, Melowic HR, Blatner NR, Tun MP, Kim Y, Källberg M, Fujiwara TK, Hong JH, Kim KP, Lu H, Kusumi A, Lee MG, Cho W. Cholesterol modulates cell signaling and protein networking by specifically interacting with PDZ domain-containing scaffold proteins. Nat Commun. 2012;3:1249.
9. Huang P, Nedelcu D, Watanabe M, Jao C, Kim Y, Liu J, Salic A. Cellular cholesterol directly activates smoothened in Hedgehog signaling. Cell. 2016;166:1176–87.

10. Liu S-L, Sheng R, Jung JH, Wang L, Stec E, O'Connor MJ, Song S, Bikkavilli RK, Winn RA, Lee D, Baek K, Ueda K, Levitan I, Kim K-P, Cho W. Orthogonal lipid sensors identify transbilayer asymmetry of plasma membrane cholesterol. Nature Chem Biol. 2016;13:268–74.
11. Molugu TR, Brown MF. Cholesterol-induced suppression of membrane elastic fluctuations at the atomistic level. Chem Phys Lipids. 2016;199:39–51.
12. Arriaga LR, Rodriguez-Garcia R, Moleiro LH, Prevost S, Lopez-Montero I, Hellweg T, Monroy F. Dissipative dynamics of fluid lipid membranes enriched in cholesterol. Adv Colloid Interface Sci. 2017;247:514–20.
13. Seddon JM. Structure of the inverted hexagonal (H_{II}) phase, and non-lamellar phase transitions of lipids. Biochim Biophys Acta. 1990;1031:1–69.
14. Seddon JM, Templer RH, Warrender NA, Huang Z, Cevc G, Marsh D. Phosphatidylcholine-fatty acid membranes: effects of headgroup hydration on the phase behaviour and structural parameters of the gel and inverse hexagonal (H_{II}) phases. Biochim Biophys Acta. 1997;1327:131–47.
15. Feigenson GW. Phase behavior of lipid mixtures. Nature Chem Biol. 2006;2:560–3.
16. Zimmerberg J, Gawrisch K. The physical chemistry of biological membranes. Nature Chem Biol. 2006;2:564–7.
17. Krepkiy D, Mihailescu M, Freites JA, Schow EV, Worcester DL, Gawrisch K, Tobias DJ, White SH, Swartz KJ. Structure and hydration of membranes embedded with voltage-sensing domains. Nature. 2009;462:473–9.
18. Phillips R, Ursell T, Wiggins P, Sens P. Emerging roles for lipids in shaping membrane-protein function. Nature. 2009;459:379–85.
19. Amazon JJ, Feigenson GW. Lattice simulations of phase morphology on lipid bilayers: renormalization, membrane shape, and electrostatic dipole interactions. Phys Rev E. 2014;89:022702.
20. Feigenson GW. Pictures of the substructure of liquid-ordered domains. Biophys J. 2015; 109:854–5.
21. Rheinstädter MC, Ollinger C, Fragneto G, Demmel F, Salditt T. Collective dynamics of lipid membranes studied by inelastic neutron scattering. Phys Rev Lett. 2004;93:108107.
22. Brown MF, Chan SI. Bilayer membranes: deuterium and carbon-13 NMR. eMagRes. 2007:1–15.
23. Tyler AI, Clarke J, Seddon J, Law R. Solid state NMR of lipid model membranes. In: Owen DM, editor. Methods in membrane lipids. New York: Springer; 2015. p. 227–53.
24. Kaiser H-J, Lingwood D, Levental I, Sampaio JL, Kalvodova L, Rajendran L, Simons K. Order of lipid phases in model and plasma membranes. Proc Natl Acad Sci U S A. 2009; 106:16645–50.
25. Orädd G, Shahedi V, Lindblom G. Effect of sterol structure on the bending rigidity of lipid membranes: a ^{2}H NMR transverse relaxation study. Biochim Biophys Acta. 2009;1788:1762–71.
26. Coskun U, Simons K. Cell membranes: the lipid perspective. Structure. 2011;19:1543–8.
27. Kaye MD, Schmalzl K, Nibali VC, Tarek M, Rheinstädter MC. Ethanol enhances collective dynamics of lipid membranes. Phys Rev E. 2011;83(5 Pt 1):050907.
28. Mallikarjunaiah KJ, Leftin A, Kinnun JJ, Justice MJ, Rogozea AL, Petrache HI, Brown MF. Solid-state ^{2}H NMR shows equivalence of dehydration and osmotic pressures in lipid membrane deformation. Biophys J. 2011;100:98–107.
29. Leftin A, Xu X, Brown MF. Phospholipid bilayer membranes: deuterium and carbon-13 NMR spectroscopy. eMagRes. 2014;3:199–214.
30. Kinnun JJ, Mallikarjunaiah KJ, Petrache HI, Brown MF. Elastic deformation and area per lipid of membranes: atomistic view from solid-state deuterium NMR spectroscopy. Biochim Biophys Acta. 2015;1848:246–59.
31. Shaghaghi M, Keyvanloo A, Huang ZH, Szoka FC, Thewalt JL. Constrained versus free cholesterol in DPPC membranes: a comparison of chain ordering ability using deuterium NMR. Langmuir. 2017;33:14405–13.
32. Thewalt JL. Essential insights into lipid membrane organization from essential fatty acids. Biophys J. 2018;114:254–5.

33. Molugu TR, Xu X, Lee S, Mallikarjunaiah KJ, Brown MF. Solid-state ^{2}H NMR studies of water-mediated lipid membrane deformation. In: Webb GA, editor. Modern magnetic resonance. Cham: Springer; 2018. p. 1–27.
34. Soubias O, Teague WE Jr, Hines KG, Gawrisch K. Rhodopsin/lipid hydrophobic matching-rhodopsin oligomerization and function. Biophys J. 2015;108:1125–32.
35. Chawla U, Jiang YJ, Zheng W, Kuang LJ, Perera SMDC, Pitman MC, Brown MF, Liang HJ. A usual G-protein-coupled receptor in unusual membranes. Angew Chem Int Ed. 2016;55:588–92.
36. Teague WE Jr, Soubias O, Petrache H, Fuller N, Hines KG, Rand RP, Gawrisch K. Elastic properties of polyunsaturated phosphatidylethanolamines influence rhodopsin function. Faraday Discuss. 2013;161:383–95.
37. Liang R, Li H, Swanson JMJ, Voth GA. Multiscale simulation reveals a multifaceted mechanism of proton permeation through the influenza A M2 proton channel. Proc Natl Acad Sci U S A. 2014;111:9396–401.
38. Soubias O, Teague WE, Hines KG, Gawrisch K. The role of membrane curvature elastic stress for function of rhodopsin-like G protein-coupled receptors. Biochimie. 2014;107:28–32.
39. Gondré-Lewis MC, Petrache HI, Wassif CA, Harries D, Parsegian A, Porter FD, Loh YP. Abnormal sterols in cholesterol-deficiency diseases cause secretory granule malformation and decreased membrane curvature. J Cell Sci. 2006;119:1876–85.
40. Kumar GA, Jafurulla M, Chattopadhyay A. The membrane as the gatekeeper of infection: cholesterol in host–pathogen interaction. Chem Phys Lipids. 2016;199:179–85.
41. Eriksson JC, Henriksson U. Bridging-cluster model for hydrophobic attraction. Langmuir. 2007;23:10026–33.
42. Goñi FM, Alonso A, Bagatolli LA, Brown RE, Marsh D, Prieto M, Thewalt JL. Phase diagrams of lipid mixtures relevant to the study of membrane rafts. Biochim Biophys Acta. 2008;1781:665–84.
43. Escriba PV, Gonzalez-Ros JM, Goni FM, Kinnunen PKJ, Vigh L, Sanchez-Magraner L, Fernandez AM, Busquets X, Horvath I, Barcelo-Coblijn G. Membranes: a meeting point for lipids, proteins and therapies. J Cell Mol Med. 2008;12:829–75.
44. Armstrong CL, Barrett MA, Hiess A, Salditt T, Katsaras J, Shi A-C, Rheinstädter MC. Effect of cholesterol on the lateral nanoscale dynamics of fluid membranes. Eur Biophys J. 2012; 41:901–13.
45. Armstrong CL, Marquardt D, Dies H, Kučerka N, Yamani Z, Harroun TA, Katsaras J, Shi A-C, Rheinstädter MC. The observation of highly ordered domains in membranes with cholesterol. Plos One. 2013;8:e66162.
46. Ackerman DG, Feigenson GW. Multiscale modeling of four-component lipid mixtures: domain composition, size, alignment, and properties of the phase interface. J Phys Chem B. 2015;119:4240–50.
47. Konyakhina TM, Feigenson GW. Phase diagram of a polyunsaturated lipid mixture: brain sphingomyelin/1-stearoyl-2-docosahexaenoyl-*sn*-glycero-3-phosphocholine/cholesterol. Biochim Biophys Acta. 2016;1858:153–61.
48. Epand RM. Lipid polymorphism and protein-lipid interactions. Biochim Biophys Acta. 1998; 1376:353–68.
49. Epand RM. Cholesterol and the interaction of proteins with membrane domains. Prog Lipid Res. 2006;45:279–94.
50. Scheidt HA, Meyer T, Nikolaus J, Baek DJ, Haralampiev I, Thomas L, Bittman R, Mueller P, Herrmann A, Huster D. Cholesterol's aliphatic side chain modulates membrane properties. Angew Chem Int Ed. 2013;52:12848–51.
51. Sodt AJ, Sandar ML, Gawrisch K, Pastor RW, Lyman E. The molecular structure of the liquid-ordered phase of lipid bilayers. J Am Chem Soc. 2014;136:725–32.
52. Levental I, Veatch SL. The continuing mystery of lipid rafts. J Mol Biol. 2016;428:4749–64.
53. Brown DA, London E. Functions of lipid rafts in biological membranes. Annu Rev Cell Dev Biol. 1998;14:111–36.

54. Golebiewska U, Scarlata S. The effect of membrane domains on the G protein-phospholipase Cβ signaling pathway. Crit Rev Biochem Mol Biol. 2010;45:97–105.
55. Simons K, Gerl MJ. Revitalizing membrane rafts: new tools and insights. Nat Rev Mol Cell Biol. 2010;11:688–99.
56. Simons K, Sampaio JL. Membrane organization and lipid rafts. Cold Spring Harb Perspect Biol. 2011;3:a004697.
57. Surma MA, Klose C, Simons K. Lipid-dependent protein sorting at the trans-Golgi network. Biochim Biophys Acta. 2012;1821:1059–67.
58. Klose C, Surma MA, Simons K. Organellar lipidomics – background and perspectives. Curr Opin Cell Biol. 2013;25:406–13.
59. Song Y, Kenworthy AK, Sanders CR. Cholesterol as a co-solvent and a ligand for membrane proteins. Prot Sci. 2014;23:1–22.
60. Day CA, Kenworthy AK. Functions of cholera toxin B-subunit as a raft cross-linker. Essays Biochem. 2015;57:135–45.
61. Keller SL, McConnell HM. Stripe phases in lipid monolayers near a miscibility critical point. Phys Rev Lett. 1999;82:1602–5.
62. Edidin M. The state of lipid rafts: from model membranes to cells. Annu Rev Biophys Biomol Struct. 2003;32:257–83.
63. Polozov IV, Gawrisch K. Characterization of the liquid-ordered state by proton MAS NMR. Biophys J. 2006;90:2051–61.
64. Veatch SL, Soubias O, Keller SL, Gawrisch K. Critical fluctuations in domain-forming lipid mixtures. Proc Natl Acad Sci U S A. 2007;104:17650–5.
65. Bartels T, Lankalapally RS, Bittman R, Beyer K, Brown MF. Raftlike mixtures of sphingomyelin and cholesterol investigated by solid-state ^{2}H NMR spectroscopy. J Am Chem Soc. 2008;130:14521–32.
66. Korade Z, Kenworthy AK. Lipid rafts, cholesterol, and the brain. Neuropharmacology. 2008;55:1265–73.
67. Wassall SR, Stillwell W. Polyunsaturated fatty acid-cholesterol interactions: domain formation in membranes. Biochim Biophys Acta. 2009;1788:24–32.
68. Camley BA, Brown FLH. Dynamic simulations of multicomponent lipid membranes over long length and time scales. Phys Rev Lett. 2010;105:148102.
69. Lingwood D, Simons K. Lipid rafts as a membrane-organizing principle. Science. 2010; 327:46–50.
70. Leftin A, Job C, Beyer K, Brown MF. Solid-state ^{13}C NMR reveals annealing of raft-like membranes containing cholesterol by the intrinsically disordered protein α-synuclein. J Mol Biol. 2013;425:2973–87.
71. Meinhardt S, Vink RLC, Schmid F. Monolayer curvature stabilizes nanoscale raft domains in mixed lipid bilayers. Proc Natl Acad Sci U S A. 2013;110:4476–81.
72. Quinn PJ. Structure of sphingomyelin bilayers and complexes with cholesterol forming membrane rafts. Langmuir. 2013;29:9447–56.
73. Leftin A, Molugu TR, Job C, Beyer K, Brown MF. Area per lipid and cholesterol interactions in membranes by separated local-field ^{13}C NMR spectroscopy. Biophys J. 2014;107:2274–86.
74. Ipsen JH, Karlström G, Mouritsen OG, Wennerström H, Zuckermann MJ. Phase equilibria in the phosphatidylcholine-cholesterol system. Biochim Biophys Acta. 1987;905:162–72.
75. Vist MR, Davis JH. Phase-equilibria of cholesterol dipalmitoylphosphatidylcholine mixtures: ^{2}H nuclear magnetic-resonance and differential scanning calorimetry. Biochemistry. 1990;29:451–64.
76. Simons K, Ikonen E. How cells handle cholesterol. Science. 2000;290:1721–6.
77. Simons K, Toomre D. Lipid rafts and signal transduction. Nat Rev Mol Cell Biol. 2000;1:31–9.
78. Ge Y, Gao J, Jordan R, Naumann CA. Changes in cholesterol level alter integrin sequestration in raft-mimicking lipid mixtures. Biophys J. 2018;114:158–67.
79. Greenwood AI, Pan J, Mills TT, Nagle JF, Epand RM, Tristram-Nagle S. CRAC motif peptide of the HIV-1 gp41 protein thins SOPC membranes and interacts with cholesterol. Biochim Biophys Acta. 2008;1778:1120–30.

80. Baier CJ, Fantini J, Barrantes FJ. Disclosure of cholesterol recognition motifs in transmembrane domains of the human nicotinic acetylcholine receptor. Sci Rep. 2011;69:1–7.
81. Fantini J, Barrantes FJ. How cholesterol interacts with membrane proteins: an exploration of cholesterol-binding sites including CRAC, CARC, and tilted domains. Front Physiol. 2013;4:1–9.
82. Koufos E, Chang EH, Rasti ES, Krueger E, Brown AC. Use of a cholesterol recognition amino acid consensus peptide to inhibit binding of a bacterial toxin to cholesterol. Biochemistry. 2016;55:4787–97.
83. Jafurulla M, Tiwari S, Chattopadhyay A. Identification of cholesterol recognition amino acid consensus (CRAC) motif in G-protein coupled receptors. Biochim Biophys Res Commun. 2011;404:569–73.
84. Vogel A, Tan K-T, Waldmann H, Feller SE, Brown MF, Huster D. Flexibility of Ras lipid modifications studied by ^{2}H solid-state NMR and molecular dynamics simulations. Biophys J. 2007;93:2697–712.
85. Weise K, Huster D, Kapoor S, Triola G, Waldmann H, Winter R. Gibbs energy determinants of lipoprotein insertion into lipid membranes: the case study of Ras proteins. Faraday Discuss. 2013;161:549–61.
86. Hubbell WL, McConnell HM. Molecular motion in spin-labeled phospholipids and membranes. J Am Chem Soc. 1971;93:314–26.
87. Semer R, Gelerinter E. Spin label study of the effects of sterols on egg lecithin bilayers. Chem Phys Lipids. 1979;23:201–11.
88. Delmelle M, Butler KW, Smith ICP. Saturation transfer electron-spin resonance spectroscopy as a probe of anisotropic motion in model membrane systems. Biochemistry. 1980;19:698–704.
89. Manukovsky N, Sanders E, Matalon E, Wolf SG, Goldfarb D. Membrane curvature and cholesterol effects on lipids packing and spin-labelled lipids conformational distributions. Mol Phys. 2013;111:2887–96.
90. Williams JA, Wassall CD, Kemple MD, Wassall SR. An electron paramagnetic resonance method for measuring the affinity of a spin-labeled analog of cholesterol for phospholipids. J Membr Biol. 2013;246:689–96.
91. Cheng C-Y, Olijve LLC, Kausik R, Han S. Cholesterol enhances surface water diffusion of phospholipid bilayers. J Chem Phys. 2014;141:22D513.
92. Lai AL, Freed JH. HIV gp41 fusion peptide increases membrane ordering in a cholesterol-dependent fashion. Biophys J. 2014;106:172–81.
93. Stepien P, Polit A, Wisniewska-Becker A. Comparative EPR studies on lipid bilayer properties in nanodiscs and liposomes. Biochim Biophys Acta. 2015;1848:60–6.
94. Vitiello G, Falanga A, Alcides Petruk A, Merlino A, Fragneto G, Paduano L, Galdiero S, D'Errico G. Fusion of raft-like lipid bilayers operated by a membranotropic domain of the HSV-type I glycoprotein gH occurs through a cholesterol-dependent mechanism. Soft Matter. 2015;11:3003–16.
95. Lippert JL, Peticolas W l. Laser Raman investigation of effect of cholesterol on conformational changes in dipalmitoyl lecithin multilayers. Proc Natl Acad Sci U S A. 1971;68:1572–6.
96. Tantipolphan R, Rades T, Strachan CJ, Gordon KC, Medlicott NJ. Analysis of lecithin–cholesterol mixtures using Raman spectroscopy. J Pharm Biomed Anal. 2006;41:476–84.
97. Mendelsohn R. Laser-Raman spectroscopic study of egg lecithin and egg lecithin-cholesterol mixtures. Biochim Biophys Acta. 1972;290:15–21.
98. Umemura J, Cameron DG, Mantsch HH. A Fourier transform infrared spectroscopic study of the molecular interaction of cholesterol with 1,2-dipalmitoyl-*sn*-glycero-3-phosphocholine. Biochim Biophys Acta. 1980;602:32–44.
99. Gagoś M, Arczewska M. FTIR spectroscopic study of molecular organization of the antibiotic amphotericin B in aqueous solution and in DPPC lipid monolayers containing the sterols cholesterol and ergosterol. Eur Biophys J. 2012;41:663–73.
100. Xu XL, London E. The effect of sterol structure on membrane lipid domains reveals how cholesterol can induce lipid domain formation. Biochemistry. 2000;39:843–9.

101. Yasuda T, Matsumori N, Tsuchikawa H, Lonnfors M, Nyholm TKM, Slotte JP, Murata M. Formation of gel-like nanodomains in cholesterol-containing sphingomyelin or phosphatidylcholine binary membrane as examined by fluorescence lifetimes and ^{2}H NMR spectra. Langmuir. 2015;31:13783–92.
102. Iwasaki F, Suga K, Okamoto Y, Umakoshi H. Characterization of DDAB/cholesterol vesicles and its comparison with lipid/cholesterol vesicles. J Nanosci Nanotechnol. 2018;18:1989–94.
103. Sparr E, Eriksson L, Bouwstra JA, Ekelund K. AFM study of lipid monolayers: III. Phase behavior of ceramides, cholesterol and fatty acids. Langmuir. 2001;17:164–72.
104. Lawrence JC, Saslowsky DE, Edwardson JM, Henderson RM. Real-time analysis of the effects of cholesterol on lipid raft behavior using atomic force microscopy. Biophys J. 2003;84:1827–32.
105. Sacchi M, Balleza D, Vena G, Puia G, Facci P, Alessandrini A. Effect of neurosteroids on a model lipid bilayer including cholesterol: an atomic force microscopy study. Biochim Biophys Acta. 2015;1848:1258–67.
106. Warschawski DE, Devaux PF. ^{1}H-^{13}C Polarization transfer in membranes: a tool for probing lipid dynamics and the effect of cholesterol. J Magn Reson. 2005;177:166–71.
107. Holland GP, Alam TM. Multi-dimensional ^{1}H-^{13}C HETCOR and FSLG-HETCOR NMR study of sphingomyelin bilayers containing cholesterol in the gel and liquid crystalline states. J Magn Reson. 2006;181:316–26.
108. Stockton GW, Polnaszek CF, Tulloch AP, Hasan F, Smith ICP. Molecular-motion and order in single-bilayer vesicles and multilamellar dispersions of egg lecithin and lecithin-cholesterol mixtures. A deuterium nuclear magnetic resonance study of specifically labeled lipids. Biochemistry. 1976;15:954–66.
109. Brown MF. Anisotropic nuclear spin relaxation of cholesterol in phospholipid bilayers. Mol Phys. 1990;71:903–8.
110. Weisz K, Gröbner G, Mayer C, Stohrer J, Kothe G. Deuteron nuclear magnetic resonance study of the dynamic organization of phospholipid/cholesterol bilayer membranes: molecular properties and viscoelastic behavior. Biochemistry. 1992;31:1100–12.
111. Martinez GV, Dykstra EM, Lope-Piedrafita S, Job C, Brown MF. NMR elastometry of fluid membranes in the mesoscopic regime. Phys Rev E. 2002;66:050902.
112. Martinez GV, Dykstra EM, Lope-Piedrafita S, Brown MF. Lanosterol and cholesterol-induced variations in bilayer elasticity probed by ^{2}H NMR relaxation. Langmuir. 2004;20:1043–6.
113. Bunge A, Mueller P, Stoeckl M, Herrmann A, Huster D. Characterization of the ternary mixture of sphingomyelin, POPC, and cholesterol: support for an inhomogeneous lipid distribution at high temperatures. Biophys J. 2008;94:2680–90.
114. Matsumori N, Yasuda T, Okazaki H, Suzuki T, Yamaguchi T, Tsuchikawa H, Doi M, Oishi T, Murata M. Comprehensive molecular motion capture for sphingomyelin by site-specific deuterium labeling. Biochemistry. 2012;51:8363–70.
115. Ferreira TM, Coreta-Gomes F, Ollila OHS, Moreno MJ, Vaz WLC, Topgaard D. Cholesterol and POPC segmental order parameters in lipid membranes: solid state ^{1}H–^{13}C NMR and MD simulation studies. Phys Chem Chem Phys. 2013;15:1976–89.
116. Shaghaghi M, Chen MT, Hsueh YW, Zuckermann MJ, Thewalt JL. Effect of sterol structure on the physical properties of 1-palmitoyl-2-oleoyl-*sn*-glycero-3-phosphocholine membranes determined using ^{2}H nuclear magnetic resonance. Langmuir. 2016;32:7654–63.
117. Vogel A, Scheidt HA, Baek DJ, Bittman R, Huster D. Structure and dynamics of the aliphatic cholesterol side chain in membranes as studied by ^{2}H NMR spectroscopy and molecular dynamics simulation. Phys Chem Chem Phys. 2016;18:3730–8.
118. Molugu TR, Lee S, Brown MF. Concepts and methods of solid-state NMR spectroscopy applied to biomembranes. Chem Rev. 2017;117:12087–132.
119. Schmidt ML, Davis JH. Liquid disordered-liquid ordered phase coexistence in lipid/cholesterol mixtures: a deuterium 2D NMR exchange study. Langmuir. 2017;33:1881–90.
120. Ivankin A, Kuzmenko I, Gidalevitz D. Cholesterol-phospholipid interactions: new insights from surface X-ray scattering data. Phys Rev Lett. 2010;104:108101.

121. Pan J, Cheng X, Heberle FA, Mostofian B, Kučerka N, Drazba P, Katsaras J. Interactions between ether phospholipids and cholesterol as determined by scattering and molecular dynamics simulations. J Phys Chem B. 2012;116:14829–38.
122. Foglia F, Lawrence MJ, Demė B, Fragneto G, Barlow D. Neutron diffraction studies of the interaction between amphotericin B and lipid-sterol model membranes. Sci Rep. 2012;2:778.
123. Armstrong CL, Haeussler W, Seydel T, Katsaras J, Rheinstädter MC. Nanosecond lipid dynamics in membranes containing cholesterol. Soft Matter. 2014;10:2600–11.
124. Toppozini L, Meinhardt S, Armstrong CL, Yamani Z, Kučerka N, Schmid F, Rheinstädter MC. Structure of cholesterol in lipid rafts. Phys Rev Lett. 2014;113:228101.
125. McConnell H. Complexes in ternary cholesterol-phospholipid mixtures. Biophys J. 2005; 88:L23–5.
126. Stanich CA, Honerkamp-Smith AR, Putzel GG, Warth CS, Lamprecht AK, Mandal P, Mann E, Hua T-AD, Keller SL. Coarsening dynamics of domains in lipid membranes. Biophys J. 2013;105:444–54.
127. Brown MF, Thurmond RL, Dodd SW, Otten D, Beyer K. Composite membrane deformation on the mesoscopic length scale. Phys Rev E. 2001;64:010901.
128. Brown MF. Membrane structure and dynamics studied with NMR spectroscopy. In: Merz KM, Roux B, editors. Biological membranes: a molecular perspective from computation and experiment. Basel: Birkhäuser; 1996. p. 175–252.
129. Leftin A, Brown MF. An NMR database for simulations of membrane dynamics. Biochim Biophys Acta. 2011;1808:818–39.
130. Kinnun JJ, Leftin A, Brown MF. Solid-state NMR spectroscopy for the physical chemistry laboratory. J Chem Educ. 2013;90:123–8.
131. Seelig J. Deuterium magnetic resonance: theory and application to lipid membranes. Q Rev Biophys. 1977;10:353–418.
132. Seelig J, Seelig A. Lipid conformation in model membranes and biological membranes. Q Rev Biophys. 1980;13:19–61.
133. Seelig J, Macdonald PM. Phospholipids and proteins in biological membranes. ^{2}H NMR as a method to study structure, dynamics, and interactions. Acc Chem Res. 1987;20:221–8.
134. Brown MF, Chan SI. Bilayer membranes: deuterium & carbon-13 NMR. In: Harris RK, Grant DM, editors. Encyclopedia of magnetic resonance. New York: Wiley; 1996. p. 871–85.
135. Brown MF, Lope-Piedrafita S, Martinez GV, Petrache HI. Solid-state deuterium NMR spectroscopy of membranes. In: Webb GA, editor. Modern magnetic resonance. Heidelberg: Springer; 2006. p. 245–56.
136. Xu X, Struts AV, Brown MF. Generalized model-free analysis of nuclear spin relaxation experiments. eMagRes. 2014;3:275–86.
137. Rose ME. Elementary theory of angular momentum. New York: Wiley; 1957.
138. Petrache HI, Dodd SW, Brown MF. Area per lipid and acyl length distributions in fluid phosphatidylcholines determined by ^{2}H NMR spectroscopy. Biophys J. 2000;79:3172–92.
139. Thurmond RL, Dodd SW, Brown MF. Molecular areas of phospholipids as determined by ^{2}H NMR spectroscopy: comparison of phosphatidylethanolamines and phosphatidylcholines. Biophys J. 1991;59:108–13.
140. Jansson M, Thurmond RL, Barry JA, Brown MF. Deuterium NMR study of intermolecular interactions in lamellar phases containing palmitoyllysophosphatidylcholine. J Phys Chem. 1992;96:9532–44.
141. Nagle JF, Tristram-Nagle S. Structure of lipid bilayers. Biochim Biophys Acta. 2000;1469: 159–95.
142. Pastor RW, Venable RM, Feller SE. Lipid bilayers, NMR relaxation, and computer simulations. Acc Chem Res. 2002;35:438–46.
143. Huber T, Rajamoorthi K, Kurze VF, Beyer K, Brown MF. Structure of docosahexaenoic acid-containing phospholipid bilayers as studied by ^{2}H NMR and molecular dynamics simulations. J Am Chem Soc. 2002;124:298–309.

144. Klauda JB, Venable RM, MacKerell AD Jr, Pastor RW. Considerations for lipid force field development. In: Feller SE, editor. Computational modeling of membrane bilayers; 2008. p. 1–48.
145. Klauda JB, Roberts MF, Redfield AG, Brooks BR, Pastor RW. Rotation of lipids in membranes: molecular dynamics simulation, ^{31}P spin-lattice relaxation, and rigid-body dynamics. Biophys J. 2008;94:3074–83.
146. Klauda JB, Eldho NV, Gawrisch K, Brooks BR, Pastor RW. Collective and noncollective models of NMR relaxation in lipid vesicles and multilayers. J Phys Chem B. 2008;112:5924–9.
147. Klauda JB, Venable RM, Freites JA, O'Connor JW, Tobias DJ, Mondragon-Ramirez C, Vorobyov I, MacKerell AD Jr, Pastor RW. Update of the CHARMM all-atom additive force field for lipids: validation on six lipid types. J Phys Chem B. 2010;114:7830–43.
148. Venable RM, Sodt AJ, Rogaski B, Rui H, Hatcher E, MacKerell AD Jr, Pastor RW, Klauda JB. CHARMM all-atom additive force field for sphingomyelin: elucidation of hydrogen bonding and of positive curvature. Biophys J. 2014;107:134–45.
149. Gruner SM. Stability of lyotropic phases with curved interfaces. J Phys Chem. 1989;93: 7562–70.
150. Gawrisch K. Tafazzin senses curvature. Nature Chem Biol. 2012;8:811–2.
151. Brown MF, Seelig J. Influence of cholesterol on the polar region of phosphatidylcholine and phosphatidylethanolamine bilayers. Biochemistry. 1978;17:381–4.
152. Oldfield E, Meadows M, Rice D, Jacobs R. Spectroscopic studies of specifically deuterium labeled membrane systems. Nuclear magnetic resonance investigation of effects of cholesterol in model systems. Biochemistry. 1978;17:2727–40.
153. Trouard TP, Nevzorov AA, Alam TM, Job C, Zajicek J, Brown MF. Influence of cholesterol on dynamics of dimyristoylphosphatidylcholine as studied by deuterium NMR relaxation. J Chem Phys. 1999;110:8802–18.
154. Salmon A, Dodd SW, Williams GD, Beach JM, Brown MF. Configurational statistics of acyl chains in polyunsaturated lipid bilayers from ^{2}H NMR. J Am Chem Soc. 1987;109:2600–9.
155. Wiedmann TS, Pates RD, Beach JM, Salmon A, Brown MF. Lipid-protein interactions mediate the photochemical function of rhodopsin. Biochemistry. 1988;27:6469–74.
156. Petrache HI, Salmon A, Brown MF. Structural properties of docosahexaenoyl phospholipid bilayers investigated by solid-state ^{2}H NMR spectroscopy. J Am Chem Soc. 2001;123:12611–22.
157. Huber T, Botelho AV, Beyer K, Brown MF. Membrane model for the G-protein-coupled receptor rhodopsin: hydrophobic interface and dynamical structure. Biophys J. 2004;86:2078–100.
158. Shaikh SR, Kinnun JJ, Leng X, Williams JA, Wassall SR. How polyunsaturated fatty acids modify molecular organization in membranes: insight from NMR studies of model systems. Biochim Biophys Acta. 2015;1848:211–9.
159. Zurzolo C, Simons K. Glycosylphosphatidylinositol-anchored proteins: membrane organization and transport. Biochim Biophys Acta. 2016;1858:632–9.
160. Ahmed SN, Brown DA, London E. On the origin of sphingolipid/cholesterol-rich detergent-insoluble cell membranes: physiological concentrations of cholesterol and sphingolipid induce formation of a detergent-insoluble, liquid-ordered lipid phase in model membranes. Biochemistry. 1997;36:10944–53.
161. Frisz JF, Lou KY, Klitzing HA, Hanafin WP, Lizunov V, Wilson RL, Carpenter KJ, Kim R, Hutcheon ID, Zimmerberg J, Weber PK, Kraft ML. Direct chemical evidence for sphingolipid domains in the plasma membranes of fibroblasts. Proc Natl Acad Sci U S A. 2013;110:E613–22.
162. Hsueh YW, Gilbert K, Trandum C, Zuckermann M, Thewalt J. The effect of ergosterol on dipalmitoylphosphatidylcholine bilayers: a deuterium NMR and calorimetric study. Biophys J. 2005;88:1799–808.
163. Baoukina S, Rozmanov D, Tieleman DP. Composition fluctuations in lipid bilayers. Biophys J. 2017;113:2750–61.
164. Honerkamp-Smith AR, Veatch SL, Keller SL. An introduction to critical points for biophysicists; observations of compositional heterogeneity in lipid membranes. Biochim Biophys Acta. 2009;1788:53–63.

165. Heberle FA, Marquardt D, Doktorova M, Geier B, Standaert RF, Heftberger P, Kollmitzer B, Nickels JD, Dick RA, Feigenson GW, Katsaras J, London E, Pabst G. Subnanometer structure of an asymmetric model membrane: interleaflet coupling influences domain properties. Langmuir. 2016;32:5195–200.
166. McConnell HM, Radhakrishnan A. Condensed complexes of cholesterol and phospholipids. Biochim Biophys Acta. 2003;1610:159–73.
167. Ali MR, Cheng KH, Huang JY. Assess the nature of cholesterol-lipid interactions through the chemical potential of cholesterol in phosphatidylcholine bilayers. Proc Natl Acad Sci U S A. 2007;104:5372–7.
168. Pandit SA, Scott HL. Multiscale simulations of heterogeneous model membranes. Biochim Biophys Acta. 2009;1788:136–48.
169. Longo GS, Schick M, Szleifer I. Stability and liquid-liquid phase separation in mixed saturated lipid bilayers. Biophys J. 2009;96:3977–86.
170. Rog T, Orlowski A, Llorente A, Skotland T, Sylvanne T, Kauhanen D, Ekroos K, Sandvig K, Vattulainen I. Interdigitation of long-chain sphingomyelin induces coupling of membrane leaflets in a cholesterol dependent manner. Biochim Biophys Acta. 2016;1858:281–8.
171. Radhakrishnan A. Phase separations in binary and ternary cholesterol-phospholipid mixtures. Biophys J. 2010;98:L41–3.
172. Hsueh YW, Weng CJ, Chen MT, Thewalt J, Zuckermann M. Deuterium NMR study of the effect of ergosterol on POPE membranes. Biophys J. 2010;98:1209–17.
173. Miao L, Nielsen M, Thewalt J, Ipsen JH, Bloom M, Zuckermann MJ, Mouritsen OG. From lanosterol to cholesterol: structural evolution and differential effects on lipid bilayers. Biophys J. 2002;82:1429–44.
174. Greenwood AI, Tristram-Nagle S, Nagle JF. Partial molecular volumes of lipids and cholesterol. Chem Phys Lipids. 2006;143:1–10.
175. Keyvanloo A, Shaghaghi M, Zuckermann MJ, Thewalt JL. The phase behavior and organization of sphingomyelin/cholesterol membranes: a deuterium NMR study. Biophys J. 2018; 114:1344–56.
176. Williams GD, Beach JM, Dodd SW, Brown MF. Dependence of deuterium spin-lattice relaxation rates of multilamellar phospholipid dispersions on orientational order. J Am Chem Soc. 1985;107:6868–73.
177. Gross JD, Warschawski DE, Griffin RG. Dipolar recoupling in MAS NMR: a probe for segmental order in lipid bilayers. J Am Chem Soc. 1997;119:796–802.
178. Gawrisch K, Eldho NV, Polozov IV. Novel NMR tools to study structure and dynamics of biomembranes. Chem Phys Lipids. 2002;116:135–51.
179. Brown MF, Deese AJ, Dratz EA. Proton, carbon-13, and phosphorus-31 NMR methods for the investigation of rhodopsin-lipid interactions in retinal rod outer segment membranes. Methods Enzymol. 1982;81:709–28.
180. Lee AG. How lipids affect the activities of integral membrane proteins. Biochim Biophys Acta. 2004;1666:62–87.
181. Ferreira TM, Medronho B, Martin RW, Topgaard D. Segmental order parameters in a nonionic surfactant lamellar phase studied with ^{1}H-^{13}C solid-state NMR. Phys Chem Chem Phys. 2008;10:6033–8.
182. Hong M, Schmidt-Rohr K, Pines A. NMR measurement of signs and magnitudes of C-H dipolar couplings in lecithin. J Am Chem Soc. 1995;117:3310–1.
183. Kobayashi M, Struts AV, Fujiwara T, Brown MF, Akutsu H. Fluid mechanical matching of H^{+}-ATP synthase subunit *c*-ring with lipid membranes revealed by ^{2}H solid-state NMR. Biophys J. 2008;94:4339–47.
184. Seelig J. General features of phospholipid conformation in membranes. Z Physiol Chem. 1978;359:1049–50.
185. Brown MF. Theory of spin-lattice relaxation in lipid bilayers and biological membranes. ^{2}H and ^{14}N quadrupolar relaxation. J Chem Phys. 1982;77:1576–99.
186. Trouard TP, Alam TM, Zajicek J, Brown MF. Angular anisotropy of ^{2}H NMR spectral densities in phospholipid bilayers containing cholesterol. Chem Phys Lett. 1992;189:67–75.

187. Barenholz Y, Thompson TE. Sphingomyelin: biophysical aspects. Chem Phys Lipids. 1999; 102:29–34.
188. Yun-Wei C, Costa-Filho AJ, Freed JH. Dynamic molecular structure and phase diagram of DPPC-cholesterol binary mixtures: a 2D-ELDOR study. J Phys Chem B. 2007;111:11260–70.
189. Smith AK, Freed JH. Determination of tie-line fields for coexisting lipid phases: an ESR study. J Phys Chem B. 2009;113:3957–71.
190. Tong J, Borbat PP, Freed JH, Shin Y-K. A scissors mechanism for stimulation of SNARE-mediated lipid mixing by cholesterol. Proc Natl Acad Sci U S A. 2009;106:5141–6.
191. Ipsen JH, Mouritsen OG, Bloom M. Relationships between lipid membrane area, hydrophobic thickness, and acyl-chain orientational order. The effects of cholesterol. Biophys J. 1990;57:405–12.
192. Chen Z, Rand RP. The influence of cholesterol on phospholipid membrane curvature and bending elasticity. Biophys J. 1997;73:267–76.
193. Filippov A, Orädd G, Lindblom G. The effect of cholesterol on the lateral diffusion of phospholipids in oriented bilayers. Biophys J. 2003;84:3079–86.
194. Ohvo-Rekilä H, Ramstedt B, Leppimäki P, Slotte JP. Cholesterol interactions with phospholipids in membranes. Prog Lipid Res. 2002;41:66–97.
195. Ramstedt B, Slotte JP. Sphingolipids and the formation of sterol-enriched ordered membrane domains. Biochim Biophys Acta. 2006;1758:1945–56.
196. Brown MF, Thurmond RL, Dodd SW, Otten D, Beyer K. Elastic deformation of membrane bilayers probed by deuterium NMR relaxation. J Am Chem Soc. 2002;124:8471–84.
197. Brown MF. Unified picture for spin-lattice relaxation of lipid bilayers and biomembranes. J Chem Phys. 1984;80:2832–6.
198. Klauda JB, Kučerka N, Brooks BR, Pastor RW, Nagle JF. Simulation-based methods for interpreting X-ray data from lipid bilayers. Biophys J. 2006;90:2796–807.
199. Brown MF. Theory of spin-lattice relaxation in lipid bilayers and biological membranes. Dipolar relaxation. J Chem Phys. 1984;80:2808–31.
200. Nevzorov AA, Brown MF. Dynamics of lipid bilayers from comparative analysis of ^{2}H and ^{13}C nuclear magnetic resonance relaxation data as a function of frequency and temperature. J Chem Phys. 1997;107:10288–310.
201. Nevzorov AA, Trouard TP, Brown MF. Lipid bilayer dynamics from simultaneous analysis of orientation and frequency dependence of deuterium spin-lattice and quadrupolar order relaxation. Phys Rev E. 1998;58:2259–81.
202. Bloom M, Evans E. Observations of surface undulations on the mesoscopic length scale by NMR. In: Peliti L, editor. Biologically inspired physics. New York: Plenum; 1991. p. 137–47.
203. Bloom M, Evans E, Mouritsen OG. Physical properties of the fluid lipid-bilayer component of cell membranes: a perspective. Q Rev Biophys. 1991;24:293–397.
204. Althoff G, Stauch O, Vilfan M, Frezzato D, Moro GJ, Hauser P, Schubert R, Kothe G. Transverse nuclear spin relaxation studies of viscoelastic properties of membrane vesicles. II. Experimental results. J Phys Chem B. 2002;106:5517–26.
205. Althoff G, Frezzato D, Vilfan M, Stauch O, Schubert R, Vilfan I, Moro GJ, Kothe G. Transverse nuclear spin relaxation studies of viscoelastic properties of membrane vesicles. I. Theory. J Phys Chem B. 2002;106:5506–16.
206. Brown MF, Ribeiro AA, Williams GD. New view of lipid bilayer dynamics from ^{2}H and ^{13}C NMR relaxation time measurements. Proc Natl Acad Sci U S A. 1983;80:4325–9.
207. Endress E, Heller H, Casalta H, Brown MF, Bayerl TM. Anisotropic motion and molecular dynamics of cholesterol, lanosterol, and ergosterol in lecithin bilayers studied by quasi-elastic neutron scattering. Biochemistry. 2002;41:13078–86.
208. Rog T, Pasenkiewicz-Gierula M, Vattulainen I, Karttunen M. What happens if cholesterol is made smoother: importance of methyl substituents in cholesterol ring structure on phosphatidylcholine-sterol interaction. Biophys J. 2007;92:3346–57.
209. Shahedi V, Orädd G, Lindblom G. Domain-formation in DOPC/SM bilayers studied by pfg-NMR: effect of sterol structure. Biophys J. 2006;91:2501–7.

210. Endress E, Bayerl S, Prechtel K, Maier C, Merkel R, Bayerl TM. The effect of cholesterol, lanosterol, and ergosterol on lecithin bilayer mechanical properties at molecular and microscopic dimensions: a solid-state NMR and micropipet study. Langmuir. 2002;18:3293–9.
211. Yeagle PL, Martin RB, Lala AK, Lin H-K, Bloch K. Differential effects of cholesterol and lanosterol on artificial membranes. Proc Natl Acad Sci U S A. 1977;74:4924–6.
212. Bloch K. Sterol structure and membrane function. CRC Crit Rev Biochem. 1983;14:47–92.
213. Yeagle PL. Lanosterol and cholesterol have different effects on phospholipid acyl chain ordering. Biochim Biophys Acta. 1985;815:33–6.
214. Cheng K-H, Lepock JR, Hui SW, Yeagle PL. The role of cholesterol in the activity of reconstituted Ca-ATPase vesicles containing unsaturated phosphatidylethanolamine. J Biol Chem. 1986;261:5081–7.
215. Yeagle PL, Albert AD, Boesze-Battaglia K, Young J, Frye J. Cholesterol dynamics in membranes. Biophys J. 1990;57:413–24.
216. Henriksen J, Rowat AC, Brief E, Hsueh YW, Thewalt JL, Zuckermann MJ, Ipsen JH. Universal behavior of membranes with sterols. Biophys J. 2006;90:1639–49.
217. Brief E, Kwak S, Cheng JTJ, Kitson N, Thewalt J, Lafleur M. Phase behavior of an equimolar mixture of N-palmitoyl-d_{31}-D-*erythro*-sphingosine, cholesterol, and palmitic acid, a mixture with optimized hydrophobic matching. Langmuir. 2009;25:7523–32.
218. Huang JY, Feigenson GW. Monte Carlo simulation of lipid mixtures: finding phase separation. Biophys J. 1993;65:1788–94.
219. Hofsäß C, Lindahl E, Edholm O. Molecular dynamics simulations of phospholipid bilayers with cholesterol. Biophys J. 2003;84:2192–206.
220. Scheidt HA, Huster D. Structure and dynamics of the myristoyl lipid modification of Src peptides determined by ^{2}H solid-state NMR spectroscopy. Biophys J. 2009;96:3663–72.
221. Penk A, Mueller M, Scheidt HA, Langosch D, Huster D. Structure and dynamics of the lipid modifications of a transmembrane α-helical peptide determined by ^{2}H solid-state NMR spectroscopy. Biochim Biophys Acta. 2011;1808:784–91.
222. Huster D. Solid-state NMR spectroscopy to study protein lipid interactions. Biochim Biophys Acta. 2014;1841:1146–60.

Effect of Cholesterol on the Dipole Potential of Lipid Membranes

Ronald J. Clarke

Abstract The membrane dipole potential, ψ_d, is an electrical potential difference with a value typically in the range 150–350 mV (positive in the membrane interior) which is located in the lipid headgroup region of the membrane, between the linkage of the hydrocarbon chains to the phospholipid glycerol backbone and the adjacent aqueous solution. At its physiological level in animal plasma membranes (up to 50 mol%), cholesterol makes a significant contribution to ψ_d of approximately 65 mV; the rest arising from other lipid components of the membrane, in particular phospholipids. Via its effect on ψ_d, cholesterol may modulate the activity of membrane proteins. This could occur through preferential stabilization of protein conformational states. Based on its effect on ψ_d, cholesterol would be expected to favour protein conformations associated with a small local hydrophobic membrane thickness. Via its membrane condensing effect, which also produces an increase in ψ_d, cholesterol could further modulate interactions of polybasic cytoplasmic extensions of membrane proteins, in particular P-type ATPases, with anionic lipid headgroups on the membrane surface, thus leading to enhanced conformational stabilization effects and changes to ion pumping activity.

Keywords Lipid headgroup · Oxysterols · Lipid packing · Hydrophobic thickness · Ion channels · Ion pumps

1 Introduction

The plasma cell membrane and organellar membranes of all animal cells contain significant amounts of cholesterol, with between 5 and 50 mol% of the total membrane lipid composed of cholesterol [1]. The largest percentages are found in the plasma membrane, between 10 and 30 mol% up to 50 mol% [2]. The membranes of intracellular organelles, in contrast, contain significantly lower percentages, with

R. J. Clarke (✉)
University of Sydney, School of Chemistry, Sydney, NSW, Australia
e-mail: ronald.clarke@sydney.edu.au

A. Rosenhouse-Dantsker, A. N. Bukiya (eds.), *Cholesterol Modulation of Protein Function*, Advances in Experimental Medicine and Biology 1115,
https://doi.org/10.1007/978-3-030-04278-3_6

the endoplasmic reticulum, Golgi apparatus and mitochondrial membranes, all with <10 mol% cholesterol [2]. It is highly likely that these variations in cholesterol composition between different animal membranes, which occur even within a single cell, are related to different functions of the plasma membrane versus organellar membranes and those of the proteins that they contain. In the subsequent volume of this series modulation of protein function by direct interactions between cholesterol and a variety of proteins is discussed. However, cholesterol is known to cause changes in a number of physical properties of lipid membranes, which could, by a variety of mechanisms, indirectly modify protein function. In this chapter we concentrated predominantly on the effect of cholesterol on the membrane dipole potential and how cholesterol-induced changes in dipole potential might modulate membrane protein function.

2 Membrane Dipole Potential

The membrane dipole potential, ψ_d, is an electrical potential difference which drops across the lipid headgroup region of a lipid bilayer (see Fig. 1), i.e., approximately from the position of the glycerol backbone of phospholipids and the nearest neighbouring aqueous solution (cytoplasm, extracellular fluid or organellar lumen, depending on the membrane concerned). It arises because of the anisotropic structure of a lipid membrane, with the polar lipid headgroups pointing towards the aqueous

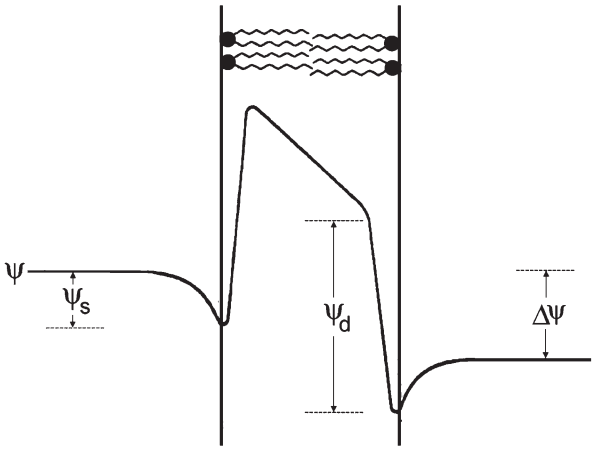

Fig. 1 Electrical potential, ψ, profile across a lipid bilayer. The transmembrane potential, $\Delta\psi$, is due to the difference in anion and cation concentrations between the two bulk aqueous phases. The surface potential, ψ_s, arises from charged residues at the membrane–solution interface. The dipole potential, ψ_d, results from the anisotropic arrangement of dipoles associated with the lipid headgroups and their solvating water molecules. It is defined at the potential drop from interior of the membrane (at the level of the linkage between lipid glycerol backbone and the hydrocarbon chains) to the adjacent aqueous solution. Reproduced from [3] with permission from Springer Nature

phase and the hydrocarbon chains pointing towards the centre of the membrane. Because the lipids are anisotropically arranged, then any dipolar groups associated with them (including hydrating water dipoles) must also be anisotropically arranged. This necessarily gives rise to an electrical potential difference, ψ_d, across the headgroup region of the membrane. The same is true for any other self-assembled molecular colloidal system, e.g., micelles and microemulsions [4, 5]. In the case of lipid membranes, although its origin is not entirely resolved, it appears likely that the major contribution to the magnitude of ψ_d is oriented water dipoles, which hydrogen-bond to the carbonyl oxygen in the ester linkage between the glycerol backbone and the *sn*-2 hydrocarbon chain of ester phospholipids [6–10].

The dipole potential is much less widely known and investigated than the transmembrane electrical potential, $\Delta\psi$, or the surface potential, ψ_s. One reason for this is that $\Delta\psi$ and ψ_s can be relatively easily directly measured or controlled by electrophysiological or electrophoretic techniques. In contrast, the measurement of ψ_d, an electrical potential difference located totally within the membrane and which drops over a distance of not more than 0.5 nm [11], relies mostly on indirect observations, e.g., the effect it has on the transport rates of ions across the membrane or the electronic polarization that it causes to membrane-bound probes [12–14]. However, just because it is difficult to measure doesn't mean that it is unimportant. Depending on the lipid concerned, the magnitude of ψ_d has been estimated to be in the range 100–400 mV, positive in the membrane interior, which would be expected to produce local electric field strengths of 10^8–10^9 V m^{-1} [13], i.e., at least an order of magnitude greater than the field strengths produced by the transmembrane potential, $\Delta\psi$, which is known to be capable of regulating the opening and closing of voltage-sensitive ion channels [15]. Thus, it seems reasonable to expect that ψ_d could play a significant role in modulating the activity of membrane proteins.

The existence of the dipole potential was discovered in 1969 by two Russian scientists, Liberman and Topaly [16]. In studies using the hydrophobic ions tetraphenylborate (TPB^-) and tetraphenylphosphonium (TPP^+) as models to investigate the carrier-mediated mechanism of ion transport, they discovered that TPB^- produced a bilayer phospholipid membrane conductance approximately 10^5 times greater than TPP^+, although the two ions have virtually identical radii and very similar chemical structures. They reasoned that there must, therefore, be a greater energy barrier for the transport of cations across the membrane than anions, i.e., dipoles associated with the lipid headgroups and their hydrating water molecules must be arranged so that the positive ends of the dipoles point on average more towards the centre of the membrane, whereas the negative ends point more towards the aqueous phase. Based on the relative magnitudes of the membrane conductances towards these two ions it is possible to estimate a value of ψ_d [7, 17, 18]. Depending on the lipid concerned, these purely experimental values vary between around 100 and 230 mV. However, as many authors have pointed out [7, 17, 18], the calculation of these values relies on an assumption that there is no difference in the free energies of hydration of TPB^- and TPP^+, and this assumption is unlikely to be completely true. Indeed, theoretical calculations indicate that TPB^- is more strongly hydrated than TPP^+ [19, 20]. Using conductance ratios again, but correcting for the difference

in hydration energies, yields values of ψ_d which are at least 60 mV more positive, i.e., in the range 150–350 mV [20]. This is in reasonable agreement with values of ψ_d estimated from the change in electrical surface potential produced on spreading a lipid monolayer above an aqueous subphase in a Langmuir trough [21, 22].

Before discussing the effect of cholesterol on ψ_d, it is useful to review the factors which have been found to influence the magnitude of ψ_d, because this will help later to explain the origin of changes caused by cholesterol. If the dipole moments of all the molecules within the lipid headgroup region of the membrane were precisely known, then, in principle, ψ_d could be theoretically calculated from the Helmholtz equation for a parallel-plate capacitor:

$$\psi_d = \frac{\mu_\perp}{A\varepsilon_0\varepsilon} \tag{1}$$

where $\mu_\perp$ is the average component of the lipid molecular dipole moment (including membrane-associated water dipoles) perpendicular to the plane of the membrane, A is surface area of the membrane, ε_0 is the permittivity of free space and ε is the local dielectric constant. From this equation it can be seen that ψ_d is directly proportional to the dipole packing density ($\mu_\perp/A$). This theoretical prediction has been borne out in experimental results. Thus, an increase in the degree of saturation of phospholipid hydrocarbon chains causes a decrease in ψ_d [23]. *Cis* double bonds produce a larger drop in ψ_d than *trans* double bonds because a *cis* double bond produces a kink in the hydrocarbon chain, and, thus, causes a greater decrease in lipid packing density than a *trans* double bond. Similarly, the introduction of a heteroatom in the hydrocarbon chain reduces ψ_d [9]. Peterson et al. [9] found that the replacement of a CH_2 carbon atom of a hydrocarbon chain by sulphur causes a drop in ψ_d, but that the magnitude of the drop depends on the position of substitution. If the substitution is near the end of the chain, close to the terminal CH_3 group, there is no significant effect on ψ_d, but if the substitution is at the other end of the hydrocarbon chain, close to the headgroup, there is a significant drop in ψ_d. This result seems perfectly logical, since one would expect that a disruption to lipid packing near the headgroup would be magnified along the chain, as the hydrocarbon tails continue to spread towards the centre of the bilayer. A further result strongly supporting the role of lipid packing as an important determinant of the magnitude of ψ_d was obtained by Warshaviak et al. [24], who showed that membrane expansion due to the exposure of lipid vesicles to osmotic stress causes a drop in ψ_d.

A further important factor in determining the magnitude of ψ_d is the chemical nature of the linkage between phospholipid hydrocarbon tails and the headgroup. As discussed earlier, a lipid with an ester linkage, i.e., including a carbonyl group, produces a significantly greater ψ_d than the corresponding lipid with an ether linkage [7, 23]. Because the carbonyl bond is itself a dipole, the cause for the difference in ψ_d between ester and ether lipids is most likely not simply due to changes in lipid packing, but rather a change in the component of the average dipole moment perpendicular to the membrane, $\mu_\perp$ (see Eq. (1)). Experiments comparing a single-chain ester phospholipid to its corresponding double-chain derivative [10] have shown that the single-chain lipid

has a much lower $\mu_{\perp}$. The likely cause of this difference is the orientation of the carbonyl group relative to the membrane surface. In a single-chain lipid the carbonyl bond is expected to be oriented on average more parallel to the membrane surface, similar to the carbonyl of an *sn*-1 hydrocarbon chain [6, 7]. In double-chain ester phospholipids, on the other hand, the carbonyl bond of the extra chain, i.e., the *sn*-2 chain, is expected to be oriented more perpendicular to the membrane, thus contributing to the membrane inside-positive polarity of ψ_d [6, 7]. However, the orientation of the *sn*-2 chain's carbonyl is likely to have a further effect on ψ_d in addition to the contribution of its dipole moment. The oxygen atom of the carbonyl can act as a hydrogen bond acceptor and thus cause an alignment of hydrating water molecules, with the positive hydrogen-end of the water dipole directed towards the membrane interior. This would further increase the positive magnitude of ψ_d.

The chemical nature of the phospholipid headgroup is another important factor which can alter the magnitude of ψ_d. In the case of the phosphatidylcholine (PC) headgroup, the P^-–N^+ dipole between the phosphate group and the nitrogen of the choline is thought to lie approximately parallel to the membrane surface and, therefore, not be a major contributor to ψ_d. Nevertheless, NMR studies have shown that the angle it makes to the membrane surface can change with the surface charge of the membrane, which could lead to a modulation in ψ_d [25]. However, substitution of the PC headgroup by the negatively charged phosphatidylserine (PS) has not been found to cause major changes in ψ_d [10, 11]. Presumably the negative charge on the carboxylate residue of the PS group is far enough out into the adjacent aqueous solution that it is effectively screened by physiological levels of salt. A similar situation seems to exist in the case of the negatively charged phosphatidylglycerol (PG) headgroup, which also shows very little effect on ψ_d relative to PC [10]. The hydroxyl dipoles of the PG headgroup are probably sufficiently far out into the aqueous phase that the electric fields they produce are screened by the surrounding water dipoles with a dielectric constant of 80. In contrast, the zwitterionic phosphatidylethanolamine (PE) headgroup causes a significant increase in ψ_d. A possible reason for this is a difference in hydration of the PE versus the PC headgroup. Rand and Parsegian [26] have shown that as the degree of methylation of the nitrogen of the headgroup increases from 0 in PE to 3 in PC, there is an increase in the number of hydrating water molecules. If the additional water molecules of PC polarize themselves so as to oppose the existing ψ_d, then this could account for the higher ψ_d of PE relative to PC. Finally, the small negatively charged headgroup of phosphatidic acid (PA) causes a significant increase in ψ_d [10]. This result stresses the importance of the precise location of charges relative to the membrane surface. The increase in ψ_d caused by PA implies that its negative phosphate group is located close to the membrane surface at the level of the negative pole of the dipole potential, so that the electrical potential gradient is magnified and ψ_d increases (see Fig. 2).

The change in ψ_d caused by PA can be compared to the effects of ion binding to the membrane from the adjacent aqueous phase. Anions with relatively low hydration energies, such as perchlorate, have been found to bind to PC membranes and cause a significant drop in ψ_d [27]. The drop could be accounted for by binding within the membrane at the level of the positive pole of the dipole potential,

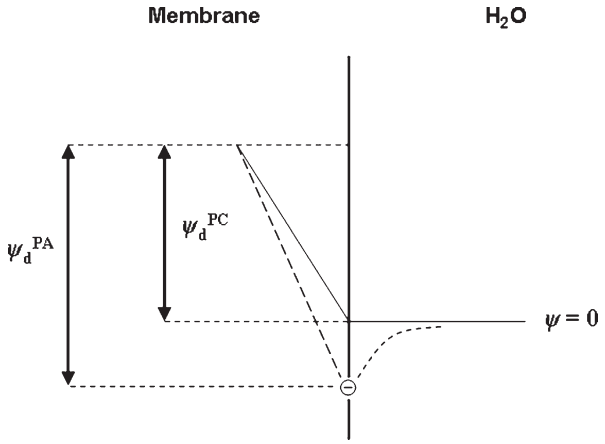

Fig. 2 Mechanism for the increase in ψ_d by the incorporation of phosphatidic acid (PA) into a phosphatidylcholine (PC) membrane. The solid lines represent the profile of the electrical potential, ψ, for PC alone. The dotted lines represent the profile of ψ for a PC membrane incorporating PA. The electrical potential is defined to be zero in the aqueous solution far from the membrane surface. ψ_d^{PC} and ψ_d^{PA} represent the dipole potentials of a pure PC membrane and one in which PA has been incorporated, respectively. PC, because it has a zwitterionic headgroup, is assumed to produce no surface potential, whereas PA with its negatively charged phosphate group produces a negative surface potential. Reproduced from [10] with permission from Springer Nature

thus yielding a partial neutralization and hence a ψ_d decrease. Binding of divalent or trivalent cations has also been found to produce a drop in ψ_d [27]. It might seem paradoxical that both anions and cations cause a change in ψ_d in the same direction. However, divalent and trivalent cations have very high hydration energies relative to monovalent anions and are, thus, unlikely to bind very deeply within membranes. Their hydrophilic nature makes it much more likely that they bind to a negatively charged polar site at the membrane surface, i.e., to the phosphate residue of PC. Binding at this position would cause a partial neutralization of the negative pole of the dipole potential, thus yielding the observed decrease in ψ_d. In principle then, because ψ_d arises from the alignment of dipoles, the membrane binding of anions and cations could produce either an increase or a decrease in ψ_d depending on where in the membrane they bind.

Before turning to the effect of cholesterol, there is one further factor worth mentioning. From the Helmholtz equation (see Eq. (1)) it can be seen that there is an inverse relationship between ψ_d and the local dielectric constant, ε, of the medium. Thus, any decrease in lipid packing density which allows further mobile water dipoles (as opposed to oriented water) to penetrate into the lipid headgroup region will result in an increase in ε. The polarization of these water molecules around existing oriented dipoles will lead to a further decrease in ψ_d, thus magnifying the drop caused by the decrease in dipole packing density alone. Similarly, any increase in lipid packing density could cause the exclusion of some mobile water from the headgroup region, thus causing a drop in ε and a further increase in ψ_d above that caused by the increase in $\mu_\perp$/A alone.

3 Influence of Cholesterol on the Dipole Potential

The fact that cholesterol is able to significantly alter the magnitude of the dipole potential of a lipid bilayer was first recognized by Szabo [28], who found that the addition of cholesterol to the membrane caused an increase in membrane conductance towards TPB^- of up to 30-fold and a decrease in conductance towards TPP^+ of up to 100-fold. Based on the conductance changes Szabo [28] estimated cholesterol-induced increases in ψ_d of up to approximately 100 mV. However, he did not speculate on the molecular origin of the effect. Subsequent studies using a variety of cholesterol derivatives have shown that sterol-induced changes in ψ_d are very sensitive to the sterol's molecular structure [29–31] (see Fig. 3). 6-Ketocholestanol, for example, causes an increase in ψ_d which is even greater than that produced by cholesterol [30, 32]. For this reason 6-ketocholestanol has sometimes been used as a ψ_d-enhancing molecule in the testing of dipole potential probes [11, 33]. Other cholesterol derivatives, however, have been found to decrease ψ_d. Thus, the

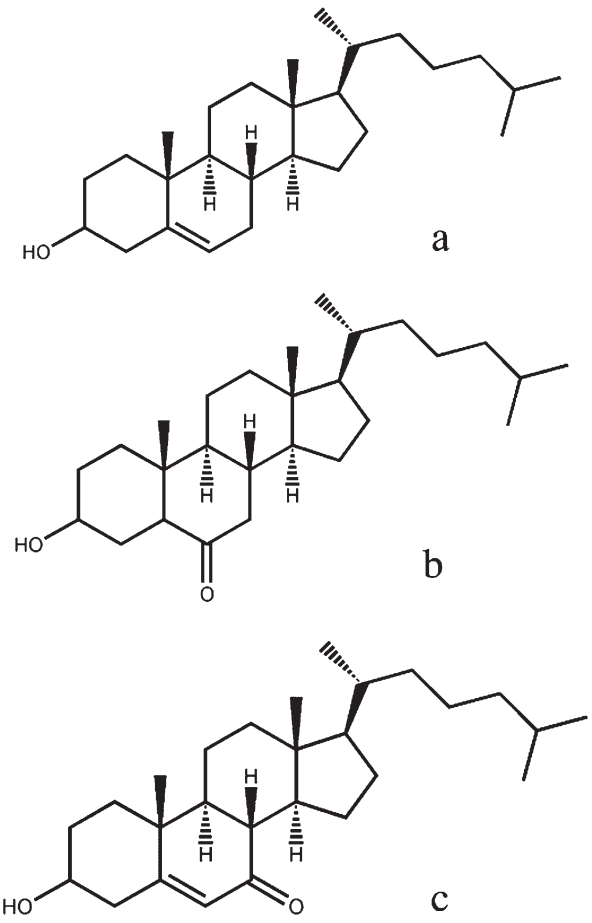

Fig. 3 Chemical structures of cholesterol and some of its oxidized derivatives. (**a**) Cholesterol, (**b**) 6-ketocholestanol and (**c**) 5-cholesten-3β-ol-7-one (7-ketocholesterol)

incorporation of 5-cholesten-3β-ol-7-one (hereafter referred to by its more common name 7-ketocholesterol) into phosphatidylcholine vesicles causes a significant drop in ψ_d [30]. It has been found [30] that the magnitude of the effect of a range of cholesterol derivatives on ψ_d correlates with the component of the derivatives' dipole moments perpendicular to the membrane, $\mu_\perp$, assuming as a first approximation that each adopts the same orientation within the membrane as cholesterol itself [34, 35]. Such a correlation would be expected based on the Helmholtz equation (Eq. (1)). However, the magnitudes of the changes in ψ_d are far too large to be accounted for by the dipole moments of the cholesterol derivatives alone. Starke-Peterkovic et al. [30] estimated that the derivative's dipole moments could only account for approximately 20% of the observed ψ_d changes.

A further important effect to consider is the influence that cholesterol and its derivatives have on lipid packing, i.e., on the value of $\mu_\perp/A$ in Eq. (1). It has long been known that cholesterol has a condensing effect on lipid membranes [36–39]. However, the observed cholesterol-induced increase in ψ_d is still significantly greater than what one would expect from the combined effect of cholesterol's dipole moment plus the increase in lipid packing density of the phospholipid [30]. Therefore, in addition to these two effects, it seems that there must be some cholesterol-induced structural reorganization of the lipid headgroup region. A possibility could be that cholesterol causes an increase in the local dielectric constant, ε, perhaps either by increasing the proportion of oriented immobilized water molecules within the membrane or by decreasing the penetration of mobile orientationally polarizable water molecules into the membrane. A decrease in ε, by either of these mechanisms, would be expected to further enhance cholesterol's effect on ψ_d (see Eq. (1)).

The effect of 7-ketocholesterol on ψ_d is particularly interesting and also physiologically relevant, because it is a major oxidation product leading from the cholesterol biosynthetic pathway. It is produced either directly from cholesterol or from its precursor in the pathway 7-dehydrocholesterol [40]. 7-Ketocholesterol has been found to accumulate in atherosclerotic plaques and to cause apoptosis in vascular cells [41, 42]. As explained above, 7-ketocholesterol has been found to cause a significant reduction in ψ_d [30], i.e., the complete opposite of the effect of cholesterol. Measurements of lipid monolayers using a Langmuir trough have shown, however, that, although significantly less effective than cholesterol, 7-ketocholesterol also causes a lipid condensation effect, i.e., an increase in lipid packing density [43–45]. In the absence of any reorganization of the lipid interface, one would expect the increase in phospholipid packing density caused by addition of 7-ketocholesterol to cause a smaller increase in ψ_d than observed on addition of cholesterol, but not to completely reverse the direction of the ψ_d change. To explain this effect one can think of ψ_d consisting of two components, one due to the phospholipids (plus associated water dipoles) within the membrane, $\mu_\perp^{\mathrm{PL}}$, and one due to 7-ketocholesterol molecules (plus associated water dipoles), $\mu_\perp^{\mathrm{KC}}$. The resultant ψ_d would then be given by an expanded form of the Helmholtz equation:

$$\psi_d = \frac{\left|\mu_\perp^{\mathrm{PL}}\right|}{A\varepsilon_0\varepsilon} - \frac{\left|\mu_\perp^{\mathrm{KC}}\right|}{A\varepsilon_0\varepsilon} \tag{2}$$

In the absence of any change in ε, the only way that addition of 7-ketocholesterol to the membrane could lead to a decrease in ψ_d would be if the modulus $|\mu_\perp^{KC}|$ is greater than $|\mu_\perp^{PL}|$. The subtraction in Eq. (2) signifies the opposite polarity of the dipole moments due to phospholipid and 7-ketocholesterol. Thus, the compression-induced drop in the component of ψ_d caused by 7-ketocholesterol must overcompensate for the increase expected from the phospholipid component of ψ_d. It is possible that this massive difference in the effects of cholesterol and its common oxidative product 7-ketocholesterol on ψ_d may to some extent be involved in 7-ketocholesterol's cytotoxic effects. It has even been proposed that a cause of neurodegenerative diseases, such as Parkinson's and Alzheimer's disease, could be an overproduction of oxysterols [46].

Another interesting effect of cholesterol and some of its oxidized derivatives on ψ_d is that the concentration profile is biphasic [30]. Thus, up to a level of approximately 40 mol%, cholesterol steadily increases ψ_d, but if one incorporates more cholesterol into the membrane, ψ_d starts to drop again. It is interesting that 40 mol% corresponds to the level of cholesterol often found physiologically in the plasma membrane of animals [1, 2]. Thus, it appears that for some reason the cholesterol content of the plasma membrane is optimized to maximize the value of ψ_d. This could perhaps be to minimize the cation permeability of the lipid component of the membrane, as suggested by Szabo [28], or it could be due to an effect of ψ_d on the activity of transmembrane proteins, which will be discussed in the following section. The precise reason why the effect of cholesterol on ψ_d goes through a maximum at 40 mol% is not entirely clear. However, it is not completely surprising. Optimal concentrations are often observed in three-dimensional solvent mixtures, e.g., boiling point maxima or minima at a particular mixture composition. These are attributed to differences in the strengths of the intermolecular forces between the components of the mixture. Cholesterol is thought to interact more strongly with the hydrocarbon chains of phospholipids than with itself [47–49]. Therefore, as the cholesterol composition increases, the overall net strength of intermolecular forces in the membrane and its stability would be expected to initially increase. However, if the cholesterol composition increases too far and the membrane becomes too cholesterol-rich, the lower strength of the forces between two cholesterol molecules relative to a cholesterol molecule and a phospholipid would be expected to cause a drop in the strength of intermolecular forces. The fact that ψ_d goes through a maximum at a particular cholesterol concentration is an indication of the key role that intermolecular forces play in determining its magnitude.

Another interesting observation is that the effect of cholesterol on the magnitude of ψ_d varies depending on the phospholipid composition of the membrane. Removal of cholesterol via treatment with methyl-β-cyclodextrin from lipid vesicles formed from lipids extracted from a variety of animal tissues has shown [30] that cholesterol makes a contribution of approximately 65 mV to the total ψ_d. However, in experiments with synthetic phospholipid vesicles, it has been found [30] that cholesterol produces a far greater increase in ψ_d when the hydrocarbon chains of the phospholipid are saturated than when they are unsaturated. This would seem to be

further evidence supporting an important role of intermolecular forces in determining cholesterol's effect on ψ_d, in this case a differential interaction between cholesterol and saturated versus unsaturated hydrocarbon chains.

4 Physical Basis of Modulation of Membrane Protein Function

The activity of many membrane proteins is critically dependent on the composition of their surrounding lipid environment, and there are many possible mechanisms by which lipid sensitivity could come about. Here the discussion is limited purely to the mechanisms by which ψ_d could modulate membrane protein activity. Because ψ_d produces an electric field within the headgroup region of the membrane, ion-transporting membrane proteins, e.g., ion channels and ion pumps, first come to mind as possible candidates that could potentially be sensitive to the value of ψ_d in their surrounding membrane. Therefore, we will first concentrate on this class of proteins.

In spite of the large electric field strength that ψ_d produces of 10^8–10^9 Vm^{-1}, it seems that, apart from small pore-forming peptides such as gramicidin and syringomycin [50, 51], ψ_d has little effect on binding or conduction of ions through membrane proteins. Theoretical calculations indicate that the reason for this is that most ion channels or pumps are so large that the electric field strength originating from ψ_d is effectively screened from the ion binding sites by the intervening protein mass [52, 53]. However, this only means that ion conduction rates are not affected, not that ion channel or ion pump activities are totally insensitive to ψ_d. As a prime example, let us consider the voltage-gated Na^+ channels of neurons.

From cell-attached patch clamp measurements of Na^+ channels of neuroblastoma cells, Zhang et al. [54] found that, although the single-channel conductance was constant regardless of where on the cell it was measured, the kinetics of activation, i.e., the gating of the channel, varied across the surface of the cell. In previous measurements [55] the same group had already found that the magnitude of ψ_d also varies spatially across the cell surface. Comparison [54] of the spatial variations of ψ_d with those of channel activation showed that they matched. This suggests, therefore, that Na^+ channel gating kinetics are dependent on the local value of ψ_d in the membrane surrounding the protein. Because the plasma membrane contains such a high proportion of cholesterol, and cholesterol is known to modulate ψ_d, Bedlack et al. [55] suggested that the local variations in ψ_d arise because of local variations in the cholesterol composition across the surface of the membrane.

The measurements of Zhang et al. [54] on ion channels are consistent with results on ion pumps. In particular, it has been found [53, 56] that the kinetics of ion occlusion reactions are dependent on the local value of ψ_d, even though, based on electrophysiological studies [57–62], ion occlusion reactions do not involve significant movement of the transported ions, i.e., they are non-electrogenic reactions. Both the ion occlusion reactions of ion pumps and the gating reactions of ion channels are

protein conformational changes. Therefore, the question is, how could a conformational change of a membrane protein be sensitive to ψ_d. A possible mechanism which has recently been presented [53, 63] will now be described.

Any conformational change of a membrane protein, whether it be a channel, pump, secondary transporter or a receptor is likely to lead to some change in the protein's hydrophobic thickness. In order to avoid any exposure of protein hydrophobic regions to the surrounding aqueous medium, the membrane can undergo local deformations around the protein so that the hydrophobic thickness of the protein matches that of the membrane [64–67]. Any distortion to the membrane must be associated with a change in the density of lipid packing and hence in the value of ψ_d (see Eq. (1)). Any membrane distortion will also involve a change in energy, which must be considered as a component of the total energetics describing the conformational change a membrane protein undergoes. Here we consider the energy changes which arise due to changes in ψ_d alone.

Because the dipoles which give rise to ψ_d are aligned more or less parallel to one another, the energy of interaction is repulsive, or destabilizing. For an infinite planar lattice of parallel dipoles the energy of interaction, E, is given by:

$$E = \frac{1}{4\pi\varepsilon_0\varepsilon}\frac{\mu^2}{r^3}M \tag{3}$$

where r is the distance between two neighbouring dipoles of dipole moment, μ, and M is termed a Madelung constant and represents the factor by which the energy changes on going from a pair of dipoles to an infinite lattice. The value of M depends on the geometrical arrangement of the lattice. For a hexagonally close-packed array of dipoles, M has been estimated to have a value of 10.2. For such a lattice, if one considers each net dipole to be associated with a single lipid within the membrane, r is related to the cross-sectional area, A, occupied by a lipid in the membrane by:

$$r = \sqrt{A / \cos 30} \tag{4}$$

Substituting this expression for r into Eq. (3) and including the value of M of 10.2 yields the following repulsive energy per mole of lipid:

$$E = \frac{8.22N_A}{4\pi\varepsilon_0\varepsilon}\frac{\mu^2}{A^{3/2}} \tag{5}$$

In order to use this equation to estimate E one first needs to know values of μ, A and ε. Based on a typical ψ_d value of 300 mV, an A of 0.65 nm^2 [23] and an ε of 75 (i.e. a polarity slightly less than water) [53, 68] one can estimate the value of μ to be 1.3×10^{-28} Cm or 39 D. Inserting these values into Eq. (5) yields a repulsive energy of interaction of 19 kJ mol^{-1}. This is comparable to the attractive energy of interaction on hydrogen bond formation. If one considers that any membrane protein is surrounded by many annular lipids and membrane distortions due to protein

conformational changes are likely to extend much further out from the protein than the annular lipids, then it is clear that the repulsive energy of interaction associated with ψ_d could play a substantial role in determining the relative stabilities of protein conformations, e.g., between the open and closed state of channels or the occluded and deoccluded states of pumps. For example, the Na^+,K^+-ATPase and the sarcoplasmic reticulum Ca^{2+}-ATPase possess approximately 35 and 20 annular lipids, respectively [69]. The repulsive energy of interaction due solely to the 35 annular lipids of the Na^+,K^+-ATPase amounts to 665 kJ mol^{-1}. Even if a membrane distortion caused a relatively small perturbation of 10% to this repulsive energy, this would be of the same order of magnitude as the energy released by ATP hydrolysis of approximately – 60 kJ mol^{-1}. Thus, even relatively small changes in ψ_d could be expected to result in significant changes in ion pump kinetics.

Now let us consider at a more molecular level the effects of ψ_d on the conformational equilibrium of a membrane protein. Figure 4 shows an exaggerated picture of a membrane protein conformational change in which a large change in protein hydrophobic thickness occurs. In the protein conformation on the left the protein has a large hydrophobic thickness. In this situation the membrane must increase its own thickness in order to cover the protein's hydrophobic domains. The only way the membrane can do this is by extending the hydrocarbon chains of the surrounding lipids. This necessarily causes an increase in lipid packing and thus an increase in the local ψ_d around the protein. Conversely, in the protein conformation on the right the protein has a small hydrophobic thickness and the membrane must, therefore, thin so that its own hydrophobic thickness matches that of the protein. The only way this can occur is if the hydrocarbon tails of the lipids spread. This naturally causes a local decrease in the lipid packing density and a decrease in ψ_d. Thus, protein conformations with a large hydrophobic thickness are expected to be associated with a large local ψ_d and conformations with a small hydrophobic thickness are expected to be associated with a small local ψ_d. Now if a molecule is added

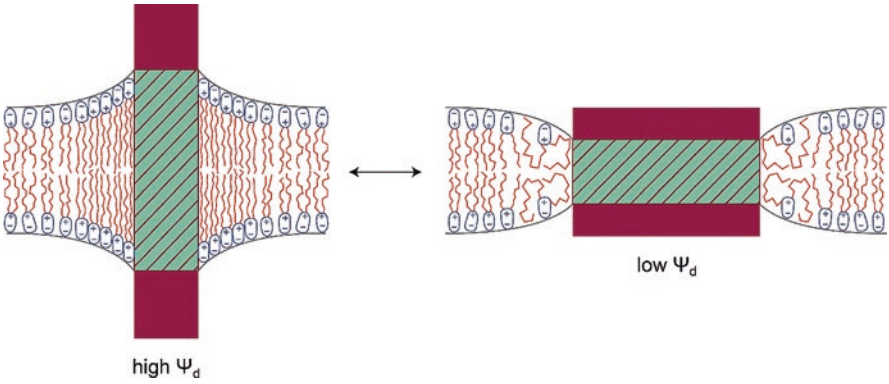

Fig. 4 Conformational transition between two membrane protein conformational states with large (left) and small (right) hydrophobic thicknesses. Adapted from [63] with permission from Elsevier

to the membrane that changes ψ_d the distribution of the protein between the two states would be expected to change. This can be explained qualitatively using Le Châtelier's principle, i.e., any equilibrium shifts in order to decrease the magnitude of a perturbation. Thus, if one adds cholesterol to a membrane, and it is known that cholesterol increases ψ_d, then the equilibrium must shift to decrease ψ_d again. This necessitates a shift to the protein conformation on the right, with a lower ψ_d. Based purely on the energetics of dipole–dipole interactions at the membrane interface, increasing cholesterol concentrations, up to the physiological level, would, therefore, be expected to favour protein conformational states with a small hydrophobic thickness. In contrast the addition of substances to the membrane which decrease ψ_d would be expected to favour protein conformational states with a large hydrophobic thickness. The theoretical framework described here for the effect of ψ_d on membrane protein conformational transitions arose out of the author's work on the lipid sensitivity of the Na^+,K^+-ATPase. Recently it has also been applied by others [70] to explain the effects of activators of the hERG (human Ether-a-go-go Related Gene) K^+ channel, which is involved in coordinating beating of the heart. Interference in the activity of the hERG channel can potentially lead to sudden death via the condition known as long QT syndrome. For this reason the Food and Drug Administration of the USA requires that all new drugs be tested for any effect on the hERG channel. If the hERG channel is in fact sensitive to ψ_d, it would seem advisable that any new drugs, whatever their planned therapeutic purpose, be initially screened for their effect on ψ_d. It is hard to imagine a more severe side effect of a drug than sudden death.

5 Membrane-Binding Terminal Extensions of Membrane Proteins

The calculations presented in the previous section indicate that any membrane bending required to accommodate changes in protein hydrophobic thickness would be expected to be associated with very significant changes in energy. However, rather than the membrane distorting to encompass a protein's changing hydrophobic thickness, another possibility is that the protein could change its orientation relative to the membrane. Thus, if a membrane protein can tilt in the membrane sufficiently so that any expansions to its hydrophobic domains are moved into the membrane, the membrane's hydrophobic thickness could remain unchanged and still fully cover the hydrophobic domains of the protein. Indeed evidence for such a mechanism has recently been found from X-ray crystallographic studies on the sarcoplasmic reticulum Ca^{2+}-ATPase [71]. This paper presented the first structures of a P-type ATPase in which the surrounding lipid bilayer could be resolved. The results revealed that between different protein conformational states, the protein tilts relative to the membrane plane by angles up to 18.4° (see Fig. 5). Such a mechanism would minimize effects of ψ_d on the protein's function via the mechanism described

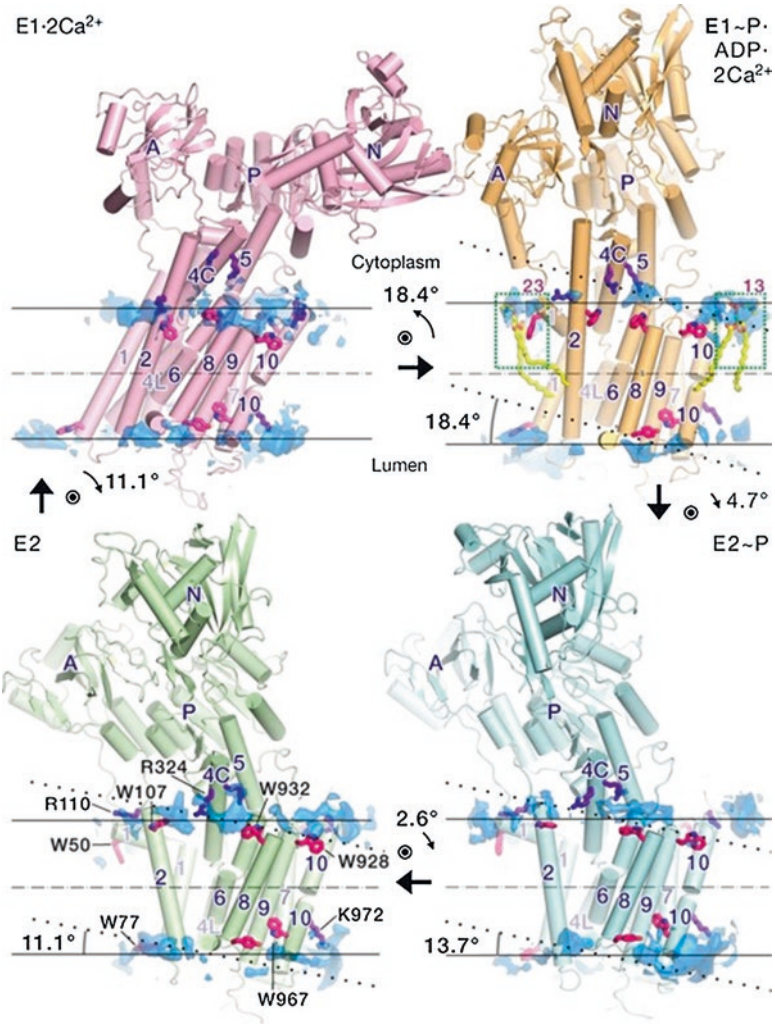

Fig. 5 Changes in orientation of the sarcoplasmic reticulum Ca^{2+}-ATPase molecule during its ion pumping reaction cycle. The horizontal solid lines show each side of the membrane. The inclined dotted lines show the previously thought position of the membrane, in alignment with the protein's M7–M10 transmembrane helices. The angle values associated with the arrows between different protein conformational states indicate the rotation of the protein relative to the membrane surface required for it to proceed to the next conformational state. Reproduced from [71] with permission from Springer Nature

in the previous section, i.e., preferential stabilization of conformational states with small protein hydrophobic thicknesses with increasing ψ_d.

However, if membrane proteins do rock backwards and forwards in the membrane in order to avoid membrane bending, other mechanisms need to be considered to

explain the effect of their membrane environment on protein activity. It is now clear that many membrane proteins contain polybasic sequences, i.e., clusters of lysine and arginine residues, which can interact with the headgroups of negatively charged phospholipids such as phosphatidylserine on the cytoplasmic face of the plasma membrane [72]. Such an interaction has been clearly shown from experiments with model membrane systems and synthetic peptides and polyamino acids (e.g. polylysine) [73–75]. Prime examples are the Na^+,K^+-ATPase and its closest relative among the P-type ATPase family, the gastric H^+,K^+-ATPase, which is responsible for the acidification of the stomach, necessary for activation of the digestive enzyme pepsin. Both of these proteins possess lysine-rich N-termini on the proteins' cytoplasmic face [76]. The N-terminus of the H^+,K^+-ATPase from the Chinese carnivorous fish *Siniperca chuatsi* even has seven consecutive lysine residues. Based on both equilibrium and kinetic experiments it appears that the N-terminus interacts electrostatically with negatively charged phospholipids in the surrounding membrane and that this interaction stabilizes the enzymes' E2 conformational state [76–78], which is the state to which K^+ ions preferentially bind. Now that it is known from the X-ray studies on the Ca^{2+}-ATPase [71] that these enzymes rock backwards and forwards in the membrane as the enzyme cycles between E1 and E2 conformations, this provides a structural basis to understand the conformational preference of the N-terminus–membrane interaction. It seems possible then that this membrane interaction could continually be switching on and off as the proteins pump ions across the membrane. What the purpose of this might be is still unclear. A possibility is that the interaction may provide a membrane anchoring, thus locking in E2-like conformations and helping to drive the pumping cycle forward by inhibiting back reactions. The interaction could also be involved in the occlusion process of the transported ions or in regulation of the proteins' activities. However, whatever the functional purpose, if a membrane interaction exists, this would seem to be an obvious locus to seek an explanation for the strong sensitivity of the activity of the Na^+,K^+-ATPase on the cholesterol content of the membrane [69, 79–82].

As mentioned earlier, cholesterol is known to cause an increase in lipid packing density [36–39]. Any increase in the cholesterol content of the inner cytoplasmic leaflet of the plasma membrane, which is known to contain a high level of negatively charged lipids such as phosphatidylserine, would be expected to increase the negative surface charge density of the membrane, thus promoting interaction with the positively charged N-terminus of the Na^+,K^+- or H^+,K^+-ATPase and stabilizing the E2 conformation. Any stabilization of one conformation over another will alter the kinetics of the entire ion pumping cycle and could lead to either pump stimulation or inhibition. What role the ψ_d may have in this mechanism of membrane protein modulation awaits further investigation. In principle this depends on the degree of penetration of the N-terminus into the membrane. If the interaction is purely at this surface, ψ_d may have minimal effect, but if the penetration extends to the level of the phospholipid glycerol backbone, where the gradient of ψ_d is expected to be at its greatest, then ψ_d may play a significant role.

6 Conclusions

It is clear that the cholesterol molecule has a significant effect on the magnitude of ψ_d. That much at least is certain. The exact origin of cholesterol's effect on ψ_d is less clear, but several possibilities have been here discussed. How and by how much cholesterol affects the function of membrane proteins via its influence on ψ_d is also in need of further investigation. Whatever the mechanism, any effects on ion-transporting membrane proteins are likely to be on the kinetics of protein conformational changes (i.e. gating or occlusion reactions), not ion conduction.

The effects of lipids, including cholesterol, on membrane proteins are normally classified as being either general membrane-mediated (i.e. due to the physical properties of the membrane) or specific (i.e. due to a direct interaction between the protein and a specific lipid). Effects of ψ_d on membrane proteins would normally be classed in the first category. However, it is worthwhile pointing out that such classifications, although sometimes useful, tend to impose a limitation to the imagination. In actual fact there is no reason why a mechanism by which cholesterol modulates membrane protein function couldn't combine both general and specific aspects. The final mechanism presented in the previous section of this chapter is a case in point. It is proposed that a specific section of a protein, its N-terminus interacts with a negatively charged membrane surface. There is no suggestion at this stage that cholesterol interacts directly with the N-terminus, but it modulates a general physical property of the membrane, namely lipid packing, and alters surface charge density (and, as described in Sect. 3, also ψ_d), thus influencing the strength of the N-terminus interaction with the membrane. This mechanism is also in need of further investigation and how widely applicable it is remains to be seen. The final message, however, is that a complete understanding of the role that cholesterol plays in membrane function requires an open mind willing to consider the possibility of complex mechanisms which are not able to be pigeon-holed as either specific or general.

Acknowledgements R.J.C. received financial support from the Australian Research Council (Discovery Grants DP-12003548, DP150103518 and DP170101732).

References

1. van Meer G, Voelker DR, Feigenson GW. Membrane lipids: where they are and how they behave. Nat Rev Mol Cell Biol. 2008;9:112–24.
2. Subczynski WK, Pasenkiewicz-Gierula M, Widomska J, Mainali L, Raguz M. High cholesterol/low cholesterol: effects in biological membranes: a review. Cell Biochem Biophys. 2017;75:369–85.
3. Clarke RJ. Electric field sensitive dyes. In: Demchenko AP, editor. Advanced fluorescence reporters in chemistry and biology I. Fundamentals and molecular design. Berlin: Springer; 2010. p. 331–44.
4. Sarkar P, Chattopadhyay A. Dipolar rearrangement during micellization explored using a potential-sensitive fluorescent probe. Chem Phys Lipids. 2015;191:91–5.

5. Sarkar P, Chattopadhyay A. Micellar dipole potential is sensitive to sphere-to-rod transition. Chem Phys Lipids. 2016;195:34–8.
6. Seelig J, Macdonald PM, Scherer PG. Phospholipid head groups as sensors of electric charge in membranes. Biochemistry. 1987;26:7535–41.
7. Gawrisch K, Ruston J, Zimmerberg J, Parsegian VA, Rand RP, Fuller N. Membrane dipole potentials, hydration forces, and the ordering of water at membrane interfaces. Biophys J. 1992;61:1213–23.
8. Mashl RJ, Scott HL, Subramaniam S, Jacobsson E. Molecular simulation of dioleoylphosphatidylcholine lipid bilayers at differing levels of hydration. Biophys J. 2001;81:3005–15.
9. Peterson U, Mannock DA, Lewis RNAH, Pohl P, McElhaney RN, Pohl EE. Origin of membrane dipole potential: Contribution of the phospholipid fatty acid chains. Chem Phys Lipids. 2002;117:19–27.
10. Starke-Peterkovic T, Clarke RJ. Effect of headgroup on the dipole potential of phospholipid vesicles. Eur Biophys J Biophys Lett. 2009;39:103–10.
11. Gross E, Bedlack RS Jr, Loew LM. Dual-wavelength ratiometric fluorescence measurement of the membrane dipole potential. Biophys J. 1994;67:208–16.
12. Brockman H. Dipole potential of lipid membranes. Chem Phys Lipids. 1994;73:57–79.
13. Clarke RJ. The dipole potential of phospholipid membranes and methods for its detection. Adv Colloid Interfac Sci. 2001;89-90:263–81.
14. Wang L. Measurements and implications of the membrane dipole potential. Annu Rev Biochem. 2012;81:615–35.
15. Hille B. Ionic channels of excitable membranes. 2nd ed. Sunderland: Sinauer Associates; 1992.
16. Liberman EA, Topaly VP. Permeability of bimolecular phospholipid membranes for fat-soluble ions. Biofizika. 1969;14:452–61. (In Russian).
17. Andersen OS, Fuchs M. Potential energy barriers to ion transport within lipid bilayers. Studies with tetraphenylborate. Biophys J. 1975;15:795–830.
18. Pickar AD, Benz R. Transport of oppositely charged lipophilic probe ions in lipid bilayer membranes having various structures. J Membr Biol. 1978;44:353–76.
19. Luzhkov V, Warshel A. Microscopic models for quantum mechanical calculations of chemical processes in solutions: LD/AMPAC and SCAAS/AMPAC calculations of solvation energies. J Comput Chem. 1992;13:199–213.
20. Schamberger J, Clarke RJ. Hydrophobic ion hydration and the magnitude of the dipole potential. Biophys J. 2002;82:3081–8.
21. Hladky SB, Haydon DA. Membrane conductance and surface potential. Biochim Biophys Acta. 1973;318:464–8.
22. Beitinger H, Vogel V, Möbius D, Rahmann H. Surface potentials and electric dipole moments of ganglioside and phospholipid monolayers: contribution of the polar headgroup at the water/lipid interface. Biochim Biophys Acta. 1989;984:293–300.
23. Clarke RJ. Effect of lipid structure on the dipole potential of phosphatidylcholine bilayers. Biochim Biophys Acta Biomembr. 1997;1327:269–78.
24. Warshaviak DT, Muellner MJ, Chachisvilis M. Effect of membrane tension on the electric field and dipole potential of lipid bilayer membrane. Biochim Biophys Acta Biomembr. 2011;1808:2608–17.
25. Semchyschyn DJ, Macdonald PM. Conformational response of the phosphatidylcholine headgroup to bilayer surface charge: torsion angle constraints from dipolar and qudripolar couplings in bicelles. Magn Reson Chem. 2004;42:89–104.
26. Rand RP, Parsegian VA. Hydration forces between phospholipid bilayers. Biochim Biophys Acta. 1989;988:351–76.
27. Clarke RJ, Lüpfert C. Influence of anions and cations on the dipole potential of phosphatidylcholine vesicles: a basis for the Hofmeister effect. Biophys J. 1999;76:2614–24.
28. Szabo G. Dual mechanism for the action of cholesterol on membrane permeability. Nature. 1974;252:47–9.
29. Krull UJ. Bilayer lipid membrane permeabilityAn empirical model based on molecular packing/fluidity and membrane dipole potentials. J Electrochem Soc. 1987;134:1910–4.

30. Starke-Peterkovic T, Turner N, Vitha MF, Waller MP, Hibbs DE, Clarke RJ. Cholesterol effect on the dipole potential of lipid membranes. Biophys J. 2006;90:4060–70.
31. Haldar S, Kanaparthi RK, Samanta A, Chattopadhyay A. Differential effect of cholesterol and its biosynthetic precursors on membrane dipole potential. Biophys J. 2012;102:1561–9.
32. Franklin JC, Cafiso DS. Internal electrostatic potentials in bilayers: measuring and controlling dipole potentials in lipid vesicles. Biophys J. 1993;65:289–99.
33. Clarke RJ, Kane DJ. Optical detection of membrane dipole potential: avoidance of fluidity and dye-induced effects. Biochim Biophys Acta Biomembr. 1997;1323:223–39.
34. Franks NP. Structural analysis of hydrated egg lecithin and cholesterol bilayers. I. X-ray diffraction. J Mol Biol. 1976;100:345–58.
35. McIntosh TJ. The effect of cholesterol on the structure of phosphatidylcholine bilayers. Biochim Biophys Acta. 1978;513:43–58.
36. De Bernard L. Molecular associations between lipids. II. Lecithin and cholesterol. Bull Soc Chim Biol Paris. 1958;40:161–4. (In French).
37. Demel RA, De Kruyff B. The function of sterols in membranes. Biochim Biophys Acta. 1976;457:109–32.
38. Hung W-C, Lee M-T, Chen F-Y, Huang HW. The condensing effect of cholesterol in lipid bilayers. Biophys J. 2007;92:3960–7.
39. Alwarawrah M, Dai J, Huang J. A molecular view of the cholesterol condensing effect in DOPC lipid bilayers. J Phys Chem B. 2010;114:7516–23.
40. Shinkyo R, Xu L, Tallman KA, Cheng Q, Porter NA, Guengerich FP. Conversion of 7-dehydrocholesterol to 7-ketocholesterol is catalysed by human cytochrome P450 7A1 and occurs by direct oxidation without an epoxide intermediate. J Biol Chem. 2011;286:33021–8.
41. Gaus K, Dean RT, Kitharides L, Jessup W. Inhibition of cholesterol efflux by 7-ketocholesterol: Comparison between cells, plasma membrane vesicles, and liposomes as cholesterol donors. Biochemistry. 2001;40:13002–14.
42. Leonarduzzi G, Biasi F, Chiarpotto E, Poli G. Trojan horse-like behavior of a biologically representative mixture of oxysterols. Mol Asp Med. 2004;25:155–67.
43. Mintzer E, Charles G, Gordon S. Interaction of two oxysterols, 7-ketocholesterol and 25-hydroxycholesterol, with phosphatidylcholine and sphingomyelin in model membranes. Chem Phys Lipids. 2010;163:586–93.
44. Telesford D-M, Verreault D, Rieck-Mitrisin V, Allen HC. Reduced condensing and ordering effects by 7-ketocholesterol and 5β,6β-epoxycholesterol on DPPC monolayers. Langmuir. 2015;31:9859–69.
45. Wnętrzak A, Makyła-Juzak K, Filiczkowska A, Kulig W, Dynarowicz-Łątka P. Oxysterols versus cholesterol in model neuronal membrane. I. The case of 7-ketocholesterol. The Langmuir monolayer study. J Membr Biol. 2017;250:553–64.
46. Leoni V, Caccia C. Oxysterols as biomarkers in neurodegenerative diseases. Chem Phys Lipids. 2011;164:515–24.
47. Ramsammy LS, Chauhan VPS, Box LL, Brockerhoff H. Interactions in the hydrogen belts of membranes: cholesterol leaving phosphatidylcholine bilayers. Biochem Biophys Res Commun. 1984;118:743–6.
48. Parker A, Miles K, Cheng KH, Huang J. Lateral distribution of cholesterol in dioleoylphosphatidylcholine lipid bilayers: cholesterol-phospholipid interactions at high cholesterol limit. Biophys J. 2004;86:1532–44.
49. Jedlovsky P, Medvedev N, Mezei M. Effect of cholesterol on the properties of phospholipid membranes. 3. Local lateral structure. J Phys Chem B. 2004;108:465–72.
50. Bamberg E, Noda K, Gross E, Läuger P. Single-channel parameters of gramicidin A, B and C. Biochim Biophys Acta. 1976;419:223–8.
51. Ostroumova OS, Malev VV, Bessonov AN, Takemoto JY, Schagina LV. Altering the activity of syringomycin E via membrane dipole potential. Langmuir. 2008;24:2987–91.
52. Jordan PC. Electrostatic modeling of ion pores. II. Effects attributable to the membrane dipole potential. Biophys J. 1983;41:189–95.

53. Mares LJ, Garcia A, Rasmussen HH, Cornelius F, Mahmmoud YA, Berlin JR, Lev B, Allen TW, Clarke RJ. Identification of electric-field-dependent steps in the Na^+,K^+-pump cycle. Biophys J. 2014;107:1352–63.
54. Zhang J, Loew LM, Davidson RM. Faster voltage-dependent activation of Na^+ channels in growth cones versus somata of neuroblastoma N1E-115 cells. Biophys J. 1996;71:2501–8.
55. Bedlack RS Jr, M-d W, Fox SH, Gross E, Loew LM. Distinct electric potentials in soma and neurite membranes. Neuron. 1994;13:1187–93.
56. Ganea C, Babes A, Lüpfert C, Grell E, Fendler K, Clarke RJ. Hofmeister effects of anions on the kinetics of partial reactions of the Na^+,K^+-ATPase. Biophys J. 1999;77:267–81.
57. Gadsby DC, Rakowski RF, De Weer P. Extracellular access to the Na,K pump: pathway similar to ion channel. Science. 1993;260:100–3.
58. Hilgemann DW. Channel-like function of the Na,K pump probed at microsecond resolution in giant membrane patches. Science. 1994;263:1429–32.
59. Wuddel I, Apell H-J. Electrogenicity of the sodium transport pathway in the Na,K-ATPase probed by charge-pulse experiments. Biophys J. 1995;69:909–21.
60. Rakowski RF, Gadsby DC, De Weer P. Voltage dependence of the Na/K pump. J Membr Biol. 1997;155:105–12.
61. Babes A, Fendler K. Na^+ transport, and the E1P-E2P conformational transition of the Na^+/K^+-ATPase. Biophys J. 2000;79:2557–71.
62. Gadsby DC, Bezanilla F, Rakowski RF, De Weer P, Holmgren M. The dynamic relationships between the three events that release individual Na^+ ions from the Na^+/K^+-ATPase. Nat Commun. 2012;3:669.
63. Clarke RJ. Dipole-potential-mediated effects on ion pump kinetics. Biophys J. 2015;109:1513–20.
64. Mouritsen OG, Bloom M. Mattress model of lipid-protein interactions in membranes. Biophys J. 1984;46:141–53.
65. Peschke J, Riegler J, Möhwald H. Quantitative analysis of membrane distortions induced by mismatch of protein and lipid hydrophobic thickness. Eur Biophys J Biophys Lett. 1987;14:385–91.
66. Mouritsen OG, Bloom M. Models of lipid-protein interactions in membranes. Annu Rev Biophys Biomol Struct. 1993;22:145–71.
67. Fattal DR, Ben-Shaul A. A molecular model for lipid-protein interactions in membranes: the role of hydrophobic mismatch. Biophys J. 1993;65:1795–809.
68. Clarke RJ, Zouni A, Holzwarth J. Voltage sensitivity of the fluorescent probe RH421 in a model membrane system. Biophys J. 1995;68:1406–15.
69. Cornelius F, Habeck M, Kanai R, Toyoshima C, Karlish SJD. General and specific lipid-protein interactions in Na,K-ATPase. Biochim Biophys Acta Biomembr. 2015;1848:1729–43.
70. Pearlstein RA, Dickson CJ, Hornak V. Contributions of the membrane dipole potential to the function of voltage-gated cation channels and modulation by small molecule potentiators. Biochim Biophys Acta Biomembr. 2017;1859:177–94.
71. Norimatsu Y, Hasegawa K, Shimizu N, Toyoshima C. Protein-phospholipid interplay revealed with crystals of a calcium pump. Nature. 2017;545:193–8.
72. Li L, Shi X, Guo X, Li H, Xu C. Ionic protein-lipid interaction at the plasma membrane: what can the charge do? Trends Biochem Sci. 2014;39:130–40.
73. Volodkin D, Mohwald H, Voegel J-C, Ball V. Coating of negatively charged liposomes by polylysine: drug release study. J Control Release. 2007;117:111–20.
74. Reuter M, Schwieger C, Meister A, Karlsson G, Blume A. Poly-L-lysines and poly-L-arginines induce leakage of negatively charged phospholipid vesicles and translocate through the lipid bilayer upon electrostatic binding to the membrane. Biophys Chem. 2009;144:27–37.
75. Hädicke A, Blume A. Binding of the cationic peptide $(KL)_4K$ to lipid monolayers at the air-water interface: effect of lipid headgroup, acyl chain length, and acyl chain saturation. J Phys Chem B. 2016;120:3880–7.
76. Garcia A, Pratap PR, Lüpfert C, Cornelius F, Jacquemin D, Lev B, Allen TW, Clarke RJ. The voltage-sensitive dye RH421 detects a Na^+,K^+-ATPase conformational change at the membrane surface. Biochim Biophys Acta Biomembr. 2017;1859:813–23.

77. Jiang Q, Garcia A, Han M, Cornelius F, Apell H-J, Khandelia H, Clarke RJ. Electrostatic stabilization plays a central role in autoinhibitory regulation of the Na^+,K^+-ATPase. Biophys J. 2017;112:288–99.
78. Nguyen K, Garcia A, Sani M-A, Diaz D, Dubey V, Clayton D, Dal Poggetto G, Cornelius F, Payne RJ, Separovic F, Khandelia H, Clarke RJ. Interaction of N-terminal peptide analogues of the Na^+,K^+-ATPase with membranes. Biochim Biophys Acta Biomembr. 2018;1860(6):1282–91.
79. Yeagle PL, Young J, Rice D. Effects of cholesterol on sodium-potassium ATPase ATP hydrolyzing activity in bovine kidney. Biochemistry. 1988;27:6449–52.
80. Cornelius F. Cholesterol modulation of molecular activity of reconstituted shark Na^+,K^+-ATPase. Biochim Biophys Acta Biomembr. 1995;1235:205–12.
81. Sotomayor CP, Aguilar LF, Cuevas FJ, Helms MK, Jameson DM. Modulation of pig kidney Na^+/K^+-ATPase activity by cholesterol: Role of hydration. Biochemistry. 2000;39:10928–35.
82. Starke-Peterkovic T, Turner N, Else PL, Clarke RJ. Electric field strength of membrane lipids from vertebrate species: membrane lipid composition and Na^+-K^+-ATPase molecular activity. Am J Physiol Regul Comp Physiol. 2005;288:R663–70.

Mass Spectrometry Imaging of Cholesterol

Stephanie M. Cologna

Abstract Mass spectrometry imaging (MSI) has evolved as a significant tool to map biomolecules in situ without tags. This chapter describes advancements in mass spectrometry imaging technology and applications focused on mapping cholesterol. Secondary ion mass spectrometry (SIMS), matrix-assisted laser desorption/ionization (MALDI), and desorption electrospray (DESI) modes are described. These MSI technologies range in spatial resolution, and therefore different levels of mapping ranging from intracellular to whole tissue can be achieved. A variety of technical examples showing methods for cholesterol and cholesterol-derived molecular imaging are provided as well as imaging results from membrane dynamics, and genetic and drug treatment models. This emerging application of MSI for mapping cholesterol in biological specimens provides a new means to gain a deeper understanding of cholesterol distribution, and thereby insights into function.

Keywords Label-free imaging · Isotope · Mapping · Cholesterol · Mass spectrometry

1 Introduction to Mass Spectrometry Imaging

Mass spectrometry imaging (MSI) is a label-free technique to spatially map molecules according to an X–Y position and accurate mass measurement. A typical experimental setup includes the surface to be analyzed and an ion beam, laser, or other source that is focused on the sample. Mass spectra are collected across the surface such that each collection represents a pixel. Following data acquisition, an ion image is generated for any given mass-to-charge (m/z) ratio. The applications of

S. M. Cologna (✉)
Department of Chemistry and Laboratory of Integrated Neuroscience, University of Illinois at Chicago, Chicago, IL, USA
e-mail: cologna@uic.edu

A. Rosenhouse-Dantsker, A. N. Bukiya (eds.), *Cholesterol Modulation of Protein Function*, Advances in Experimental Medicine and Biology 1115,
https://doi.org/10.1007/978-3-030-04278-3_7

MSI are diverse and cross many different disciplines. This chapter is focused on the modern methods for MSI with a focus on the analysis of cholesterol. Ionization modes, applications, and novel methodologies are presented.

2 Cholesterol

Cholesterol is a critical component of cell membranes [1] that serves as a signaling molecule for a number of cellular processes [2, 3]. Disturbances in cholesterol homeostasis, synthesis, and signaling have been implicated in a number of human diseases ranging from cancer to cardiovascular disease and neurodegeneration among others [4–7]. Therefore, the ability to map cholesterol location and abundance has been at the forefront of a growing number of biophysical studies. Furthermore, cholesterol dysregulation is implicated in a number of human diseases, and therefore has significant clinical importance.

Mass spectrometry (MS)-based measurements of cholesterol have encompassed a variety of ionization modes and instrumentation. Gas chromatography (GC) coupled with electron ionization is one of the most standardized methodologies to measure cholesterol amounts. More recently, liquid chromatography (LC) coupled with either electrospray ionization (ESI) or chemical ionization has been implemented for routine cholesterol measurements [8, 9]. While these hybrid mass spectrometry approaches have proven extremely valuable for identification and quantification of cholesterol from a variety of sources, the absence of spatial information highlights the need for more advanced techniques. This need is further heightened in view of the limited number of resources for molecular approaches (e.g., chemical stains, and antibodies) to address this need. Recent advancements in MSI technology and their applications to cholesterol mapping are discussed in the sections below.

3 Secondary Ion Mass Spectrometry

Secondary ion mass spectrometry (SIMS) utilizes an ion beam or cluster to generate secondary ions following bombardment of the sample of interest [10]. The choice of primary ion beam in part dictates the type of secondary ions that are generated. For example, high-energy sources typically cause the fragmentation of molecules into individual atomic or polyatomic species, and is thereby referred to as atomic SIMS. Significant efforts have been focused on the development of source conditions, techniques, and experimental approaches to generate molecular ions in SIMS experiments. This approach allows for the direct measurement of molecular species according to accurate mass measurement, and benefits from large mass range measurements [11]. With regard to cholesterol, two approaches can be used,

either incorporation of an isotope label or observation of the molecular ion [12]. Owing to the relatively small (micro- to nanometer scale) source beam size, the spatial resolution obtained on SIMS instruments is high [13].

Cholesterol imaging using SIMS instruments has been widely implemented in a number of biological applications (Fig. 1). These include plasma membrane

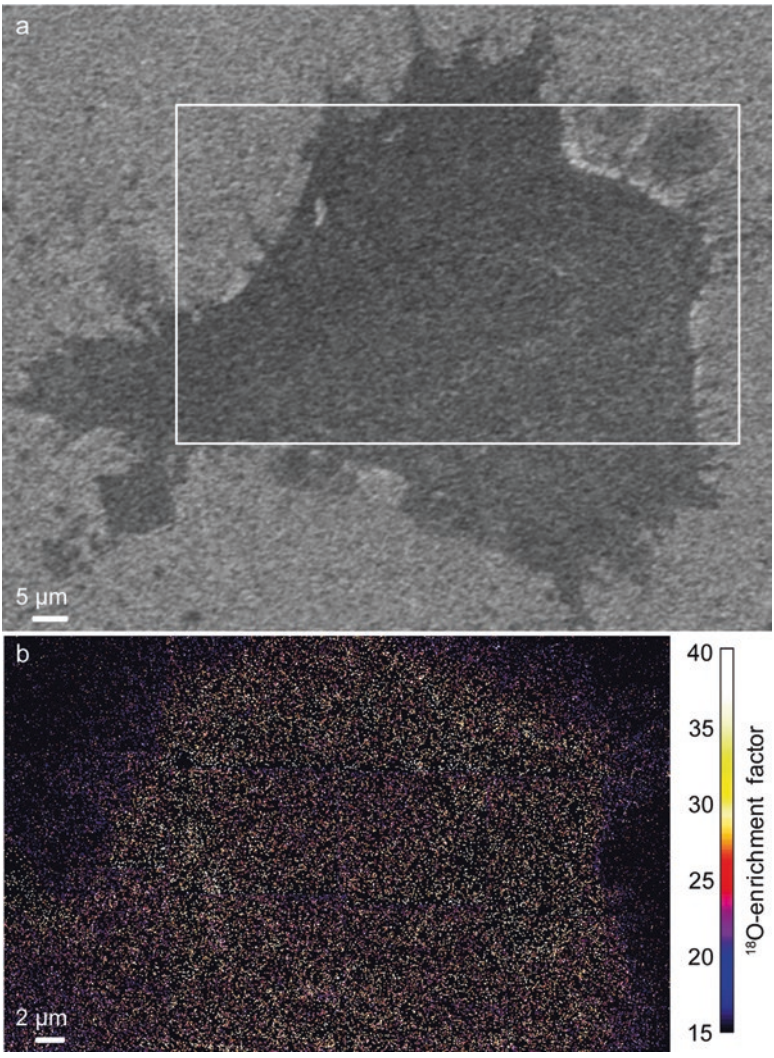

Fig. 1 SIMS imaging of cholesterol in NIH3T3 fibroblasts. (**a**) Image of approximate MSI analysis area. (**b**) Distribution of cholesterol based upon metabolic incorporation of ^{18}O. Image courtesy of Mary L. Kraft, University of Illinois—Urbana Champaign. Reproduced with permission from [14] under the Creative Commons Attribution License

distributions of cholesterol in blood cells [15], and mapping of cholesterol in macrophages [16, 17] as well as in other single-cell systems [18]. Additionally, a variety of tissue sections including brain [19, 20], kidney [21], cartilage [22], and colon tissue [23] among others have been investigated to understand normal and perturbed cholesterol distributions.

Another area of imaging using SIMS instrumentation has been in artificial systems such as lipid membrane mimics. For example, Sostarecz et al. [24] imaged cholesterol in Langmuir–Blodgett model membrane of cholesterol while investigating phospholipid composition differences. More recently, the effect of the chemical composition of the leaflets of a cell membrane on membrane domain formation has also been studied using a similar approach [25]. Similarly, SIMS imaging coupled with atomic force microscopy has been utilized to study the effect of cholesterol on a predominant phospholipid in the inner leaflet of the cellular membrane [26].

4 Matrix-Assisted Laser Desorption/Ionization (MALDI)

MALDI-MS has been employed for imaging experiments successfully for a number of years and across many disciplines. MALDI as a soft ionization method is ideal for measuring protonated and de-protonated molecules and when coupled with time-of-flight (TOF) or ion cyclotron resonance (ICR) mass analyzers can result in the collection of high and ultrahigh mass resolution. For MALDI imaging, the sample is typically adhered to a stainless steel plate or conductively coated glass slide. Matrix application techniques have included inkjet printing [27], sublimation [28], spraying devices [29], and most recently, 3D printing devices [30], among others. For data collection, the laser (commonly UV) is rastered across the sample in which a mass spectrum is collected at each "pixel." Reconstructed images are obtained for any given m/z value measured in the experiments. The spatial resolution obtained from these instruments is dictated by the laser spot size and the crystal size. Modern commercial instruments have recently boasted 5-μm lateral spatial resolution, and this will be a continually developing area for such instruments [31, 32].

Work using MALDI-MS for imaging has spanned over two decades. An example of cholesterol imaging by MALDI in the cerebellum of a mouse is provided in Fig. 2. Regarding cholesterol imaging, Zaima et al. [33] reported the images of cholesterol esters in atherosclerosis lesions, while cholesterol sulfate mapping was reported on skin tissue sections. In addition to tissue section mapping, a study by Schober and coworkers [34] focused on single-cell imaging in which cholesterol has been mapped on individual HeLa cells. Other examples of cholesterol imaging by MALDI demonstrating changes in cholesterol levels include traumatic brain injury [35], atherosclerosis aortic plaques [36], and materials suitable for joint implants [37].

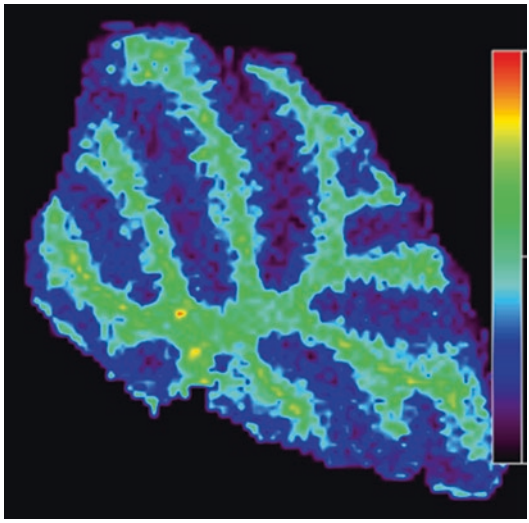

Fig. 2 Example of cholesterol (m/z 369) imaging by MALDI-MS on a sagittal section of mouse cerebellum. Animal age was 9 weeks

5 Desorption Electrospray Ionization

Desorption electrospray ionization (DESI) was first introduced in 2004 by Graham Cook's laboratory [38]. The working principle of DESI is desorption of analytes on surfaces by introducing electrosprayed droplet sources focused to the surface. The original studies provided proof-of-concept ionization of a wide range of molecules from various surfaces [38]; however, ionization of cholesterol itself remained challenging to achieve by traditional DESI. Not surprising, the benefit of this ionization mode for imaging applications was quickly realized, albeit with lower lateral spatial resolution compared to MALDI and SIMS. Rat brain tissue was evaluated for cholesterol distribution using DESI coupled with charge labeling [39]. Subsequently, similar studies were performed in atheroma [40] and adrenal tissue [41] as well. DESI imaging has been widely used as a screening tool for cancer. In particular, cholesterol sulfate has been mapped in human prostate cancer tissues [42, 43]. An example of prostate cancer imaging is depicted in Fig. 3. As evident in these examples, DESI imaging is still in its infancy, and with regard to cholesterol imaging, new approaches are needed for spatial mapping.

6 Novel Methodologies for Imaging

There have been numerous reports of novel strategies to map cholesterol. Each of these strategies has relied on derivatives of the core approaches described above. For this reason, only examples of novel approaches to perform mass spectrometry imaging with a focus on cholesterol are provided.

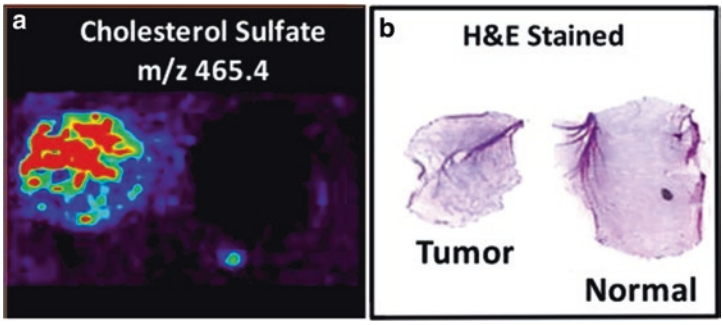

Fig. 3 Cholesterol sulfate imaging of human prostate tissue. (**a**) DESI imaging of cholesterol sulfate in prostate tissue. (**b**) H&E staining of respective tissues. Adapted from Eberlin et al. [42] with permission

Matrix Enhanced (ME)-SIMS One approach of a hybrid methodology has been the combination of SIMS and MALDI features for imaging applications. Matrix enhanced-SIMS includes deposition of an organic acid followed by analysis using traditional SIMS imaging. A unique feature of this approach is the extension in m/z range that can be measured. Cholesterol mapping from the freshwater snail *Lymnaea stagnalis* has been imaged in such a manner [44]. Other applications include ionic liquid matrices [45] as well as imaging of brain tissue using ME-SIMS [46].

3D Imaging While imaging of biological specimens including cells and tissues has been invaluable, a challenge has been in representing a 3D structure in 2D space. Therefore, efforts have been focused on developing an approach that would adequately represent 3D structures. One such approach, which is related to SIMS imaging, involves depth profiling that allows image reconstruction in the Z-axis. Cholesterol images in 3D have been obtained in oocytes from *Xenopus laevis* [47]. 3D imaging has also been performed on kidney cells using metabolic labeling for cholesterol [48]. More recently, SIMS has been coupled with the ultrahigh resolution mass analyzer, the orbitrap, for multidimensional labeling [49].

IR-MALDESI A hybrid approach to traditional MALDI imaging has been reported with the coupling of an infrared (IR) laser to an electrospray source [50]. This approach has been termed IR-MALDESI [51]. In addition to offering a new way for ionization and detection of various analytes, IR-MALDESI has also been incorporated in the imaging mode [52]. The IR-MALDESI approach has been successfully utilized to perform imaging experiments of cholesterol in tissue sections [53].

Metal Incorporation The addition of metals in imaging experiments of cholesterol has spanned multiple ionization modes. In SIMS experiments, rat kidney sections were treated with a thin silver layer, and signals were compared to untreated sections [54]. Generally, signal enhancement was observed for treated sections that included

silver cationized cholesterol. Similarly, gold has been added for SIMS imaging of neuroblastoma cells in which enhanced cholesterol signals were observed [55].

The neutral nature of the cholesterol structure makes protonation difficult in soft ionization experiments. The most commonly observed ion for cholesterol (denoted M) mapping is the dehydrated, protonated molecule ($[M - H_2O + H]^+$). Efforts to enhance cholesterol signal in tissue imaging include the addition of silver ions to the matrix [56] as well as silver sputtering [57]. Furthermore, addition of silver nanoparticles or implantation [35] of such nanoparticles has also been investigated in conjunction with MSI experiments [58]. These ever-evolving methodologies indicate the interest in cholesterol imaging and also the continual efforts to improve ionization efficiency, speed, and resolution.

7 Implications for Biophysical and Biomedical Applications

With these new technological advances in place, the scope of applications that can be utilized to elucidate cholesterol dynamics is clearly broad. Investigators must understand, however, the limitations of these approaches, particularly with lateral spatial resolution required for evaluating either cell culture populations or more broadly tissue sections. The ability to gain functional insight either by drug treatment or via genetic manipulation using mass spectrometry imaging of cholesterol has been demonstrated in several studies. For example, co-localization studies provide insight into cell membrane structure and organization. As shown in Fig. 4, Frisz et al. [14] used nanoSIMS to investigate the sphingolipid and cholesterol localization in the plasma membrane of fibroblasts. While sphingolipids (Fig. 4b) appear to be nonuniformly dispersed, the authors observe cholesterol to be uniformly distributed (Fig. 4c).

In an example from a genetic model, Smith–Lemli–Opitz syndrome (SLOS) which is caused by mutations of *DHCR7*, the enzyme that reduces 7-dehydrocholesterol to cholesterol in biosynthesis (as reviewed in [59]). Patients with SLOS have elevated 7-dehydrocholesterol levels compared to unaffected controls. Xu and coworkers [60] performed silver sputtering to visualize silver adducts of cholesterol and 7-dehydrocholesterol on cell monolayers using MALDI coupled with ion mobility mass spectrometry. Image alignment and co-localization provided pixel-based ratios of the two sterols. The authors suggested that this was a rapid methodology to obtain sterol ratios as compared to more standard approaches.

Very recently, the effects of cisplatin treatment on pheochromocytoma cells (PC12) was investigated with a focus on lipid imaging [61]. In general, the authors observed a decrease in lipid species upon drug treatment. With regard to cholesterol, a decrease was observed upon treatment with cisplatin. Notably, similar observations were made in a study that employed tissue imaging experiments [62]. Based on these results, the authors proposed an exocytotic mechanism, and eventually apoptosis [61].

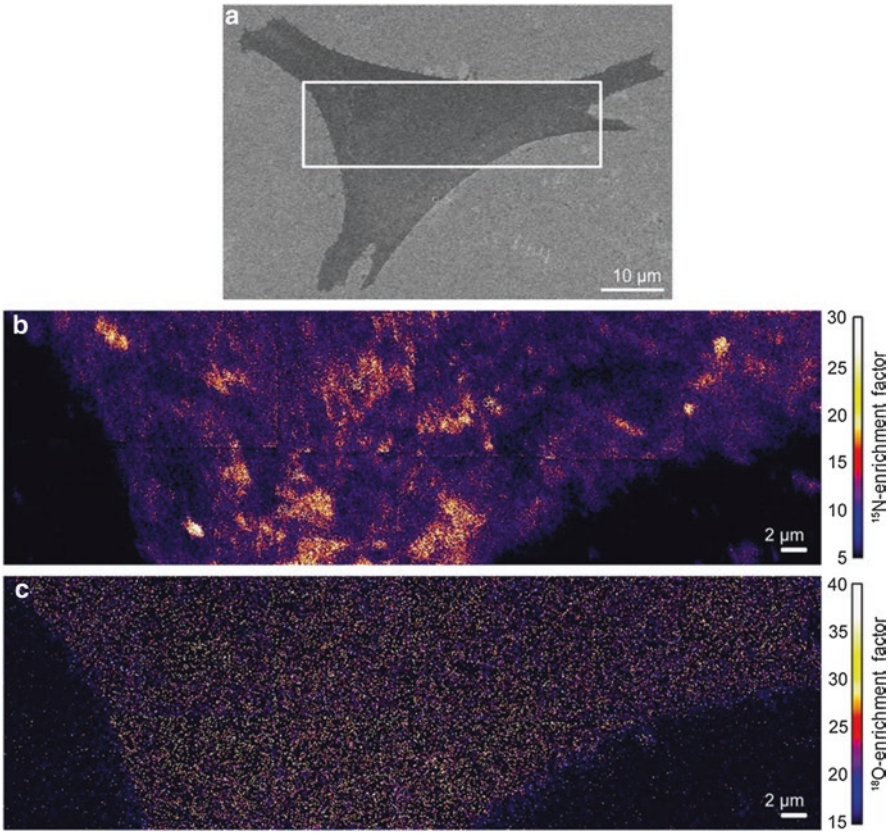

Fig. 4 Fibroblast imaging. (**a**) Scanning electron microscopy image of a fibroblast cell. (**b**) Distribution of sphingolipids in the plasma membrane. (**c**) Cholesterol imaging in the same cell plasma membrane. Reproduced with permission from [14] under the Creative Commons Attribution

8 Concluding Remarks

This chapter has provided a summary of technological and experimental approaches to image cholesterol in biological specimens. The ability to perform imaging in situ without the need for tags highlights the strength of mass spectrometry imaging. While advances have improved the lateral spatial resolution achieved, continued efforts are being focused on further improving the spatial resolution.

The application of MSI to studies involving cholesterol specifically continues to expand, and has been included in a variety of biomedical and biophysical applications. These include membrane dynamics, genetic modification, and drug-induced changes. The potential impact of MSI in understanding cholesterol dynamics in biological systems is endless. While single-molecule tracking is not available currently with these methods, individual cell types can be analyzed to

evaluate differences in cholesterol distribution, and include membrane changes at the subcellular level.

In terms of diagnostics, DESI imaging demonstrates significant promise in clinical applications for disease diagnosis. While currently premature to rely on this approach solely, many examples of DESI imaging show feature differences in disease versus control tissues suggesting that this approach is providing new technologies for clinical diagnostics. The different technological methods presented here highlight the array of options for mapping cholesterol. Furthermore, the range in biological specimens analyzed also underscores the potential application of these technologies for mapping whole organismal samples. New applications of MSI continue to be reported regularly, and the ability to utilize these approaches for uncovering the diverse functions and distribution of cholesterol in biological systems will remain paramount to biomedical research.

References

1. Spector AA, Yorek MA. Membrane lipid composition and cellular function. J Lipid Res. 1985;26(9):1015–35.
2. Luu W, Sharpe LJ, Gelissen IC, Brown AJ. The role of signalling in cellular cholesterol homeostasis. IUBMB Life. 2013;65(8):675–84.
3. Paik YK, Jeong SK, Lee EY, Jeong PY, Shim YH. *C. elegans*: an invaluable model organism for the proteomics studies of the cholesterol-mediated signaling pathway. Expert Rev Proteomics. 2006;3(4):439–53.
4. Edwards PA, Ericsson J. Signaling molecules derived from the cholesterol biosynthetic pathway: mechanisms of action and possible roles in human disease. Curr Opin Lipidol. 1998;9(5):433–40.
5. Zhang Y, Ma KL, Ruan XZ, Liu BC. Dysregulation of the low-density lipoprotein receptor pathway is involved in lipid disorder-mediated organ injury. Int J Biol Sci. 2016;12(5):569–79.
6. Fessler MB. Regulation of adaptive immunity in health and disease by cholesterol metabolism. Curr Allergy Asthma Rep. 2015;15(8):48.
7. Vance JE. Dysregulation of cholesterol balance in the brain: contribution to neurodegenerative diseases. Dis Model Mech. 2012;5(6):746–55.
8. Becker S, Rohnike S, Empting S, Haas D, Mohnike K, Beblo S, et al. LC-MS/MS-based quantification of cholesterol and related metabolites in dried blood for the screening of inborn errors of sterol metabolism. Anal Bioanal Chem. 2015;407(17):5227–33.
9. Blondelle J, Pais de Barros JP, Pilot-Storck F, Tiret L. Targeted lipidomic analysis of myoblasts by GC-MS and LC-MS/MS. Methods Mol Biol. 2017;1668:39–60.
10. Gamble LJ, Anderton CR. Secondary ion mass spectrometry imaging of tissues, cells, and microbial systems. Micros Today. 2016;24(2):24–31.
11. Nunez J, Renslow R, Cliff JB 3rd, Anderton CR. NanoSIMS for biological applications: current practices and analyses. Biointerphases. 2017;13(3):03B301.
12. Kraft ML. Plasma membrane organization and function: moving past lipid rafts. Mol Biol Cell. 2013;24(18):2765–8.
13. Klitzing HA, Weber PK, Kraft ML. Secondary ion mass spectrometry imaging of biological membranes at high spatial resolution. In: Sousa AA, Kruhlak MJ, editors. Nanoimaging: methods and protocols. Totowa: Humana Press; 2013. p. 483–501.
14. Frisz JF, Klitzing HA, Lou K, Hutcheon ID, Weber PK, Zimmerberg J, et al. Sphingolipid domains in the plasma membranes of fibroblasts are not enriched with cholesterol. J Biol Chem. 2013;288(23):16855–61.

15. Sjovall P, Lausmaa J, Nygren H, Carlsson L, Malmberg P. Imaging of membrane lipids in single cells by imprint-imaging time-of-flight secondary ion mass spectrometry. Anal Chem. 2003;75(14):3429–34.
16. Ostrowski SG, Kurczy ME, Roddy TP, Winograd N, Ewing AG. Quantitative SIMS imaging of cholesterol in the membranes of individual cells from differentially treated populations. Anal Chem. 2007;79(10):3554–60.
17. Ostrowski SG, Kurczy ME, Roddy TP, Winograd N, Ewing AG. Secondary ion MS imaging to relatively quantify cholesterol in the membranes of individual cells from differentially treated populations. Anal Chem. 2007;79(10):3554–60.
18. Georgi N, Cillero-Pastor B, Eijkel GB, Periyasamy PC, Kiss A, van Blitterswijk C, et al. Differentiation of mesenchymal stem cells under hypoxia and normoxia: lipid profiles revealed by time-of-flight secondary ion mass spectrometry and multivariate analysis. Anal Chem. 2015;87(7):3981–8.
19. Lazar AN, Bich C, Panchal M, Desbenoit N, Petit VW, Touboul D, et al. Time-of-flight secondary ion mass spectrometry (TOF-SIMS) imaging reveals cholesterol overload in the cerebral cortex of Alzheimer disease patients. Acta Neuropathol. 2013;125(1):133–44.
20. Sjovall P, Lausmaa J, Johansson B. Mass spectrometric imaging of lipids in brain tissue. Anal Chem. 2004;76(15):4271–8.
21. Nygren H, Borner K, Hagenhoff B, Malmberg P, Mansson JE. Localization of cholesterol, phosphocholine and galactosylceramide in rat cerebellar cortex with imaging TOF-SIMS equipped with a bismuth cluster ion source. Biochim Biophys Acta. 2005;1737(2–3):102–10.
22. Cillero-Pastor B, Eijkel G, Kiss A, Blanco FJ, Heeren RM. Time-of-flight secondary ion mass spectrometry-based molecular distribution distinguishing healthy and osteoarthritic human cartilage. Anal Chem. 2012;84(21):8909–16.
23. Brulet M, Seyer A, Edelman A, Brunelle A, Fritsch J, Ollero M, et al. Lipid mapping of colonic mucosa by cluster TOF-SIMS imaging and multivariate analysis in cftr knockout mice. J Lipid Res. 2010;51(10):3034–45.
24. Sostarecz AG, McQuaw CM, Ewing AG, Winograd N. Phosphatidylethanolamine-induced cholesterol domains chemically identified with mass spectrometric imaging. J Am Chem Soc. 2004;126(43):13882–3.
25. Baker MJ, Zheng L, Winograd N, Lockyer NP, Vickerman JC. Mass spectral imaging of Glycophospholipids, cholesterol, and Glycophorin a in model cell membranes. Langmuir. 2008;24(20):11803–10.
26. McQuaw CM, Sostarecz AG, Zheng L, Ewing AG, Winograd N. Lateral heterogeneity of dipalmitoylphosphatidylethanolamine−cholesterol Langmuir−Blodgett films investigated with imaging time-of-flight secondary ion mass spectrometry and atomic force microscopy. Langmuir. 2005;21(3):807–13.
27. Baluya DL, Garrett TJ, Yost RA. Automated MALDI matrix deposition method with inkjet printing for imaging mass spectrometry. Anal Chem. 2007;79(17):6862–7.
28. Hankin JA, Barkley RM, Murphy RC. Sublimation as a method of matrix application for mass spectrometric imaging. J Am Soc Mass Spectrom. 2007;18(9):1646–52.
29. Li S, Zhang Y, Liu J, Han J, Guan M, Yang H, et al. Electrospray deposition device used to precisely control the matrix crystal to improve the performance of MALDI MSI. Sci Rep. 2016;6:37903.
30. Tucker LH, Conde-Gonzalez A, Cobice D, Hamm GR, Goodwin RJA, Campbell CJ, et al. MALDI matrix application utilizing a modified 3D printer for accessible high resolution mass spectrometry imaging. Anal Chem. 2018;90(15):8742–9.
31. Duenas ME, Feenstra AD, Korte AR, Hinners P, Lee YJ. Cellular and subcellular level localization of maize lipids and metabolites using high-spatial resolution MALDI mass spectrometry imaging. Methods Mol Biol. 2018;1676:217–31.
32. Feenstra AD, Duenas ME, Lee YJ. Five Micron high resolution MALDI mass spectrometry imaging with simple, interchangeable, multi-resolution optical system. J Am Soc Mass Spectrom. 2017;28(3):434–42.

33. Zaima N, Sasaki T, Tanaka H, Cheng XW, Onoue K, Hayasaka T, et al. Imaging mass spectrometry-based histopathologic examination of atherosclerotic lesions. Atherosclerosis. 2011;217(2):427–32.
34. Schober Y, Guenther S, Spengler B, Rompp A. Single cell matrix-assisted laser desorption/ionization mass spectrometry imaging. Anal Chem. 2012;84(15):6293–7.
35. Roux A, Muller L, Jackson SN, Post J, Baldwin K, Hoffer B, et al. Mass spectrometry imaging of rat brain lipid profile changes over time following traumatic brain injury. J Neurosci Methods. 2016;272:19–32.
36. Castro-Perez J, Hatcher N, Kofi Karikari N, Wang SP, Mendoza V, Shion H, et al. In vivo isotopically labeled atherosclerotic aorta plaques in ApoE KO mice and molecular profiling by matrix-assisted laser desorption/ionization mass spectrometric imaging. Rapid Commun Mass Spectrom. 2014;28(22):2471–9.
37. Frohlich SM, Archodoulaki VM, Allmaier G, Marchetti-Deschmann M. MALDI-TOF mass spectrometry imaging reveals molecular level changes in ultrahigh molecular weight polyethylene joint implants in correlation with lipid adsorption. Anal Chem. 2014;86(19):9723–32.
38. Takats Z, Wiseman JM, Gologan B, Cooks RG. Mass spectrometry sampling under ambient conditions with desorption electrospray ionization. Science. 2004;306(5695):471–3.
39. Wu C, Ifa DR, Manicke NE, Cooks RG. Rapid, direct analysis of cholesterol by charge labeling in reactive desorption electrospray ionization. Anal Chem. 2009;81(18):7618–24.
40. Manicke NE, Nefliu M, Wu C, Woods JW, Reiser V, Hendrickson RC, et al. Imaging of lipids in atheroma by desorption electrospray ionization mass spectrometry. Anal Chem. 2009;81(21):8702–7.
41. Wu C, Ifa DR, Manicke NE, Cooks RG. Molecular imaging of adrenal gland by desorption electrospray ionization mass spectrometry. Analyst. 2010;135(1):28–32.
42. Eberlin LS, Dill AL, Costa AB, Ifa DR, Cheng L, Masterson T, et al. Cholesterol sulfate imaging in human prostate cancer tissue by desorption electrospray ionization mass spectrometry. Anal Chem. 2010;82(9):3430–4.
43. Pirro V, Eberlin LS, Oliveri P, Cooks RG. Interactive hyperspectral approach for exploring and interpreting DESI-MS images of cancerous and normal tissue sections. Analyst. 2012;137(10):2374–80.
44. Altelaar AF, van Minnen J, Jimenez CR, Heeren RM, Piersma SR. Direct molecular imaging of *Lymnaea stagnalis* nervous tissue at subcellular spatial resolution by mass spectrometry. Anal Chem. 2005;77(3):735–41.
45. Fitzgerald JJD, Kunnath P, Walker AV. Matrix-enhanced secondary ion mass spectrometry (ME SIMS) using room temperature ionic liquid matrices. Anal Chem. 2010;82(11):4413–9.
46. Dowlatshahi Pour M, Malmberg P, Ewing A. An investigation on the mechanism of sublimed DHB matrix on molecular ion yields in SIMS imaging of brain tissue. Anal Bioanal Chem. 2016;408(12):3071–81.
47. Fletcher JS, Lockyer NP, Vaidyanathan S, Vickerman JC. TOF-SIMS 3D biomolecular imaging of *Xenopus laevis* oocytes using buckminsterfullerene (C60) primary ions. Anal Chem. 2007;79(6):2199–206.
48. Yeager AN, Weber PK, Kraft ML. Three-dimensional imaging of cholesterol and sphingolipids within a Madin-Darby canine kidney cell. Biointerphases. 2016;11(2):02A309.
49. Passarelli MK, Pirkl A, Moellers R, Grinfeld D, Kollmer F, Havelund R, et al. The 3D OrbiSIMS-label-free metabolic imaging with subcellular lateral resolution and high mass-resolving power. Nat Methods. 2017;14(12):1175–83.
50. Sampson JS, Hawkridge AM, Muddiman DC. Generation and detection of multiply-charged peptides and proteins by matrix-assisted laser desorption electrospray ionization (MALDESI) Fourier transform ion cyclotron resonance mass spectrometry. J Am Soc Mass Spectrom. 2006;17(12):1712–6.
51. Barry JA, Muddiman DC. Global optimization of the infrared matrix-assisted laser desorption electrospray ionization (IR MALDESI) source for mass spectrometry using statistical design of experiments. Rapid Commun Mass Spectrom. 2011;25(23):3527–36.

52. Robichaud G, Barry JA, Muddiman DC. IR-MALDESI mass spectrometry imaging of biological tissue sections using ice as a matrix. J Am Soc Mass Spectrom. 2014;25(3):319–28.
53. Nazari M, Muddiman DC. Cellular level mass spectrometry imaging using infrared matrix assisted laser desorption electrospray ionization (IR-MALDESI) by oversampling. Anal Bioanal Chem. 2015;407(8):2265–71.
54. Nygren H, Johansson BR, Malmberg P. Bioimaging TOF-SIMS of tissues by gold ion bombardment of a silver-coated thin section. Microsc Res Tech. 2004;65(6):282–6.
55. Altelaar AF, Klinkert I, Jalink K, de Lange RP, Adan RA, Heeren RM, et al. Gold-enhanced biomolecular surface imaging of cells and tissue by SIMS and MALDI mass spectrometry. Anal Chem. 2006;78(3):734–42.
56. Meier F, Garrard KP, Muddiman DC. Silver dopants for targeted and untargeted direct analysis of unsaturated lipids via infrared matrix-assisted laser desorption electrospray ionization (IR-MALDESI). Rapid Commun Mass Spectrom. 2014;28(22):2461–70.
57. Dufresne M, Thomas A, Breault-Turcot J, Masson JF, Chaurand P. Silver-assisted laser desorption ionization for high spatial resolution imaging mass spectrometry of olefins from thin tissue sections. Anal Chem. 2013;85(6):3318–24.
58. Muller L, Kailas A, Jackson SN, Roux A, Barbacci D, Schultz JA, et al. Lipid imaging within the normal rat kidney using silver nanoparticles by matrix-assisted laser desorption/ionization mass spectrometry. Kidney Int. 2015;88(1):186–92.
59. Porter FD, Herman GE. Malformation syndromes caused by disorders of cholesterol synthesis. J Lipid Res. 2011;52(1):6–34.
60. Xu L, Kliman M, Forsythe JG, Korade Z, Hmelo AB, Porter NA, et al. Profiling and imaging ion mobility-mass spectrometry analysis of cholesterol and 7-dehydrocholesterol in cells via sputtered silver MALDI. J Am Soc Mass Spectrom. 2015;26(6):924–33.
61. Mohammadi AS, Li X, Ewing AG. Mass spectrometry imaging suggests that cisplatin affects exocytotic release by alteration of cell membrane lipids. Anal Chem. 2018;90(14):8509–16.
62. Moreno-Gordaliza E, Esteban-Fernandez D, Lazaro A, Humanes B, Aboulmagd S, Tejedor A, et al. MALDI-LTQ-Orbitrap mass spectrometry imaging for lipidomic analysis in kidney under cisplatin chemotherapy. Talanta. 2017;164:16–26.

Cholesterol-Dependent Gating Effects on Ion Channels

Qiu-Xing Jiang

Abstract Biomembranes separate a live cell from its environment and keep it in an off-equilibrium, steady state. They contain both phospholipids and nonphospholipids, depending on whether there are phosphate groups in the headgroup regions. Cholesterol (CHOL) is one type of nonphospholipids, and one of the most abundant lipid molecules in humans. Its content in plasma membranes and intracellular membranes varies and is tightly regulated. Voltage-gated ion channels are universally present in every cell and are fairly diversified in the eukaryotic domain of life. Our lipid-dependent gating hypothesis postulates that the controlled switch of the voltage-sensor domains (VSDs) in a voltage-gated potassium (Kv) channel between the "down" and the "up" state (gating) is sensitive to the ratio of phospholipids:nonphospholipids in the annular layer around the channel. High CHOL content is found to exert strong inhibitory effects on Kv channels. Such effects have been observed in *in vitro* membranes, cultured cells, and animal models for cholesterol metabolic defects. Thermodynamic analysis of the CHOL-dependent gating suggests that the inhibitory effects of CHOL result from collective interactions between annular CHOL molecules and the channel, which appear to be a more generic principle behind the CHOL effects on other ion channels and transporters. We will review the recent progress in the CHOL-dependent gating of voltage-gated ion channels, discuss the current technical limitations, and then expand briefly the learned principles to other ion channels that are known to be sensitive to the CHOL–channel interactions.

Keywords Annular lipids · Cholesterol packing · bSUMs · Cholesterol organization · Inhibitory effects · Voltage-sensor conformation

Q.-X. Jiang (✉)
Department of Microbiology and Cell Science, IFAS, University of Florida, Gainesville, FL, USA
e-mail: qxjiang@ufl.edu

A. Rosenhouse-Dantsker, A. N. Bukiya (eds.), *Cholesterol Modulation of Protein Function*, Advances in Experimental Medicine and Biology 1115,
https://doi.org/10.1007/978-3-030-04278-3_8

1 Introduction

All lipids in eukaryotic cell membranes contain hydrophilic headgroups and hydrophobic fatty acyl tails. They belong to two main groups—phospholipids (group I) and nonphospholipids (group II) (Fig. 1). Group I includes glycerophospholipids and sphingomyelin phospholipids, both of which contain phosphate groups in their headgroup regions in an equivalent location. Group II includes mainly cholesterol (CHOL), glycolipids, and other sphingolipids and cationic lipids. The molar ratio of phospholipids to nonphospholipids (PL/non-PL) varies from cell to cell or from one membrane patch to another in the same cell. In a major fraction of human cells, PL/non-PL ratio may be significantly smaller than unity, meaning that Group II lipids may be an overwhelming majority in certain cell membranes.

Group I lipids include mainly phosphatidylcholine (PC), cardiolipin, phosphatidylethanolamine (PE), phosphatidyl-glycerol (PG), phosphatidylserine (PS), phosphatidyl-inositols (PI), phosphatidic acid (PA), and sphingomyelin. Their acyl tails can vary in length and unsaturation level. Phospholipids are known to be important for the functions of specific ion channels. Anionic phospholipids, such as PS, PG, cardiolipin, PA, etc., are important for the normal function of bacterial MscL channels [1, 2]. Phosphatidyl-inositol-4,5-bisphosphate (PIP_2) is known to regulate specific ion channels [3–9]. PG was found to be associated with the KcsA channel and important for its function [10, 11]. Crystallographic studies revealed potential phospholipid-binding sites in a Kv2.1 chimera channel and PIP_2-binding pockets in the IRK channel [4, 12]. PC content was found to be a key regulator for the topogenesis of lactose permease in bacteria [13]. Cardiolipin is a structural and functional component for the supercomplex of the electron transport chain in

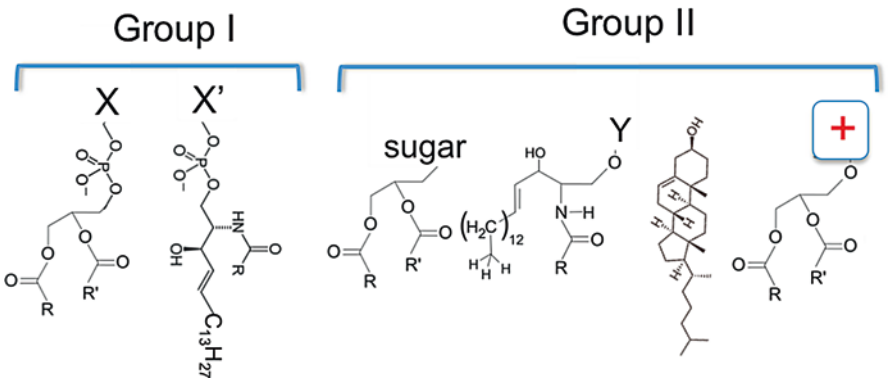

Fig. 1 Two main groups of lipid molecules in eukaryotic cell membranes. Group I are phospholipids, include (1) glycerol-phospholipids. The group X could be choline (PC), ethanolamine (PE), glycerol (PG), serine (PS), inositol (PIs), or proton (PA). (2) Sphingosine phospholipids. Group X' refers to mainly choline. Group II are non-phospholipids, and include (3) glycerol-glycolipids; (4) Sphingosine-glycolipids. Group Y represents different sugar groups, mono-saccharides or oligo-saccharides. (5) Cholesterol (CHOL). (6) Cationic glycerol-lipids

mitochondria [14, 15]. Because of the relative random distribution of the phospholipids in their specific leaflets of asymmetric cell membranes and the fact that nearly all known monogenic lipid metabolic defects in humans affect the cellular and systems homeostasis of nonphospholipids (group II), we will not focus our discussions on the effects of different types of phospholipids on ion channels.

Group II lipids are both structural and signaling components [16]. Figure 1 shows the structures of four main types of Group II lipids. C40-based ether lipids, which are usually seen in extremophiles, are not diagramed here, nor are the derivatives of cholesterol, monoacyl-glycerol, ceramides, or long unsaturated fatty acids. Diacylglycerol (DAG), a product from the hydrolysis of phosphatidylinositol 4,5-bisphosphate (PIP2) by phospholipase C (PLC), is a second messenger that activates protein kinase C (PKC). DAG also is a ligand for MunC13, which is a critical regulator for the fusion competence of synaptic vesicles [17, 18], and a coactivator for transient receptor potential canonical (TRPC) cation channels (TRPC3/6/7) [19–22]. Cerebrosides, which include both monoglycosylceramides and oligoglycosylceramides, are important structural constituents in the plasma membranes of animal muscle and nerve cells, may cause higher phase-transition temperatures of biological membranes, and are capable for forming multidentate H-bonding interactions among them in order to stabilize membranes containing them [23]. Galactosylceramides are major constituents of gray matter (2% dry weight) and white matter (12% dry weight) in nervous tissues [23–25]. Cholesterol (CHOL) is literally the most abundant nonphospholipids in mammalian cells. It is the precursor for different steroid hormones. Its analogs in fungi and protozoans are called ergosterols and in plants phytosterols. *Xenopus* oocyte membranes contain ~21 mol% cholesterol [26, 27]. For the CHOL-dependent gating of voltage-gated ion channels, we will discuss animal sterols (dominantly CHOL), and phytosterols and ergosterols may share strong chemical similarities. We therefore will focus on CHOL content in the plasma membranes of animal cells. The average CHOL levels in plasma membranes (PMs) are between 15 and 50 mol% whereas net content of 5–10 mol% CHOL is present in endoplasmic reticulum (ER) membranes. However, CHOL in PMs is distributed between CHOL-poor and CHOL-rich areas, which depends on the organization of proteins and various types of lipids. In humans, brain contains ~25% of total body CHOL even though it normally accounts for merely 2–3% of body weight [28], suggesting high CHOL content in both neuronal and glial cells. CHOL affects nAChR, Kir, BK, and TRPV channels [29].

Voltage-gated ion channels are a must for all cells [32]. Their dysfunction may cause severe diseases [33–45]. Except voltage-gated proton channels, all known canonical voltage-gated channels have four subunits/domains, each of which has six transmembrane segments (TMs). They contain a pore domain flanked by four VSDs (Fig. 2A). Gating of a voltage-gated channel refers to a controlled switch of its VSDs or the pore between "down" and "up" or between "closed" and "open" states, respectively. The fourth TM (S4) of a VSD has evenly spaced positively charged residues believed to move inside a *gating pore* (Fig. 2B). Outer (or "upper") and inner (or "lower") crevices of the gating pore are separated by a central "hydrophobic gasket," also called the *gating charge transfer center* [30, 46]. The gating charge

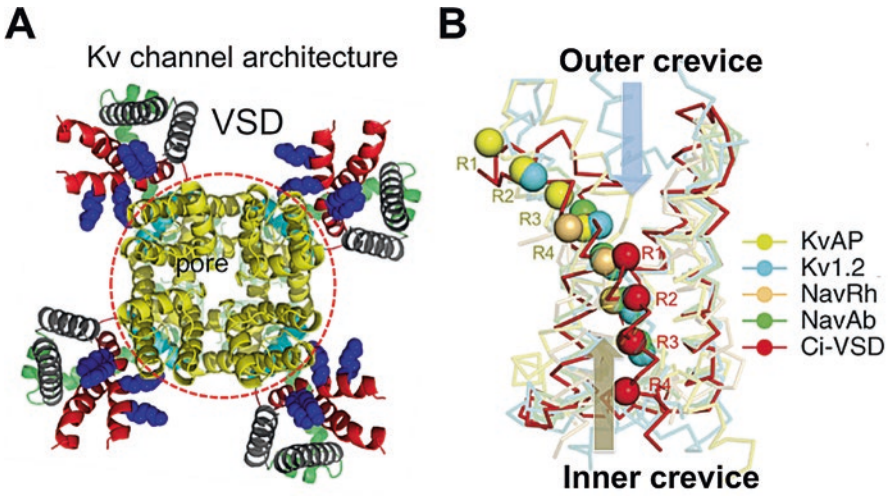

Fig. 2 Architecture of a Kv channel and variations in VSD structures. (**A**) KvAP model after the Kv2.1 structure showing a central pore domain (red circle) and four VSDs. (**B**) Five VSD structures in alignment. Arginine residues on S4 are aligned across the gating pore. Outer (upper) and inner (lower) crevices separated by a hydrophobic gasket (red). In a full resting (down) state, all four Arg residues move to the inner crevice, and drive the pore domain into the closed state [30, 31]. Panel B was modified from [30]

selectivity was proposed to rely on a conserved Phe residue, which is missing in some of the VSDs, possibly allowing structural variations in the modes of the proposed charge movements. Structures of multiple VSDs in detergents determined by X-ray or cryoEM represent "up" or "intermediately closed" states and exhibit significant structural diversity among VSDs and in the coupling of VSDs to pore domains [47–54]. Recently reported Kv structures by cryoEM further strengthened the structural diversity [50, 51, 53, 55].

Past biophysical and physiological studies have revealed abundant information about the voltage-gated ion channels at the protein level [12, 30, 31, 49, 56–102]. Key residues contributing to voltage sensing and chemical basis for ion selectivity are established, revealing a broad range of gating charge per channel [49, 85, 103–113]. Multiple structures reveal significant differences among "up" and intermediately "down" states of the VSDs. More congruent structural features in the pore domains are established, but the allosteric coupling between VSDs and pore domains may vary strikingly (Fig. 2b) [12, 46, 49–51, 53, 55, 72, 75, 85–87, 114–118]. The published data have proposed that the voltage-driven conformational changes of the VSDs may have the following components of physical movement: (1) a simple sliding of the S4 helix "up" and "down" in the gating pore to pass individual arginine (or lysine in some channels) residues through the gating charge transfer center, with or without possible switch of one short segment of the S4 between a regular alpha helix and a 3_{10} helix; (2) a short sliding and rotation of the S4 helix through the focused electrostatic field across the "hydrophobic plug; (3) the toggling of the

VSDs between "outward-facing" and "inward-facing" conformations as a transporter when the tilting of helices is rearranged; and (4) the movement of S3 together with S4 and the leaning of the S1/S2 helical pairs against the S3/S4 helical pairs.

Structural studies of the VSDs from *Ciona* voltage-sensitive phosphatase (*Ci*-VSP) in two different states revealed a one-register movement (~5 Å translation and ~60° rotation) of the S4 and minor changes in the other three VSD helices, which largely accord with the intermediately "down" states seen in the NavAb and TPCs [47–49, 84]. This mode of movement, to some extent, agrees with a short vertical movement of the KvAP voltage-sensor paddle in the gating pore (not directly in lipids), an S4 movement of 6–10 Å for the focused field model, or the sliding 3_{10}-helix in the S4 by a similar distance as predicted by Rosetta modeling of the NavAb [56, 74, 75, 78, 90], even though *the structural diversity in VSDs may still allow different conformational changes to achieve functional differences*. Despite these models, a structure has so far not been available for a canonical voltage-gated ion channel that is fully kept in the resting state with all four VSDs in a complete "down" state. It is still not feasible to compare directly the VSDs of the same channel in "up" and "down" states. In the past, it has been taciturnly assumed that despite the diversified VSDs in sequence, the voltage-driven conformational changes among all, or at least a majority, of VSDs are very similar, if not identical. The structural variations in Fig. 2b, the functional diversities among various different types of voltage-gated ion channels, especially the Kv channels, and the altered gating properties of voltage-gated ion channels in different cell types or in different locations of the same cells make it plausible to consider that an alternative thinking may be needed to reconcile the different views of the voltage-gating mechanisms. Lipid-dependent gating hypothesis represents a new proposal in this direction.

2 Overview of CHOL Effects on Voltage-Gated Ion Channels

As integral membrane proteins, Kv channels are expected to be sensitive to their lipid environments. When *Xenopus* oocytes were used as a heterogeneous expression system for Kv channels and cell-attached patches were formed to record channel activity, it has been long known that functional Kv channels on the surface of the oocytes appear clustered in hot spots, especially in regions of the animal pole that are close to the boundary between the dark-colored animal pole and the faintly colored vegetal pole. When a pore-blocking toxin, CTX or AgTx2, was mutated and conjugated with a nanogold particle, and used to detect *Shaker* K channel on the surfaces of *Xenopus* oocytes, it was observed that the channels were randomly distributed on the surfaces (QXJ, unpublished observations). Similar observations of nonfunctional voltage-gated ion channels were made on the surface of cultured cells and neurons. These could be attributed either to channel proteins that were not fully matured or to the lipid environments in cell membranes [119, 120]. For example, Kv2.1 is delivered to different regions of a neuronal cell, but only a fraction of the

channels are functional when recorded by cell-attached patches. When expressed in cultured cells, the Kv2.1 channels in puncta, which refer to microdomains that consist of both proteins and special lipids, are usually not active [121, 122]. Phosphorylation and dephosphorylation were proposed as a possible mechanism. In view of the strong lipid-dependent gating effects and well-known or characterized cholesterol-rich domains, it is very likely that the special lipids around the proteins might contribute to the inhibitory effects on the channel activity [122].

Chemical treatments to alter CHOL content led to either inhibitory or stimulatory effects on voltage-gated ion channels [123–138]. The partial or nearly complete depletion of CHOL with methyl-β-cyclodextrin (MBCD) in different cells has caused different effects. Changes in current density, activation/deactivation kinetics, inactivation rate, and shifts in G–V relation were reported. For example, 1 mM MBCD treatment of NG108-15 neurons overexpressing Kv3.1 channels led to slower activation/deactivation and decrease in firing frequency of action potential (AP's) [124]. Contrastingly, in rat hippocampal neurons, MBCD treatment increased the firing frequency of AP's by increasing the current density of delayed rectifier Kv channels and accelerating the activation and deactivation of the A-type Kv channels [126]. The opposite effects for different Kv channels in neurons and other cells have been puzzling. On the other hand, MBCD treatment has been demonstrated to cause severe structural changes in cells. 1–3 mM MBCD treatment of mouse fetal skeletal muscle cells for 1 h at 37 °C caused obvious decrease in caveolae and T-tubule area [131]. *Such complications from chemical treatment raised serious concerns and cast strong doubt on all past data collected from voltage-gated ion channels in MBCD-treated cells.*

More consistent data, however, were obtained in cells loaded with MBCD–CHOL, where the inhibitory effects of higher CHOL content were observed for L-type Ca^{2+} channels (Cav1.2) in mouse fetal skeletal muscle cells [131], Kv1.3 in T lymphocytes [127, 132, 136], L-type Ca^{2+} channels in coronary artery smooth muscle cells [139], Kv11.1 in adult canine ventricular myocytes [140], and Kv channels in coronary arteriolar smooth muscle cells [139]. The main reason for such consistency among different channels in cultured cells or in primary tissues is probably attributable to intrinsic effects of high content of CHOL and its analogs on membrane stability and the voltage-gated ion channels, which could only be quantitatively studied in a well-controlled membrane system.

3 Lipid-Dependent Gating Predicts Strong CHOL-Dependent Inhibition of Kv Channels

My laboratory started the investigation of the lipid-dependent effect in a well-controlled system, where the channels were completely pure and the lipids in defined composition formed fluidic membranes. Under such conditions, we first discovered that the phosphate groups in the lipid bilayers were essential for a Kv channel to reach its open state [73], which was echoed by findings from Dr. Zhe Lu's lab where

sphingomyelinases were used to treat cell membranes and alter activities of various eukaryotic Kv channels [141, 142]. After carefully studying the conformational states of both the voltage-sensor domains and the channel pore in different lipids, we concluded that *in homogeneous membranes, Group II lipids favor the KvAP in a resting state with its VSDs in the "down" conformation. Moreover, the lipid-stabilized "resting" state is equivalent or tightly connected to the native one driven by hyperpolarization in transmembrane electrostatic potential* [143], leading to our hypothesis of "*lipid-dependent gating*" (Fig. 3) [144]. Physicochemically, we may speculate that the lipid-dependent gating mainly stems from the nonphospholipids in the annulus around a channel. These lipids cause energetic difference between different gating states of the VSDs. This hypothesis explains partial gating charge immobilization caused by sphingomyelinase treatment of cells [141] and may explain the clusters of nonconducting Kv channels in cholesterol-rich domains in cultured cells [120] or gating charge immobilization of the Kv4.3 channels in midbrain dopamine neurons directly caused by endocannabinoids (besides faster inactivation effect) [145]. Similar lipid-dependent conformational changes in the VSDs were reported for hyperpolarization-activated MVP channels [146].

Studies by my laboratory and later by other groups in other channels suggest a self-coherent explanation for various lipid effects we have observed. There is thus a good reason to believe that our hypothesis of lipid-dependent gating may underlie a more general inhibitory effect of nonphospholipids on Kv channels. Among all the Group II lipids, CHOL is probably the most studied because of its importance to public health and the available technologies and reagents in analyzing CHOL in different cells and tissues. The lipid-dependent gating hypothesis predicts that CHOL exerts strong inhibitory effects on a variety of eukaryotic Kv channels. *We will call this prediction the CHOL-dependent gating of Kv channels*. As reported before, hypercholesterolemia caused inhibitory effects on Cav2.1 channels in coronary arterial smooth muscle cells [134]. The CHOL-dependent gating effects may be expanded to both Cav and voltage-gated Na^+ (Nav) channels, depending on the accessibility of their VSDs [147]. On the other hand, such gating effects might

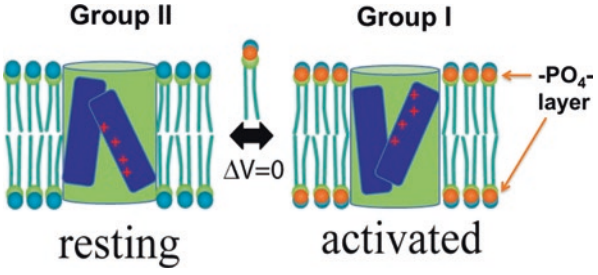

Fig. 3 Simplified scheme for lipid-dependent gating. A VSD (blue bars with + charges in red) flanking a pore domain (green cylinder) switches between resting ("down" state of the VSDs) and activated ("up" state of the VSDs) state in Group II and Group I lipids at $\Delta V = 0$, showing the inner and outer crevices of the gating pore. The VSD is assumed to take an inward-facing conformation in the resting state and an out-ward-facing conformation in the activated state

be less prominent for voltage-gated Na^+ (Nav) or Ca^{2+} (Cav) channels [123–138], probably because eukaryotic Nav and Cav have four different VSDs and their VSDs may be shielded (at least partially) from annular lipids by auxiliary transmembrane subunits [54, 94, 148, 149]. Recent results did show that Nav1.9 in DRG neurons could be relieved from CHOL-dependent inhibition when inflammation lowers cholesterol content in these neurons and causes Nav1.9 to be repartitioned from "CHOL-rich lipid rafts to CHOL-poor non-raft regions" [147]. It is therefore necessary to take into account potential complications from channel proteins, accessory proteins, and lipid environments when we apply the lipid-dependent gating effects to experimental observations.

4 Cholesterol Distribution in Membranes and Cholesterol-Dependent Phase Separation

As a key component in cell membrane, CHOL may be equally or asymmetrically distributed between two leaflets. Even though the small polar headgroup (–OH) of CHOL allows relatively easy flipping across the hydrophobic core, transbilayer asymmetry of CHOL has been observed in plasma membranes of different mammalian cells due to active transport from the inner to the outer leaflet and the retention of CHOL in the outer leaflet [150]. The cholesterol content in plasma membranes of a cell may vary in the range of 15–50 mol%. Presence of CHOL fills in crevices between packed fatty acyl tails in the hydrophobic region and leaves gaps in the layer of the headgroups such that CHOL-rich membranes tend to have smooth phase transition, instead of a sharp switch from the fluidic phase to the crystalline gel phase during cooling. The gaps left by CHOL molecules in the headgroup layer are believed to increase the disorder of the headgroup layer.

Preferential packing of CHOL and sphingomyelin (SPhM) has been proposed to form dynamic lipid rafts in membranes or more stable structures like caveolae [152–156]. Super-resolution imaging suggests that the dynamic lipid rafts might be of 120–150 nm in diameter in cell membranes [157]. Secondary ion mass spec (SIMS) imaging indeed failed to detect large structures made by co-clustering of sphingomyelin and CHOL [158, 159]. Physicochemical studies also showed that in a ternary system made of PC/SPhM/CHOL, all lipids might be organized into a CHOL-poor phase with individual CHOL-rich islands [160, 161]. CHOL-dependent gating thus depends on the distribution of voltage-gated ion channels in the CHOL-rich domains, CHOL-sparse phase, or the boundary between the two.

Unfortunately with the current super-resolution fluorescence microscopy or high-resolution cryo-electron microscopy, it is still not possible to discern individual lipid molecules around each ion channel in a cell membrane. Quantitative analysis of CHOL-dependent gating thus requires a homogeneous system, which allows more precise control of lipid composition, CHOL content, phase behavior, channel density, and orientation. We developed a bead-supported unilamellar membrane system (bSUM) in order to achieve these effects (Fig. 4) [151]. In this system,

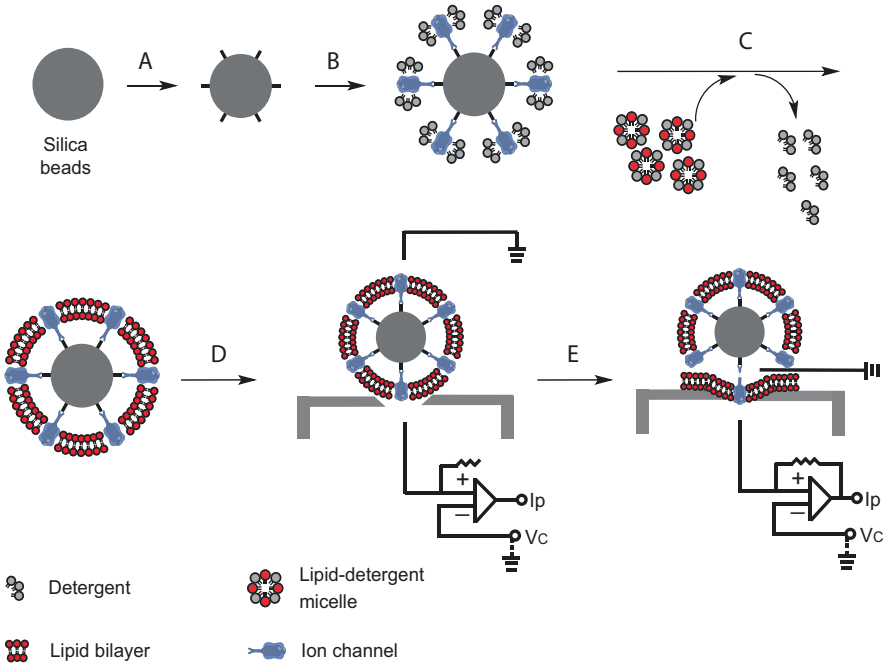

Fig. 4 bSUMs for preferred directional insertion of ion channels in CHOL-rich membranes. Chemical functionalization added ligand to the surface of silica beads (**A**). Channels bind to the ligands and orient themselves (**B**). Addition of detergent-solubilized lipids and slow removal of the detergents by BioBeads (**C**) leads to the formation of one bilayer membranes around each bead (**D**), which is the bSUM. The channels in bSUMs can be patched using a planar glass electron for electrical recordings (**E**). Adapted from [151]

a high density of surface ligands on a bead is used to sequester and select affinity-tagged channel proteins. The bSUM is advantageous in several aspects: (a) A majority of channels, if not all, are in the same orientation; (b) channels mediate the formation of the lipid bilayer; (c) there is one and only one bilayer; (d) lipids are changeable and the bead sizes can be varied from 0.1 to 20 μm; (e) channels can be recorded by patch clamp; (f) fast voltage-clamp speed (0.2–0.5 ms) is suitable for studying Kv channels with fast kinetics; and (g) it is suitable to measure the fluidity or phase separation in the membranes. Because of the fast gating kinetics of Nav, Cav, and many eukaryotic Kv channels, bSUMs will be better than almost all of the other in vitro membrane systems, such as bilayer membranes, glass-supported biomembrane, etc., and more stable than giant unilamellar vesicles (GUVs).

Cholesterol differs from phospholipids in another peculiar aspect. Chemical structures showed in Fig. 2 suggest that the electronegative OH group endows partial positive charges at the hydrophobic terminus of cholesterol. The stronger ester groups in a phospholipid for linking the fatty acyl chains endow higher partial positive charges to the hydrophobic core than a cholesterol molecule. It means that with the incorporation of more cholesterol, the positive potential in the middle of a

regular phospholipid bilayer would become weakened. A decrease of the hydrophobic core dipole potential from ~+500 mV to ~+200 mV in the membrane might be a contributing factor to favor the VSDs of a Kv channel in a specific gating state [162]. Such an effect has not been studied, and still awaits future investigations.

5 A Thermodynamic Model for Lipid–Channel Interactions

A canonical gating model for the *Shaker* K^+ channel can be used to address the energetics behind the CHOL-dependent gating effects (Fig. 5). In this model, the switch of four VSDs from the "down" to the "up" state must happen first before a concerted coupling of the VSDs and the pore domain that leads to the pore opening ($C_x \rightarrow O$) [110]. We assume that all the low-affinity binding sites for the CHOL

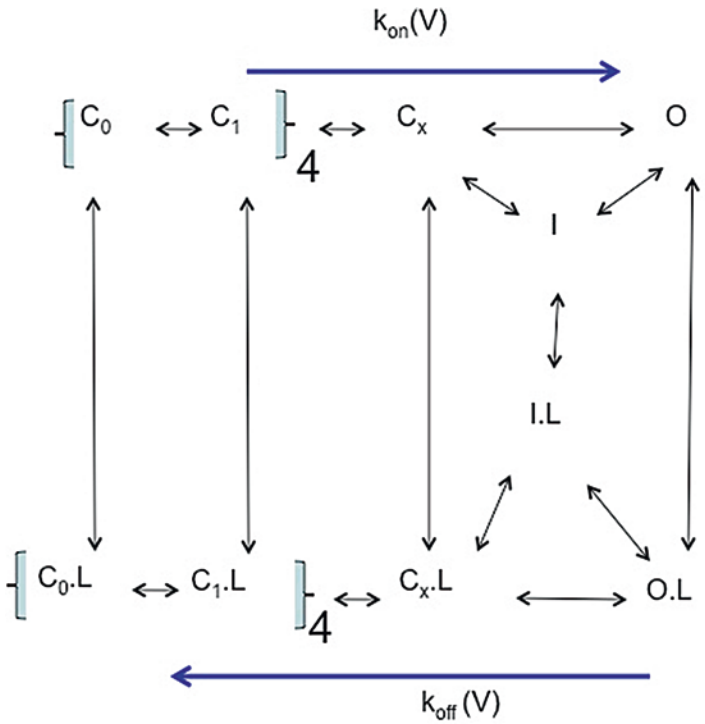

Fig. 5 A gating model for CHOL-dependent gating. The fully resting state (C_0) switches to the C_1 state in four independent steps because of four VSDs. The concerted coupling between four VSDs and the pore domain leads to the closed state immediately before the channel opening (C_x). The open state (O) can become inactivated (I) so as the closed state (C_x as an example). Cholesterol as the ligand (L) can be partitioned around channels in each state. The measured activation rate [$k_{on}(V)$] will be determined by the forward rate-limiting step. The deactivation rate [$k_{off}(V)$] will be determined by the closing rate of O

molecules in the annular layer of lipids next to the channel remain even though these sites may change their affinity during the gating transition. The general ON-rate (the activation rate) for channel opening represents the allosteric change from a closed state to the open state. The ON-rate is dominated by the rate-limiting step or the combination of a few steps that together determine the apparent rate of voltage-dependent activation. The OFF-rate for closing the open channel is defined by a combination of the kinetic constants for the two pathways that are connected to the O state. The OFF-rate can be determined from the mean life-time of the O state, assuming that there is one and only one open state here.

CHOL-dependent inhibition of the channel activity is ultimately to shift the channels away from the two open states—the O and O.L states. Collectively, the difference in free-energy change *(ΔΔG)* between the closed states and the open states is resulted from the binding of CHOL to multiple sites on probably different subunits with similar or quite different affinities for CHOL. Based on the dimension of a Kv channel and the diameter of a typical lipid molecule, there is enough space for ~120 lipid molecules in the annular layer next to each channel. A significant $\Delta\Delta G$ may come from a combination of a few high-affinity binding sites and/or low-affinity binding sites among the ~10 mol% CHOL among these annular lipids if each CHOL contributes an energetic difference of ~3 kT, which is equivalent to merely a three to eightfold change in the apparent binding affinity at each binding site. The summed energetic change of ~25 kT is sufficient to cause a significant shift of the Q–V (gating charge versus membrane potential) or G–V (relative conductance versus membrane potential) curve by 100–200 mV with an apparent gating charge similar to a *Shaker*-like K channel, which has a total gating charge of 10–13 elementary charges, and an apparent charge of ~4 elementary charges from its G–V relation. Such a consideration suggests that a small change in binding affinity for multiple CHOL-binding sites together can cause a major shift in G–V and Q–V.

More numerical calculations for the kinetic model will not be presented here. Instead, we will use the macroscopic $k_{on}(V)/k_{off}(V)$ to reach a conceptual understanding. The rate-limiting forward step leading to the opening of the channel and the rate-limiting deactivation step will dominate the distribution of the channels between the closed states and the open state. CHOL binding to multiple low-affinity binding sites may decrease the $k_{on}(V)/k_{off}(V)$ and exert strong inhibitory effects on the channel opening, and disfavor the activated state (Fig. 3). The scheme in Fig. 5 may make it more complicated if the cholesterol effect is caused by the energetic difference in the switching of the VSDs. It might cause a similar increase in $k_{on}(V)$ *and* $k_{off}(V)$*, leading to only small apparent shift of G–V, but a decrease in open channel activity (current density) through changes in open probability and dwell time for the open state*. Direct measurement of VSDs movement will be needed in such cases.

Because the details in the gating scheme may differ among the various Kv channels, especially the rate-limiting steps in the forward transition, the possible subconductance steps, the inactivation steps, and the movement of the VSDs in different lipid conditions, it is expected that the inhibitory effects of CHOL-dependent gating may be manifested differently when we compare the activation/deactivation/inactivation rates, the G–V/Q–V curve shifts, the open probability and dwell time of open

states, the steady-state currents after inactivation, etc. Other complicating factors such as channel density, lipid composition around individual channels, cell conditions under chemical modifications or genetic manipulations, etc. may also complicate the effects. These considerations will be necessary when direct lipid–channel interactions are used to account for CHOL-dependent gating or lipid-dependent gating in cell membranes.

6 Kv Channels Are Sensitive to Cholesterol Content

The above considerations make it important to use a well-controlled system to study the fundamental principles behind the CHOL-dependent gating without the interferences from uncontrolled factors in cellular environments. We initially used a solvent-based planar lipid bilayer system and found that a small amount of CHOL likely introduced significant inhibitory effects [143]. The lipid bilayer system has three limits: (1) It was difficult to control the fusion of CHOL-containing vesicles with the bilayer membrane; (2) the chemical nature of CHOL might drive its selective partition into the solvent (decane) islands or annulus in a bilayer membrane; and (3) the clamp speed is slow such that channel activity with fast gating kinetics cannot be resolved well. These limitations might have contributed to the observations by Finol-Urdaneta et al., who detected no CHOL-dependent gating when fusing KvAP channels in PE/PG vesicles into bilayer membranes made of PE/PG/CHOL, due to possible partition of cholesterol into the decane phases [125].

Our bSUMs were developed in order to overcome these technical limitations [151], and we were able to control CHOL content in membranes using a predefined molar ratio (mol%). With ~10 mol% CHOL, KvAP only started to show activity when the membrane potential (V_m) was > +60 mV [151]. Studies of DOPC/CHOL membranes showed that 9.6 mol% CHOL membrane is highly fluidic [163]. The channel identity was verified with a 33H1Fv, which was derived from a monoclonal antibody. The reconstitution process removed all detergents and achieved random insertion of both CHOL and DOPC into the bSUMs, which allows the predefinition of DOPC/CHOL ratio. Comparing the G–V curves of KvAP in DOPC with 4.0 and 9.6 mol% CHOL (Fig. 6A, B) revealed significant shifts, which are +210 mV in 9.6 mol% CHOL and +160 mV in 4.0 mol% (brown and red traces in Fig. 6C). Consistent with our hypothesis, 9.6 ml% CHOL stabilized KvAP in a closed state by ~18 kcal/mol*, using the apparent gating charge of 4.0 elementary charges*. Such a free-energy change *(ΔΔG)* could only be partially accounted for by changes in ON- and OFF-rates (~3.3 kcal/mol; not shown), suggesting that CHOL effects on VSDs probably dominate the stabilizing effect, which differs from the proposed replacement of phospholipids bound at the S4/S5 linkers to affect the concerted opening step during activation [8, 138]. In a homogeneous membrane, the CHOL effect is much stronger than what was reported in chemically treated cells [130, 132], which were probably lessened by the presence of CHOL-free domains, changes in types and levels of membrane proteins, vesicle fusion, or endocytosis. Without these complications, our analysis in bSUMs is direct and more accurate and quantitative.

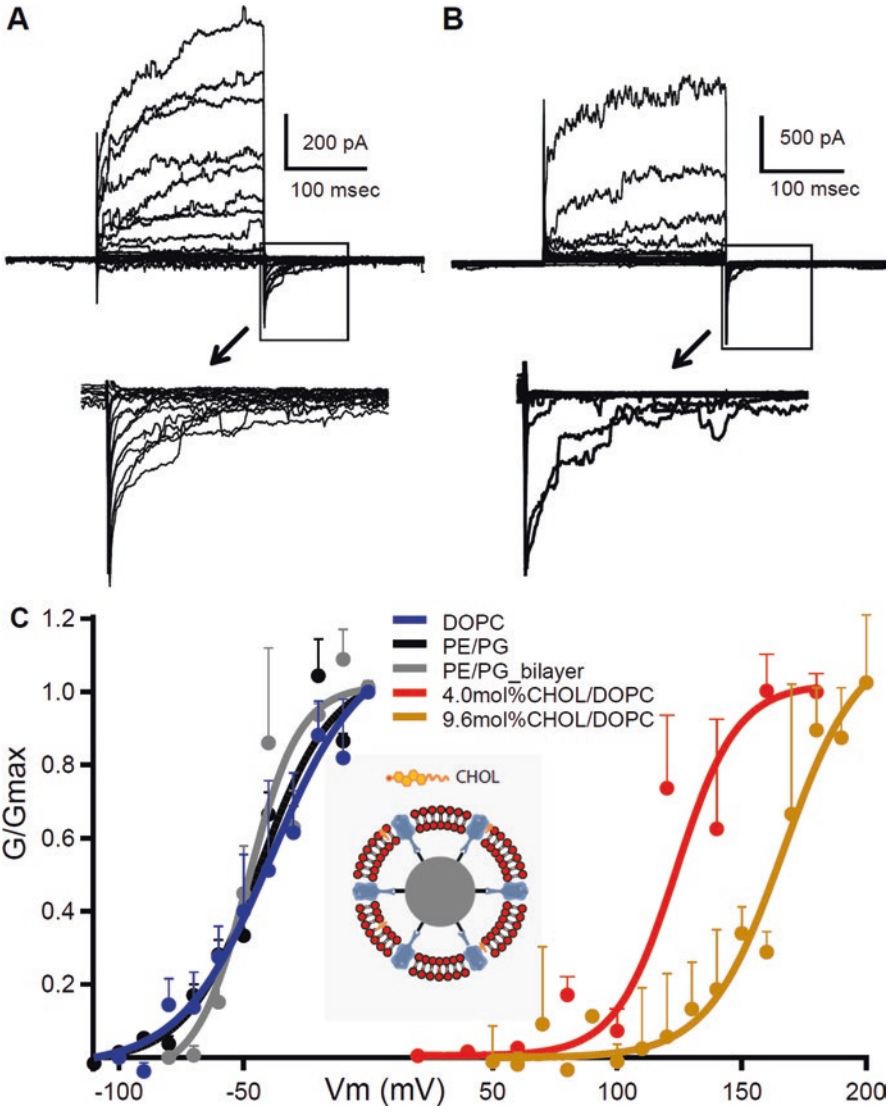

Fig. 6 CHOL inhibits KvAP in bSUMs. (**A**) Activity of KvAP in bSUMs made of PE:PG (3:1), pulsed from −160 to 180 mV at 10 mV steps. (**B**) Recordings from KvAP channels in bSUMs made of DOPC with 9.6 mol% of CHOL. (**C**) G–V for KvAP in bSUMs of DOPC (blue; $n = 3$), PE:PG (3:1, black; $n = 4$), DOPC/CHOL (4.0 mol% in red and 9.6% in brown; $n = 3$) and PE/PG 3:1 BLMs (grey; $n = 3$). Boltzmann fittings (solid lines) yielded ($Z\delta$, $V_{1/2}$) (e_0, mV) for channels in BLM (3.0, −47.5), PE/PG bSUMs (2.0, −45), DOPC bSUMs (1.6, −42.0), 4.0 mol% CHOL (1.6, 118) and 9.6 mol% CHOL (2.0, 162) in DOPC bSUMs. Error bars: *s.d*

7 Genetic Mutations that Affect Cholesterol Content in Cell Membranes

Virtually, all human lipid metabolic defects affect Group II lipids [164], and all may cause severe neurological defects and early death [165–167]. Recently in the acutely isolated dopaminergic neurons, it was found that the endocannabinoids and its analogs directly inhibit Kv4.3 channels by altering the inactivation rate and causing partial immobilization of gating charge [145]. The endocannabinoids are analogs of Group II lipids, and their effects suggest that distribution of the Group II lipids or their analogs around the channels is important to the cholesterol-dependent gating.

There are three pathways for cholesterol homeostasis in a human cell: uptake of LDL particles from outside, de novo synthesis of cholesterol in the ER, and the recycling of cholesterol from lysosome to the plasma membranes. Autophagosomes may contribute to the recycling pathway. There are different knockout mouse models for multiple genes in the pathway for cholesterol synthesis. Nonfunctional enzymes for cholesterol synthesis will lead to the decrease of cholesterol level in ER and ultimately in other cell membranes. NPC1 and NPC2 are the two enzymes responsible for the recycling of cholesterol [168, 169]. Their malfunction leads to severe lysosome-storage disease due to the accumulation of cholesterol in the lysosomes and autophagolysosomes. In cultured cells, knockout of NPC1 and NPC2 leads to significantly lower cholesterol content. In knockout mice, both NPC1-/- and NPC2-/- cause severe neurological symptoms, mirroring the severe neurological phenotypes in human patients [170]. The LDL-uptake is achieved through receptor-mediated endocytosis. Disruption of one or more of the three pathways will decrease cholesterol content in cell membranes and exert strong effects on at least some of the voltage-gated ion channels by removing part of the CHOL-dependent inhibition. The decreased cholesterol content in plasma membranes has the potential to cause higher activity of Kv channels and in turn lower excitability in the neurons that are affected. If such effects are more prominent in the inhibitory pathways, the net effect will become excitatory and cause hyperexcitability. Studies of Kv channels in cultured cells or knockout mice with defects in the three pathways will provide important information on the physiological significance of the CHOL-dependent gating of Kv channels in the future.

Structural comparison in Fig. 1 of the nonphospholipids and phospholipids suggests that there is a special role of the phosphate layer in shaping the electrostatic field across the bilayer, which has not been well understood. In the current molecule dynamics model, the difference between the DOTAP membrane and the DOPC bilayer was thought to be trivial because the salts in solution appeared sufficient to shield the effects of phosphates [171]. But, the experimental difference was very dramatic when a voltage-gated channel (or its VSDs) was used as a lipid sensor. Without a good atomistic model for these two types of lipids, calculations for energetic difference of any protein in them would fail to certain extent. The nature of the force field for the two groups of lipids might need to be better defined in order to

make good testable predictions. Quantum mechanical treatment of the atoms around the phosphodiesters plus molecular dynamics will be a possible avenue towards understanding the role of phosphates in distinguishing the Group I and II lipids.

8 Kv Channels as Sensors for Changes in Cholesterol Content

Our studies of KvAP in bSUMs (Fig. 6) demonstrated significant sensitivity of the VSDs to changes in CHOL content. In eukaryotic systems, multiple Kv channels have been found to be co-localized with marker proteins for lipid rafts or caveolae [131, 172–174]. The Kv channels in cholesterol-rich domains are expected to experience significant inhibitory effects. It appears that the Kv channels are much more sensitive because all four VSDs must undergo significant conformational changes in order to gate the channel pore and all VSDs are directly exposed to annular lipids (CHOL). No previous study has been able to determine specific factors that affect the delivery of a Kv channel into the CHOL-rich domains. Nor has it been possible to count the channels in CHOL-rich domains, CHOL-poor phases, and the boundary between them.

From an evolutionary viewpoint, our hypothesis predicts that the diversified sequences of Kv channels, especially the VSD sequences, and the distribution of various Kv channels in different cells with contrastingly different lipids may reflect the coevolution of specific Kv channels and the lipid environments in specific cells. For example, the lipid composition of the plasma membranes in a glial cell, a neuron, and an adipocyte is known to be fairly different. A glial cell has high content of plasmalogens [175]. A neuronal cell harbors high level of gangliosides. An adipocyte contains a large fraction of surface area covered by caveolae. Kv channels in these cells are expected to experience contrastingly different lipid environments and therefore may manifest the CHOL-dependent gating effects to different extents. It might be feasible to transduce these native cells with a viral vector to overexpress Kv2.1 or other channels in order to study their gating property in different regions of the cell membranes.

On the other hand, the current patch clamp techniques and imaging methods are not sufficient to reveal the annular lipids around individual channels. Other methods need to be tested. For example, a combination of super-resolution imaging of fluoresterol or other probes for CHOL and a labeled Kv channel (say Kv2.1) with cell-attached patch clamp recordings using a small-bore electrode will likely be suitable to reveal new insights on the direct distribution of cholesterol around a small number of Kv channels in cells. But, the limited resolution at 50–200 nm is not able to reach single-lipid resolution. CryoEM analysis of individual channels will need to average images of hundreds or thousands of ion channels in order to reveal the positions of stably bound structural lipids, not necessarily the lipids that are involved in gating modulation [176]. Secondary ion mass spectrometry is not able to reach single-

lipid resolution for imaging individual lipids, either. Molecular dynamic simulations using better force field to account for the differences between Group I and Group II lipids may be feasible in the near future. A completely new experimental method is thus needed in order to reach high-resolution imaging of annular lipids around individual channels. It is speculated that exposure to high-brilliance beam of either X-ray or electrons will potentially allow the structure determination for small membrane patches from a high-density sampling of Fourier components.

9 Other Ion Channels that Are Sensitive to Change in Cholesterol Content

Ion channel sensitivity to CHOL content has been more extensively studied for nAChR (nicotinic acetylcholine receptor) and G-protein-gated inward rectifier K channel (GIRK) [29, 177–180]. nAChR has an annular CHOL at the interface between M4 and M1 + M3, in proximity to the pore-lining M2 transmembrane helix. The M4 lipid sensor model proposes that the binding of lipids at the M4 site in the outer leaflet has direct effects on the transition of the channel into an uncoupling state. CryoEM averaging revealed recently potential empty spaces at the M1 and M4 interface for an annular CHOL in the outer leaflet, consistent with the M4 lipid sensor model deduced from the functional studies, even though still being complicated by uncertainty in averaging out the density for a disordered headgroup [176]. Further, the bound lipids are proposed to exert strong gating control to the channel. DAG was proposed to be a strong nAChR activator, which might be able to account for the empty space in the cryoEM density equally well. The biophysical nature of the CHOL and DAG binding in terms of their positions and functional effects on ion channels needs further characterization.

For GIRK interaction with CHOL in a stereo-sensitive manner, there are a few recent reviews discussing high-affinity binding sites based on structural studies [29]. CHOL binding acts mainly as an agonist in potentiating the function, and as an antagonist in a few cases. The “principal” CHOL-binding site in the crevice between the TM1 and TM2 in the outer leaflet is in proximity to the selectivity filter. The “transient” binding site in the inner leaflet is next to the inner gate and the coupling site at the intracellular surface, close to the PIP_2-binding site. In consideration of the relatively equal distribution of cholesterol in both leaflets, it is likely that these identified CHOL-binding sites will play a significant role when the channels are relocated between CHOL-rich and CHOL-poor regions in cell membranes.

In both nAChR and IRKs, CHOL binding is in close coupling to the gate of the channel pore and the stability of the open state. It is not expected that CHOL binding or unbinding would cause major conformational changes despite the proposed M4-movement for the nAChR after cholesterol binding. This view is fairly different from the proposed conformational changes of the VSDs in the Kv channels (Fig. 3).

Many other channels may have direct sensors for the annular lipids. Nav1.9 channels were recently identified as a sensor for plasma membrane cholesterol in DRG

(dorsal root ganglion) neurons that sense inflammatory pain. The pain sensitivity was higher when Nav1.9 channels were redistributed from CHOL-rich domains to CHOL-poor ones [147]. TRPV1 was found to have stably bound lipids in the nanodiscs which do not have a complete annular layer of lipids [181]. It would be interesting to study the lipid-dependent gating of TRPV1 in a well-controlled lipid environment, such as the bSUMs, or in native cell membranes after genetic manipulations of lipid homeostasis of the neurons. The same is probably true for multiple other TRPs, especially those that function in plasma membranes and lysosomal membranes.

10 General Conclusions and Future Perspectives

The lipid-dependent gating is probably a more general steady-state gating modality for voltage-gated ion channels. The chemical treatment by MBCD–CHOL to increase CHOL content has shown consistent inhibitory effects on different voltage-gated ion channels in different cells, all of which agree with the strong inhibitory effects observed in bSUMs (Fig. 6). The depletion of CHOL by MBCD is expected to cause severe structural heterogeneity and functional changes in cells and may alter channel density and its delivery to or retrieval from the cell membrane. Voltage-gated ion channels are thus adapted to their physiological lipid environments, and sensitive to changes in lipid composition caused by lipid metabolic defects in their native niches, some of which result in significant changes in the gating properties of voltage-gated ion channels and severe pathological phenotypes. Multiple low-affinity binding sites in the annular layer are sufficient to exert strong collective effects and change the gating property of a Kv channel. So far, we still lack a high-resolution tool to reveal the dynamic interactions between annular CHOL and voltage-gated ion channels. Structural studies of a Kv channel in a CHOL-rich bilayer membrane may provide a direct view in the future.

Acknowledgments Over the years, the main body of research in my laboratory on lipid-dependent gating has been funded by NIH (R01GM111367, R01GM093271 & R01GM088745), AHA (12IRG9400019), CF Foundation (JIANG15G0), Welch Foundation (I-1684), and CPRIT (RP120474). I am indebted to many colleagues in the ion channel field and in lipid research for their valuable suggestions and advice. I have tried my best to cover most, if not all, published work closely related to CHOL-dependent gating effects on ion channels, and would apologize to those whose work is not cited here.

References

1. Powl AM, East JM, Lee AG. Anionic phospholipids affect the rate and extent of flux through the mechanosensitive channel of large conductance MscL. Biochemistry. 2008;47(14):4317–28.
2. Powl AM, East JM, Lee AG. Lipid-protein interactions studied by introduction of a tryptophan residue: the mechanosensitive channel MscL. Biochemistry. 2003;42(48):14306–17.

3. Zaydman MA, et al. Kv7.1 ion channels require a lipid to couple voltage sensing to pore opening. Proc Natl Acad Sci U S A. 2013;110(32):13180–5.
4. Whorton MR, MacKinnon R. X-ray structure of the mammalian GIRK2-betagamma G-protein complex. Nature. 2013;498(7453):190–7.
5. Rittenhouse AR. PIP2 PIP2 hooray for maxi K+. J Gen Physiol. 2008;132(1):5–8.
6. Lee J, et al. PIP2 activates TRPV5 and releases its inhibition by intracellular Mg2+. J Gen Physiol. 2005;126(5):439–51.
7. Xiao J, Zhen XG, Yang J. Localization of PIP2 activation gate in inward rectifier K+ channels. Nat Neurosci. 2003;6(8):811–8.
8. Zaydman MA, Cui J. PIP2 regulation of KCNQ channels: biophysical and molecular mechanisms for lipid modulation of voltage-dependent gating. Front Physiol. 2014;5:195.
9. Furst O, D'Avanzo N. Isoform dependent regulation of human HCN channels by cholesterol. Sci Rep. 2015;5:14270.
10. Valiyaveetil FI, Zhou Y, MacKinnon R. Lipids in the structure, folding, and function of the KcsA K+ channel. Biochemistry. 2002;41(35):10771–7.
11. Valiyaveetil FI, et al. Glycine as a D-amino acid surrogate in the K(+)-selectivity filter. Proc Natl Acad Sci U S A. 2004;101(49):17045–9.
12. Long SB, et al. Atomic structure of a voltage-dependent K+ channel in a lipid membrane-like environment. Nature. 2007;450(7168):376–82.
13. Dowhan W, Bogdanov M. Lipid-dependent membrane protein topogenesis. Annu Rev Biochem. 2009;78:515–40.
14. Zhang M, Mileykovskaya E, Dowhan W. Cardiolipin is essential for organization of complexes III and IV into a supercomplex in intact yeast mitochondria. J Biol Chem. 2005;280(33):29403–8.
15. Mileykovskaya E, Zhang M, Dowhan W. Cardiolipin in energy transducing membranes. Biochemistry (Mosc). 2005;70(2):154–8.
16. Alberts B, et al. Molecular biology of the cell. 5th ed. New York: Garland Science; 2007.
17. Palfreyman M, Jorgensen EM. PKC defends crown against Munc13. Neuron. 2007;54(2): 179–80.
18. de Jong AP, et al. Phosphorylation of synaptotagmin-1 controls a post-priming step in PKC-dependent presynaptic plasticity. Proc Natl Acad Sci U S A. 2016;113(18):5095–100.
19. Kalwa H, et al. Phospholipase C epsilon (PLCepsilon) induced TRPC6 activation: a common but redundant mechanism in primary podocytes. J Cell Physiol. 2015;230(6):1389–99.
20. Zhang X, Trebak M. Transient receptor potential canonical 7: a diacylglycerol-activated non-selective cation channel. Handb Exp Pharmacol. 2014;222:189–204.
21. Itsuki K, et al. PLC-mediated PI(4,5)P2 hydrolysis regulates activation and inactivation of TRPC6/7 channels. J Gen Physiol. 2014;143(2):183–201.
22. Venkatachalam K, Zheng F, Gill DL. Control of TRPC and store-operated channels by protein kinase C. Novartis Found Symp. 2004;258:172–85; discussion 185-8, 263-6.
23. Schmitt S, Castelvetri LC, Simons M. Metabolism and functions of lipids in myelin. Biochim Biophys Acta. 2015;1851(8):999–1005.
24. Smaby JM, et al. Cholesterol-induced interfacial area condensations of galactosylceramides and sphingomyelins with identical acyl chains. Biochemistry. 1996;35(18):5696–704.
25. Di Biase A, Salvati S, Serlupi Crescenzi G. Lipid profile of rat myelin subfractions. Neurochem Res. 1990;15(5):519–22.
26. Hill WG, et al. Isolation and characterization of the Xenopus oocyte plasma membrane: a new method for studying activity of water and solute transporters. Am J Physiol Renal Physiol. 2005;289(1):F217–24.
27. Sadler SE. Low-density caveolae-like membrane from Xenopus laevis oocytes is enriched in Ras. J Cell Biochem. 2001;83(1):21–32.
28. Orth M, Bellosta S. Cholesterol: its regulation and role in central nervous system disorders. Cholesterol. 2012;2012:292598.
29. Levitan I, Singh DK, Rosenhouse-Dantsker A. Cholesterol binding to ion channels. Front Physiol. 2014;5:65.

30. Li Q, et al. Structural mechanism of voltage-dependent gating in an isolated voltage-sensing domain. Nat Struct Mol Biol. 2014;21(3):244–52.
31. Long SB, Campbell EB, Mackinnon R. Crystal structure of a mammalian voltage-dependent Shaker family K+ channel. Science. 2005;309(5736):897–903.
32. Hille B. Ion channels of excitable membranes. 3rd ed. Sunderland: Sinauer Associates; 2001.
33. Shribman S, et al. Voltage-gated potassium channelopathy: an expanding spectrum of clinical phenotypes. BMJ Case Rep. 2013;2013:bcr2012007742.
34. Poolos NP, Johnston D. Dendritic ion channelopathy in acquired epilepsy. Epilepsia. 2012;53(Suppl 9):32–40.
35. Baig SM, et al. Loss of Ca(v)1.3 (CACNA1D) function in a human channelopathy with bradycardia and congenital deafness. Nat Neurosci. 2011;14(1):77–84.
36. Xie G, et al. A new Kv1.2 channelopathy underlying cerebellar ataxia. J Biol Chem. 2010;285(42):32160–73.
37. Tremblay J, Hamet P. Genetics of pain, opioids, and opioid responsiveness. Metabolism. 2010;59(Suppl 1):S5–8.
38. Pietrobon D. CaV2.1 channelopathies. Pflugers Arch. 2010;460(2):375–93.
39. Rajakulendran S, et al. Episodic ataxia type 1: a neuronal potassium channelopathy. Neurotherapeutics. 2007;4(2):258–66.
40. Kordasiewicz HB, Gomez CM. Molecular pathogenesis of spinocerebellar ataxia type 6. Neurotherapeutics. 2007;4(2):285–94.
41. Howard RJ, et al. Structural insight into KCNQ (Kv7) channel assembly and channelopathy. Neuron. 2007;53(5):663–75.
42. Estevez M. Invertebrate modeling of a migraine channelopathy. Headache. 2006;46(Suppl 1):S25–31.
43. Cox JJ, et al. An SCN9A channelopathy causes congenital inability to experience pain. Nature. 2006;444(7121):894–8.
44. Bjerregaard P, Jahangir A, Gussak I. Targeted therapy for short QT syndrome. Expert Opin Ther Targets. 2006;10(3):393–400.
45. Poolos NP. The h-channel: a potential channelopathy in epilepsy? Epilepsy Behav. 2005;7(1):51–6.
46. Tao X, et al. A gating charge transfer center in voltage sensors. Science. 2010;328:67–73.
47. Kintzer AF, Stroud RM. Structure, inhibition and regulation of two-pore channel TPC1 from Arabidopsis thaliana. Nature. 2016;531(7593):258–62.
48. Guo J, et al. Structure of the voltage-gated two-pore channel TPC1 from Arabidopsis thaliana. Nature. 2016;531(7593):196–201.
49. Payandeh J, et al. The crystal structure of a voltage-gated sodium channel. Nature. 2011;475(7356):353–8.
50. Wang W, MacKinnon R. Cryo-EM structure of the open human ether-a-go-go-related K(+) channel hERG. Cell. 2017;169(3):422–430.e10.
51. Lee CH, MacKinnon R. Structures of the human HCN1 hyperpolarization-activated channel. Cell. 2017;168(1-2):111–120.e11.
52. Hite RK, MacKinnon R. Structural titration of Slo2.2, a Na+−dependent K+ channel. Cell. 2017;168(3):390–399.e11.
53. Whicher JR, MacKinnon R. Structure of the voltage-gated K(+) channel Eag1 reveals an alternative voltage sensing mechanism. Science. 2016;353(6300):664–9.
54. Wu J, et al. Structure of the voltage-gated calcium channel Cav1.1 complex. Science. 2015;350(6267):aad2395.
55. Sun J, MacKinnon R. Cryo-EM structure of a KCNQ1/CaM complex reveals insights into congenital long QT syndrome. Cell. 2017;169(6):1042–1050.e9.
56. Vargas E, et al. An emerging consensus on voltage-dependent gating from computational modeling and molecular dynamics simulations. J Gen Physiol. 2012;140(6):587–94.
57. Villalba-Galea CA, et al. Charge movement of a voltage-sensitive fluorescent protein. Biophys J. 2009;96(2):L19–21.

58. Vargas E, Bezanilla F, Roux B. In search of a consensus model of the resting state of a voltage-sensing domain. Neuron. 2011;72(5):713–20.
59. Villalba-Galea CA, et al. S4-based voltage sensors have three major conformations. Proc Natl Acad Sci U S A. 2008;105(46):17600–7.
60. Chanda B, Bezanilla F. A common pathway for charge transport through voltage-sensing domains. Neuron. 2008;57(3):345–51.
61. Bezanilla F. The voltage-sensor structure in a voltage-gated channel. Trends Biochem Sci. 2005;30(4):166–8.
62. Sigg D, Bezanilla F. A physical model of potassium channel activation: from energy landscape to gating kinetics. Biophys J. 2003;84(6):3703–16.
63. Bezanilla F, Perozo E. The voltage sensor and the gate in ion channels. Adv Protein Chem. 2003;63:211–41.
64. Bezanilla F. Voltage sensor movements. J Gen Physiol. 2002;120(4):465–73.
65. Bezanilla F. The voltage sensor in voltage-dependent ion channels. Physiol Rev. 2000;80(2):555–92.
66. Papazian DM, Bezanilla F. Voltage-dependent activation of ion channels. Adv Neurol. 1999;79:481–91.
67. Cha A, Bezanilla F. Structural implications of fluorescence quenching in the Shaker K+ channel. J Gen Physiol. 1998;112(4):391–408.
68. Sigg D, Bezanilla F. Total charge movement per channel. The relation between gating charge displacement and the voltage sensitivity of activation. J Gen Physiol. 1997;109(1):27–39.
69. Cha A, Bezanilla F. Characterizing voltage-dependent conformational changes in the Shaker K+ channel with fluorescence. Neuron. 1997;19(5):1127–40.
70. Bezanilla F, Stefani E. Voltage-dependent gating of ionic channels. Annu Rev Biophys Biomol Struct. 1994;23:819–46.
71. Shenkel S, Bezanilla F. Patch recordings from the electrocytes of electrophorus. Na channel gating currents. J Gen Physiol. 1991;98(3):465–78.
72. Lee SY, et al. Structure of the KvAP voltage-dependent K+ channel and its dependence on the lipid membrane. Proc Natl Acad Sci U S A. 2005;102(43):15441–6.
73. Jiang QX, Wang DN, MacKinnon R. Electron microscopic analysis of KvAP voltage-dependent K+ channels in an open conformation. Nature. 2004;430(7001):806–10.
74. Jiang Y, et al. The principle of gating charge movement in a voltage-dependent K+ channel. Nature. 2003;423(6935):42–8.
75. Jiang Y, et al. X-ray structure of a voltage-dependent K+ channel. Nature. 2003;423(6935):33–41.
76. Ahern CA, et al. Electrostatic contributions of aromatic residues in the local anesthetic receptor of voltage-gated sodium channels. Circ Res. 2008;102(1):86–94.
77. Horn R. How ion channels sense membrane potential. Proc Natl Acad Sci U S A. 2005;102(14):4929–30.
78. Ahern CA, Horn R. Focused electric field across the voltage sensor of potassium channels. Neuron. 2005;48(1):25–9.
79. Ahern CA, Horn R. Specificity of charge-carrying residues in the voltage sensor of potassium channels. J Gen Physiol. 2004;123(3):205–16.
80. Horn R. Coupled movements in voltage-gated ion channels. J Gen Physiol. 2002;120(4):449–53.
81. Horn R. A new twist in the saga of charge movement in voltage-dependent ion channels. Neuron. 2000;25(3):511–4.
82. Horn R. Conversation between voltage sensors and gates of ion channels. Biochemistry. 2000;39(51):15653–8.
83. Yang N, Horn R. Evidence for voltage-dependent S4 movement in sodium channels. Neuron. 1995;15(1):213–8.
84. Li Q, et al. Structural basis of lipid-driven conformational transitions in the KvAP voltage-sensing domain. Nat Struct Mol Biol. 2014;21(2):160–6.

85. Tang L, et al. Structural basis for Ca2+ selectivity of a voltage-gated calcium channel. Nature. 2014;505(7481):56–61.
86. Catterall WA. Structure and function of voltage-gated sodium channels at atomic resolution. Exp Physiol. 2014;99(1):35–51.
87. Payandeh J, et al. Crystal structure of a voltage-gated sodium channel in two potentially inactivated states. Nature. 2012;486(7401):135–9.
88. Catterall WA. Voltage-gated calcium channels. Cold Spring Harb Perspect Biol. 2011;3(8):a003947.
89. Catterall WA. Ion channel voltage sensors: structure, function, and pathophysiology. Neuron. 2010;67(6):915–28.
90. Yarov-Yarovoy V, Baker D, Catterall WA. Voltage sensor conformations in the open and closed states in ROSETTA structural models of K(+) channels. Proc Natl Acad Sci U S A. 2006;103(19):7292–7.
91. Sokolov S, Scheuer T, Catterall WA. Ion permeation through a voltage- sensitive gating pore in brain sodium channels having voltage sensor mutations. Neuron. 2005;47(2):183–9.
92. Yu FH, Catterall WA. Overview of the voltage-gated sodium channel family. Genome Biol. 2003;4(3):24.
93. Catterall WA. Structure and function of voltage-gated ion channels. Annu Rev Biochem. 1995;64:493–531.
94. Catterall WA. Molecular properties of voltage-sensitive sodium and calcium channels. Braz J Med Biol Res. 1988;21(6):1129–44.
95. Tombola F, Ulbrich MH, Isacoff EY. Architecture and gating of Hv1 proton channels. J Physiol. 2009;587(Pt 22):5325–9.
96. Pathak MM, et al. Closing in on the resting state of the Shaker K(+) channel. Neuron. 2007;56(1):124–40.
97. Tombola F, Pathak MM, Isacoff EY. How does voltage open an ion channel? Annu Rev Cell Dev Biol. 2006;22:23–52.
98. Tombola F, Pathak MM, Isacoff EY. Voltage-sensing arginines in a potassium channel permeate and occlude cation-selective pores. Neuron. 2005;45(3):379–88.
99. Gandhi CS, Isacoff EY. Molecular models of voltage sensing. J Gen Physiol. 2002;120(4):455–63.
100. Mannuzzu LM, Isacoff EY. Independence and cooperativity in rearrangements of a potassium channel voltage sensor revealed by single subunit fluorescence. J Gen Physiol. 2000;115(3):257–68.
101. Mannuzzu LM, Moronne MM, Isacoff EY. Direct physical measure of conformational rearrangement underlying potassium channel gating. Science. 1996;271(5246):213–6.
102. Larsson HP, et al. Transmembrane movement of the shaker K+ channel S4. Neuron. 1996;16(2):387–97.
103. Heginbotham L, et al. Mutations in the K+ channel signature sequence. Biophys J. 1994;66(4):1061–7.
104. Heginbotham L, MacKinnon R. Conduction properties of the cloned Shaker K+ channel. Biophys J. 1993;65(5):2089–96.
105. Aggarwal SK, MacKinnon R. Contribution of the S4 segment to gating charge in the Shaker K+ channel. Neuron. 1996;16(6):1169–77.
106. Starace DM, Bezanilla F. Histidine scanning mutagenesis of basic residues of the S4 segment of the shaker k+ channel. J Gen Physiol. 2001;117(5):469–90.
107. Seoh SA, et al. Voltage-sensing residues in the S2 and S4 segments of the Shaker K+ channel. Neuron. 1996;16(6):1159–67.
108. Islas LD, Sigworth FJ. Electrostatics and the gating pore of Shaker potassium channels. J Gen Physiol. 2001;117(1):69–89.
109. Islas LD, Sigworth FJ. Voltage sensitivity and gating charge in Shaker and Shab family potassium channels. J Gen Physiol. 1999;114(5):723–42.
110. Schoppa NE, Sigworth FJ. Activation of Shaker potassium channels. III. An activation gating model for wild-type and V2 mutant channels. J Gen Physiol. 1998;111(2):313–42.

111. Schoppa NE, et al. The size of gating charge in wild-type and mutant Shaker potassium channels. Science. 1992;255(5052):1712–5.
112. Zhou Y, MacKinnon R. Ion binding affinity in the cavity of the KcsA potassium channel. Biochemistry. 2004;43(17):4978–82.
113. Zhou Y, MacKinnon R. The occupancy of ions in the K+ selectivity filter: charge balance and coupling of ion binding to a protein conformational change underlie high conduction rates. J Mol Biol. 2003;333(5):965–75.
114. Zhang X, et al. Crystal structure of an orthologue of the NaChBac voltage-gated sodium channel. Nature. 2012;486(7401):130–4.
115. Takeshita K, et al. X-ray crystal structure of voltage-gated proton channel. Nat Struct Mol Biol. 2014;21(4):352–7.
116. Clayton GM, et al. Combining electron crystallography and X-ray crystallography to study the MlotiK1 cyclic nucleotide-regulated potassium channel. J Struct Biol. 2009;167(3):220–6.
117. Tao X, Hite RK, MacKinnon R. Cryo-EM structure of the open high-conductance Ca2+-activated K+ channel. Nature. 2017;541(7635):46–51.
118. Hite RK, Tao X, MacKinnon R. Structural basis for gating the high-conductance Ca2+-activated K+ channel. Nature. 2017;541(7635):52–7.
119. Fox PD, Loftus RJ, Tamkun MM. Regulation of Kv2.1 K(+) conductance by cell surface channel density. J Neurosci. 2013;33(3):1259–70.
120. O'Connell KM, Loftus R, Tamkun MM. Localization-dependent activity of the Kv2.1 delayed-rectifier K+ channel. Proc Natl Acad Sci U S A. 2010;107(27):12351–6.
121. O'Connell KM, Tamkun MM. Targeting of voltage-gated potassium channel isoforms to distinct cell surface microdomains. J Cell Sci. 2005;118(Pt 10):2155–66.
122. Martens JR, et al. Isoform-specific localization of voltage-gated K+ channels to distinct lipid raft populations. Targeting of Kv1.5 to caveolae. J Biol Chem. 2001;276(11):8409–14.
123. Purcell EK, et al. Cholesterol influences voltage-gated calcium channels and BK-type potassium channels in auditory hair cells. PLoS One. 2011;6(10):e26289.
124. Huang CW, Wu YJ, Wu SN. Modification of activation kinetics of delayed rectifier K+ currents and neuronal excitability by methyl-beta-cyclodextrin. Neuroscience. 2011;176:431–41.
125. Finol-Urdaneta RK, et al. Modulation of KvAP unitary conductance and gating by 1-alkanols and other surface active agents. Biophys J. 2010;98(5):762–72.
126. Guo J, et al. Effects of cholesterol levels on the excitability of rat hippocampal neurons. Mol Membr Biol. 2008;25(3):216–23.
127. Pottosin II, et al. Methyl-beta-cyclodextrin reversibly alters the gating of lipid rafts-associated Kv1.3 channels in Jurkat T lymphocytes. Pflugers Arch. 2007;454(2):235–44.
128. Balijepalli RC, et al. Kv11.1 (ERG1) K+ channels localize in cholesterol and sphingolipid enriched membranes and are modulated by membrane cholesterol. Channels (Austin). 2007;1(4):263–72.
129. Abi-Char J, et al. Membrane cholesterol modulates Kv1.5 potassium channel distribution and function in rat cardiomyocytes. J Physiol. 2007;582(Pt 3):1205–17.
130. Xia F, et al. Disruption of pancreatic beta-cell lipid rafts modifies Kv2.1 channel gating and insulin exocytosis. J Biol Chem. 2004;279(23):24685–91.
131. Pouvreau S, et al. Membrane cholesterol modulates dihydropyridine receptor function in mice fetal skeletal muscle cells. J Physiol. 2004;555(Pt 2):365–81.
132. Hajdu P, et al. Cholesterol modifies the gating of Kv1.3 in human T lymphocytes. Pflugers Arch. 2003;445(6):674–82.
133. Rudakova E, et al. Localization of Kv4.2 and KChIP2 in lipid rafts and modulation of outward K+ currents by membrane cholesterol content in rat left ventricular myocytes. Pflugers Arch. 2015;467(2):299–309.
134. Bowles DK, et al. Hypercholesterolemia inhibits L-type calcium current in coronary macro-, not microcirculation. J Appl Physiol (1985). 2004;96(6):2240–8.
135. Heaps CL, Tharp DL, Bowles DK. Hypercholesterolemia abolishes voltage-dependent K+ channel contribution to adenosine-mediated relaxation in porcine coronary arterioles. Am J Physiol Heart Circ Physiol. 2005;288(2):H568–76.

136. Balajthy A, et al. 7DHC-induced changes of Kv1.3 operation contributes to modified T cell function in Smith-Lemli-Opitz syndrome. Pflugers Arch. 2016;468:1403.
137. Chun YS, et al. Cholesterol modulates ion channels via down-regulation of phosphatidylinositol 4,5-bisphosphate. J Neurochem. 2010;112(5):1286–94.
138. Coyan FC, et al. A long QT mutation substitutes cholesterol for phosphatidylinositol-4,5-bisphosphate in KCNQ1 channel regulation. PLoS One. 2014;9(3):e93255.
139. Heaps CL, et al. Effects of exercise training and hypercholesterolemia on adenosine activation of voltage-dependent K+ channels in coronary arterioles. J Appl Physiol. 2008;105(6):1761–71.
140. Balijepalli SY, et al. Mechanism of loss of Kv11.1 K+ current in mutant T421M-Kv11.1-expressing rat ventricular myocytes: interaction of trafficking and gating. Circulation. 2012;126(24):2809–18.
141. Xu Y, Ramu Y, Lu Z. Removal of phospho-head groups of membrane lipids immobilizes voltage sensors of K+ channels. Nature. 2008;451(7180):826–9.
142. Ramu Y, Xu Y, Lu Z. Enzymatic activation of voltage-gated potassium channels. Nature. 2006;442(7103):696–9.
143. Zheng H, et al. Lipid-dependent gating of a voltage-gated potassium channel. Nat Commun. 2011;2:250.
144. Jiang Q-X, Gonen T. The influence of lipids on voltage-gated ion channels. Curr Opin Struct Biol. 2012;22:529–36.
145. Gantz SC, Bean BP. Cell-autonomous excitation of midbrain dopamine neurons by endocannabinoid-dependent lipid signaling. Neuron. 2017;93(6):1375–1387.e2.
146. Randich AM, et al. Biochemical and structural analysis of the hyperpolarization-activated K(+) channel MVP. Biochemistry. 2014;53(10):1627–36.
147. Amsalem M, et al. Membrane cholesterol depletion as a trigger of Nav1.9 channel-mediated inflammatory pain. EMBO J. 2018;37(8):e97349.
148. Calhoun JD, Isom LL. The role of non-pore-forming beta subunits in physiology and pathophysiology of voltage-gated sodium channels. Handb Exp Pharmacol. 2014;221:51–89.
149. Hofmann F, Belkacemi A, Flockerzi V. Emerging alternative functions for the auxiliary subunits of the voltage-gated calcium channels. Curr Mol Pharmacol. 2015;8(2):162–8.
150. Liu SL, et al. Orthogonal lipid sensors identify transbilayer asymmetry of plasma membrane cholesterol. Nat Chem Biol. 2017;13(3):268–74.
151. Zheng H, et al. bSUM: a bead-supported unilamellar membrane system facilitating unidirectional insertion of membrane proteins into giant vesicles. J Gen Physiol. 2016; 147(1):77–93.
152. Lingwood D, Simons K. Lipid rafts as a membrane-organizing principle. Science. 2010;327(5961):46–50.
153. Kaiser HJ, et al. Order of lipid phases in model and plasma membranes. Proc Natl Acad Sci U S A. 2009;106(39):16645–50.
154. Coskun U, Simons K. Membrane rafting: from apical sorting to phase segregation. FEBS Lett. 2009;28:28.
155. Anderson RG. The caveolae membrane system. Annu Rev Biochem. 1998;67:199–225.
156. Anderson RG. Transendothelial movement and caveolae. Nat Biotechnol. 2008;26(4):380–1; author reply 381-2.
157. Mizuno H, et al. Fluorescent probes for superresolution imaging of lipid domains on the plasma membrane. Chem Sci. 2011;2:1548.
158. Klitzing HA, Weber PK, Kraft ML. Secondary ion mass spectrometry imaging of biological membranes at high spatial resolution. Methods Mol Biol. 2013;950:483–501.
159. Kraft ML. Sphingolipid organization in the plasma membrane and the mechanisms that influence it. Front Cell Dev Biol. 2016;4:154.
160. Richard M, Raquel F. Non-raft forming sphingomyelin-cholesterol mixtures. Chem Phys Lipids. 2004;132(1):37–46.
161. Dietrich C, et al. Lipid rafts reconstituted in model membranes. Biophys J. 2001;80(3): 1417–28.

162. Wang L, Bose PS, Sigworth FJ. Using cryo-EM to measure the dipole potential of a lipid membrane. Proc Natl Acad Sci U S A. 2006;103(49):18528–33.
163. Nyholm TK, et al. Construction of a DOPC/PSM/cholesterol phase diagram based on the fluorescence properties of trans-parinaric acid. Langmuir. 2011;27:8339.
164. Kolter T, Sandhoff K. Sphingolipid metabolism diseases. Biochim Biophys Acta. 2006;1758(12):2057–79.
165. Cheng SH. Gene therapy for the neurological manifestations in lysosomal storage disorders. J Lipid Res. 2014;55:1827.
166. Bolsover FE, et al. Cognitive dysfunction and depression in Fabry disease: a systematic review. J Inherit Metab Dis. 2014;37(2):177–87.
167. Bellettato CM, Scarpa M. Pathophysiology of neuropathic lysosomal storage disorders. J Inherit Metab Dis. 2010;33(4):347–62.
168. Millard EE, et al. The sterol-sensing domain of the Niemann-Pick C1 (NPC1) protein regulates trafficking of low density lipoprotein cholesterol. J Biol Chem. 2005;280(31):28581–90.
169. Millard EE, et al. Niemann-pick type C1 (NPC1) overexpression alters cellular cholesterol homeostasis. J Biol Chem. 2000;275(49):38445–51.
170. Praggastis M, et al. A murine Niemann-Pick C1 I1061T knock-in model recapitulates the pathological features of the most prevalent human disease allele. J Neurosci. 2015;35(21):8091–106.
171. Andersson M, et al. Structural dynamics of the S4 voltage-sensor helix in lipid bilayers lacking phosphate groups. J Phys Chem B. 2011;115(27):8732–8.
172. O'Connell KM, Martens JR, Tamkun MM. Localization of ion channels to lipid Raft domains within the cardiovascular system. Trends Cardiovasc Med. 2004;14(2):37–42.
173. Martens JR, O'Connell K, Tamkun M. Targeting of ion channels to membrane microdomains: localization of KV channels to lipid rafts. Trends Pharmacol Sci. 2004;25(1):16–21.
174. Martens JR, et al. Differential targeting of Shaker-like potassium channels to lipid rafts. J Biol Chem. 2000;275(11):7443–6.
175. Bichenkov E, Ellingson JS. Temporal and quantitative expression of the myelin-associated lipids, ethanolamine plasmalogen, galactocerebroside, and sulfatide, in the differentiating CG-4 glial cell line. Neurochem Res. 1999;24(12):1549–56.
176. Unwin N. Segregation of lipids near acetylcholine-receptor channels imaged by cryo-EM. IUCrJ. 2017;4(Pt 4):393–9.
177. Sun J, Comeau JF, Baenziger JE. Probing the structure of the uncoupled nicotinic acetylcholine receptor. Biochim Biophys Acta. 2017;1859(2):146–54.
178. Brannigan G. Direct interactions of cholesterol with pentameric ligand-gated ion channels: testable hypotheses from computational predictions. Curr Top Membr. 2017;80:163–86.
179. daCosta CJ, et al. A distinct mechanism for activating uncoupled nicotinic acetylcholine receptors. Nat Chem Biol. 2013;9(11):701–7.
180. Barrantes FJ. Cell-surface translational dynamics of nicotinic acetylcholine receptors. Front Synaptic Neurosci. 2014;6:25.
181. Gao Y, et al. TRPV1 structures in nanodiscs reveal mechanisms of ligand and lipid action. Nature. 2016;534(7607):347–51.

Correction to: Cholesterol Effects on the Physical Properties of Lipid Membranes Viewed by Solid-state NMR Spectroscopy

Trivikram R. Molugu and Michael F. Brown

Correction to:
Chapter 5 in: A. Rosenhouse-Dantsker, A. N. Bukiya (eds.), *Cholesterol Modulation of Protein Function*, Advances in Experimental Medicine and Biology 1115, https://doi.org/10.1007/978-3-030-04278-3_5

Chapter 5 was published without including the research grant details in the acknowledgement section, which has been updated in the chapter now.

The updated version of this chapter can be found at
https://doi.org/10.1007/978-3-030-04278-3_5

A. Rosenhouse-Dantsker, A. Bukiya (eds.), *Cholesterol Modulation of Protein Function*, Advances in Experimental Medicine and Biology 1115,
https://doi.org/10.1007/978-3-030-04278-3_9

Index

A. Rosenhouse-Dantsker, A. N. Bukiya (eds.), *Cholesterol Modulation of Protein Function*, Advances in Experimental Medicine and Biology 1115,
https://doi.org/10.1007/978-3-030-04278-3